Advanced Composites and Hybrid Materials (2025) 8:30
https://doi.org/10.1007/s42114-024-01078-z

REVIEW

Recent progress in the development of cellulose-derived organic-nanopolymer and coordination network platforms for application as optical chemosensors

Ratish R. Nair[1] · Joo Hee Hyun[2] · Jahyun Kim[3] · Kyung Oh Jung[4] · Dokyoung Kim[1,2,3,5,6]

Received: 11 August 2024 / Revised: 12 October 2024 / Accepted: 21 November 2024

Abstract
Cellulosic materials are attractive hybrid combinations that avail an array of hitherto unachievable properties by conjugating with organic, inorganic,and nano- and polymeric compounds. Cellulose-based materials have established great potential in several fields, such as air purification, water remediation, adsorbents, gas storage, biomedicine and optical chemosensing. Cellulose is among the cheapest materials available and is easily modifiable into different materials. The review summarises the chemical modification of cellulose materials and their applications in optical chemosensing. The review briefs the utilization of cellulose in fabrication, doping, and modification with organic, nano and polymeric chromo and fluorophores. Cellulose-fabricated materials like films, fibres, crystals, hydrogel and coordination networks are accurately highlighted. Discussion on the applicability of cellulosic hybrids for the detection of toxic metal ions, anions, aromatic vapours, explosives, pH, bioimaging, 3D-printing, coating and anti-counterfeiting by utilizing optical sensing approaches such as UV and fluorescence spectroscopy is pursued. Finally, the elaboration of upcoming investigations, challenges and opinions observed in utilising cellulose hybrid materials for optical chemosensing applications are discussed. We believe that this review will drive more and more curiosity and attention from the scientific community, industries and laboratories working with the synthesis of cellulose-based hybrid materials for widespread optical chemosensing applications.

Keywords Hybrid material · Chemosensor · Coordination platform · Cellulose-based materials · Optical sensing

1 Introduction

Globally, the demand for products generated from renewable and sustainable resources that possess qualities of biodegradability, carbon neutral, non-petroleum based and have low environmental, biological health and safety risks is progressively gaining popularity. Cellulose, starch and lignin fall under the class of excellent and low-cost biopolymers derived from natural resources, which can generate an array of eco-friendly, cheap and sustainable functional materials. Cellulose is a biomolecule found and produced in abundance with an exceptional annual production rate of 1.5×10^{12} tons [1]. For thousands of years, different forms of natural cellulose-based materials (wood, hemp, cotton,

✉ Ratish R. Nair
ratish222@gmail.com

✉ Kyung Oh Jung
kojung@cau.ac.kr

✉ Dokyoung Kim
dkim@khu.ac.kr

[1] Medical Research Center for Bioreaction to Reactive Oxygen Species and Biomedical Science Institute, Core Research Institute (CRI), Kyung Hee University, Seoul 02447, Republic of Korea

[2] Department of Biomedical Science, Graduate School, Kyung Hee University, Seoul 02447, Republic of Korea

[3] Department of Precision Medicine, Graduate School, Kyung Hee University, Seoul 02447, Republic of Korea

[4] Department of Anatomy, College of Medicine, Chung-Ang University, Seoul 06974, Republic of Korea

[5] Department of Anatomy and Neurobiology, College of Medicine, Kyung Hee University, Seoul 02447, Republic of Korea

[6] KHU-KIST Department of Converging Science and Technology, Kyung Hee University, Seoul 02447, Republic of Korea

Published online: 09 December 2024

linen, etc.) have been used by human societies as engineering solutions accounting in high economic gains [2]. Natural products when reinforced into cellulose gain high-end physical properties like elasticity along with flexibility, excellent functionality including high tensile and mechanical strength/weight, aiding in the transformation of hierarchical structure design that ranges from nanoscale to supramolecular and macroscopic dimensions. However, traditional cellulosic materials also have disadvantages like durability, functionality and uniformity, which are essential properties for the construction of next-generation efficient engineering materials [2]. Hence, it is important to imbibe modern technology and generate high-end solutions for producing cellulosic materials with highly applicable properties. Cellulose is used as precursor in the production of a wide range of materials like nanomaterials, polymers and organic and inorganic chemicals.

Cellulose is a natural polymer constituting D-glucose monomers, which is obtained by processing of natural raw materials like algae, wood, plants, tunicate and bacteria. Cellulose as substrate yields composite materials which include organic, inorganic and nano- and polymers. Applications of cellulose have been pursued in a wide range of environmental (adsorption of metals [3], water treatment [4], self-decontaminated textiles [5], defence from dangerous ultraviolet radiation [6], food-safe paper [7] and antifouling membranes[8]), energy-based (electronics [9], supercapacitors [10], fuel cells [11], flexible devices [12], triboelectric nanogenerators [13] and thermal insulators [14]) and biomedical applications (antifouling [15], drug delivery [16], antibacterial [17], tissue engineering [18] and wound healing vascular grafts [19], bone repair materials [20], sensing in cells [21] and bioimaging [22]).

Cellulose possesses excellent chemical, physical and mechanical properties (Fig. 1), such as high tensile strength, chirality, high stability under acidic conditions, good elastic modulus (130–150 GPa), low density (1.6 g/cm^3), high wettability and high biodegradability [23]. Owing to the notable features of cellulose has been used extensively in biomedical applications (Fig. 1a–d) like diagnostics and theranostics [24–29]. Moreover, the size compatibility of cellulose allows it to be used in the development of materials with various sizes ranging from nano to supramolecular or macromolecules and also comes with the potential to be spun into wearable devices. Cellulose with varied sizes can be generated by using different procedures like chemical treatment, mechanical treatment (milling processes, valorisation) and enzymatic treatment. Figure 2 illustrates various methods involved in the extraction of cellulose from mediums like biomass, bacteria and food waste, resulting in different nano and polymeric cellulose products. The extracted or synthesised cellulose materials have also found deep applications in the development of various sensors (Table 1).

In the current scenario, higher attention is paid on the development of sensors with fast response, high sensitivity, long-term stability and many more characteristics for the monitoring of environmentally and biologically important and hazardous analytes. Sensors which include strain sensors [166], tactile sensors [167], skin and sweat monitoring [168, 169], non-contact switches [170], plant growth monitoring [171], baby diapers [172], humidity sensors [173] and, most importantly, optical chemosensors [174]. Moreover, cellulose-derived materials are also utilised in the separation of enantiomeric molecules [175] and the immobilization of proteins [176] and peptides [177] (including antibodies [178] and enzymes [179]). Furthermore, the reinforcing ability and strength of cellulose matrix permit its usage as a composite in combination with synthetic polymers and biopolymers as a support medium for several applications in sensing and biosensing devices [180–182]. In the nanocellulose scenario, the cellulose nanofibres have entangled network structures with a high aspect ratio, which allows contact, penetration and concentration of the target molecules, facilitating in proving the specificity and sensitivity of sensing materials [183]. Also, nanostructures encompass inherent chiral assembly and dielectric characteristics [184]. Bacterial cellulose is widely used in the development of polymeric materials, a result of its high degree of polymerisation (up to 8000) and exceptional mechanical strength along with 3D network structure [185]. The intrinsic physical and chemical properties of cellulose aids its modification into hydrogels, aerogels, papers, films and membranes [186]. Considering organic materials, cellulose constitutes linear β−1, 4-linked D-glucose units with abundant hydroxyl (–OH) active groups. The free hydroxyl groups in cellulose allow it to form bonds with different optical materials, aiding its applicability in chemosensors. Moreover, high crystallinity, robustness, large surface area, high aspect ratio and high thermal resistance make cellulose an ideal substrate for sensing devices [187].

To date, there are several reviews that focus on putting together different aspects and applications of cellulose [23, 174, 182, 188–201]. However, only a few reviews focus on discussions related to cellulose application in sensing platforms [174, 182, 189–196]. Nevertheless, these reviews discuss a small portion of the scope of cellulose-derived materials and their applications. Table 2 depicts the contents and limitations of prior reviews related to the topic of current review.

In the current review, we have first illustrated and summarised the basic structure and synthetic routes for different cellulose-derived materials consisting of organic, inorganic and nano and polymers. Further, proper evaluation of the application of the developed cellulose-derived materials in optical chemosensing via colourimetric and fluorimetric techniques is performed. Finally, the advantages and

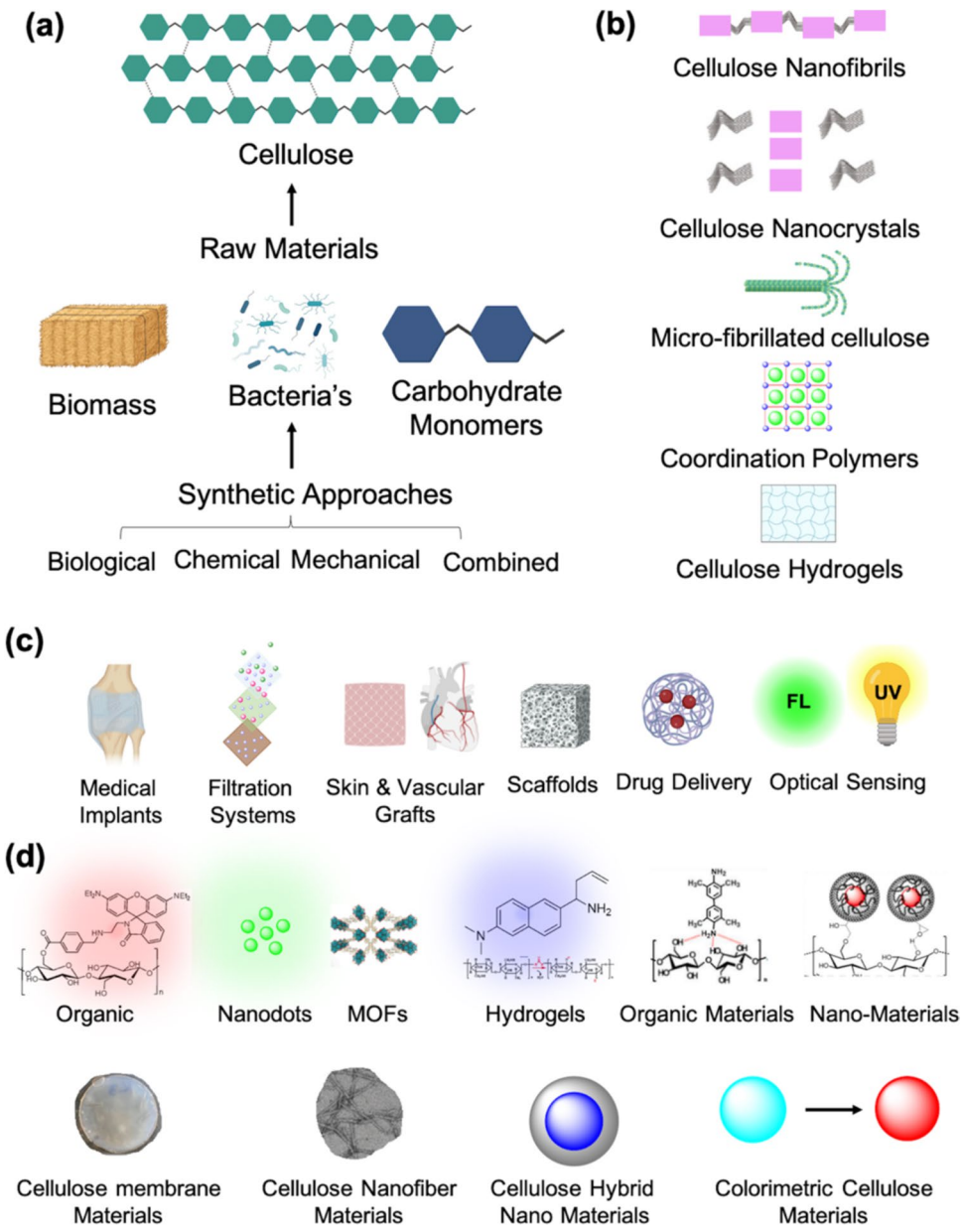

Fig. 1 Schematic representation of **a** cellulose structure and substrates, **b** different cellulose products, **c** application of cellulose-derived materials and **d** different optical chemosensing platforms

concerns faced by the employment of cellulose-derived materials in optical chemosensing will be summarised. The review will be concluded on the note of challenges and prospects in the area of cellulosic materials and their applications in the development of optical chemosensors.

2 Cellulose-derived organic materials (Cello-Org)

In the past few decades, optical chemosensors with organic profiles have shown great potential for monitoring environmentally and biologically important and hazardous materials [202–223]. Substantial research endeavours are channelled into the progression of sophisticated sensing mechanisms for the recognition of different analyte species [202–224]. Organic molecules are well-used in both colourimetric and fluorimetric techniques of optical chemosensing. Organic molecules constitute different heteroatoms that act as binding sites for various analytes, along with a colourimetric or fluorimetric unit and a mechanism for communication between these two sites [205]. As discussed in the Sect. 1, the abundant hydroxyl (–OH) active groups in cellulose allow organic molecules to bind with cellulose forming excellent templates for applications in chemosensing. Cellulose substrates like methyl cellulose, ethyl cellulose, hydroxyethyl methylcellulose, hydroxypropyl cellulose and carboxymethyl cellulose are great

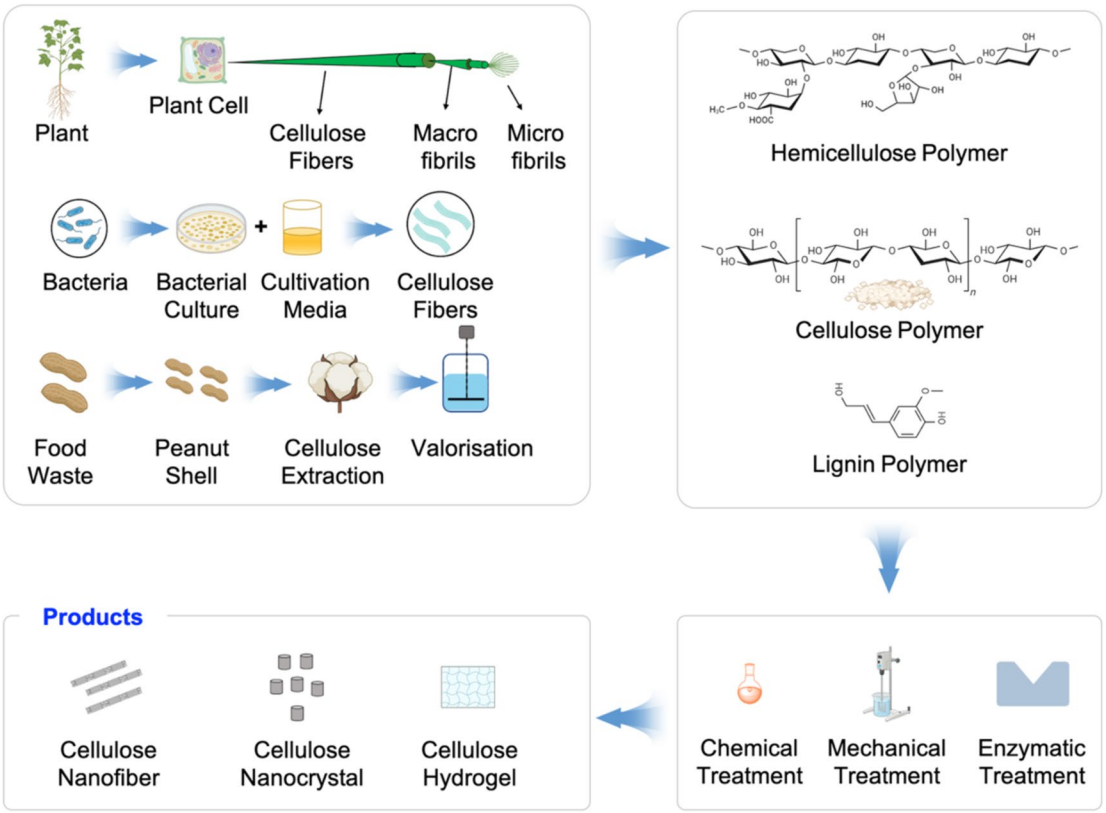

Fig. 2 Schematic illustration of synthetic strategies for extraction and production of cellulose materials, cellulosic products, different techniques and functionalised materials

substituents for binding with organic molecules. Moreover, cellulose papers are used as adsorbents for fluorescent and colourimetric materials utilised for the purpose of optical and naked eye chemosensing. In this review, we will not go into the details of such adsorbent materials but instead focus on reaction-based cellulose materials. However, it will not be justified if we do not attribute some of the notable cellulose paper-based dye-adsorbent chemosensors reported every year starting from '2012 to 2024'. In 2012, Das and their team utilised an azo dye–based compound for the dual recognition of Hg^{2+} and Cr^{3+} ions. The highly selective azo dye–derived molecular probe was adsorbed on the surface of cellulose paper for the selective naked-eye visualization of Hg^{2+} and Cr^{3+} [225]. Guo and co-workers employed a rhodamine-derived molecular fluorescent probe for selective colourimetric and fluorimetric detection of Hg^{2+} ions. Cellulose paper was modified by adsorbing rhodamine molecules and, in turn, used for the real-time detection of Hg^{2+} ions [226]. In 2014, Rurack and their group developed a BODIPY-linked hydrogen-bonding receptor for the fluorometric detection of fluoride ions in aqueous media. A test strip–based device of a BODIPY-based probe for fluoride ions was prepared and used for real-time monitoring of F^- ions [227]. Li and co-workers developed a relay strategy based on AIEgen for probing Hg^{2+} in aqueous media. Test strips based on cellulose were appended with the AIEgen dye and applied for the real-time monitoring of Hg^{2+} [228]. In 2016, Zhao and their group reported dimethyl yellow-based colourimetric chemosensors for the detection of Cr^{3+} in aqueous media. The dimethyl yellow–based receptor was suspended on cellulose paper for the naked eye colourimetric detection of Cr^{3+} [229]. Chatterjee and co-workers developed a rhodamine-based molecular probe capable of chelating Cu^{2+}. The rhodamine-based chemosensor was adsorbed on the surface of the paper and used for the naked-eye real-time colourimetric and fluorimetric detection of Cu^{2+} [230]. In 2018, Niamnont et al. introduced three salicylidene fluorophores capable of detecting volatile organic compounds (VOCs). The salicylidene probes were modified on cellulose paper by using an adsorption technique and further utilised in the naked eye detection of VOCs [231]. Pandya et al. reported a luminescent pyrene-allied calix [4] arene-based molecular probe for the determination of Zn^{2+}, Hg^{2+} and I^- ions. Further, the Calix-arene probe was appended on cellulose paper for the easy visualization of Zn^{2+}, Hg^{2+} and I^- ions [232]. Later, in 2021, Kumaresan and co-workers utilised a coumarin-based chemosensor for the

Table 1 Source of cellulose materials used in the development of sensors used in the current review

Probe	Source of cellulose	Material used in application	Reference
1	Bacterial cellulose	Cotton gauze wound dressing	[30]
3	Bacterial cellulose	BC filter paper	[31]
5	Wood pulp	Whatman 42 filter paper	[32]
7	High alpha wood cellulose	Hydroxyethyl cellulose	[33]
8	Waste cellulose papers	Activated cellulose papers	[34]
10	Wood pulp	Cellulose paper strip	[35]
13	Purified cellulose from wood pulp	Cellulose acetate	[36]
14	Cellulose powder from wood pulp	Cellulose filter paper	[37]
16	Biomass	Cellulose filter paper	[38]
17	Cotton pulp	Cellulose fibres	[39]
18	Cellulose from cotton pulp	α-cellulose	[40]
19	Purified cellulose from wood pulp	Cellulose acetate fibres	[41]
22	Wood pulp	Whatman 42 filter paper	[42]
24	Cotton pulp	Cellulose textiles	[43]
26	Biomass	Cellulose nanofibres	[44]
30	Wood pulp	High-purity cellulose membranes	[45]
36	Biocomposites	Semi-crystalline cellulose	[46]
37	Cotton pulp	Modified cellulose paper	[47]
38	Renewable wood pulp	Lignin nanoparticles	[48]
39	Cotton pulp	Cellulose filter papers	[49]
40	Wood/cotton pulp/biomass	Carboxymethyl cellulose	[50]
41	Wood/cotton pulp/biomass	Carboxymethyl cellulose	[51]
42	Wood/cotton pulp	Cellulose paper microzone plate	[52]
43	Wood/cotton pulp	Cellulose paper strips	[53]
45	Bacterial cellulose	Cellulose nanofibril	[54]
46	Bacterial cellulose	Quaternised cellulose	[55]
48	Natural plant fibre	Cellulose nanofibril	[56]
49	Wood/cotton pulp	Cellulose papers	[57]
50	Cotton pulp	Modified cellulose paper	[58]
51	Cotton pulp	Cellulose nanocrystal	[59]
53	Cellulose from wood/cotton pulp	Carboxylethyl quaternised cellulose	[60]
54	Bacterial cellulose	Cellulose nanopaper	[61]
55–57	Softwood pulp	Mixed cellulose ester paper	[62]
58	Wood/cotton pulp	Cellulose papers	[63]
59	Wood/cotton pulp	Modified cellulose membrane	[64]
60	Bacterial cellulose	Cellulose nanofibres	[65]
62	Wood/cotton pulp	Cellulose papers	[66]
63	Wood/cotton pulp	Cellulose nanowhiskers	[67]
64	Natural plant fibre	Cellulose fibre strip	[68]
66	Wood/cotton pulp	Cellulose nanocrystals	[69]
67	Cotton pulp	Modified cellulose fibres	[70]
68	Wood/cotton pulp	Cellulose nanocrystals	[71]
69	Wood/cotton pulp	Cellulose nanocrystals	[72]
70	Bacterial cellulose	Cellulose nanofibres	[73]
72	Wood/cotton pulp	Cellulose nanocrystals	[74]
73	Wood/cotton pulp	Cellulose nanocrystals	[75]
74	Wood/cotton pulp	Cellulose nanocrystals	[76]
75	Bacterial cellulose	Cellulose acetate nanofibres	[77]
76	Wood/cotton pulp	Cellulose nanocrystals	[78]
78	Wood/cotton pulp	Cellulose nanocrystals	[79]
79	Bacterial cellulose	Cellulose nanofibres	[80]

Table 1 (continued)

Probe	Source of cellulose	Material used in application	Reference
80	Wood/cotton pulp	Cellulose nanocrystals	[81]
81	Wheat straw	Cellulose nanofibres	[82]
83	Cotton pulp	Microcrystal cellulose	[83]
84	Wood/cotton pulp	Cellulose nanocrystals	[84]
85	Microcrystalline cellulose	Cellulose nanocrystals	[85]
87	Natural plant fibre	Cellulose nanofibres	[86]
88	Algae	Cellulose nanocrystals	[87]
89	Biomass	Spherical nanocellulose	[88]
90	Bacterial cellulose	Cellulose paper	[89]
91	Bacterial cellulose	Cellulose paper	[90]
92	Biomass	Cellulose paper	[91]
93	Bacterial cellulose	Cellulose nanofibres	[92]
94	Wood pulp	Microcrystalline cellulose	[93]
95	Bacterial cellulose	Cellulose nanofibres	[94]
96	Wood pulp	Modified cellulose paper	[95]
97	Bacterial cellulose	Cellulose membranes	[96]
98	Biomass	Cellulose-based biowaste	[97]
99	Bacterial cellulose	Nano cellulose	[98]
100	Cellulose nanofibres from cotton	Aerogel	[99]
101	Carboxymethyl cellulose	Cellulose sponge	[100]
103	Wood pulp	Whatman cellulose filter paper	[101]
105	Softwood pulp	Oxidised cellulose	[102]
106	Wood pulp	Sodium carboxymethyl cellulose	[103]
108	Discarded cigarette filters	Cellulose diacetate	[104]
110	Bacterial cellulose	Cellulose nanofibres	[105]
111	Cellulose endonuclease	Nano fibrillated cellulose	[106]
114	Bacterial cellulose	Cellulose nanocrystal	[107]
116	Carboxymethyl cellulose	Cellulose polymer dots	[108]
117	Cellulose nanocrystal	Cholesteric nanocellulose film	[109]
118	Bacterial cellulose	Cellulose nanofibres	[110]
119	Wood/cotton pulp	Cellulose paper	[111]
120	Biomass	Lignin	[112]
122	Wood pulp	Cellulose nanocrystals	[113]
123–125	Wood pulp	Cellulose nanocrystals	[114]
126	Microcrystalline cellulose	Nanocellulose	[115]
127	Biomass	Cellulose nanofibres	[116]
128	Microcrystalline cellulose	Nanocellulose	[117]
129	Carboxymethyl cellulose	Oxidised carboxymethyl cellulose	[118]
130	Wood pulp	Sodium carboxymethyl cellulose	[119]
131	Carboxymethyl cellulose	Oxidised carboxymethyl cellulose	[120]
132	Biomass	Cellulose nanofibres	[121]
133	Wood pulp	Cellulose nanocrystals	[122]
134	Cotton pulp	Cotton cellulose	[123]
135	Biomass	Cellulose gel	[124]
136	Biomass	Cellulose nanofibres	[125]
137	Microcrystalline cellulose	Cellulose hydrogel	[126]
138	Cotton pulp	Oxidised cellulose nanofibril	[127]
141	Wood/cotton pulp	Cellulose nanofibres/nanocrystals	[128]
142	Biomass	Cellulose nanofibres	[129]
143	Cotton pulp	Cellulose fibre	[130]
144	Cotton pulp	Immobilised cellulose	[131]

Table 1 (continued)

Probe	Source of cellulose	Material used in application	Reference
146	Cellulose nanofibre	Nanocellulose film	[132]
147	Bacterial cellulose	Cellulose nanofibre	[133]
149	Wood pulp	Cellulose nanocrystals	[134]
150	Bacterial cellulose	Cellulose nanofibre	[135]
152	Wood pulp	Cellulose	[136]
153	Natural plant pulp	Nanofibrillated cellulose	[137]
155	Cotton pulp	Modified cellulose	[138]
156–161	Natural plant pulp	Allyl cellulose	[139]
162	Cotton pulp	Cellulose fibres	[140]
164	Wood pulp	Cellulose acetate	[141]
166	Cotton pulp	Cellulose strips	[142]
167	Wood pulp	Cellulose acetate	[143]
168	Cellulose pulp powder	Cellulose	[144]
174	Wood pulp	Microcrystalline cellulose	[145]
175	Microcrystalline cellulose	Dialdehyde cellulose	[146]
180	Wood pulp	Carboxymethyl cellulose	[147]
181	Wood pulp	Cellulose acetate	[148]
182	Cellulose pulp powder	Cellulose	[149]
183	Wood pulp	Cellulose polymer chain	[150]
184	Microcrystalline cellulose	Dialdehyde cellulose	[151]
185	Wood pulp	Cellulose acetate	[152]
186	Wood pulp	Cellulose acetate	[153]
187	Wood pulp	Ethyl cellulose	[154]
188	Microcrystalline cellulose	Chlorocellulose	[155]
193	Wood pulp	Cellulose powder	[156]
194	Microcrystalline cellulose	Chlorocellulose	[157]
196	Microcrystalline cellulose	Acetoacetate cellulose	[158]
198	Wood pulp	Cellulose nanocrystals	[159]
199	Wood pulp	Cellulose microcrystals	[160]
200	Cotton pulp	Cellulose strips	[161]
201	Biomass	Dialdehyde cellulose	[162]
202	Biomass	Cellulose membranes	[163]
203	Waste paper	Cellulose-based composite	[164]
204	Microcrystalline cellulose	Acetoacetate cellulose	[165]

detection of cyanide anions via nucleophilic addition in a pure aqueous environment. Further, the coumarin probe was adsorbed on the surface of cellulose paper applicable for naked-eye detection of cyanide [233]. Kim et al. introduced a pentafluorobenzene functionalised AIEgen dye for the detection of gold ions. The naked-eye detection of gold ions was achieved by adsorbing AIEgen dye on the surface of cellulose paper [234]. Later, Kim and co-workers developed a single-benzene–based ratiometric fluorescent probe for recognition of hydrazine. The probe was converted into a dip-in-naked-eye sensor by appending it on cellulose paper [235]. In this part, the review will concentrate on organic molecules functionalised on cellulose surfaces and their application in optical chemosensing (colourimetric and fluorimetric).

2.1 Fluorescence-based organic material

Organic materials are used as an excellent precursor for application in fluorescence-based chemosensing. Cellulose-bound organic fluorophores are used as solutions for real-time sensing of various environmental and biological analytes. Bioactive surfaces are extensively applied in biomedical applications as they are capable of detecting pathogens and endogenous enzymes. Cotton cellulose is extensively used to prepare such bioactive surfaces. However, such bioactive materials suffer following irregularities in the release of chromo and fluorophores. To address this challenge, Brumer and their group (2016) devised a reverse-substrate approach, wherein the chromogenic or fluorophore moiety, rather than the biomolecular component, is attached

Table 2 Contents and limitations of reported reviews on cellulose materials and their applications in sensing

Reference	Contents	Limitations
[23]	Development of nanocellulose in 1.—Antibacterial agents 2.—Antifouling agents 3.—Wound healing 4.—Gene and drug delivery 5.—Tissue engineering	1.—Only covers biomedical application 2.—No mention of sensors 3.—Only covers literature reports until 2022
[174]	Preparation, properties and application of cellulose materials in 1.—Biosensing 2.—Electrochemical sensing 3.—Immunoassays	1.—Organic molecular probes are not covered 2.—Only covers literature reports until 2022
[182]	Application of nanocellulose in sensing and biosensing like 1.—Optical biosensing 2.—Electrical biosensing 3.—Bioimaging	- Only covers application of nanocellulose in limited areas - Other fields of cellulose derived sensors not mentioned - Only covers literature reports until 2017
[189]	Features, preparation and application of cellulose in 1.—Wearable sensors 2.—Health monitoring	1.—Only covers fabricated and wearable devices 2.—Does not cover sensors applicable in environmental monitoring 3.—Only covers literature reports until 2021
[190]	1.—Cellulose powder-based sensors 2.—Cellulose nanocrystal-based sensors 3.—Cellulose fibre-based sensors 4.—Carbon dot-based sensors 5. – Nanocomplex-based sensors 6. – Paper-based sensors	1. Only mentions sensors for the selective detection of metal ions 2. Does not cover polymeric materials 3. Only covers literature reports until 2020
[191]	Preparation and properties of cellulose-based MOFS and applications in 1.—Water treatment 2.—Air purification 3.—Biomedical application 4.—Sensing and biosensing application	1.—The authors have specifically attributed the review to cellulose-based MOF materials 2.—Only covers literature reports until 2022
[192]	Features, preparation and application of cellulose in 1.—Sensor arrays 2.—Intelligent films 3.—Paper platforms 4.—Dual sensors 5.—PADs and μPADs	1.—Application of cellulose materials in development of gas sensors is only covered
[193]	Preparation and alignment of cellulose nanocrystal and application of aligned material in - Sensing applications	1.—Only covers specific modules of cellulose nanocrystal application 2.—Does not cover organic, inorganic and hybrid nano and polymeric materials 3.—Only covers literature reports until 2020
[194]	Preparation and properties of cellulose-based MOFS and applications in 1.—Water remediation 2.—Air purification 3.—Energy storage and conversion devices 4.—Biomedical applications	1.—The authors have specifically attributed the review to cellulose based MOF materials 2.—Does not cover all the fields of sensing 3.—Only covers literature reports until 2022
[195]	Features, preparation and application of cellulose in 1.—Humidity sensors	1.—The title of the review is its limitation as it only covers humidity sensors
[196]	Cellulose based fluorescent materials for 1.—Cations detection 2.—Anions detection 3.—Nitroaromatic detection 4.—pH sensors 5.—Hydrogels and aerogels	1.—The authors have not mentioned polymeric cellulose materials 2.—Only covers literature reports until 2020

Table 2 (continued)

Reference	Contents	Limitations
[200]	Features, preparation and application of cellulose in 1.—Composite films 2.—Hydrogels 3.—Photonic films 4.—Nanofibre films 5.—Flexible sensors 6.—Aerogel 7.—Electronic skins	1.—The review only covers physical sensors 2.—Only covers literature reports until 2022
[201]	Features, preparation and application of cellulose nanocrystals in - Sensing applications	1.—Only covers cellulose nanocrystal materials and its application in sensing

to the insoluble cellulosic substrate (obtained from bacterial cellulose (Table 1)). The methodology was illustrated by the detection of an important enzyme esterase. For this purpose, the fluorogenic selected was fluorescein (Fig. 3a). The mentioned approach completely relies on the intrinsically strong binding interaction between the plant cell wall matrix polysaccharide xyloglucan (XyG) and cellulose. Cellulosic material **1** is generated by the enzymatic click reaction between the cellulosic template and fluorophore. The cellulosic material **1** shows 'turn-on' emission in the presence of enzyme esterase. Simplifying, in the presence of enzyme esterase, the biomolecule tag linked with fluorophore cellulose unit is cleaved resulting in the 'turn-on' emission of the cellulosic material **1**.

Figure 3 b depicts the use of cellulose pad **2** for the efficient detection of esterase in the naked eye under a UV lamp. Utilizing the approach employed in the report, future-developed materials can overcome problems like signal attenuation and probable toxicity caused by the diffusion of chromo and fluorophore after substrate cleavage [30]. Transition metal ions are vital for the sustenance of living organisms. Copper ions are critical for human beings as they play the role of catalytic cofactor for a variety of metalloenzymes, which include cytochrome c oxidase, tyrosinase and superoxide dismutase. However, copper toxicity is related to many neurodegenerative diseases such as Alzheimer's and Wilson's diseases [236]. Hence, it is very important to monitor levels of copper in foods and the human body. In early 2018, Pisitak and his group utilised the spirolactam ring opening mechanism of rhodamine to develop a rhodamine-based fluorimetric and colourimetric molecular probe **3** for the target-specific detection of Cu^{2+} ions (Fig. 3c). The authors have asserted the importance of naked eye detection in the manuscript. In the presence of Cu^{2+} ions, the spirolactam ring in rhodamine dye opens, resulting in the formation of a highly emissive fluorescent copper complex. The authors have fabricated probe **3** on the surface of bacterial cellulose for the selective detection of Cu^{2+}. Figure 3 d depicts the fluorescence selectivity profile of **3** in the presence of different cations. The naked eye detection of Cu^{2+} by cellulose (Table 1) fabricated probe **3** can be viewed in Fig. 3e. The interaction between hydroxyl groups of cellulose and probe molecule does not result in the reduction of the detection profile of the optical probe, proving the utility and efficacy of cellulose-based optical probes [31].

The detection and quantification of anions are challenging because of their complex geometries, strong hydration energy and pH dependence. Sulfur dioxide (SO_2) is one such air pollutant prevalent in the atmosphere, resulting from extensive combustion of fossil fuels. The actual toxicity of sulfur dioxide is attributed to its derivatives like sulphite (SO_3^{2-}) and bisulphite (HSO_3^-). In 2018, Das and coworkers introduced a water-soluble fluorogenic probe **5** for the ratiometric detection of SO_3^{2-}. Figure 3 f illustrates the detection mechanism of probe **5** for SO_3^{2-}. In brief, **5** undergoes nucleophilic attack at cite C4 from SO_3^{2-}, resulting in the formation of **5**-SO_3^{2-} adduct as represented in Fig. 3f. Probe **5**, when doped on polystyrene-coated cellulose paper, can be used for the real-time detection of SO_3^{2-}. As depicted in Fig. 3g, polystyrene-coated cellulose paper–doped **5** changes glow from orange to blue under a UV lamp in the presence of SO_3^{2-}. The different regions of **5** doped polystyrene-coated cellulose paper (μPAD) are demonstrated in Fig. 3h. The limit of detection of **5** for SO_3^{2-} is estimated as 8.45 ppb. The **5** doped μPAD shows the change in fluorescence in the presence of SO_3^{2-} (Fig. 3i). The authors have also tested the biological potential of targeting mitochondria by using probe **5** in the detection of SO_3^{2-} using HeLa cells (Fig. 3j). The different hydrogen bonding functionalities in cellulose μPAD do not interfere in the detection mechanism of **5** towards SO_3^{2-}. All mechanisms, be chemical, biological or biochemical processes, are dependent on pH. The detection of pH is very important to monitor the chemical, biological or biochemical changes taking place in the surroundings. Most used pH detection devices revolve around paper strips and thin films [32].

Aqueous solution of cellulose can be a template for nature-friendly inks. In 2019, Li and the group illustrated a combination of aqueous hydroxyethyl cellulose (ink) and 1,3,6,8-pyrene sulfonic acid sodium salt (PTSA) as a

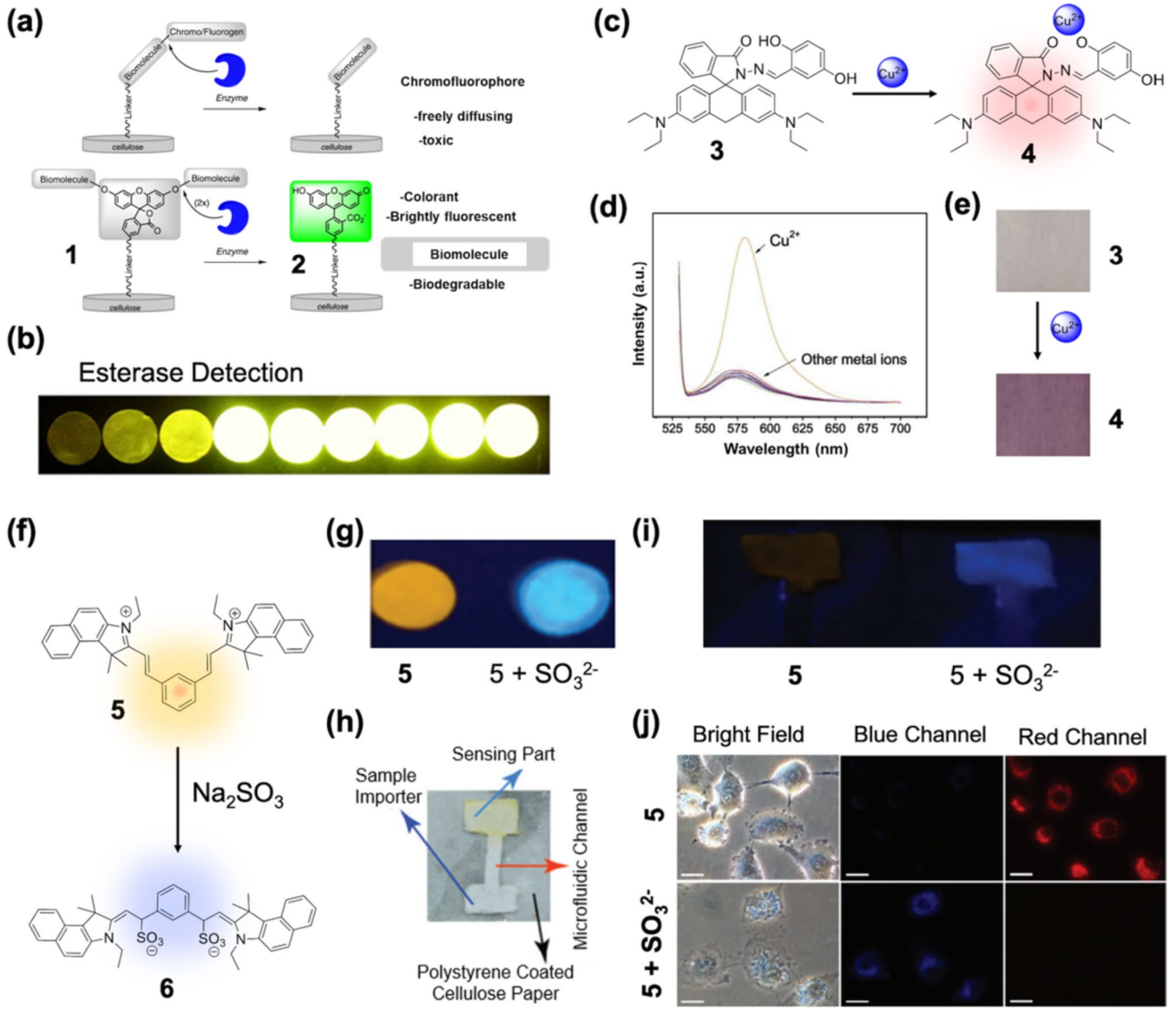

Fig. 3 **a** Detection mechanism of esterase utilised by **1**. **b** UV light detection of esterase immobilised on cellulose paper. (Refer to the web version of this article for the legend colour). Reproduced from Ref. 30 with permission of ACS. **c** Detection profile of **3** towards Cu^{2+} ion. **d** Selectivity plot of **3** for Cu^{2+} ions in the presence of different counter cations. **e** Naked eye detection of Cu^{2+} ions using **3** modified cellulose paper. (Refer to the web version of this article for the legend colour). Reproduced from Ref. 31 with permission of Elsevier. **f** Schematic representation of SO_3^{2-} detection by **5**. **g**, **h**, **i** Naked eye detection of SO_3^{2-} using **5** modified cellulose papers. **j** Detection of SO_3^{2-} using **5** treated HeLa cells. (Refer to the web version of this article for the legend colour). Reproduced from Ref. 32 with permission of RSC

water-soluble fluorescent dye utilised as a promising candidate for anti-counterfeiting applications (Fig. 4a).

The report depicts an excellent example of simple methods for the incorporation of fluorescent dyes into cellulose scaffolds and their exceptional application. Sulphonation reaction between pyrene-1-sulfonic acid sodium salt (PyS) and oleum produced **7**. Red, blue and green colours were achieved by using a combination of different pigments with **7**. Excellent thixotropic and rheological properties were noticed for **7** (Fig. 4b). Further, cellulose paper was immobilised with **7** by using inkjet and screen-printing techniques. The main advantage of cellulose ink **7** is the fact that it is highly water soluble and hence can be erased easily after use. The authors claim that cellulosic ink **7** can be used to detect counterfeiting and, hence, can be used indirectly to control duplicating and counterfeiting (Fig. 4c) [33].

As discussed earlier, rhodamine molecules, when bound with cellulose, do not lose their spirolactam ring opening property. Hence, Pulpoka and group utilised rhodamine as a fluorophore unit and fabricated it onto a cellulose matrix for

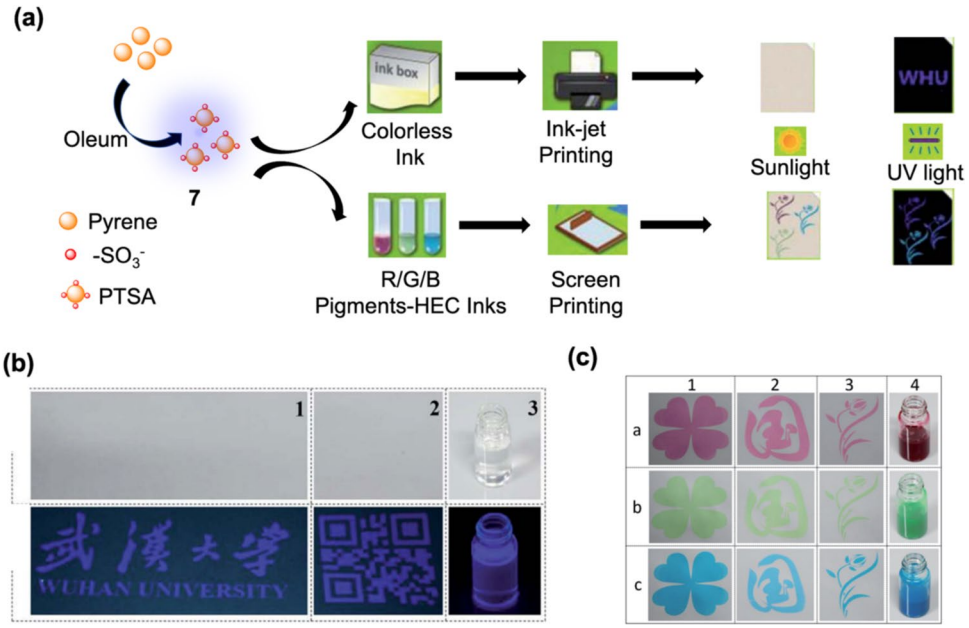

Fig. 4 **a** Chemical structure and ingredients of the developed cellulose ink **7**. **b** Different anti-counterfeiting patterns using inkjet printing on a non-background paper, under (top) white light and (bottom) 365 nm UV light. **c** RGB colour patterns by screen printing using multi-colour inks. (Refer to the web version of this article for the legend colour). Reproduced from Ref. 33 with permission of RSC

the early-stage determination of biological and environmental pH. Rhodamine-derived fluorophore was dropped on the surface of cellulose paper forming material **8**. The mechanistic approach of **8** for changing pH is represented in Fig. 5a. In acidic conditions, the spirolactam ring of rhodamine in **8** is opened resulting in both colourimetric and fluorimetric changes. The fluorimetric changes of material **8** in the presence of different pH are illustrated in Fig. 5b. Cellulose-cast probe **8** showed a rapid response in the pH range 1–8 through colour and fluorescence changes. This report opens a wide applicability of rhodamine-cellulose combination for the real-time visualization of pH changes system [34].

Transition metal zinc is known to be the second most abundant metal ion in the human body and plays crucial roles in various bodily functions. However, excess zinc in the human body and metabolism can lead to different diseases such as human ischemic stroke, Alzheimer's and epilepsy. Similarly, inorganic phosphates are also crucial biological molecules. However, the excess of inorganic phosphates such as dihydrogen phosphate ($H_2PO_4^-$) decreases the levels of dissolved oxygen which is a cause of several bodily problems. It is well known that the binding affinity of metal ion zinc towards phosphates is very high. Utilizing this knowledge, Kumar and his group introduced a quinoline derivative **10** for selective relay detection of Zn^{2+} and $H_2PO_4^-$ (Fig. 5c). Probe **10** forms a complex with Zn^{2+} (**11**), resulting in turn-on emission (Fig. 5d, e). The interaction between quinoline nitrogen, amide group nitrogen and diethyl amine nitrogen with Zn^{2+} results in the formation of turn-on coordination complex **11**. Further, complex **11** confronts $H_2PO_4^-$ causing the regeneration of **10**. Probe **11** shows selective turn off in the presence of $H_2PO_4^-$ (Fig. 5d, e). The estimated LOD of **10** and **11** for Zn^{2+} and $H_2PO_4^-$ are 8 nM and 55 nM, respectively. As illustrated in Fig. 5f, merging **10** with cellulose paper aided in the formation of dipstick technology for the real-time detection of Zn^{2+} and $H_2PO_4^-$. In this paper, the authors demonstrated that cellulose-fabricated probes can be used for complexation with metals and secondary detection of anions [35].

Later, Zhang and co-workers developed a phenanthroline-conjugated cellulose system for the visual and versatile detection of different amines and anions. The cellulose chain was used as a skeleton for the generation of molecular probe **13** (Fig. 5g). As depicted in Fig. 5h, probe **13** shows an exceptional detection for different anions. The detection of amines and anions is credited to the amplification effect of cellulose polymer chain (purified cellulose generated from wood pulp (Table 1)) and the differentiated interactions between the sensor and analytes. Moreover, Fig. 5i demonstrates the application of cellulosic material **13** for the detection of amines. The authors claim that probe **13** is capable of multi-responsive and chromogenic detection of amines and anions [36].

Another important metal is Fe^{3+}, which plays a vital role in the creation of haemoglobin and in the transport and storage of oxygen to tissues. Iron also plays a substantial role in fermentation processes and metabolism by enduring as a stabiliser, enzyme activator and functional component of proteins. However, high concentrations of iron in the blood can result in various health conditions like depression, coma, respiratory problems and cardiac arrest. In 2020, Yilmaz and his team developed a paper-based BODIPY probe to produce a low-cost and environmentally sensitive material for the removal and detection of Fe^{3+} ions. To achieve material **14**,

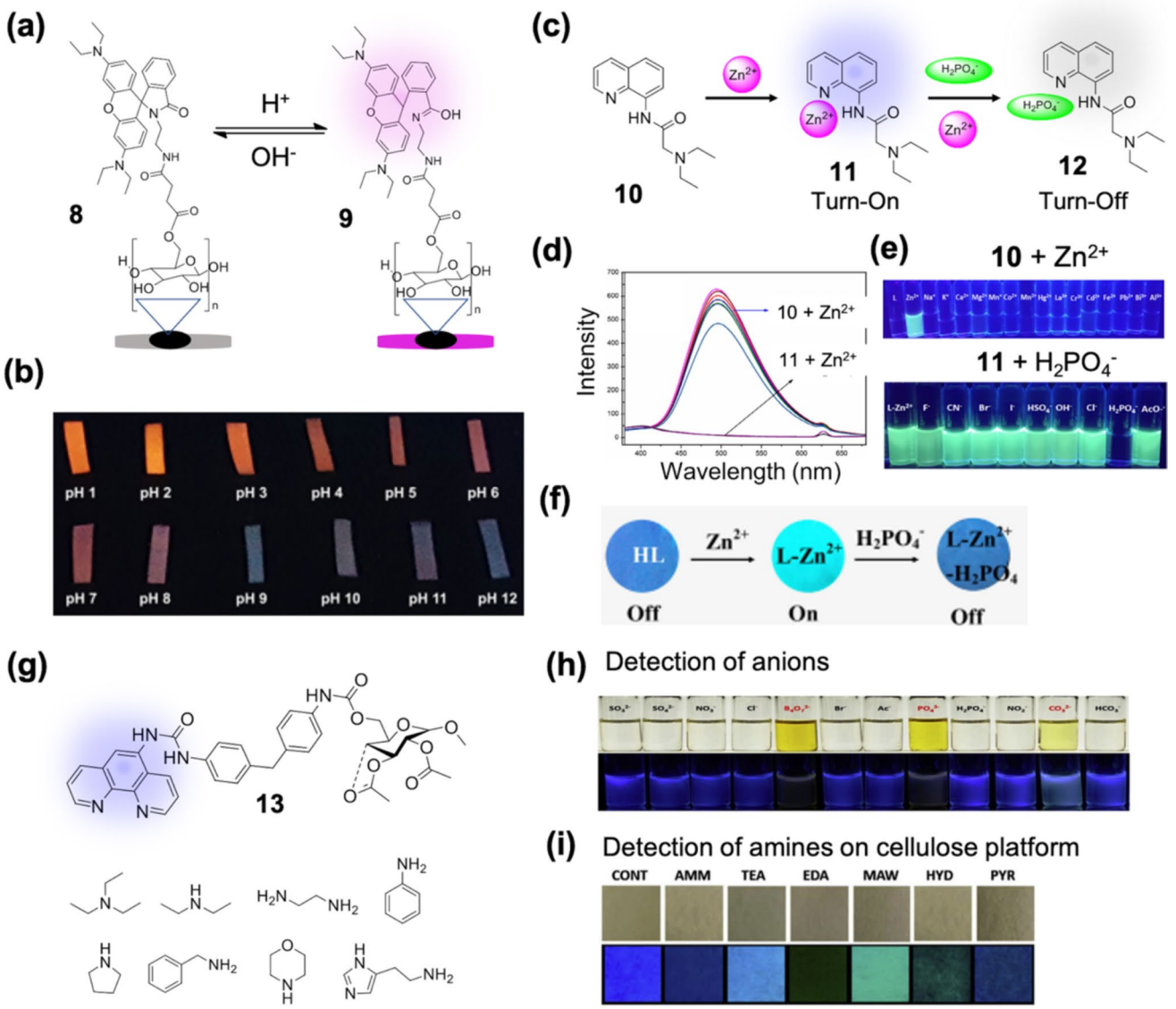

Fig. 5 **a** Mechanism of estimating pH using rhodamine probe **8**. **b** Visual colour changes of **8** coated test strips with varying pH. (Refer to the web version of this article for the legend colour). Reproduced from Ref. 34 with permission of Wiley. **c** Reversible detection mechanism of **10** for Zn^{2+} and $H_2PO_4^-$. **d** Selectivity profile towards Zn^{2+} by **10**. **e** Naked eye detection of Zn^{2+} and $H_2PO_4^-$ by probe 10 under a 365-nm UV lamp. **f** Visual detection of Zn^{2+} and $H_2PO_4^-$ by **10** doped cellulose paper. (Refer to the web version of this article for the legend colour). Reproduced from Ref. 35 with permission of Elsevier. **g** Chemical structure of anion and amine detecting probe **13**. **h** Naked eye detection of anions under UV lamp 365 nm. **i** Detection of amines by **13** doped cellulose paper. (Refer to the web version of this article for the legend colour). Reproduced from Ref. 36 with permission of Elsevier

raw cellulose powder (Table 1) was fabricated by immobilizing hexamethylene diisocyanate and modification with BODIPY. The mechanism of **14** for the detection of Fe^{3+} is represented in Fig. 6a. The observed quenching effect in **14** on addition of Fe^{3+} is attributed to the interaction of paramagnetic Fe^{3+} ions with the donor O and N atoms of **14**. Cellulosic material **14** shows selective detection for Fe^{3+} (**15**). Figure 6 b illustrates the naked eye detection profile of cellulose material **14** in the presence of Fe^{3+}. The authors claim that organic conjugate **14** is capable of the selective detection and removal of Fe^{3+}. In this report, the authors have proved the easy and efficient binding of BODIPY dye on cellulose surfaces and its competent use in the detection of Fe^{3+} ions [37]. Cellulose-based materials have also found applications in the estimation of toxic and explosive materials like picric acid and many others. Picric acid is a highly water-soluble chemical species and has a wide range of utility in the manufacturing of explosives, pharmaceutics, leather and fireworks industries. Picric acid in contact with the human body can cause dermatitis, bronchial issues,

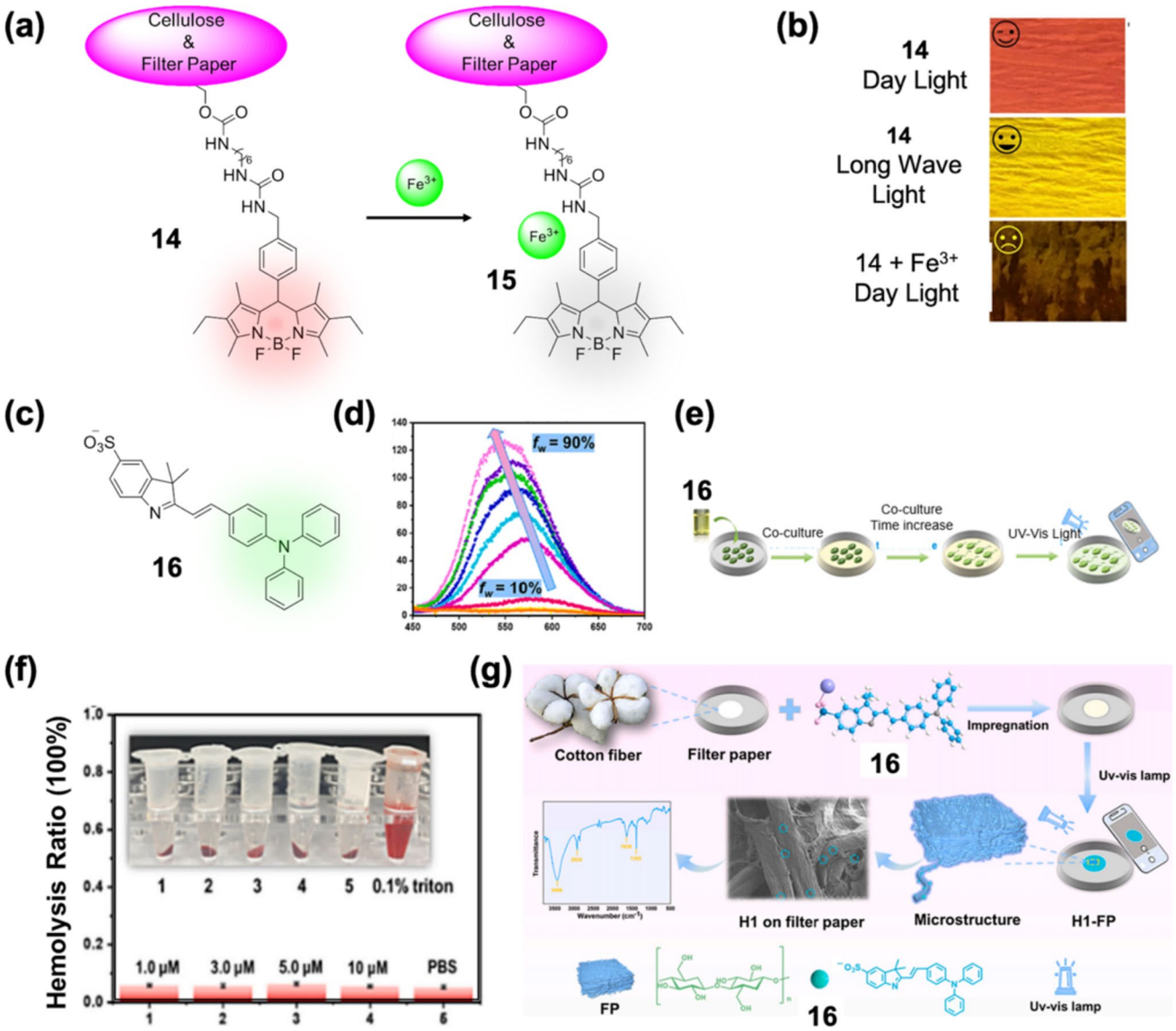

Fig. 6 **a** Detection mechanism of Fe^{3+} by BODIPY-based probe **14**. **b** Visual detection of Fe^{3+} by **14** doped cellulose strips. (Refer to the web version of this article for the legend colour). Reproduced from Ref. 37 with permission of Elsevier. **c** Chemical structure of probe **16**. **d** Fluorescence emission spectra of **16** with varying ratios of EtOH–water. **e** Schematic depiction of operation procedure at neutral conditions. **f** Haemolysis test evaluation of **16** using sheep blood. **g** Schematic representation of **16** doped cellulose paper making and colourimetric changes. (Refer to the web version of this article for the legend colour). Reproduced from Ref. 38 with permission of Elsevier

heart failure and many other serious disorders. Huang and co-workers introduced an indole-derived fluorescent sensor composited with cellulose paper **16** (Fig. 6c) for the detection of picric acid in food and environmental samples. The indole cellulose composite **16** exhibited turn-off-based selectivity for picric acid with a fast reaction rate (< 30 s), unique specificity, excellent selectivity and high sensitivity. The electrostatic interaction between **16** and picric acid is attributed for the fluorescence quenching of **16**. The titration profile of **16** with varying solvent ratios between H_2O-EtOH is depicted in Fig. 6d. The limit of detection of **16** for picric acid is estimated at 34 nM. The efficacy of **16** was tested in biological samples (Fig. 6e) like sheep blood (Fig. 6f) and zebrafish samples. In Fig. 6g, the authors have demonstrated the complete operation procedure of composite **16** for determining colourimetric changes under different conditions by virtue of smartphone. The authors claim that composite **16** is an intelligent platform for the selective monitoring of picric acid levels in biological and environmental samples [38].

In 2023, Dashti and co-workers reported photoluminescent nanoparticles for applications in organic light-emitting diodes, anti-counterfeiting, information encryption and optical detection of scratch. Amide-functionalised copolymer nanoparticles with particle sizes 42–139 nm were obtained

by the successful emulsion copolymerization of methylmethacrylate (MMA) and methacrylamide (MAAm). Further, material **17** was formed by the oxazolidine modification on surface of the amide-functionalised copolymer nanoparticles (Fig. 7a). When applied on polar substrates like cellulose paper and polymer sheets, nanomaterial **17** displayed remarkable stability. Owing to these properties, the nanomaterials **17** were utilised for the development of water-based anti-counterfeiting inks, OLEDs and photo-detection of scratches (Fig. 7b) [39].

2.2 Colourimetric-based organic material

Colourimetric materials used as optical molecular chemosensors are related to high sensitivity and good selectivity. Colourimetric organic probes have the added benefit of being used as naked eye chemosensors in real-time detection of various environmental analytes. Colourimetric molecular probes have been widely used for the rapid detection of analytes like proteins, DNA, metallic cations, viruses, small molecules and others. Cellulosic materials have been extensively employed as support materials with organic molecules for the formation of real-time usable sensors [237]. In this section, reports related to cellulose-supported organic molecular colourimetric probes are reviewed. Recently, tetrahedral oxyanion hydrogen sulphate has got profound notice from the scientific community. Excess ingestion of hydrogen sulphate can cause kidney malfunction. Hence, it is vital to estimate the concentration of hydrogen sulphate in food products [238]. Felpin and co-workers (2016) utilised the hydrogen bonding–based spirolactam ring opening phenomenon of rhodamine chromophore and modified it on cellulose paper for application as a smart sensor device for colourimetric and optical detection of hydrogen sulphate in water. Figure 8a represents the structure of material **18** formed by linking rhodamine with cellulose using a benzaldehyde linker. Probe **18** showed high selectivity with colour change from colourless to pink in the presence of HSO_4^- anion (Fig. 8b). The hydrogen bonding phenomenon between **18** and HSO_4^- is responsible for the colourimetric and fluorescence turn-on emission profile. The lower hydrogen donor properties of HPO_4^{2-} results in lower interference and higher selectivity of HSO_4^- by **18**. The estimated limit of detection of **18** for HSO_4^- is 120 µmol. As depicted in Fig. 8c, the cellulosic material **18** is also reusable even after two successive reuses. The naked eye selectivity and titration profile of **18** for HSO_4^- even in the presence of other amphiphilic anions is demonstrated in Fig. 8d. The authors claim that the cellulosic device will hold an important place in the detection of HSO_4^- in analytical and environmental samples [40].

In another interesting report, Kamel and his group introduced a cellulose-derived halochromic test strip for the optical detection of gaseous and aqueous analytes. The authors have used pH-triggered chemosensor based on a push-π conjugation-pull system, consisting of a tricyanofuran moiety (**19**) as an electron-withdrawing unit and a hydrazine moiety that works as an electron-donor unit upon deprotonation (Fig. 8e). Tricyanofuran (**19**) is embedded on the surface of halochromic polyester cellulose-acetate (**19**) and is further utilised for colourimetric sensing of alkaline vapours and analytes. Variations in pH environments of **21** are illustrated in Fig. 8f, g. The representation of gas phase detection (ammonia gas) by **21** is demonstrated in Fig. 8h. The authors

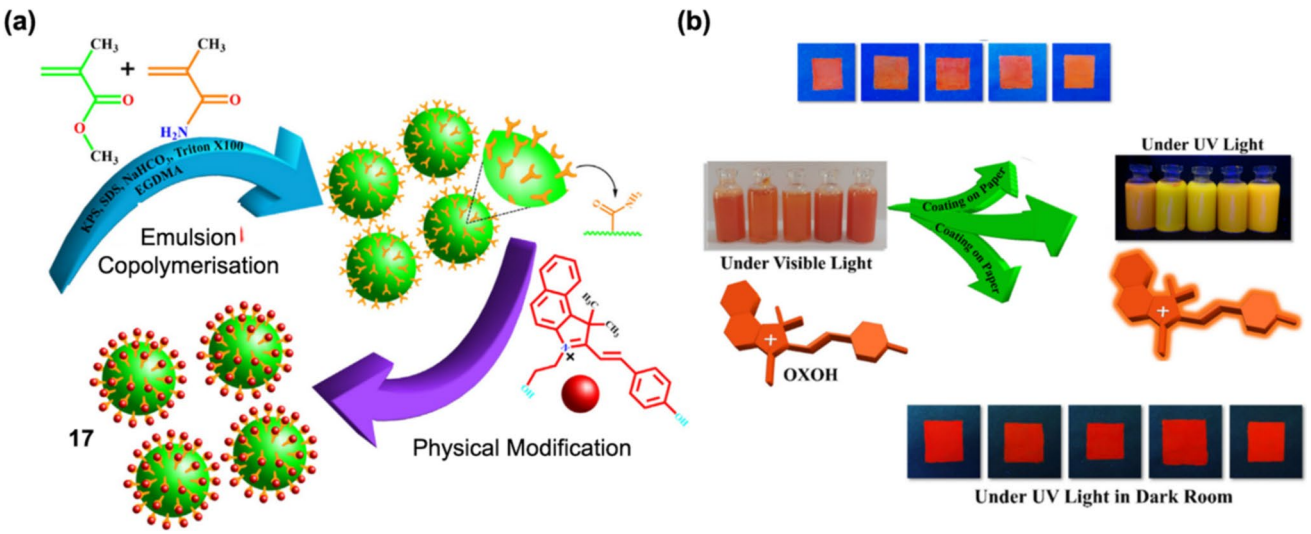

Fig. 7 **a** Schematic synthetic procedure of amide functionalised copolymer nanoparticles and modification with OXOH forming **17**. **b** Fluorescence and colour-based profile of developed photoluminescent copolymer nanoparticles and representative photoluminescence cellulose papers. (Refer to the web version of this article for the legend colour). Reproduced from Ref. 39 with permission of Elsevier

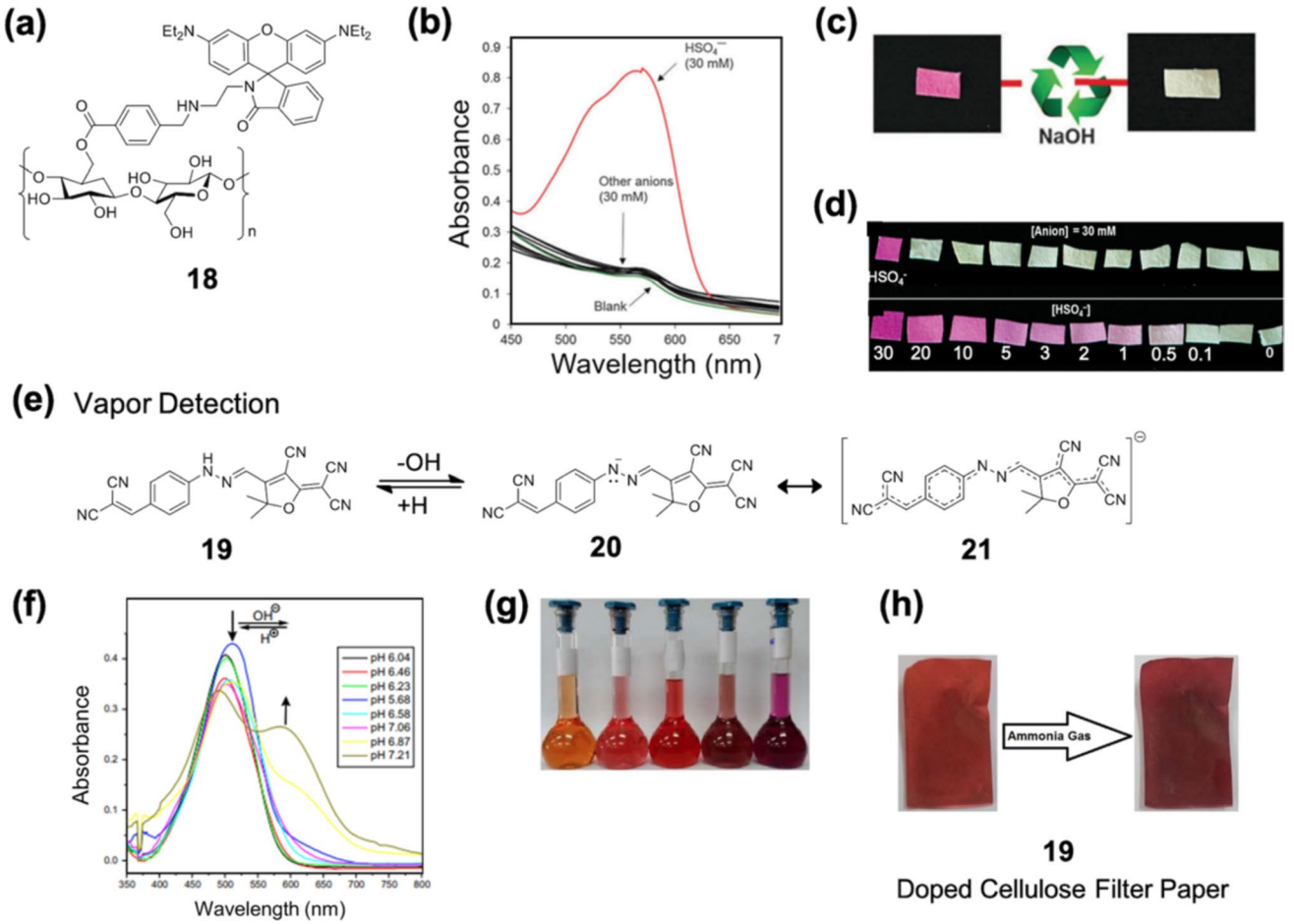

Fig. 8 **a** Chemical structure of cellulose based probe **18** used for the detection of HSO_4^-. **b** Absorbance-based selectivity profile of **18** for HSO_4^- in the presence of different counter anions (OH^-, NO_3^-, I^-, Br^-, Cl^-, F^-, CN^-, ClO_4^-, HPO_4^{2-} and AcO^- at 30 mM). **c** pH-based variation in colour of **18** doped test strips. **d** Visual eye selectivity and titration profile of **18** for HSO_4^-. (Refer to the web version of this article for the legend colour). Reproduced from Ref. 40 with permission of RSC. **e** Working mechanism of **19** for the detection of ammonia gas. **f** Changes in the absorbance profile of **19** with variation in the pH. **g** Naked eye colour change in the aqueous sample of **19** with pH. **h** Naked eye colour change on irradiation with ammonia gas on **19** doped cellulose paper. (Refer to the web version of this article for the legend colour). Reproduced from Ref. 41 with permission of Elsevier

claim that the colourimetric probe **21** can be used as an efficient tool for the detection of bacteria, infectious diseases and bacterial contamination in food packaging, protective dressings and wound healing probes [41].

In 2019, Patil and his team developed a phthalimide-based chemosensor **22** for selective spectrophotometric detection of Cu^{2+} ions (Fig. 9a) in aqueous medium. The phthalimide material **22** was supported by cellulose paper for real-time detection of Cu^{2+} in aqueous samples. Even in the presence of various cations, **22** can only selectively detect Cu^{2+} ions. Cellulosic material **22** is engaged in 1:1 stoichiometric interaction with Cu^{2+} ions resulting in the formation of Cu^{2+} complex with specific colour change. Probe **22** can detect Cu^{2+} ions as low as 1.65 µM. On dipping the **22** doped cellulosic paper in Cu^{2+} contaminated solution, the colour of the strip changed from colourless to yellow (Fig. 9b) [42]. Later in the same year, Said and co-workers utilised an azo-dye conjugated cellulosic material for the selective and specific detection of Cu^{2+} ions (Fig. 9c). Cellulose-supported azo dye **24** is capable of discriminating Cu^{2+} with a colour change from pink-to orange (Fig. 9d), even in the presence of various counter analytes. Cellulosic material **24** forms a complex with copper in 2:1 stoichiometric ratio with subsequent colour change. As a colourimetric sensor, probe **24** can detect 4.3×10^{-6} mol L (LOD) of Cu^{2+} in aqueous solution. The authors claim that cellulosic material **24** is cheap and can be utilised for the detection of Cu^{2+} in real samples [43].

In a different work (2022), Lee and his group conjugated azo dye with cellulose nanofibres (CNFs) (Fig. 10a) to generate CNF-azo films (**26**) and utilised it for the selective colourimetric detection of nerve agent diethyl chlorophosphate

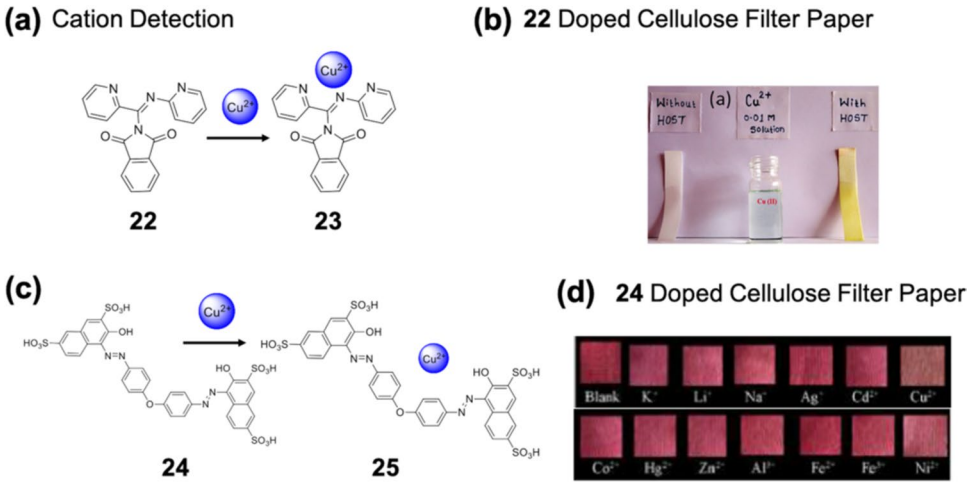

Fig. 9 **a** Chemical structure and detection mechanism of **22** for Cu^{2+}. **b** Colour change from colourless to yellow on dipping **22** doped test strips Cu^{2+} into solution. (Refer to the web version of this article for the legend colour). Reproduced from Ref. 42 with permission of Elsevier. **c** Chemical structure and detection mechanism of **24** for Cu^{2+}. **d** Visual selectivity profile of **24** for Cu^{2+} in the presence of different counter cations. (Refer to the web version of this article for the legend colour). Reproduced from Ref. 43 with permission of Springer

(DCP). The colourimetric change in the profile of **26** in the presence of DCP is shown in Fig. 10b. Probe **26** is highly selective for DCP even with the addition of different counternerve agents. The selectivity profile of cellulosic material **26** for DCP is depicted in Fig. 10c, d. On addition of DCP solution to **26**, the hydroxyl oxime group of **26** disappears, facilitating intramolecular charge transfer mechanism, resulting in the colour change from yellow to pink. The authors have also focussed on the promising advantages of **26** for DCP in real-time samples [44]. Finally, in 2023, Luo and co-workers introduced 3,3′,5,5′-tetramethylbenzidine functionalised cellulosic material **30** for selective detection of Ag^{+} and Hg^{2+}. Figure 10 e depicts the complete synthetic and selectivity mechanism of **30** for the detection of Ag^{+} and Hg^{2+}. In the presence of Ag^{+} and Hg^{2+} (strong oxidising agents), **30** is oxidised aiding in the change in colour from colourless to blue. The experimental results showed that visually, **30** can detect 10 µM levels of Ag^{+} and Hg^{2+}. Cellulosic material **30** shows good stability and reusability (Fig. 10f). The authors recognise the conjugation of cellulose forming **30** as responsible for uniform colour development and stable colour, which effectively increased the colourimetric sensing response and stability [45].

In the case of clinical, biological and environmental applications, cellulose-based solid matrices are used in the development of optical chemosensors for on-site direct detection of analytes. In laboratory testing, aqueous matrices are used for the direct sample testing.

3 Cellulose-derived nanomaterials (Cello-Nano)

For decades, cellulose has been marketed in different forms, which include bacterial cellulose, microcrystalline cellulose (MCC), microfibrillated cellulose (MFC), microfibrils, cellulose nanofibres (CNF) and cellulose nanocrystals (CNCs). The size ranges of cellulose are like nano, micro and polymeric forms, which aids in the formation of different cellulosic materials. Reports have estimated the size of cellulose variants as CNCs: 10–100 nm, microfibrils: 2–20 nm, microfibril cellulose: 10–15 nm, bacterial cellulose (BC): 10–75 nm, microcrystalline cellulose (MCC): > 1000 nm. They also home different functional groups such as OH, OSO_3H, COOH and CHO. Different methods employed for the modification of nanocellulose surface include covalent bond formation, chemical modification, surface functionalization and adsorption [239]. Cellulose colloids have high charge coefficient which ensures high stability avoiding nanoparticle aggregation. However, nanoparticles, when appended on the surface of cellulose paper, can also be used in bioassays. Moreover, the cellulose-modified nanoparticle materials act as a high-capillary-action matrix to retain small-volume materials and also carry out biochemical reactions [240]. In this section, there is a discussion related to different variants and applications of nanoparticles like cellulose-modified nanohybrids, cellulose-nanocrystals nanofibres and cellulose-modified nanodots. Recent technological advancements and high-end nanoarchitecture strategies have intrigued the interests of several scientific groups in improving the scope of optical chemosensing.

3.1 Hybrid nanomaterials

Nanohybrids are very important materials in all aspects as they are the combination of different nanoelements in a single packet. Diverse nanohybrid structures, such as yolk-hell, core–shell, heterodimer, Janus, nano branches, dot-on-nanorod and dot-in-nanotube, are designed and prepared for performing several applications. A great number of combinations are employed, such as magnetic and luminescent particles, magnetic and catalytic particles and plasmonic and catalytic for achieving different physical properties, increasing the library of nanohybrid materials.

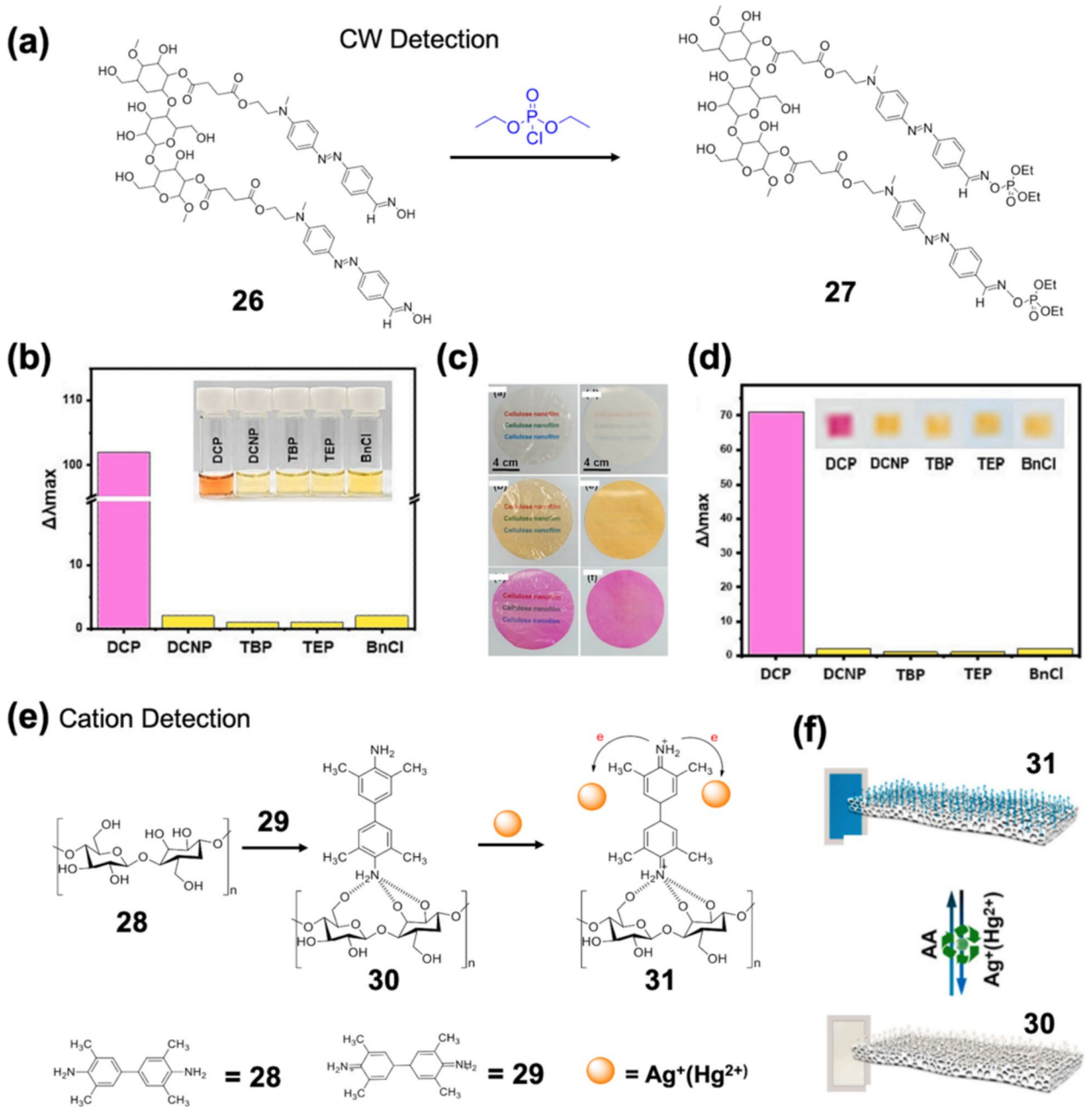

Fig. 10 **a** Schematic representation of detection mechanism of **26** for DCP. **b** Selectivity profile of **26** for DCP in the presence of different reagents. **c**, **d** Visual eye colourimetric changes in test strips doped with **26** in the presence of DCP. (Refer to the web version of this article for the legend colour). Reproduced from Ref. 44 with permission of Elsevier. **e** Chemical structure and estimation mechanism of Ag^{+} and Hg^{2+} by **30**. **f** Scheme showing the reversible detection of Ag^{+} and Hg^{2+} by **30**. (Refer to the web version of this article for the legend colour). Reproduced from Ref. 45 with permission of Elsevier

Nanohybrids with cellulose conjugation can be extensively used in different applications as they are bound by strong hydrogen bonding. Cellulose nanohybrids have outstanding mechanical, chemical and physical properties, which aid in their utilization as high-end materials. Here, the different combinations of cellulose and nanohybrids will be discussed.

3.1.1 Fluorescence-based hybrid nanomaterials

Nanohybrids have improved the prospects of application in fluorescent chemosensing technology. The inherent properties of nanohybrids, when combined with cellulose, improve the flexibility, stability and utility of the developed materials. Fluorescent tools have launched great insights into the

understanding of cellular mechanisms and dynamics at the single-cell level. Fluorescent labels permit target-specific imaging in living cells. Nanohybrids are an excellent solution for molecule-specific imaging in cell line.

In 2015, Siegwart and his team used a new charge transfer (CT) nanoparticle **32** and derivatives utilizing a bio-inspired cellulose template. Pyrene-modified 2,3-di-*O*-methyl cellulose formed charge transfer complexes with 7,7,8,8-tetracyanoquino-dimethane (TCNQ), 1,2,4,5-tetracyano-benzene (TCNB) and tetracyanoethylene (TCNE) and exhibited aggregation-induced emission (AIE) in aqueous medium on the formation of nanoparticles (Fig. 11a). Lower concentrations of TCNQ, TCNB and TCNE in reaction caused the formation of linear **33** complexes (**34**), and higher concentrations yielded crosslinked CT complex **36**. The cellulose backbone in **33** and derivatives enabled the control of orientation along with the environment of the donor and acceptor molecules of the new charge transfer particles (**33** and derivatives). Probe **34** and derivatives showed multicoloured fluorescence excimer state emission at 370–400 nm, 602 and 777 nm when excited at 330, 485 and 620 nm. The biological application of the charge transfer nanoparticle (Fig. 11b, c) was evaluated using in vitro analysis using HeLa cells. In this work, the authors have presented an excellent illustration of the charge transfer mechanism utilizing nanohybrids on cellulose templates [46].

In another work, Qu and co-workers (2015) developed an upconversion nanoparticle (UCNP) modified cellulose paper assay **37** for the specific detection of telomerase activity. In this process, UCNPs are conjugated with the telomerase reaction products (TRPs) and then appended on cellulose paper. The authors report that compared with many solution phase systems, the cellulose-based solid-state platforms are highly stable and can be easily stored. Cellulose matrix serves as a high capillary action unit which helps in the storage and distribution of **37** for the detection of telomerase.

As depicted in Fig. 12a, the interaction between telomerase and cellulose template nanoprobe **37** results in green emission. Figure 12 b–d represent the detection profile of **37** in different telomerase variants. The assay shows lower bio-background interference and higher photostability owing to the presence of UCNPs in **37**. The authors confirm that the fluorescent telomerase detection assay **37** has the potential to be used as testing materials in point-of-care clinical approaches [47]. In 2016, Chu and co-workers developed a fluorescent renewable lignin-derived nanoparticle functionalised using pyrene (**38**) and studied their photochemical properties. The lignin nanoparticles were reacted with 3-aminopropyl triethoxysilane (APTES) to garner the lignin nanoparticles with the amino group. The surface functionalization of amino-lignin nanoparticles with pyrene molecules is depicted in Fig. 12e. The excimer emission profile of **38** on excitation at 345 nm is presented in Fig. 12f. The authors claim that the lignin nanomaterial **38** can be used in the future as nanosensors. However, the authors did not report any screening tests to confirm the usability of **38** as a

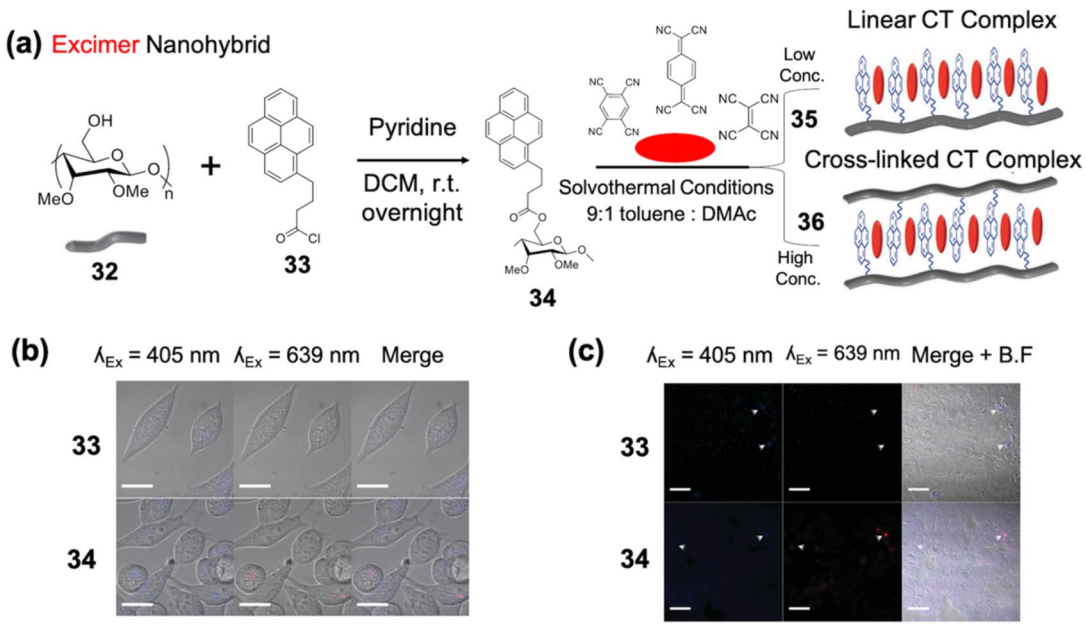

Fig. 11 **a** Synthetic mechanism of material **35** and **36**. **b** Cellular uptake of TCNQ-CT-cellulose NPs **33** into HeLa cells in vitro. Scale bar = 20 mm. **c** Imaging of TCNQ-CT-cellulose NPs **33** in vivo in mice bearing RPMI-7951 melanoma xenograft tumour models. Arrows indicate regions of concentrated NPs. Scale bar = 20 mm. (Refer to the web version of this article for the legend colour). Reproduced from Ref. 46 with permission of RSC

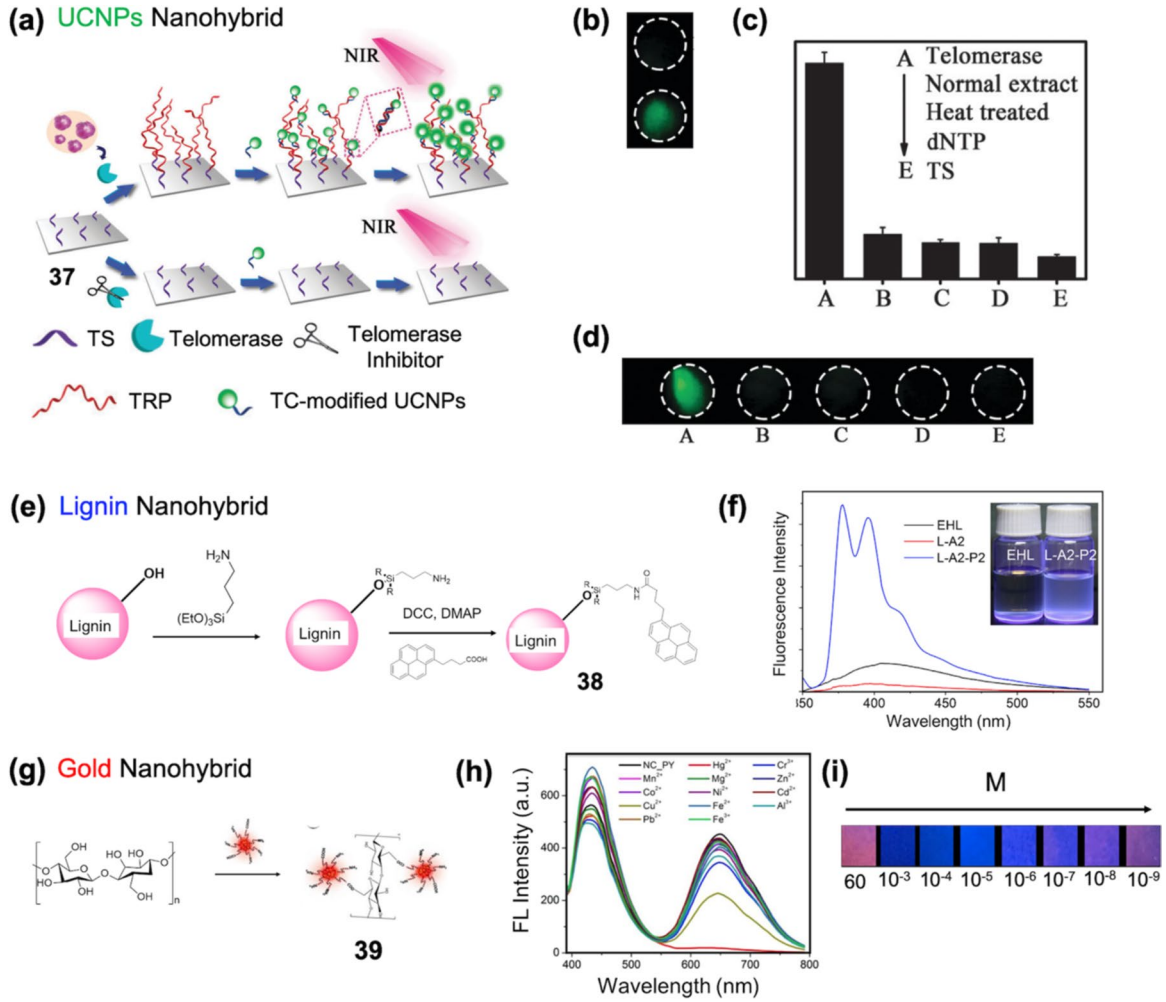

Fig. 12 **a** Schematic illustration of visual assay **37** designed on paper for testing telomerase activity coupled with TC-modified UCNPs. **b** Naked eye upconversion luminescence of the paper substrates (bottom) substrate incubated with the test solution (top) compared with the blank solution; **c** the fluorescence intensity of telomerase-incubated substrates: normal cell extract, heat-treated telomerase, dNTPs and TS. **d** The photos of A to E are in sequence. (Refer to the web version of this article for the legend colour). Reproduced from Ref. 47 with permission of RSC. **e** Construction of the lignin nanohybrid **38**. **f** Emission spectra of **38** in presence of different substrates in THF. (Refer to the web version of this article for the legend colour). Reproduced from Ref. 48 with permission of Elsevier. **g** Synthetic scheme for gold nanohybrid **39**. **h** Selectivity profile of **39** for the detection of Hg^{2+} in the presence of different counter cations. **i** Naked eye titration profile of **39** for Hg^{2+}. (Refer to the web version of this article for the legend colour). Reproduced from Ref. 49 with permission of Elsevier

nanosensor [48]. Sahoo and co-workers developed pyridoxal conjugated red fluorescent gold nanoclusters and chemically embedded them on the surface of cellulose strips (Fig. 12g) forming **39** and utilised it as a chemosensor for the detection of Hg^{2+} ions. The gold nanoclusters were synthesised using bovine serum albumin in a one-pot approach. Further, vitamin B6 cofactor pyridoxal was conjugated with the fluorescent gold nanoclusters. The fluorescence of **39** got quenched in the presence of Hg^{2+} even in the presence of different counter analytes (Fig. 12h). Upon addition of Hg^{2+} to **39**, the colour change can be noticed in Fig. 12i. The chelation of Hg^{2+} with **39** facilitates the change in surface state of **39**, resulting in fluorescence colour change. The detection limit of **39** for Hg^{2+} was estimated as 1 nM. The authors have employed cellulosic nanohybrid **39** for determining Hg^{2+} levels in fish, river water and tap water [49].

Liu and co-workers reported carboxymethyl cellulose supported gold nanoparticles for the fluorescent-sensitive detection of Hg^{2+}. The nanohybrid **40** is formed by utilising carboxymethyl cellulose as a capping and reducing agent in the synthesis. The average particle size of carboxymethyl cellulose (CMC)-capped gold nanoparticles **40** is 20.3 nm, confirmed by high transmission electron microscopy, energy-dispersive X-ray spectroscopy, dynamic light scattering and area electron diffraction pattern. The synthesised nanohybrid **40** has an SPR absorption band of 522 nm and

was employed as a fluorescent probe for the selective detection of Hg^{2+} ions.

Figure 13 a and b depict the selective detection mechanism and profile of **40** for Hg^{2+}. On interaction with Hg^{2+} ions, silver nanocluster **40** gets aggregated aiding in the quenching of fluorescence. The estimated limit of detection (LOD) of **40** for Hg^{2+} is 3.6 nM. This report is the first time that a cellulose-derived molecule was used as a reducing agent for the formation of gold nanohybrid [50]. Similar to other heavy metals, Mn^{2+} is also an important cation, the excess of which can inflict neuro damages leading to disorders such as Alzheimer's and Parkinson's diseases. Hence, it is necessary to monitor the concentrations of Mn^{2+} in industrial effluents and drinking water. Xiong and his team developed a rapid, highly selective and sensitive fluorescent probe **41** for the detection of Mn^{2+} formed by the interaction of carboxymethyl cellulose (CMC) with Tb^{3+}. Probe **41** shows a turn-off detection in the presence of Mn^{2+}. The fluorescence quenching of **41** in presence of ions is attributed both to static quenching by the reaction of quenchers with a ground-state fluorescein and the dynamic quenching by the reaction of quenchers with the excited-state fluorescein. Figure 13 c represents the quenching titration profile of **41** in the presence of increasing levels of Mn^{2+}. Probe **41** can detect Mn^{2+} as low as 0.046 μM with a fluorescence emission intensity of 544 nm. The authors have used 61 for the determination of Mn^{2+} in real samples like tap water [51].

In another illustration of up-converting fluorescence material, Zhu and co-workers developed a portable cellulose paper substrate **42** for the detection of cancer biomarker telomerase. Cellulose-supported microzone plate 42 can be used for the dual-mode colourimetric and up-conversion-based detection of telomerase. Probe **42** was generated by the functionalization of cellulose paper with telomerase substrate oligonucleotide (telomerase capturing unit). The telomerase substrate oligonucleotide was labelled with methylene blue or up-converting nanoparticles (UCNPs) and was further employed as the colourimetric or up-conversion fluorescence reporting nano labels (Fig. 14a). The experimental results for the prepared paper microzone plate 42 with the blank solution and test solution (HeLa cells extraction) are illustrated in Fig. 14b. The authors consider the cellulose-supported microzone plate material assay **42** as capable of detecting telomerase and applications in point-of-care and medical diagnostic devices [52]. Sahoo and co-workers developed a glutathione-stabilised fluorescent copper nanocluster loaded with pyridoxamine (vitamin B6) **43** for the surface of nanocellulose forming **43** and used for the real-time detection of picric acid. Using Stern Volmer equation, the authors elucidated that static quenching phenomenon is involved in the detection of picric acid by **43**. In the presence of picric acid, the fluorescence of **43** at 410 and 625 nm was selectively quenched because of the resonance energy transfer and the photo-induced electron transfer mechanisms. The authors claim that probe 63 can detect 27.4×10^{-7} M levels of picric acid without any interference from other tested nitro-aromatic compounds. The cellulose-modified nanohybrids **43** can be used to visualise picric acid as low as 1 μM [53].

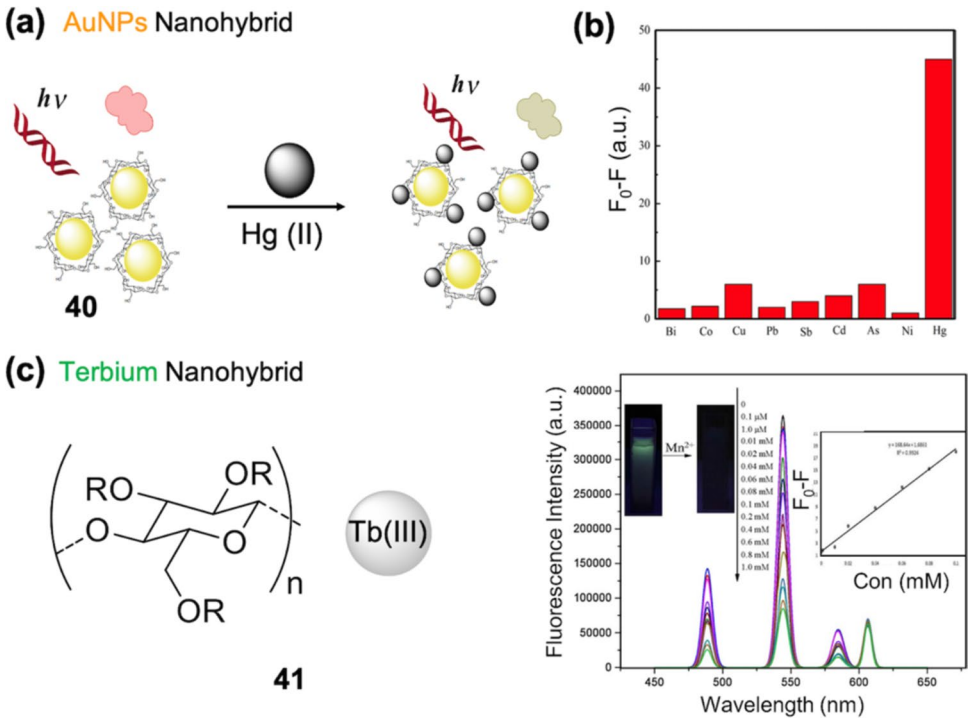

Fig. 13 **a** Schematic illustration of mechanism of **40** for the detection of Hg^{2+}. **b** Selectivity profile of **40** for in the presence of different counter cations. (Refer to the web version of this article for the legend colour). Reproduced from Ref. 50 with permission of Springer. **c** Chemical structure and fluorescence selectivity profile of **41** for Mn^{2+}. (Refer to the web version of this article for the legend colour). Reproduced from Ref. 51 with permission of Elsevier

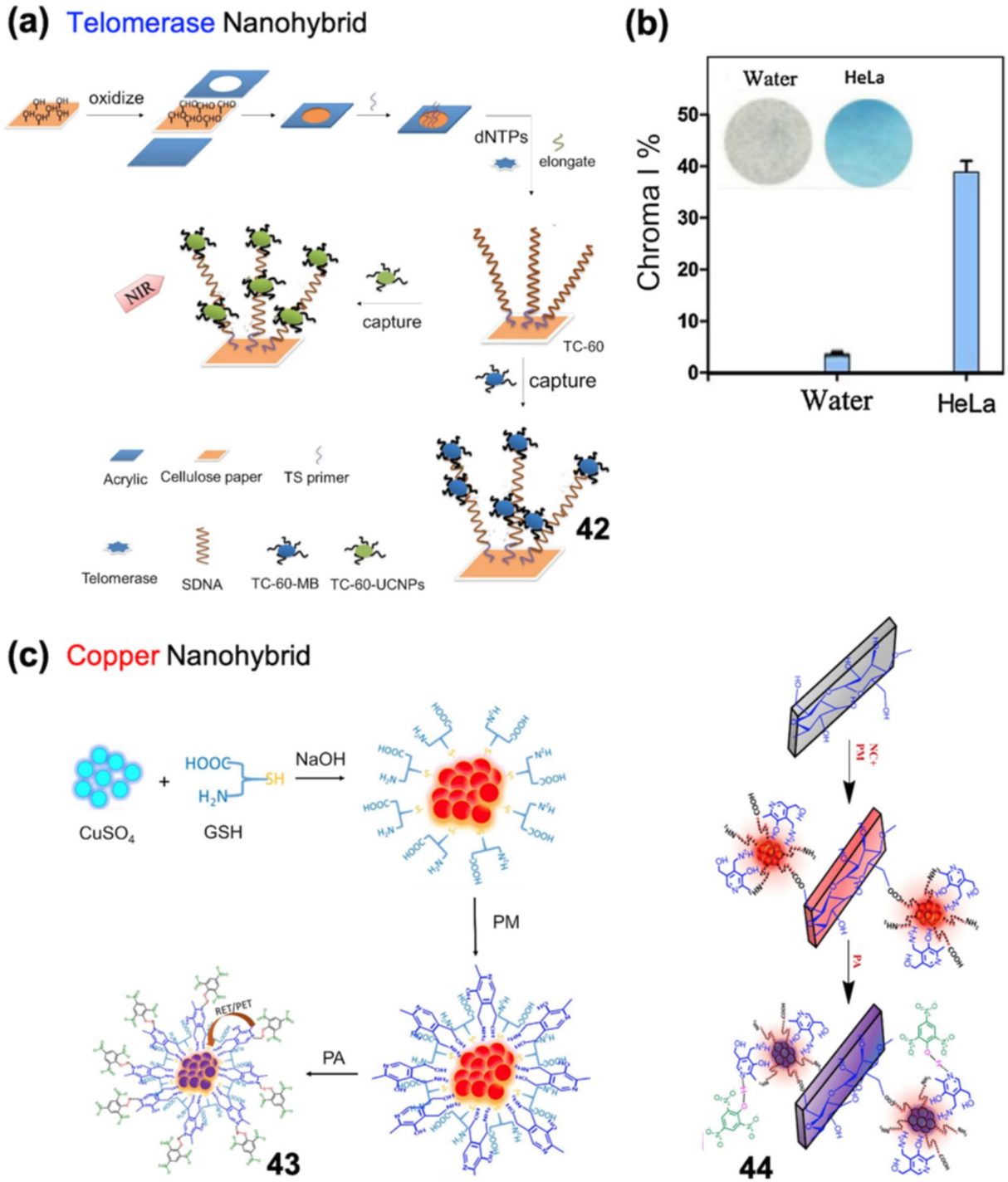

Fig. 14 **a** Schematic depiction of telomerase-cellulose material **42**. **b** Study of **42** in HeLa cells and water. (Refer to the web version of this article for the legend colour). Reproduced from Ref. 52 with permission of Elsevier. **c** Schematic representation of Cu^{2+}-based nanohybrid **43** for the detection of picric acid. **d** Detection mechanism involved in the detection of picric acid by **43**. (Refer to the web version of this article for the legend colour). Reproduced from Ref. 53 with permission of Elsevier

Feng et al. developed g-C_3N_4@TCNF nanoconjugates by chemically coupling tunicate cellulose nanofibrils containing –COOH groups with –NH_2/–NH– functionalised g-C_3N_4 nanosheets in the presence of EDC/NHS. Further, g-C_3N_4@TCNF hybrid nanopaper **45** was achieved by employing pressure extrusion technique (Fig. 15a). The so-developed nanopaper reflected qualitative properties like luminescence, transparency, high thermal stability and

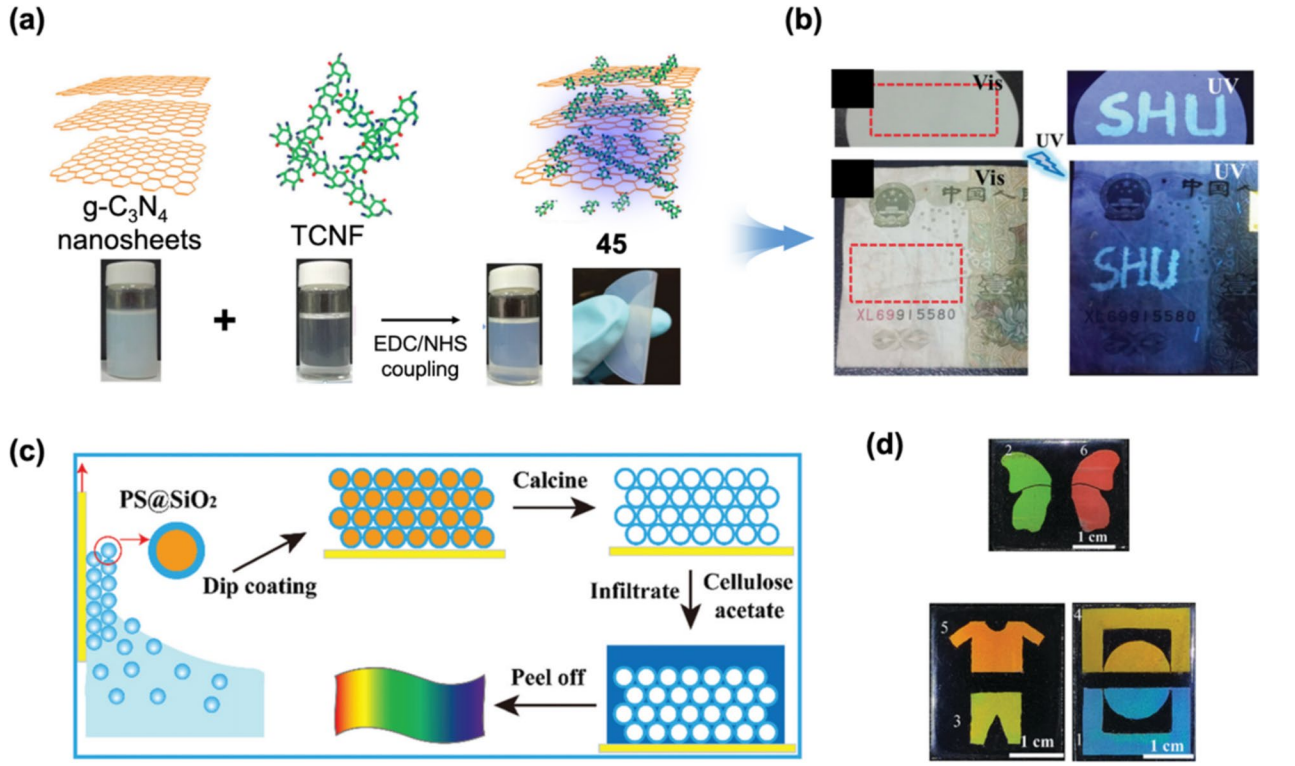

Fig. 15 **a** Schematic depiction of preparation of cellulose paper **45**. **b** Utility of **45** on banknote under UV lamp. **c** Coating mechanism of **45** and **d** detection patterns in **45** doped cellulose papers. (Refer to the web version of this article for the legend colour). Reproduced from Ref. 54 with permission of RSC

mechanical flexibility (credited to the addition of tunicate cellulose nanofibrils) (Fig. 15b). When combined with water, **45** was applied as ink for estimating banknote security and information encryption. Visibility of encrypted **45** can only be noticed under UV lamp proving its capability in anti-counterfeiting applications. Moreover, the nanopaper shows good UV shielding performance, thermal stability and mechanical properties [54]. In 2019, Zhou and his group introduced a fluorescent chemosensor based on aggregation-induced emission (AIE) for the selective detection of Fe^{3+} ions. The Fe^{3+} chelating probe **46** was formed by fabricating 1,1,2-triphenyl-2-[4- (3-sulfonatopropoxyl)-phenyl]-ethene sodium salt (SPOTPE) on quaternised cellulose (QC) via electrostatic interaction (Fig. 16a). The characterization of nanohybrid **46** was performed using transmission electron microscopy (TEM), spectrofluorophotometry and dynamic laser light scattering techniques. Figure 16 b depicts the change in intensity of nanohybrid **46** by varying the levels of quaternised cellulose. In the presence of Fe^{3+}, on exciting nanohybrid **46** (336 nm), the enhanced blue emission was quenched and observed at 472 nm. The authors observed that the cellulosic part in **46** formed more compact composites with Fe^{3+} over other metal ions. The strong electrostatic binding between AIE fluorophore and cellulose terminal aided in the formation of a stable complex with Fe^{3+}, resulting in the aggregation and quenching profile of **46**. The nanohybrid **46** is highly stable over a wide pH range of 5.0–10.0. The cellulose-modified nanohybrid **46** is capable of the real-time detection of Fe^{3+} in aqueous solution [55]. In early 2020, Liu and co-workers utilised a green and transparent cellulose nanofibre substrate supported by luminescent gold nanoparticles for the stable and sensitive solid-state sensing membrane for Hg^{2+} detection. A transparent cellulose nanofibre obtained from natural wood was combined with gold nanoparticles (Fig. 16c) to form **48**. The solid-state membrane **48** showed selective red fluorescence (Fig. 16c, d) in the presence of Hg^{2+} ions. The red fluorescence emission is attributed to the high-affinity metallophilic Hg^{2+}–Au(I) interaction. The authors consider probe **48** can be extended to detect Hg^{2+} and broader application in environmental sampling and monitoring. Another toxic heavy metal that has accumulated a lot of attention is Pb^{2+}. The toxic effect of heavy metal Pb^{2+} can cause a humongous impact on the nervous system and reproductive systems. It is vital to control levels of Pb^{2+} in drinking water. Hence, fluorescent and colourimetric materials are crucial for the monitoring of Pb^{2+} concentrations in real samples [56].

In 2020, Mahdavian and their team combined 7-acryloxycoumarin (7-AC) with methyl methacrylate and glycidyl methacrylate via copolymerization and emulsion

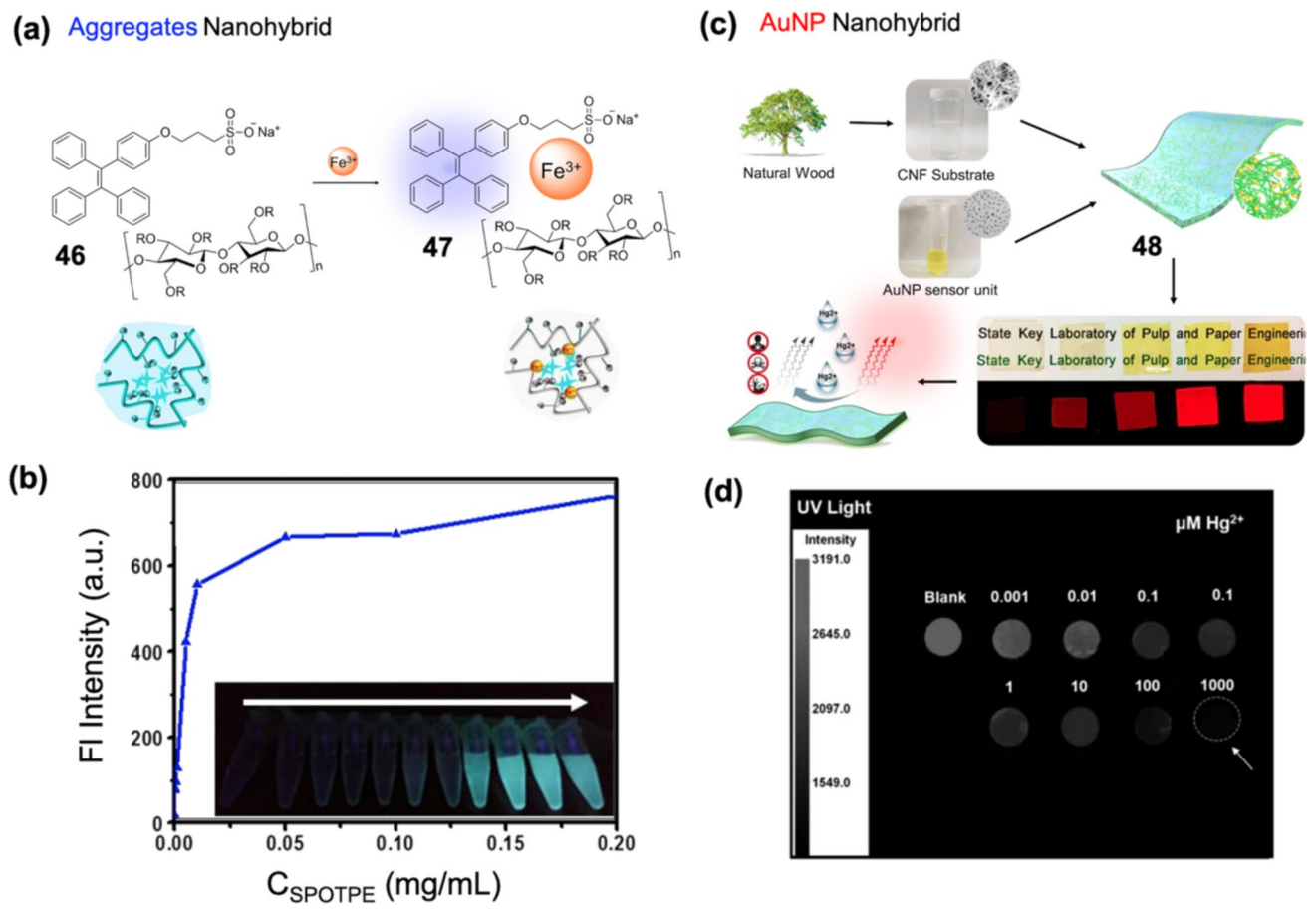

Fig. 16 **a** Schematic illustration of detection mechanism of cellulose linked AIE material **46** for detection of Fe^{3+}. **b** Titration profile of **46** in the presence of varying amounts of Fe^{3+}. (Refer to the web version of this article for the legend colour). Reproduced from Ref. 55 with permission of MDPI. **c** Schematic representation on preparation of AuNP nanohybrid paper **48** utilised for the detection Hg^{2+}. **d** Visual detection of Hg^{2+} by using **48** doped membranes under UV lamp. (Refer to the web version of this article for the legend colour). Reproduced from Ref. 56 with permission of Elsevier

polymerization to generate epoxy-functionalised fluorescent polymer nanoparticles (Fig. 17). The so-developed spherical polymeric nanoparticles were integrated into cellulose pulp papers (**49**) via smart and efficient chemical modification. Enhanced fluorescence intensity for **49** was achieved as a result of the immobilization of 7-AC into the hydrophobic acrylic copolymer substrate. The authors consider cellulosic material **49** for potential application in the development of anti-counterfeiting inks and security documents [57]. Park and his team generated amino acid and peptide-stabilised gold nanoclusters and chemically modified them on the surface of cellulose paper for measurement of lead in plasma samples. The gold nanocluster **50** was produced (Fig. 17c) using a single-pot approach, wherein histidine and glutathione were used as reducing and protecting agents. The synthesised nanohybrid **50** exhibits bright green emission at 502 nm with an excitation at 420 nm. The nanohybrid **50** shows selective quenching (Fig. 17d) in emission for Pb^{2+} even in the presence of other counter analytes. In **50**, GSH is bound to the Histidine-Au nanocluster surface via Au–S bond, enabling one amine and two carboxylic groups to freely bind with Pb^{2+} ions. The oxyphilic nature of Pb^{2+} ions promotes its selective binding with **50**. Probe **50** can detect Pb^{2+} at nanomolar levels (1.0 nM). The quantum yield of the nanohybrid is estimated at 7.5%. Image (Fig. 17e) displays the quenching profile of **50** with increasing levels of Pb^{2+}. The authors prefer to use the **50** modified cellulose paper for real-time detection of Pb^{2+} in environmental contaminants [58].

Reactive oxygen species (ROSs) are formed by the single-electron reduction of oxygen. There are a variety of ROS species which include superoxide anion radicals ($\cdot O_2^-$), hydroxyl radical (•OH), hydrogen peroxide (H_2O_2), peroxynitrite ($ONOO^-$) and hypochlorite radical (ClO^-). Highly reactive oxygen species (hROS) (•OH, $ONOO^-$, ClO^-) show higher reactivity than ROS and can directly cause the oxidation of nucleic acids, proteins and lipids. Excessive accumulation of hROS species in the human body can

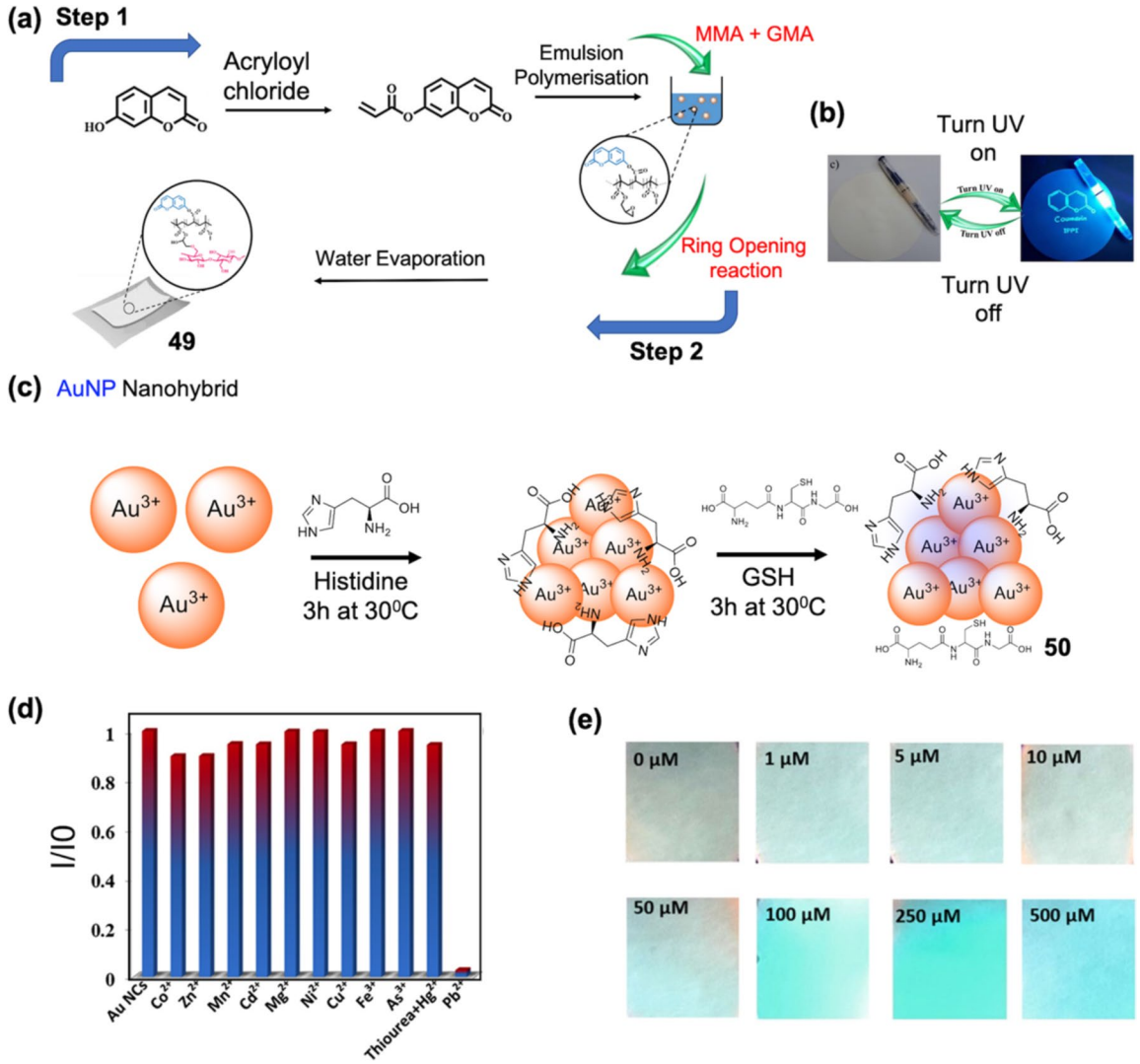

Fig. 17 **a** Fluorescence enhancement mechanism of cellulose polymeric nanohybrid **49**. **b** Reversible detection fluorescence turn on and off phenomenon in **49**. (Refer to the web version of this article for the legend colour). Reproduced from Ref. 57 with permission of Elsevier. **c** Preparation of gold nanohybrid material **50**. **d** Quenching-based selectivity profile of 50 for Pb^{2+} in the presence of other counter cations. **e** Naked eye titration profile of **50** doped cellulose papers with increasing concentrations of Pb^{2+}. (Refer to the web version of this article for the legend colour). Reproduced from Ref. 58 with permission of Elsevier

induce oxidative stress, resulting in a variety of diseases, including liver injury, inflammation, tumours and septicaemia. In early 2022, He and co-workers developed a bioinspired ratiometric fluorescence probe **51** based on cellulose nanocrystal-stabilised gold nanoclusters for the live-cell and zebrafish imaging of highly reactive oxygen species. Probe **51** utilises a combination of cellulose nanocrystals (CNCs) as carriers and stabilisers of gold nanoclusters and o-phenylenediamine (Fig. 18a) as an anti-interference internal standard for ROSs. In this work, the authors have used CNCs gained from biocompatible biomass which consist of high carboxyl density and needle-shaped and rod-like structures which resist the easy aggregation and instability of gold nanoclusters. The so-prepared ratiometric fluorescent nanohybrid **51** was inspired by the natural form of a chameleon changing (Fig. 18b) its colour in the presence of environmental stimuli. On the addition of hROS species to **51**, the fluorescence of the nanohybrid changes from blue to yellow. The selectivity profile of **51** in the presence of hROS at emission intensities of 488 and 580 nm is shown in Fig. 18b. The applicability of cellulosic material **51** for hROS was determined using biological samples like living cells and zebrafish (Fig. 18c). The authors consider **51** to have high efficacy for practical application in biological systems [59].

Other than ROS species, catecholamines are crucial hormones in the peripheral endocrine and central nervous systems. Catecholamines like dopamine are produced in nerves both in cellular bodies and at the terminals. Catecholamines

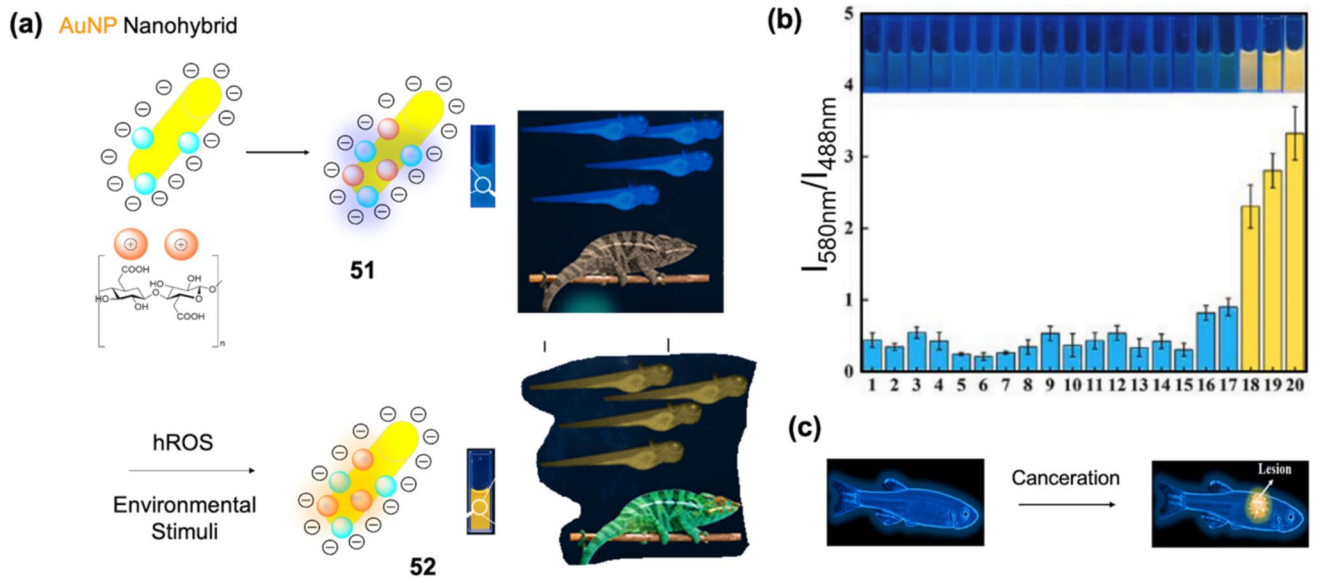

Fig. 18 **a** Scheme for the preparation of gold cellulose nanohybrid **51** utilised for the detection of hROS species. **b** Selectivity profile of **51** for different hROS species. **c** Utilisation of **51** for detection of hROS species in fish samples. (Refer to the web version of this article for the legend colour). Reproduced from Ref. 59 with permission of Elsevier

are important brain neurotransmitters and can act as biomarkers for neurodisorders like Alzheimer's and Parkinson's diseases. In the first half of 2023, Nabavi and co-workers accomplished bacterial cellulose-incorporated europium nanohybrid **53** for smartphone-based detection of levodopa and dopamine and its application in point-of-care diagnosis of Parkinson's disease. As depicted in Fig. 19a, the nanohybrid consists of europium, lithium and strontium metals as the main unit. Figure 19 b demonstrates the quenching of fluorescence and high selectivity profile of **53** for dopamine and levodopa. Nanohybrid material **53** was 3D-printed on a bacterial cellulose PAD platform and used for the detection of dopamine and levodopa (Fig. 19b). The authors consider the smartphone-based unit of **53** capable of real-time monitoring of dopamine and levodopa in biological samples (Fig. 19c) [60].

3.1.2 Colourimetric-based hybrid nanomaterials

Colourimetric nanohybrids are promising and important in both environmental and diagnostic applications. Colourimetry allows better visualization of analytes and hence can be used for real-time monitoring of different hazardous analytes. In 2013, Kondo and his group developed gold nanoparticle templated cellulose polyampholyte (carboxyethyl quaternised cellulose (CEQC)) for the colourimetric off–on detection of environmentally hazardous Hg^{2+} ions and biologically essential cysteine. Here, gold nanoparticles are stabilised using CEQC forming **54**. The addition of Cys to **54** causes aggregation, resulting in a colour change from pink to black (Fig. 19d). Further, a redispersion of **54** takes place with the addition of Hg^{2+} to **54** + Cys solution, as Hg^{2+} is known to have more affinity for thiols than AuNCs (Fig. 19d). The cellulose-stabilised assay **54** can detect very low levels of Cys and Hg^{2+} (20 and 40 nM). The naked eye detection ability of Cys and Hg^{2+} by **54** gives it an upper edge for real-time applicability [61].

Other than cations and amino acids, dihydronicotinamide adenine dinucleotide (NADH) and its oxidised form, nicotinamide adenine dinucleotide (NAD^+), are prevalent biomolecules that are associated with cellular energy metabolism, both in prokaryotic and eukaryotic organisms. NADH and NAD^+ couples are considered as indispensable cofactor for more than 300 dehydrogenase enzymes. Several reports claim the involvement of increased activity dehydrogenases and aldehyde dehydrogenase in human cancers [241]. Hence, monitoring the functions related to NADH/NAD^+ can help in identifying and treating cancers at an early stage. Xiao and his group described a paper-based device that enabled sensitive room-temperature and rapid detection of NADH through a colourimetric readout, demonstrating its value for monitoring NAD^+-driven enzymatic reactions. The paper-based device consists of a gold nanoparticle-cetyltrimethylammonium bromide solution.

As shown in Fig. 20a, the Au^{3+}-CTAB combination without the addition of NADH causes complete dissolution; low NADH relates to partial dissolution and high NADH causes no dissolution forming **55**, **56** and **57**, respectively. Figure 20 b depicts the strategy employed in the preparation of a paper-based device. The paper-based device was

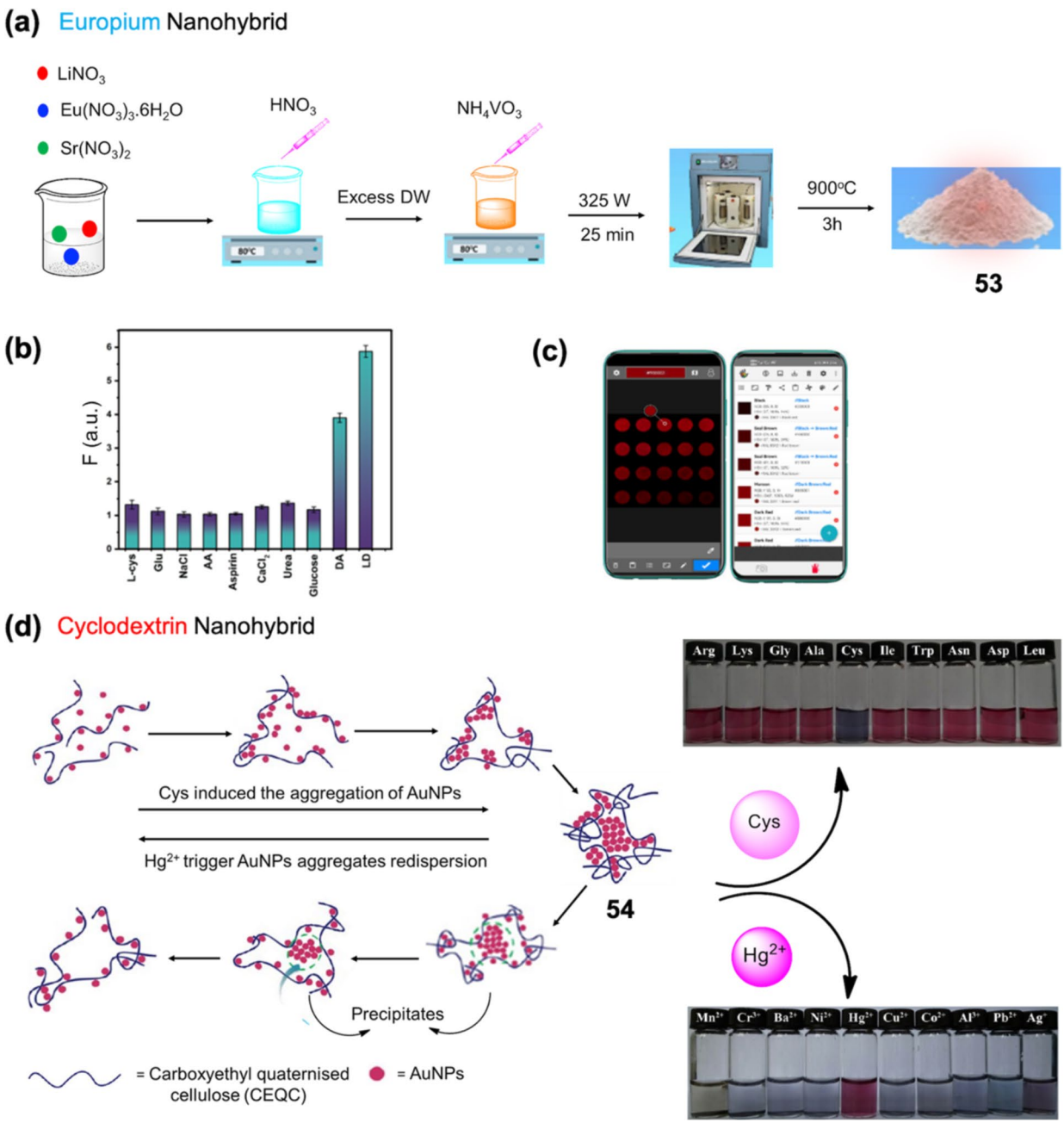

Fig. 19 **a** Scheme for the preparation of europium nanohybrid **53**. **b** Selectivity profile of **53** for L-dopa and dopamine in the presence of other neurotransmitters. **c** Visual detection of neurotransmitters in mobile phone using cellulose papers. (Refer to the web version of this article for the legend colour). Reproduced from Ref. 60 with permission of RSC. **d** Scheme for the preparation of cyclodextrin nanohybrid **54** capable of reversible detection of Cys and Hg^{2+}, naked eye selectivity profile of **54** for (top) Cys and bottom (Hg^{2+}). (Refer to the web version of this article for the legend colour). Reproduced from Ref. 61 with permission of ACS

fabricated using cellulose ester paper featuring a wax-encircled, gold nanoparticle–coated film atop a cotton absorbent layer, sandwiched between two plastic cover layers. On adding NADH, the Au^{3+} complex is quickly reduced to Au^{+}, resulting in the dissolution forming **56** and **57**. The increase in the concentration of NADH results in complete reduction and dissolution (Fig. 20b). The authors believe that the developed paper-based device can be applicable for monitoring NAD^{+}-associated enzymatic reactions and screening for dehydrogenase inhibitors in a variety of testing contexts with the reduction in cost and high-value addition [62]. Like metal ions, anions, ROS species and explosives pesticides are also a cause of serious threat to the world. Among different pesticides, organophosphorous (OPs) pesticides are

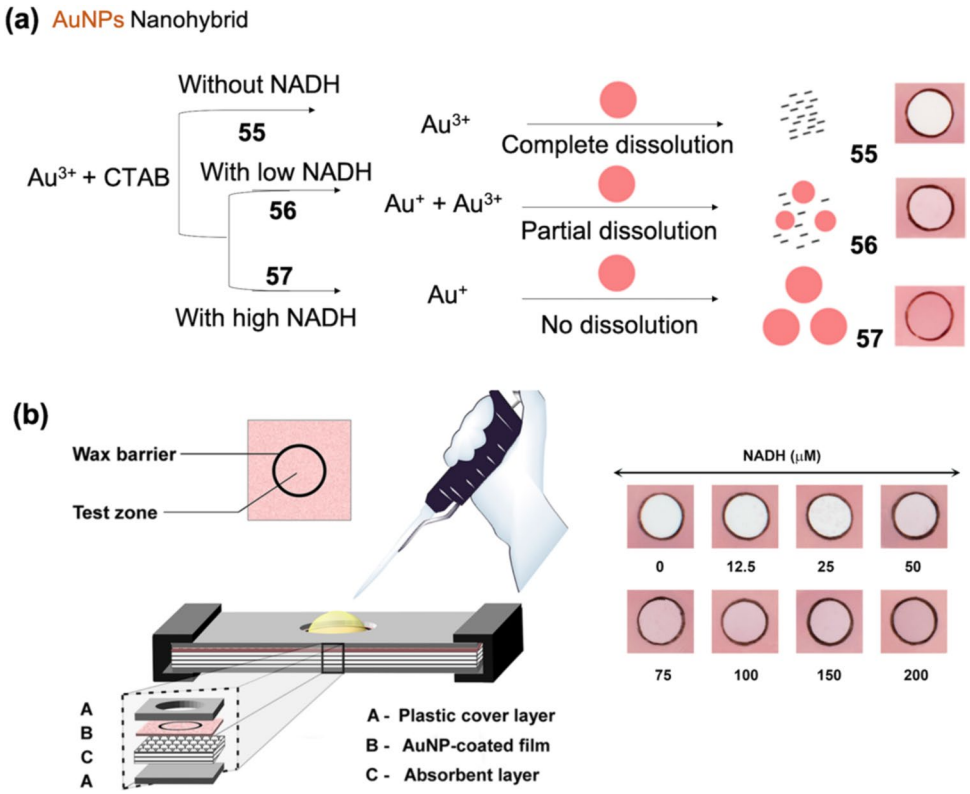

Fig. 20 **a** Scheme representation of different mechanism for preparation of **55**, **56** and **57**. **b** Coating of **55**, **56** and **57** on cellulose surface (left) and titration profile of **55**–**57** in the presence of NADH. (Refer to the web version of this article for the legend colour). Reproduced from Ref. 62 with permission of ACS

considered to have wide usage in agriculture. Moreover, organophosphorous pesticides also have a relatively long half-life time. Hence, residues of OPs can create serious water and environmental pollution problems.

Wang and co-workers introduced another colourimetric Au^{3+}-CTAB-based colourimetric device **58** for the selective determination of organophosphorous pesticides (OPs). Here, **58** is also a dissolution-based colourimetric semi-quantitative assay for OPs. Nanohybrid **58** is incomplete (Fig. 21a) without the addition of enzymatic hydrolysis product thiocholine (TCh). As depicted in Fig. 21a, in the absence of OPs, TCh consumes almost all Au^{3+} and prevents the colour change of **58**. However, in the presence of OPs, the enzymatic TCh is not enough to consume all the Au^{3+}, and the residual Au^{3+} dissolves **58**. Figure 21 b illustrates the preparation of a **58**-based paper device and its colour change in the presence of varying concentrations of parathion. Such paper-based devices make it easy for the real-time monitoring of pesticide-contaminated environments and reduce the cost burden [63]. Later, Zhou and his team developed a colourimetric sensor **59** based on an indicator displacement mechanism for the detection of trace amounts of Ni^{2+} ions. The nanohybrid **59** consists of organometallic reagent zinc incorporated into $ZnSiO_3$ nanospheres and Na_2-EDTA as a masking agent (Co-ionophore) (Fig. 21c). On interaction with Ni^{2+}, the blue colouration of **59** fades (Fig. 21d). On increasing the concentration of Ni^{2+}, the competition is amplified, resulting in the displacement of Zn^{2+} ions. The paper-based assay **59** can detect Ni^{2+} ions as low as 83 nM. The paper-based assay enables the naked-eye differentiation of nickel ions down to 0.1 μM (Fig. 21e). The paper-based nanohybrid **59** an estimate levels of Ni^{2+} ions in real environmental samples [64].

Separation and recognition of enantiomers are requisite in many diverse areas, such as biology, chemistry, health science and pharmaceutics. Chromatography is the major technique employed for the detection and separation of enantiomers. However, fluorescent and chromophore indicators can be more sustainable and cheap techniques for the determination of enantiomers. Individual researcher Zor describes silver nanoparticle-embedded nanopaper as a colourimetric platform for the enantioselective recognition of chiral analytes. The paper was prepared utilizing bacterial cellulose (Table 1), and silver nanoparticles were embedded on their surface, generating **60** (Fig. 22a). The authors have tested the ability of **60** for the enantioselective chiral detection of D-cysteine in both solution and nanopaper phases. The colourimetric changes of **60** in the presence of D-cysteine are represented in Fig. 22b, c. Nanohybrid **60** showed a discriminative sensing response towards D-cysteine with a LOD value of 4.88 μM. Here, the inherently chiral AgNPs (**60**) undergo aggregation on reacting with enantiomers displaying a significant colour change from yellow to purple, brown in both aqueous phase and nanopaper. For

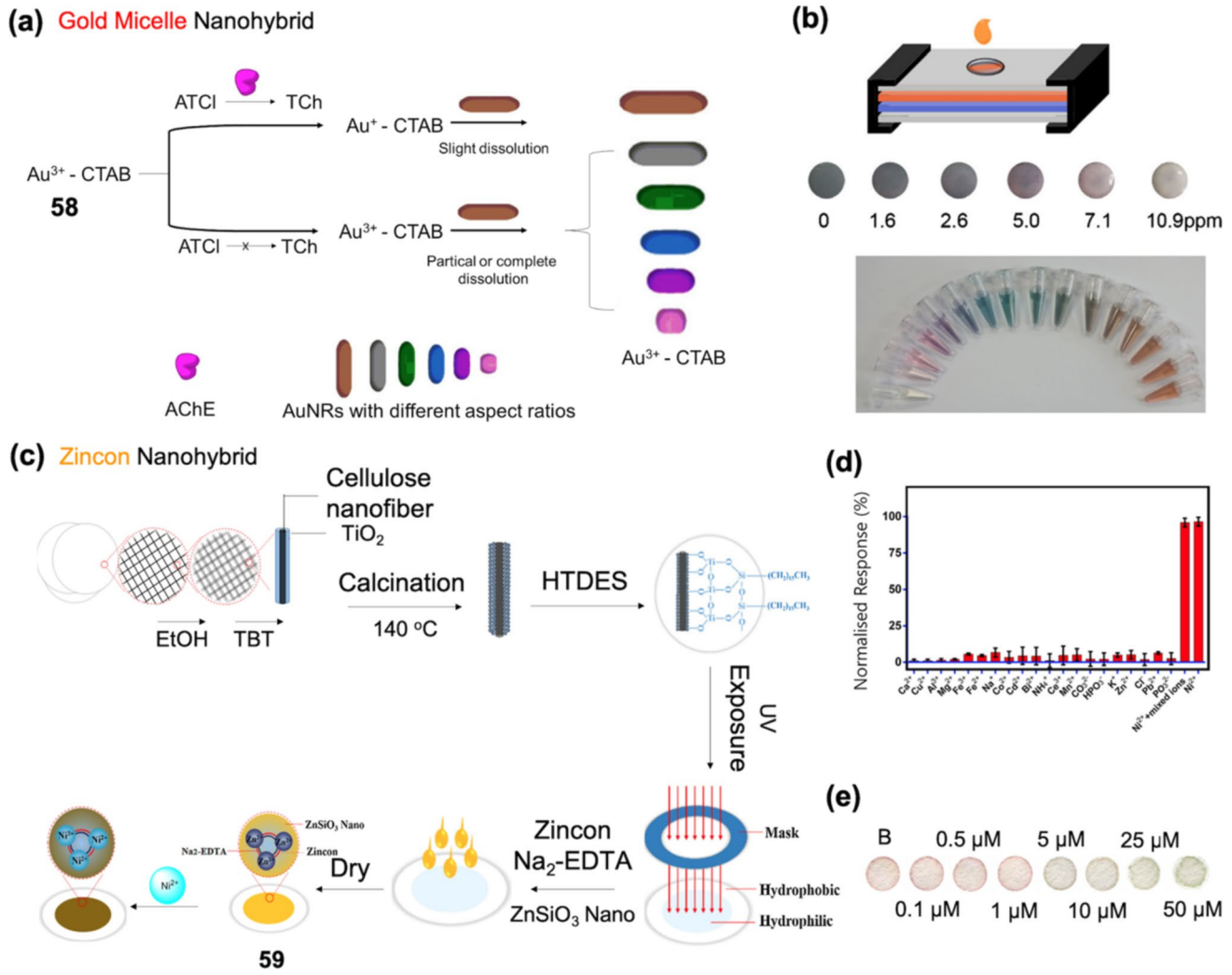

Fig. 21 **a** Scheme depicting the preparation and mechanism of gold nanohybrid **58**. **b** Casting of **58** on cellulose surface to form a paper-based device (top), Colourimetric changes on interaction with different levels of parathion (bottom). (Refer to the web version of this article for the legend colour). Reproduced from Ref. 63 with permission of Springer. **c** Schematic illustration of preparation of zincon nanohybrid **59**. **d** Colourimetric selectivity profile of **59** for detection of Ni^{2+}. **e** Naked eye titration of **59** coated cellulose with varying concentrations of Ni^{2+}. (Refer to the web version of this article for the legend colour). Reproduced from Ref. 64 with permission of Elsevier

practical use, the plasmonic nanopaper **60** was punched into circular pieces and inserted into a wax-printed PET film to produce a disposable 2D cuvette, which can be applied in an ordinary spectrophotometer.

The report is a first on the utility of cellulose material in the detection of enantioselective chiral molecules [65]. Saraji and his team reported a gold nanoparticle–embedded paper-based colourimetric assay for the selective determination of selenium (Se(IV)). Headspace single-drop microextraction utilizing a microdrop containing unmodified gold nanoparticles (AuNPs) was used as both the extractant and the colourimetric unit for the sensitive and selective estimation of Se(IV). Figure 22 d depicts a complete synthetic track for the synthesis of gold nanohybrid **62**. Nanohybrid **62** was spotted on cellulose paper and was used for the detection of Se(IV). The cellulosic nanohybrid **62** paper showed excellent selectivity for Se(IV) in the presence of different countercations. The colour change of **62** was attributed to the adsorption of in situ-generated hydrogen selenide on the surface of AuNPs. The limit of quantification of **62** for Se(IV) was reported as 12 μg L^{-1}. The repeatability of the method of cellulosic paper **62** in the presence of was studied by the calculation of intraday and interday precision of standard solutions at concentrations of 20 and 70 μg L^{-1}. The authors consider that cellulosic nanohybrid material **62** can be used for the determination of Se(IV) in real samples [66].

In the same year, Correa and co-workers utilised a combination of silver nanoparticles and cellulose nanowhiskers for the selective detection of hydrogen peroxide (H_2O_2). Nanohybrid material **63** was formed by the combination

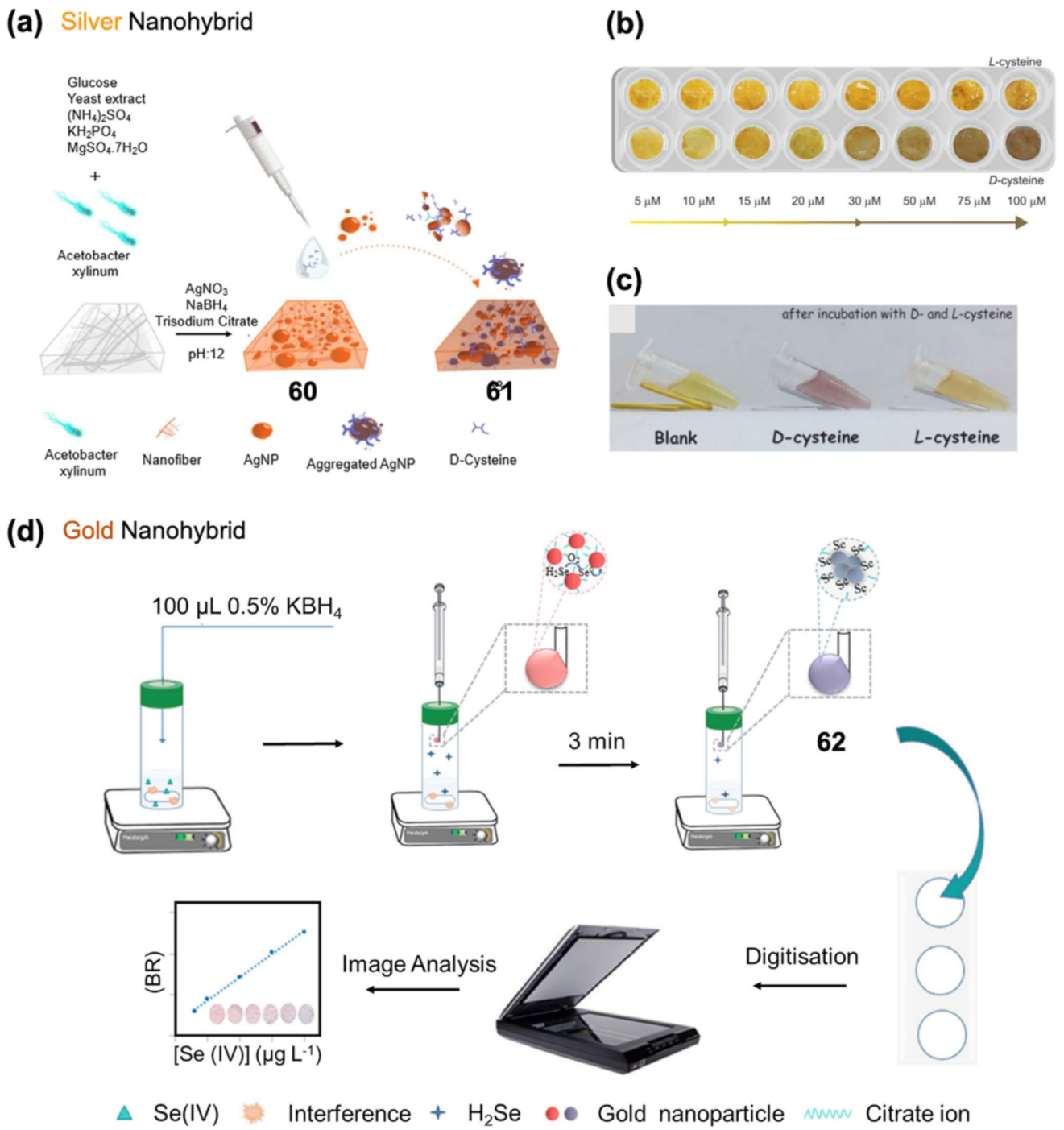

Fig. 22 **a** Preparatory procedure for the synthesis of silver nanohybrid **60** and **61**. **b**, **c** Colourimetric detection and titration profile **60** and **61** for cysteine. (Refer to the web version of this article for the legend colour). Reproduced from Ref. 65 with permission of Elsevier. **d** Complete preparation of **62** and detection mechanism for Se(IV). (Refer to the web version of this article for the legend colour). Reproduced from Ref. 66 with permission of Springer

of silver nanoparticles and nanostructured polysaccharide (cellulose nanowhiskers). When exposed to H_2O_2, the silver nanoparticles undergo catalytic decomposition, resulting in the decrease of the AgNP absorption band at 410 nm in relation to H_2O_2 concentrations (Fig. 23). The LOD of cellulosic-silver-nanohybrid **63** for H_2O_2 was estimated 0.014 and 112 μM. The authors confirm that material **63** is easy to interpret and can also be used for the real-time analysis of H_2O_2 in real samples, even in the presence of other interfering substances [67].

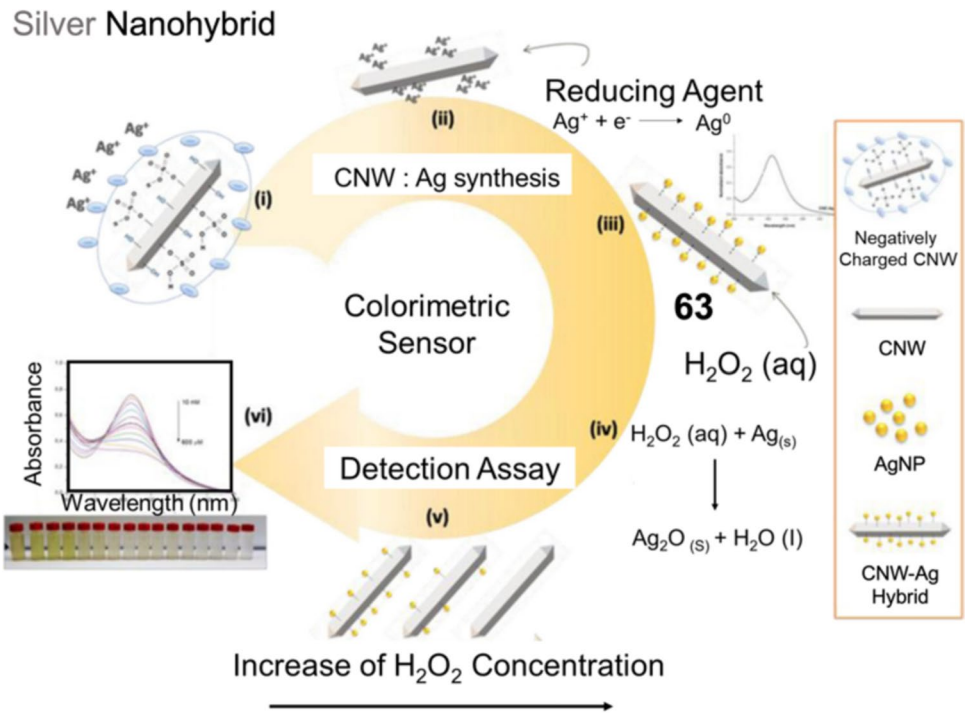

Fig. 23 Synthesis of silver nanohybrid, coating on cellulose, detection and selectivity profile of **63** for H_2O_2. (Refer to the web version of this article for the legend colour). Reproduced from Ref. 67 with permission of Elsevier

In the first report, Choi and co-workers utilised citrate-capped Pt nanoparticles (PtNPs) and doped them with cellulose paper for selective colourimetric detection of uric acids in real samples. The citric acid-capped Pt nanoparticles came with a particle size of 8–10 nm. The cellulose paper strip used in this work was prepared by pretreatment with PVA, TMB + H_2O_2 and PtNPs respectively (Fig. 24). Here, PtNPs functioned as enzyme catalytic activity. TMB was the

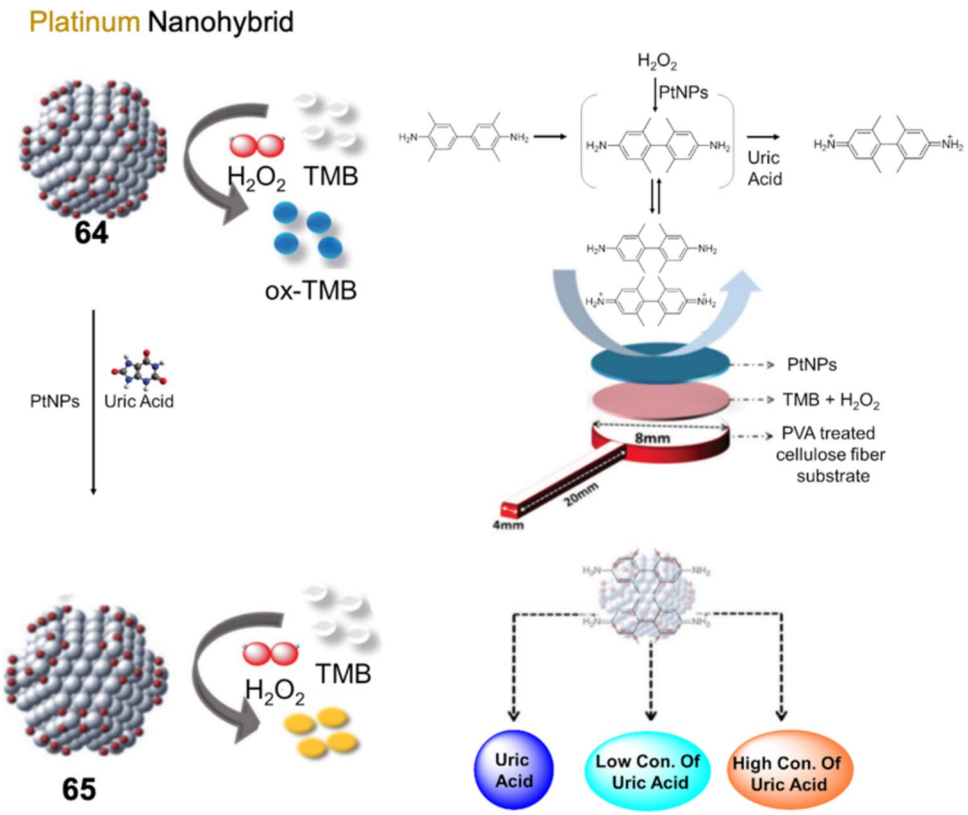

Fig. 24 Illustration of uric acid detection by **64** and protocol for doping on cellulose surface. (Refer to the web version of this article for the legend colour). Reproduced from Ref. 68 with permission of RSC

hydrogen donor group inducing the reduction of H_2O_2. A calculated LOD of 4.2 µM and a linear range of 7 mM was achieved on engaging uric acid with the cellulosic nanohybrid material **64**. The authors confirm the use of **64** as a tool for the quantitative detection of uric acid in the physiological range in urine samples. This report is a good illustration which shows that not only gold, silver or copper but transition heavy metals such as platinum-based nanomaterials can also be easily doped on cellulose surfaces [68].

In 2021, Lim and his group developed 2,2,6,6-tetramethylpiperidin-1-piperidinyloxy (TEMPO)-oxidised cellulose nanocrystal (TEMPO-CNC) capped gold nanoparticles (AuNPs) **66** for the colourimetric detection of unamplified pathogenic DNA oligomers of methicillin-resistant *Staphylococcus aureus* (Fig. 25a). The authors have characterised the nanohybrid **66** by using transmission electron microscopy, UV–visible spectroscopy, dynamic light scattering and atomic force microscopy. The average diameter of gold nanoparticles used in the generation of **66** is approximately 30 nm. Under ionic conditions, **66** undergoes a red-to-blue (Fig. 25b) colour transformation in the presence of the target DNA. On the addition of DNA to **66**, aggregation of AuNPS results in the colour change from red to blue. Nanohybrid molecule **66** demonstrated a colourimetric detection limit of 20 fM for pathogenic DNA. The authors consider nanohybrid **66** as an efficient and straightforward solution as a biosensor [69].

Recently, Mahdavian and co-workers (2024) reported spiropyran and leuco-dye doped nanocapsules and embedded them on the surface of dual-chromic cellulose paper for the colourimetric detection of heavy metal cations. Figure 26 a depicts the synthetic approach for the generation of nanohybrid **67**. Cellulosic nanohybrid **67** is capable of colourimetrically detecting Fe^{2+}, Pb^{2+} and Sn^{2+} ions. The selectivity profile of cellulosic-nanohybrid material **67** for reported heavy metals is represented in Fig. 26b, c. Opto-chemical results indicated that the LODs of nanohybrid **67** for Fe^{2+}, Pb^{2+} and Sn^{2+} ions are 0.0013 µM, 0.0023 µM and 0.0028 µM, respectively. The authors confirm the applicability of nanohybrid **67** for the detection of reported heavy metal ions with high sensitivity, instant responsivity, wide linear detection range and low detection limit in real samples [70].

3.2 Cellulose nanofibres and nanocrystals

As discussed in Sect. 1, cellulose is found to be the most abundant bio-based green polymer. The structure of cellulose is found in the form of a lignocellulosic natural

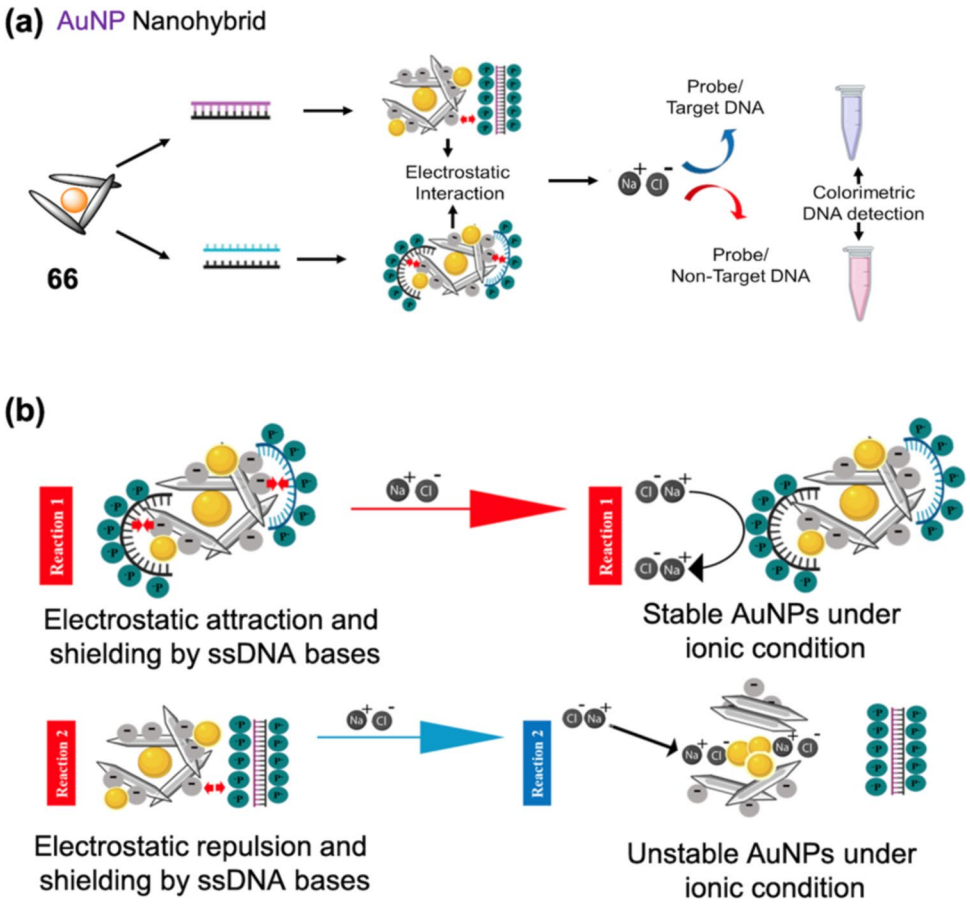

Fig. 25 **a**, **b** Depiction of the proposed mechanism of the interaction between target (upper panel) and non-target (lower panel) generating TEMPO-CNC-stabilised AuNPs (TC-AuNPs) **66** under ionic conditions for the sequence-specific detection of pathogenic DNA. (Refer to the web version of this article for the legend colour). Reproduced from Ref. 69 with permission of ACS

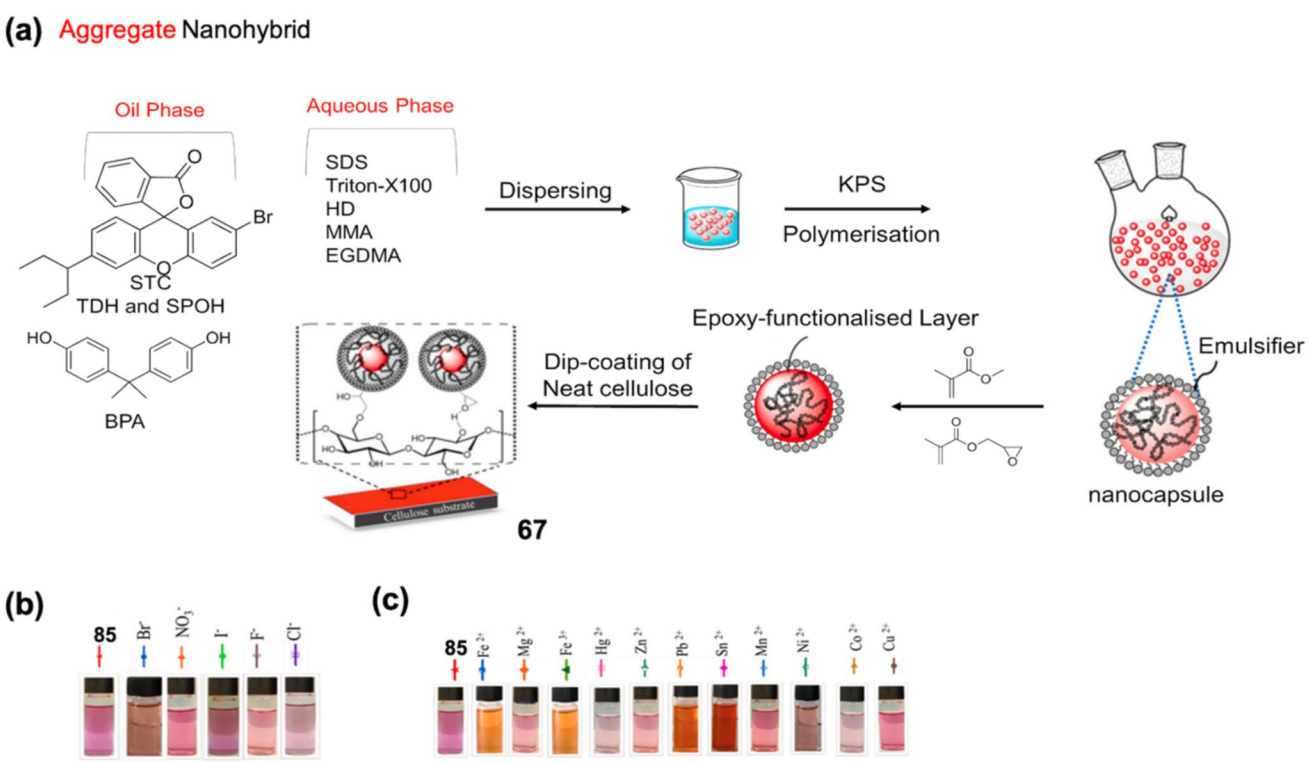

Fig. 26 **a** Structures of dyes for doping **67**. Preparation of dual-stimuli responsive latex nanocapsules via mini-emulsion polymerization. **b** Visible images of **67** in the presence of different anions and metal cations (50 μM) in 4/1 (V/V) ethanol/H_2O solutions and the corresponding visual colour changes. (Refer to the web version of this article for the legend colour). Reproduced from Ref. 70 with permission of Elsevier

fibre, and its microstructure consists of five main components: amorphous (hemicellulose), crystalline nature of α-cellulose, aromatic (lignin), wax and pectin [242]. In the past few decades, many cellulose-based materials in nanoform have replaced their counterparts. Cellulose nanomaterials have excellent benefits like high sustainability and biodegradability, low production cost, better interfacial area, high strength and modulus, high aspect ratio and low density [243]. Nanocellulose materials are classified into two main categories which are cellulose nanocrystals (CNCs) and cellulose nanofibres (CNFs). The properties of the cellulose nanomaterials (CNMs) are highly dependent on the cellulosic substrates and their processing conditions. As depicted in Fig. 2, nanocellulose materials are formed from raw cellulose via chemical, mechanical and enzymatic treatments. In this section, fluorescent and colourimetric optical chemosensors based on CNCs and cellulose nanofibres (CNFs) will be discussed.

3.2.1 Fluorescence-based nanofibres and nanocrystals

In 2015, Wilkins and co-workers utilised Alexa Fluor for labelling cellulose nanocrystals, producing **68** and application in bioimaging. In the first approach, the cellulose surface was modified with aldehyde groups by reaction with limiting amounts of sodium periodate. Further, reductive amination reactions were applied to bind Alexa Fluor dyes with terminal amino groups on the linker cellulose nanocrystals, generating **68**. In the other approach, Alexa Fluor dye was modified to conjugate chloro-substituted triazine ring at the end of the linker section and was further reacted with cellulose nanocrystals at high temperature, producing **68**. The chemical structure of Alexa Fluor–modified cellulose nanocrystal is represented in Fig. 27a. As shown in Fig. 27b, material **68** was applied for bioimaging in the pore throat of a pore network micromodel. The authors anticipate that cellulosic crystal material can be useful in evaluating how candidates of mixed microbial communities associate with solid cellulose deposits [71].

In another work, Huang and his group utilised cellulose nanocrystals with an amino acid spacer and grafted it with pH-sensitive fluorescein moiety forming **69**. Figure 27 c illustrates the structure of nanocellulose-modified material **69**. The conjugation of cellulose nanocrystals with fluorescein was achieved using L-Leucine amino acid as a spacer linker. CNC material **69** was designed for sensitive sensing of pH. The naked eye fluorescence changes of **69** for pH sensing are depicted in Fig. 27c. The authors have

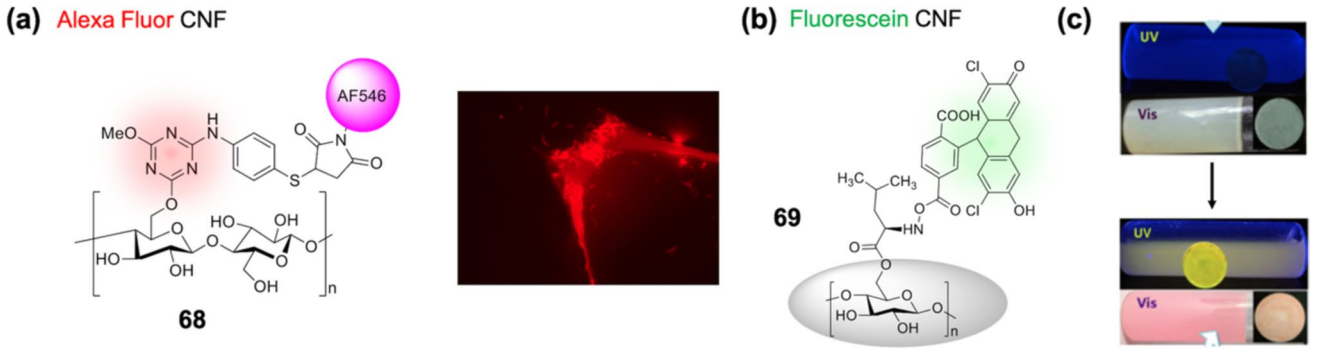

Fig. 27 **a** Chemical structure of cellulose-based imaging agent **68**. (Refer to the web version of this article for the legend colour). Reproduced from Ref. 71 with permission of ACS. **b** Chemical structure of cellulose-derived fluorescent agent **69**. **c** Illuminated suspension of **68** under UV lamp. (Refer to the web version of this article for the legend colour). Reproduced from Ref. 72 with permission of ACS

estimated that the fluorescence intensity of **69** increases with pH of the buffer from 2.28 to 12.66. The authors confirm that CNC material **69** is an excellent candidate for the estimation of pH with high biocompatibility and biological activity [72]. In 2017, Li and his team introduced a cellulose-anchored carbon nanotube and doped it with 1,4-dihydroxyanthraquinone as a fluorophore unit for the efficient detection of Cu^{2+} and Cr^{3+} ions in the aqueous solution (Fig. 28a, b). Probe **70** has excellent metal sorption capacity supporting the selective quenching of fluorescence in presence of Cu^{2+}. Further, when Cu^{2+}-contaminated **70** is treated with Cr^{3+}, replacement

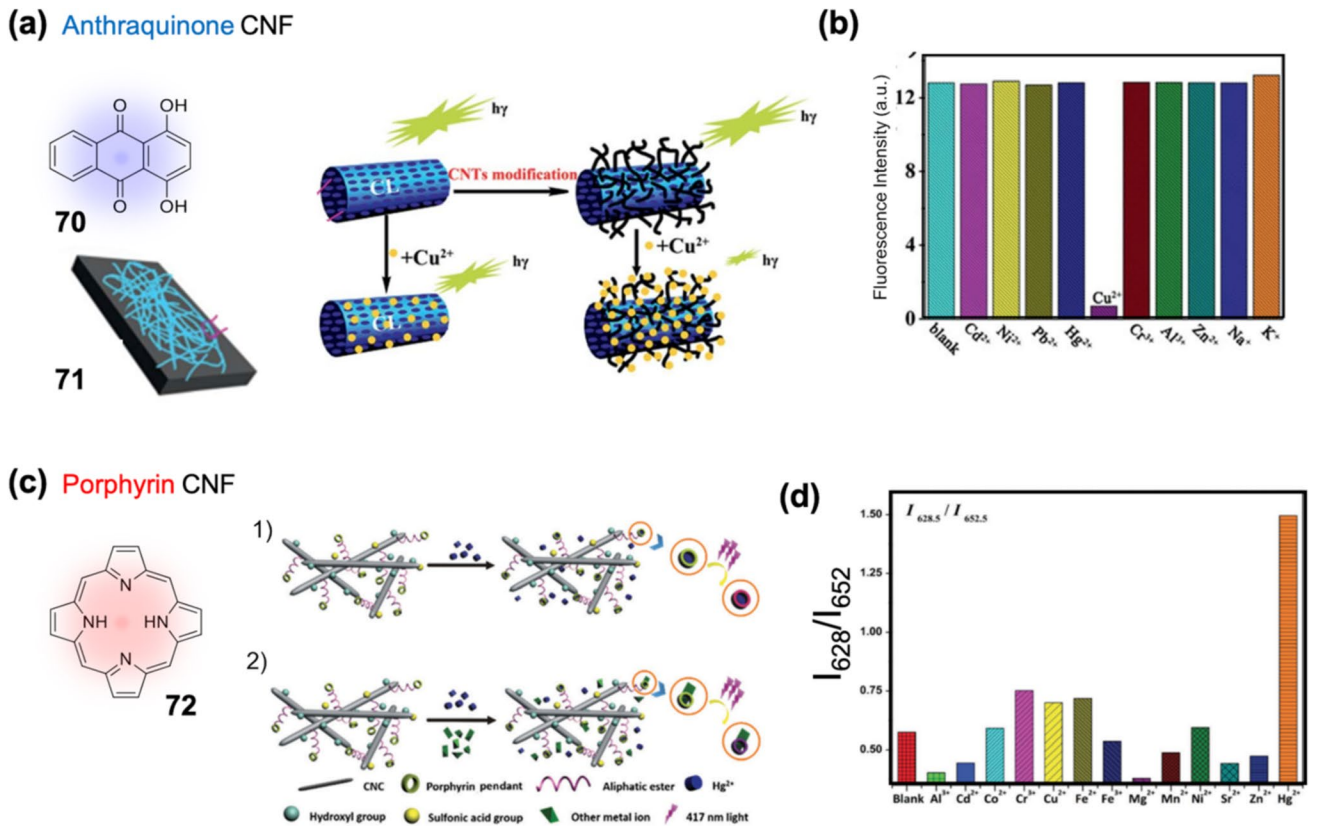

Fig. 28 **a** Schematic depiction of **70** and **71** with detection mechanism. **b** Selectivity profile of **70** and **71** for Cu^{2+}. (Refer to the web version of this article for the legend colour). Reproduced from Ref. 73 with permission of RSC. **c** Chemical structure of **72** and mechanism involved. **d** Selectivity profile of **72** for Hg^{2+}. (Refer to the web version of this article for the legend colour). Reproduced from Ref. 74 with permission of RSC

phenomenon takes place, leading to the recovery of fluorescence for **70**. The authors claim their designed material **70** is a reusable, highly sensitive and selective probe for the detection of important heavy metal ions like Cu^{2+} and Cr^{3+} ions [73].

Later, in 2017, Li and co-workers strategised a fluorescent nanoprobe **72** based on cellulose nanocrystals with pendant porphyrin molecules for the selective and quantitative detection of trace amounts of Hg^{2+}. As depicted in Fig. 28c, the nanoprobe **72** consists of CNC, porphyrin pendant, aliphatic ester group, hydroxyl group and sulfonic acid group. Nanoprobe **72** shows ratiometric turn-on detection of Hg^{2+} even in the presence of different counter analytes at an emission intensity of 628 and 652 nm (Fig. 28d). The detection limit of Hg^{2+} by nanomaterial **72** is estimated as 50 nM. According to the authors, the good dispersion of CNCs and the high selectivity of porphyrin pendants resulted in the efficient and selective detection of Hg^{2+} in water [74].

Haung and his group applied a chemical modification technique for the fabrication of CNCs with fluorescent coumarin moiety for the formation of **73** and later employed it for the selective detection of Cu^{2+} ions (Fig. 29a). At first, the CNC surface was modified with ethylenediaminetetraacetic dianhydride (EDTAD) which aided in achieving a high degree of carboxylation, crystalline structure and surface integration utilizing the TEMPO oxidation method. Further, the modified CNCs were doped with fluorescent 7-amino-4-methylcoumarin (AMC) to generate **73**. Cellulose material **73** is capable of selectively detecting Cu^{2+} with turn-off emission. Probe **73** showed good chelating property for Cu^{2+} ions. However, the quenching profile achieved is quite weak and so lags behind other reported probes in the field. The fluorescence quenching phenomenon of **73** in the presence of Cu^{2+} was estimated at 390 versus 440 nm. Probe **73** can detect Cu^{2+} as low as 0.5 ppm. The authors think that the proposed strategy of material **73** for Cu^{2+} is applicable

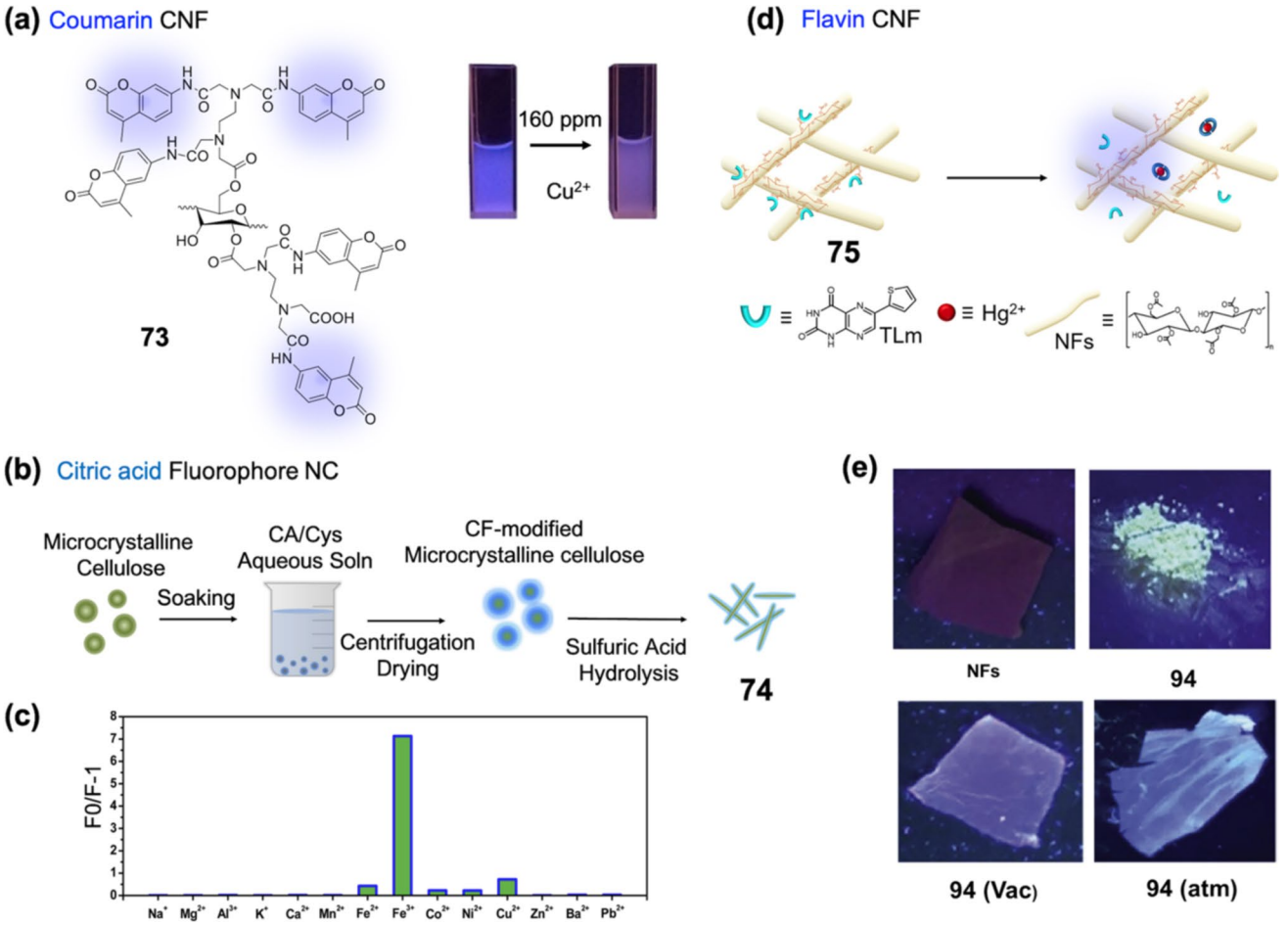

Fig. 29 **a** Chemical structure of cellulosic probe **73** and thereby visible detection of Cu^{2+}. (Refer to the web version of this article for the legend colour). Reproduced from Ref. 75 with permission of Springer. **b** Method for the preparation of **74**. **c** Fluorescence selectivity profile of **74** for Fe^{3+}. (Refer to the web version of this article for the legend colour). Reproduced from Ref. 76 with permission of Elsevier. **d**, **e** Preparation and utility of **75** for detection of Hg^{2+}. (Refer to the web version of this article for the legend colour). Reproduced from Ref. 77 with permission of Elsevier

for optical imaging and real-time sensing of the important analyte [75]. In 2019, Xu and his team utilised fluorophore-modified CNCs **74** as a biocompatible fluorescent probe for the detection of ferric ions and intracellular imaging. As depicted in Fig. 29b, the citrate-derived fluorophore modified on CNC **74** was prepared by using sulphuric acid hydrolysis of citric acid/cysteine-treated microcrystalline celluloses. The CNC **74** had a rod-like structure having an average length of 156 nm and width of 7.9 nm. The conjugation of citric-fluorophores aided in typical fluorescence characteristics of CNC material **74**. Probe **74** showed fluorescence emission at 435 nm on exciting at 350 nm. Probe **74** displayed good photostability and high quantum yields of 83%. Figure 29 c shows the selective quenching profile of **74** for Fe^{3+} ions, even in the presence of different cations. The free carboxylic groups in **74** aid in the selective chelation of Fe^{3+} ions, instantly leading to fluorescence quenching of **74**. CNC material **74** exhibits negligible cytotoxicity and is easily internalised by cells. Hence, CNC material **74** can be applied for the detection of Fe^{3+} ions in living cells [76]. Saleh and co-workers introduced 6-thienyllumazine (TLm) fluorophores into cellulose acetate nanofibres (CNFs) to produce **75** and used them for the detection of mercuric acetate salts (Fig. 29d, e). In the solution state, the excited-state proton transfer (ESPT) from TLm to water molecules was tested in the pH range 2–12. Probe **75** was used for the detection of mercury acetate in the solid state. In the presence of mercury acetate, the solid-state emission of **75** is quenched. Moreover, the quenching phenomenon of **75** was also observed for Hg^{2+} ions in aqueous media. The coordination of Hg^{2+} ions with sulphur, oxygen and nitrogen atoms in **75** with a stoichiometry of 2:1 ligand to metal is responsible for the fluorescence quenching phenomenon. The nanofabricated sensor **75** can detect mercuric ions at a concentration of 50 pM. The interaction between CNF material **75** and mercuric ions creates a non-fluorescent ground state complex. The authors consider CNF material **75** for the real-time application of mercury ions [77].

Gao and his group developed a chiral photonic crystal membrane **76** based on CNCs by molecular assembly for the detection of formaldehyde (HCHO). As depicted in Fig. 30a, CNC material **76** constitutes **77** and a PEG 2000 moiety. CNC material **76** forms a hypersensitive fluorescent off–on switch, well characterised by changes in the UV–Vis spectrum and the texture of the liquid crystal. As the concentration of HCHO increases, a significant red shift in the reflectance peak of the membrane is noticed from 498 to 736 nm. Moreover, the changes in colour and fluorescence of **76** in the presence of HCHO can be observed by the naked eye. Photo-induced electron transfer (PET) is observed between hydrazine moiety and the naphthalimide fluorophore in **76**. The addition of formaldehyde to 76 causes the inhibition of PET mechanism, causing turn on in the emission profile of **76**.The detection mechanism and naked eye changes of **76** in HCHO are shown in Fig. 30b [78].

Another interesting illustration of a cellulose nanocrystal-based Hg^{2+} sensor was provided by Zhou and co-workers. In their work, Zhou and his group labelled CNCs with rhodamine and applied it as a selective colourimetric and fluorescence sensor for Hg^{2+} in an aqueous solution. The average dimension of **78** was about 18–20 nm in width and 160–180 nm in length. The detection mechanism of probe **78** for Hg^{2+} is depicted in Fig. 31a. Briefly, Rhodamine B-CNC (**78**) has a closed spirolactam ring responsible for colourless and quenched nature of probe **78**. The chelation of Hg^{2+} ions with 78 leads to the spirolactam ring opening phenomenon aiding in pink colouration and fluorescence turn-on profile of **78**. Moreover, probe **78** shows a selective turn-on (Fig. 31b) profile towards Hg^{2+} even in the presence of various counter analytes. CNC material **78** is capable of detecting Hg^{2+} in the pH range of 3–12. The fluorescent and colourimetric detection limits for **78** towards Hg^{2+} were determined as 232 nM and 746 nM, respectively. The authors assume that CNC **78** can be used for chemosensing, bioimaging and sewage treatment–based applications [79]. Fox and his group utilised another fluorescent dye, BODIPY, to label cellulose nanofibres to create 7**9** for the determination of environmental health and safety. The authors aimed to synthesise chemically and enzymatically stable BODIPY-labelled CNF **79** for imaging in biological systems such as the gastrointestinal tract system (Fig. 31c). CNF **79** can show fluorescence in a wide pH range between 2 and 10. The toxicity of **79** was tested in in vitro small intestinal epithelial models and in vivo zebrafish (Fig. 31d) experiments [80].

In a similar report, by Zhu and co-workers, an AIE luminogen was labelled with cellulose nanocrystals (CNCs) for the rapid detection of Fe^{3+} in aqueous solutions. Here, the authors have modified CNCs with tetraphenylethylene (TPE)-based AIE active fluorophore to form CNC material **80** (Fig. 31e). CNC **80** has high selectivity (quenching) (Fig. 31f) and sensitivity for Fe^{3+} in the pH window 4 to 10. The 'O' and 'N' groups in **80** are attributed for the selective complexation of Fe^{3+}. However, Fe^{3+} is known to be a paramagnetic quencher with unfilled *d*-shell. These unfilled *d*-shell in Fe^{3+} engage in energy or electron transfer mechanism with the fluorophore (TPE), resulting in the fluorescence quenching of **80**. The limit of detection of **80** for Fe^{3+} was determined as 264 nM. The authors predict that CNC material **80** can be utilised for the visual detection of Fe^{3+} in drinking water quality. However, CNC **80** is a quenching probe and hence applicability is doubtful [81]. Kaushik and her team (2022) decorated fluoranthene with cellulose nanofibres, producing **81** (Fig. 31g) applicable for the ultra-trace level detection and annihilation of Arsenic(III) (Fig. 31h). The fluorescence response of 81 is accredited to the metal chelation and simultaneous inhibition

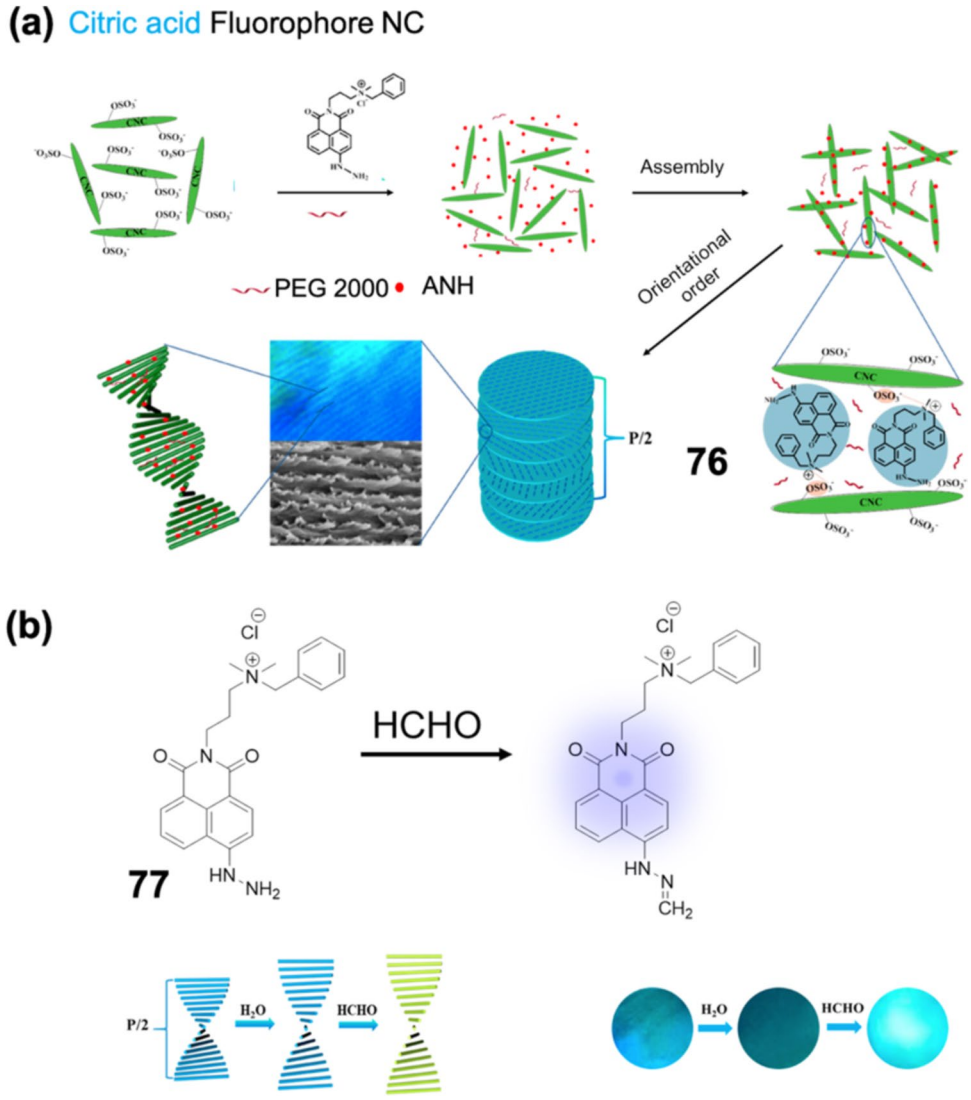

Fig. 30 **a** Procedure for the synthesis of **76** used for the detection of HCHO. **b** Detection mechanism of **77** for HCHO and its visual detection. (Refer to the web version of this article for the legend colour). Reproduced from Ref. 78 with permission of ACS

of PET phenomenon of 81 in the presence of Arsenic(III). The cellulose nanofibres used in this work were sourced from biomass wheat straw. The morphological and thermal properties of **81** were confirmed using FTIR, TGA, XRD, FESEM, EDS and TEM. The LOD for metal ion chelation (Arsenic (III)) by **81** was estimated as 2.8 ng L^{-1}. The CNF material **81** showed excellent stability and reusability. However, the authors do not mention the real-time applicability of material **81** [82].

In 2021, Cai and their team utilised functionalised nanocrystal cellulose with a 'rigidity-tensile' joint approach, for generating acicular geometry and high crystallinity of formed heterogeneous nuclei–based polyurethane crystals **82** and **83**. Use of functionalised nanocrystal cellulose is credited for the improved tensile strength and Young's modulus of **82** and **83**. As represented in Fig. 32a, the dual network structure of **82** and **83** consists of three different components such as a functionalised nanocrystal cellulose unit, a polyurethane moiety, and fluorescent agents. The so-developed cellulosic materials **82** and **83** depict reversible shape memory characteristics and diverse on and off display patterns under UV light (Fig. 32b). Therefore, the authors see a potential for the application of **82** and **83** in anti-counterfeiting applications [83]. As mentioned several times in this review, the abundance of hydroxyl groups on the surface of CNC allows it to hybridise with multiple optically active components. Taking the mentioned fact into consideration, Zhang et al. developed a multimodal switchable chiral optical platform **84** by adhering fluorescent lanthanide complexes on the surface on CNC and further utilizing it for anti-counterfeiting applications (Fig. 32c). The so-developed CNC material **84** displayed a full-colour appearance and bright photoluminescence with a genuine fluorescent lifetime of 510 µs accompanied by a quantum yield of 66.7%. Moreover, the developed **84** films exhibit a rare right-handed circular polarisation emission with an

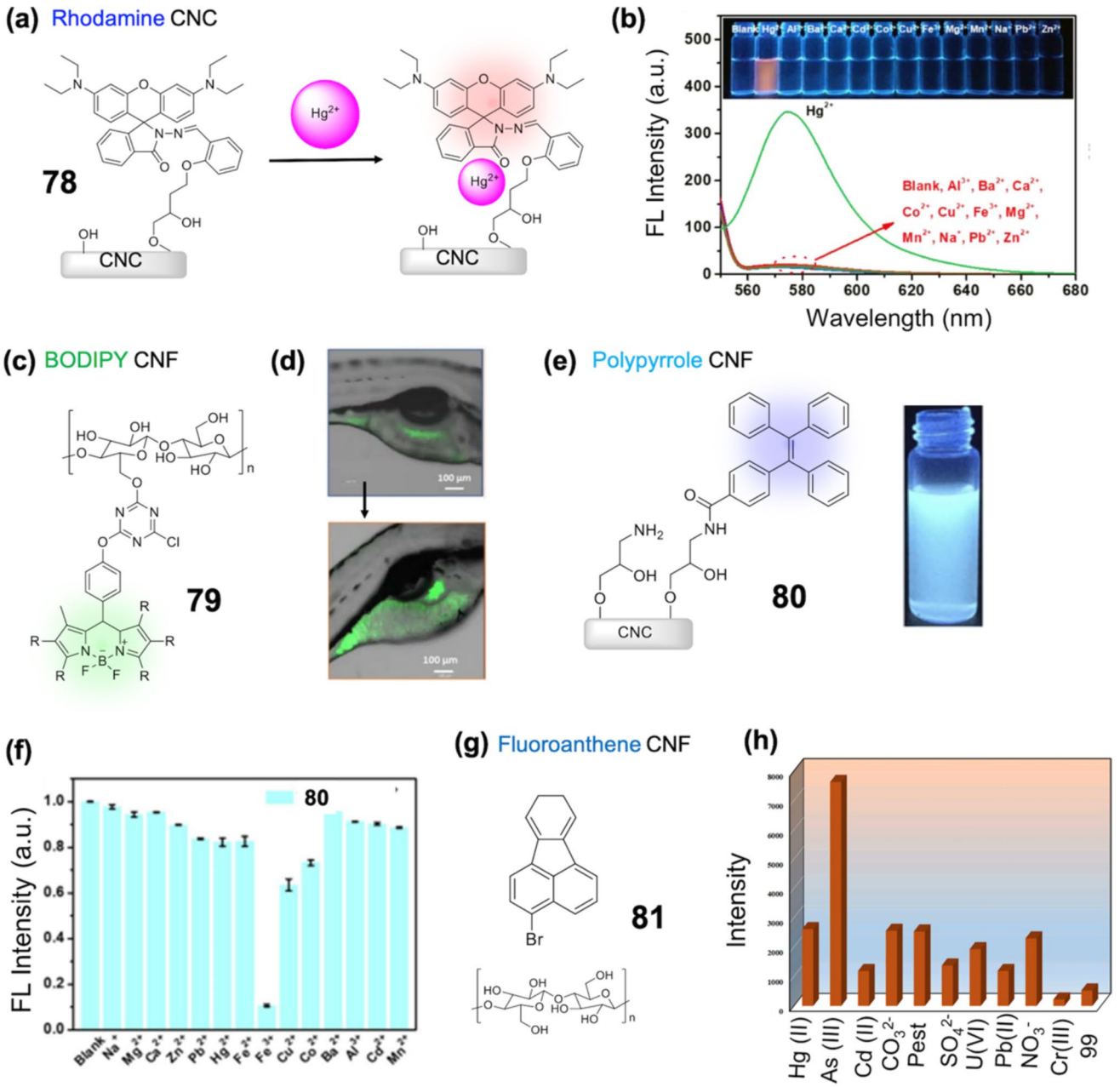

Fig. 31 **a** Chemical structure and detection mechanism of **78** for Hg^{2+}. **b** Fluorescence selectivity profile of **78** for Hg^{2+}. (Refer to the web version of this article for the legend colour). Reproduced from Ref. 79 with permission of Springer. **c** Chemical structure of BODIPY CNF molecule **79** for application in imaging. **d** **79** labelled in vitro study for estimation of toxicity. (Refer to the web version of this article for the legend colour). Reproduced from Ref. 80 with permission of MDPI. **e** Chemical structure of CNC molecule **80**. **f** Utilisation of **80** for the fluorescence quenching–based selectivity of Fe^{3+}. (Refer to the web version of this article for the legend colour). Reproduced from Ref. 81 with permission of RSC. **g** Chemical structure of CNF-based probe 81. **h** Fluorescence selectivity of As(III) by **81**. (Refer to the web version of this article for the legend colour). Reproduced from Ref. 82 with permission of Elsevier

elevated asymmetry factor of − 0.36. Moreover, the film **84** also displayed dynamic polarisation-sensitive colour switching. In the current work, the authors have integrated different features like chiral optical properties, structural colour, fluorescent colour and circularly polarised luminescence (CPL) into a single composite **84** with the logical and autonomous encoding of each optical state (Fig. 32d). The authors consider **84** to have great potential for utility as a multi-modal anti-counterfeiting label on model banknotes and other practical applications [84].

From earlier reports, it can be concluded that CNCs have distinct chiral nematic structures which help in enhancing

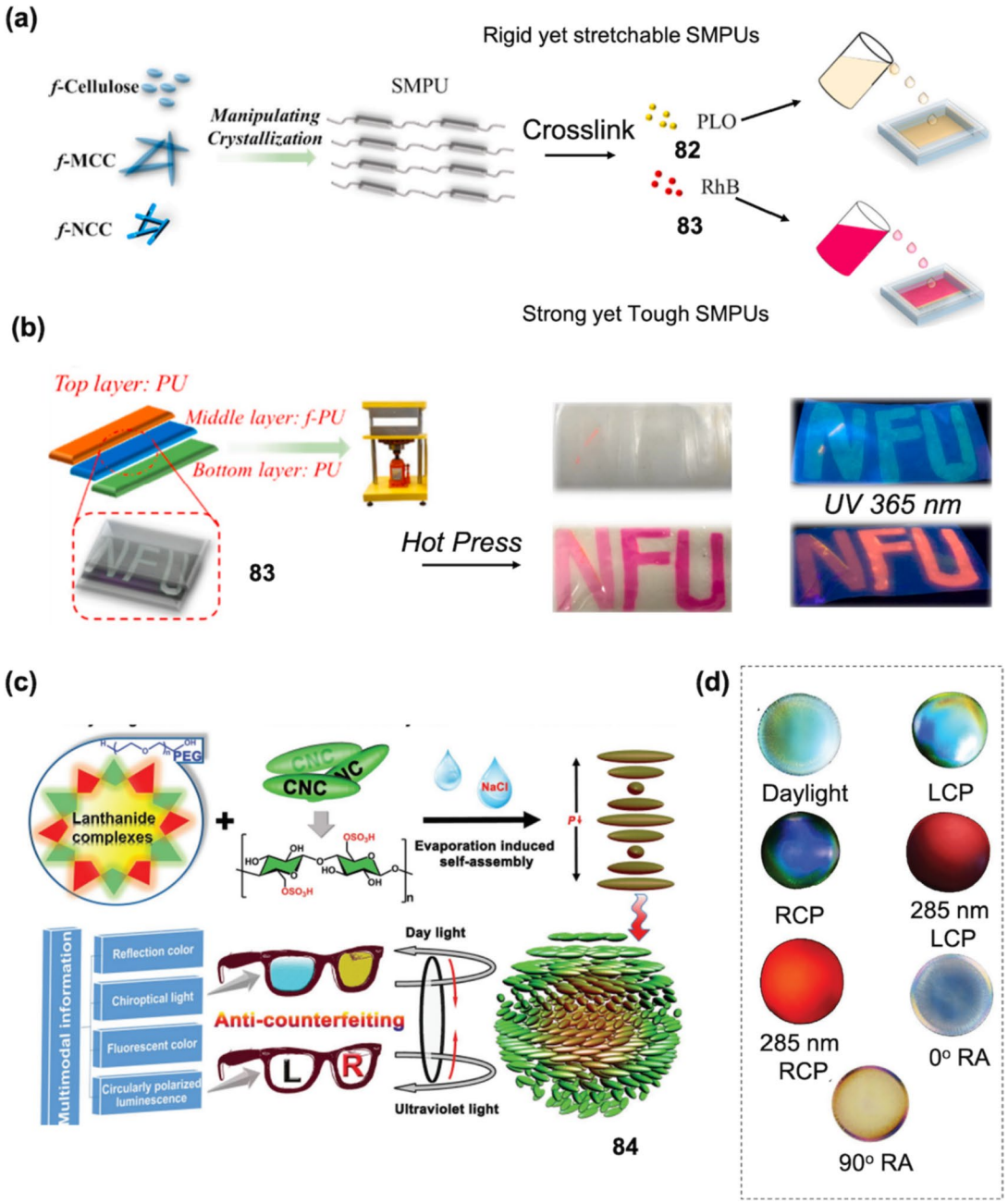

Fig. 32 **a** Method and mechanism involved in the preparation of **82** and **83** accompanied by utility in anti-counterfeiting. **b** Mechanism of application of **83** in anti-counterfeiting applications by developing a device. (Refer to the web version of this article for the legend colour). Reproduced from Ref. 83 with permission of Elsevier. **c** Complete illustration of generation and working mechanism of **84**. **d** Chiro optical characterisation performed for **84**. (Refer to the web version of this article for the legend colour). Reproduced from Ref. 84 with permission of Wiley

the optical properties of materials. However, CNCs lack in mechanical performance and have poor hydrophobicity resulting in lower practicality. In 2022, Yuan and coworkers developed chiral nematic composite films **85** and **86** by incorporating polyethylenimine (PEI) in the prolonged CNC film matrix (Fig. 33c, d). The so-developed CNC films **85** and **86** exhibited improvement in physical qualities like toughness and strain accompanied with extremely high folding resistance. Moreover, CNC films **85** and **86** displayed superior cryptographic properties with excellent optical responding capability. Moreover, to create a 3D crosslinked network, a water-soluble substrate polyethylene glycol diacrylate (PEGDA) was introduced into **85** and **86** by UV curing technique. Moreover, the crosslinking network in

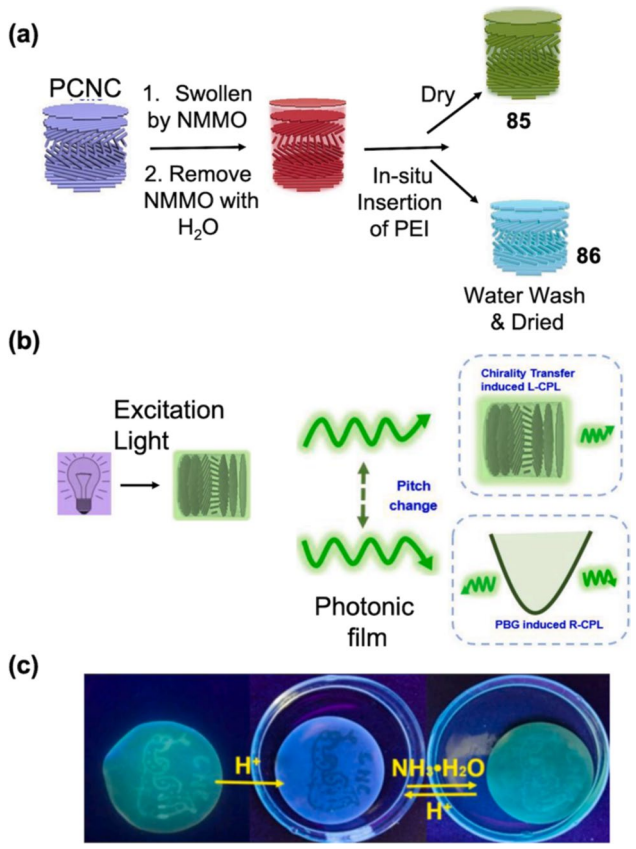

Fig. 33 **a** Schematic diagram depicting the fabrication of chiral nematic **85** and **86** composite films. **b** Example of the possible mechanism involved in chiral photonic films **85** and **86**. **c** Reversible fluorescence emission of the snake-patterned film, which is quenched by addition of 0.01 mol L^{-1} HCl solution and then recovered by 0.01 mol L^{-1} ammonia solution. (Refer to the web version of this article for the legend colour). Reproduced from Ref. 85 with permission of Elsevier

85 and **86** aided in improving its water resistance capabilities (Fig. 33e). In these works, variant crosslinking degree materials of **85** and **86** are formed, which ultimately aided in improving the practical applicability and cyclic stability as anti-counterfeiting labels [85].

3.2.2 Colourimetric-based nanofibres and nanocrystals

In early 2016, Shankaran and co-workers developed curcumin-loaded biocompatible nanofibres (CNFs) **87** (Fig. 34a) for Pb^{2+} ion detection. The Pb^{2+} probe **87** was synthesised by combining cellulose acetate nanofibres with curcumin. The average diameter of the optimised CNF material **87** was determined as 104 nm. CNF material **87** showed high selectivity with naked-eye colourimetric change (Fig. 34b) for Pb^{2+} in the presence of other counter cations. In the presence of Pb^{2+}, curcumin-Pb^{2+} complex is formed that allows the colourimetric changes in **87**. CNF material **87** can detect very low levels of Pb^{2+} (20 µM) in the aqueous solution. The authors claim that **87** was the first reported material for Pb^{2+} detection based on curcumin nanofibres. They also confirm that CNF material **87** shows promising effects if used for the development of low-cost disposable sensors for rapid and real-time applications [86]. Later in 2018, Lee and his group introduced cellulose nanocrystal-derived coloured thin films for the colourimetric detection of aldehyde gases. The CNC film **88** was created by dip-and-pull process by aiding the close packing of CNC on a solid surface by utilizing ionic-liquid (1-butyl-3-methylimidazolium) molecules which also helps in screening the repelling electrostatic charges between CNCs. The thickness of the film was controlled between 100 to 300 nm. The CNC film **88** was surface-modified with amine functionalities using APTES (Fig. 34c, d). The amine groups aided the binding of aldehyde moieties to **88**, which caused colourimetric changes to the film (Fig. 34e). The authors expect that this approach (i.e., **88**) will enable rapid and inexpensive colourimetric detection of volatile organic compounds and also on-site monitoring capabilities [87].

Chauhan and his team developed a spherical nanocellulose-based material **89** for the efficient and rapid multifunctional naked-eye detection of Cr(VI). In the presence of Cr(VI), selective colourimetric change in **89** was observed from colourless to orange (Fig. 35a). The efficient absorption Cr(VI) of onto **89** is attributed to the selective colour change of **89**. The spherical nano cellulose **89** can detect Cr(VI) as low as 30 ppb at naked eyes. The mild antimicrobial activity of **89** was also tested [88]. In another work, Khayatian and co-workers (2019) reported a nanocellulose-based colourimetric assay kit for efficient smartphone sensing of Fe^{3+} and Fe^{3+}-chelating deferoxamine drug in biofluids. The colourimetric assay kit **90** was produced by embedding curcumin in transparent bacterial cellulose (BC) nanopaper (Fig. 35b). In the presence of Fe^{3+} and Fe^{3+}-chelating deferoxamine drugs, the absorbance/colour intensity of **90** is decreased (Fig. 35c). The formation of Fe^{3+}-curcumin complex decreases the colour intensity of curcumin embedded on bacterial cellulose nanopaper surface (Table 1) of **90**. Further, owing to the stronger chelation property of deferoxamine for Fe^{3+}, the Fe^{3+}-curcumin complex disrupts, resulting in recovery of the colour intensity of **90**. Material **90** was utilised for detection of Fe^{3+} and Fe^{3+}-chelating deferoxamine drug concentrations in biofluid samples like human serum blood samples, revealing the clinical applicability of the developed assay kit. The authors consider that cellulosic material **90** can be applicable for the sensitive, selective and easy diagnosis of iron-related diseases [89]. In the same year, Maghsoudi and his group developed a curcumin-fabricated bacterial nanocellulose material as an assay kit **91** for albumin (Fig. 35d). The authors claim that **91** has excellent optical transparency, porosity, high flexibility, biodegradability and printability. For the attachment of albumin onto **91**, the hydrophilic zones

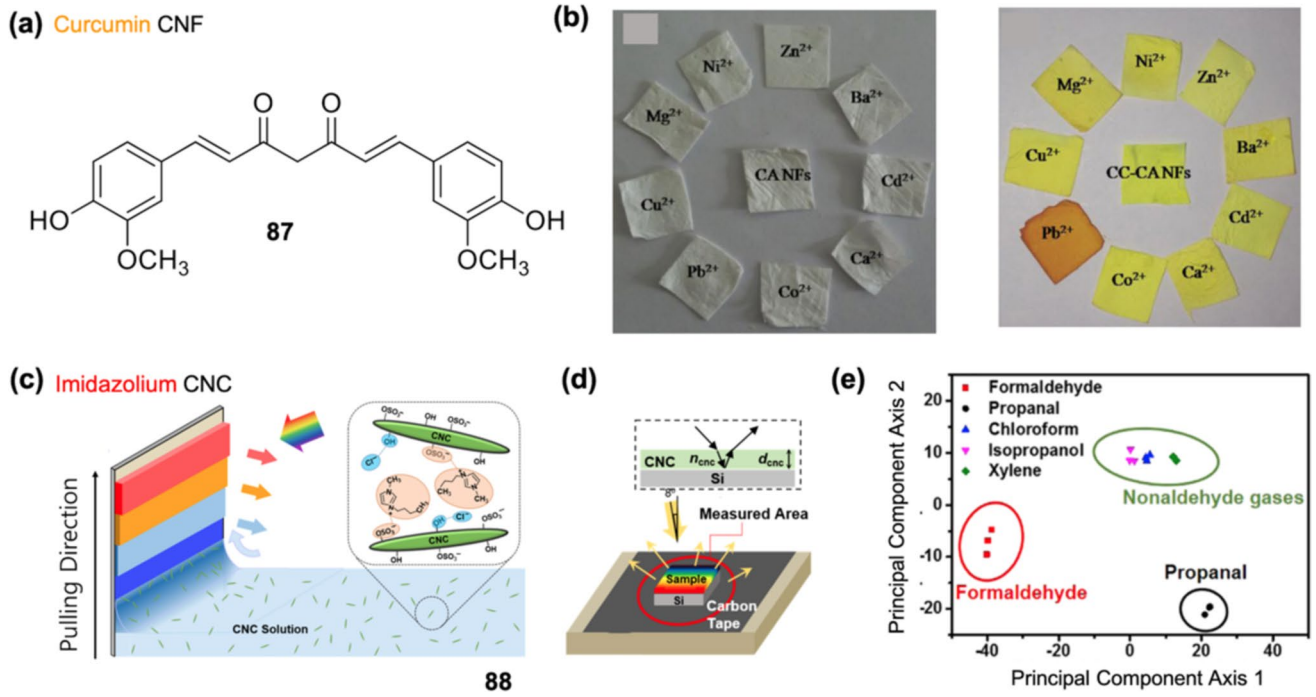

Fig. 34 **a** Chemical structure of curcumin-CNF material **87**. **b** Visual eye selectivity profile of **87** for Pb^{2+}. (Refer to the web version of this article for the legend colour). Reproduced from Ref. 86 with permission of Elsevier. **c** Schematic depicting the complete fabrication and preparation of **88**. **d** Schematic illustration of the optical measurement setup. **e** Principal component analysis (PCA) plot of the colour shifts of both aldehyde (black, red) and other nonaldehyde gases (magenta, blue, green) showing the selectivity profile of the colour film sensor **88**. (Refer to the web version of this article for the legend colour). Reproduced from Ref. 87 with permission of ACS

are created on the fabricated bioplatform by creating hydrophobic walls utilising laser printing technology (Fig. 35e). The colour change of **91** is accredited to the inhibitory effect of HSA on the curcumin degradation in alkaline solutions. Cellulosic material **91** can be applied for the visual detection of human serum albumin (HSA) in the concentration range 10–300 µM and 25–400 µM. The authors predict the applicability of cellulosic assay **91** for HSA for the development of next-generation optical biosensing platforms [90].

3.3 Cellulose nanodots

Carbon or quantum dots are generally defined as an interesting class of carbon nanoparticles that majorly consists of carbons with sizes of approximately 10 nm [244]. Carbon and quantum dots show strong fluorescent and colourimetric properties due to their strong quantum confinement with tunable optoelectronic and photoluminescence [245]. Carbon and quantum dots are widely used in many fields like in vivo imaging [246], cell imaging [247], drug delivery [248], photocatalysis [249], fluorescence sensing [250], multicolour light-emitting diodes (LEDs) [251], energy conversion and storage [252]. Carbon and quantum dots are synthesised using top-down (electrochemical oxidation [253], arc discharge [254] and laser ablation [255]) and bottom-up approaches (pyrolysis [256], micro-wave assisted method [257], ultrasonic method [258] and solvothermal method [259]). The raw materials for the synthesis of carbon and quantum dots are classified as organic and inorganic carbon sources. However, in practice, organic carbon sources such as organic natural products and biomass waste (cellulose comes under this category) and organic compounds are extensively utilised in the preparation of carbon and quantum dots [260]. In this section, carbon and quantum nanodots either generated from cellulose substrates or modified on cellulose molecules and their application in the development of fluorescent chemosensors will be discussed.

Zhang and co-workers implemented a hydrothermal strategy for the synthesis of water-stable fluorescent carbon dots (CDs) as nanosensors for monitoring pH and temperature. The carbon dots **92** was achieved by the hydrothermal treatment of glucose (GLC) in the presence of glutathione (GSH) (Fig. 36a). The hydrothermal method of synthesis aids the simultaneous formation and surface passivation of CDs. Reaction temperature, feed ratio (GSH/GLC) and reaction time influence the photoluminescence properties of CDs. Figure 36 b and c depict the utility of **92** in the detection of pH. Probe **92** has a pronounced temperature dependence and underwent temperature and pH-induced aggregation. The authors claim that CDs **92** if combined with cellulose

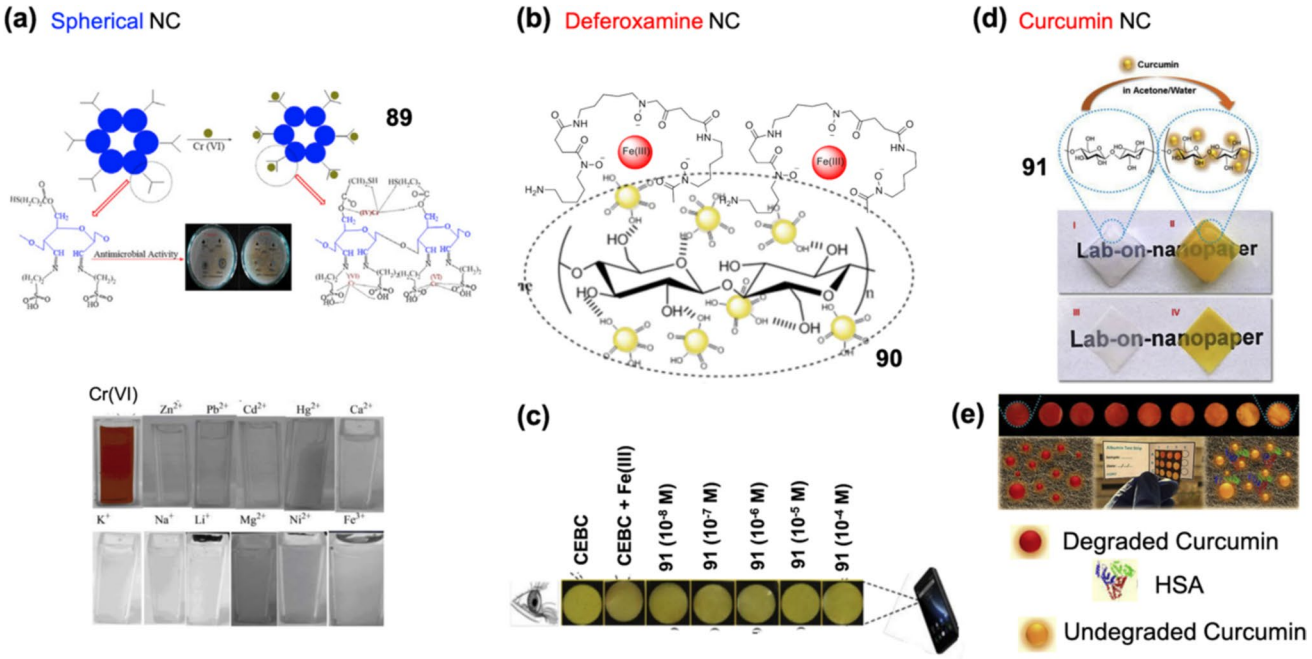

Fig. 35 **a** Chemical structure and mechanism for the development of **89** (top) with visible colourimetric change in the presence of Cr(VI) (bottom). (Refer to the web version of this article for the legend colour). Reproduced from Ref. 88 with permission of Elsevier. **b** Chemical structure of the deferoxamine nanocrystal. **c** Colourimetric naked eye changes occurring in **90** after addition of varied concentrations of Fe^{3+}. (Refer to the web version of this article for the legend colour). Reproduced from Ref. 89 with permission of Elsevier. **d** Structural components in nanopaper **91**. **e** Visible detection of HSA by **91**. (Refer to the web version of this article for the legend colour). Reproduced from Ref. 90 with permission of Elsevier

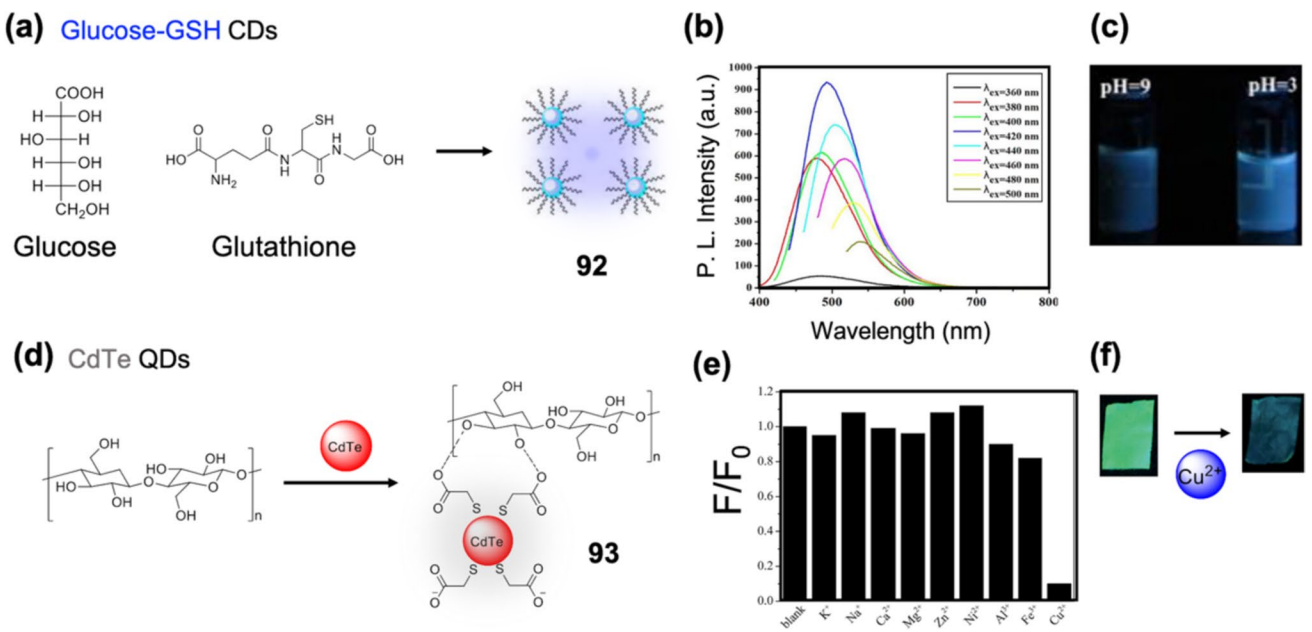

Fig. 36 **a** Synthetic method for the formation of **92**. **b** Photophysical property of **92** at variant wavelengths. **c** Visible fluorescence changes in the profile of **92** with varying pH. (Refer to the web version of this article for the legend colour). Reproduced from Ref. 91 with permission of Elsevier. **d** Synthetic procedure for the preparation of CdTe QDs/BC nanocomposite **93**. **e** Quenching-based selectivity profile of **93** for Cu^{2+} in the presence of other counter analytes. **f** **93** doped cellulose paper for the visual detection of Cu^{2+}. (Refer to the web version of this article for the legend colour). Reproduced from Ref. 92 with permission of RSC

paper can be used for the real-time monitoring of pH and temperature in real samples [91].

In the same year, Wang and his group utilised a different strategy for the development of colour-tunable luminescent CdTe quantum dots (QDs). In the report, CdTe-derived QDs were transformed into sensor membranes by fabricating with bacterial cellulose (BC) forming **93** (Fig. 36d). In the synthesis of CdTe, no N2 protection, special ligand or a particular treatment was required. Cellulosic Qd material **93** showed selective quenching (Exi = 370 nm) for Cu^{2+} even in the presence of different counter metal ions (Fig. 36e, f). Surface defects are generated on the quantum dots when combined with Cu^{2+} ions to a non-radiative recombination of the excitons followed by fluorescence quenching. Cellulosic QD material **93** can detect Cu^{2+} as low as 0.016 mM. The CdTe QDs on BC membranes **93** show high detectability and applicability for the detection of Cu^{2+} in real samples. However, the efficacy of **93** for $Cu.^{2+}$ is doubtful owing to the quenching profile [92]

Later, Zhuo and co-workers introduced CDs as versatile carbon-based nanomaterials developed using acidic ionic liquid as catalysts. As depicted in Fig. 37a, the CDs **94** were prepared from microcrystalline cellulose (MCC) using 1-butyl-3-methylimidazolium chloride ([Bmim]Cl) as a solvent and SO_3H-functionalised acidic ionic liquid (SO_3H-IL) as a catalyst. The cellulosic QDs **94** show excellent water solubility and photostability. In the presence of Hg^{2+}, the photoluminescence profile of cellulosic QDs **94** was quenched (turn-off) with excitation wavelength at 360 nm and emission at 450 nm (Fig. 37a, b). **94** can detect Hg^{2+} in the concentration range of 6 to 80 µM (Fig. 37c). The authors assume that the carboxylic and hydroxyl groups in **94** are favourable for Hg^{2+} over other metal ions. The authors confirm that **94** can be utilised for the detection of inorganic Hg^{2+} in drugs, biological products and fish samples [93]. In 2016, Tang and his team reported acidophilic S-doped carbon quantum dots (CQDs) **95** synthesised from cellulose fibres capable of detecting metal ions in extremely strong acid environments. The CQDs **95** was synthesised from widely available cellulose fibres. The cellulose fibres act as carbon precursors and sulphuric acid was utilised as the carbonization agent and dopant in the formation of **95** (Fig. 37d). The CQD material **95** demonstrated extremely acidophilic high luminescence and high quantum yields of 32% in strong acid solutions. Cellulosic CQDs **95** exhibited a very high selectivity accompanied by fluorescence quenching for Fe^{3+} ions. The high selectivity is attributed to the rapid electron transfer between Fe^{3+} ions and the surface of electron-rich oxygen containing CQDs. The detection limit of **95** for Fe^{3+} was estimated as 0.96 µM. The cellulosic CQDs **95** exhibited excellent selectivity and sensitivity for the detection of Fe^{3+} at very acidic pH (Fig. 37e, f). The limit of detection of **95** for Fe^{3+} at pH 0 is estimated as 0.96 µM. The authors claim that **95** CQDs lay the foundation for the detection of metal ions at acidic pH [94].

Krull and co-workers, in 2017, employed aptamer-linked QD **96** and fabricated it on cellulose paper for the detection of cancer biomarker protein. Cellulose-modified QD **96** showed FRET-based detection of epithelial cell adhesion molecule (EpCAM) (Fig. 38a). Probe **96** constitutes aptamer-linked QDs and Cy3 labelled complementary DNA (cDNA), which act as a donor and acceptor, respectively. Competitive binding of EpCAM with cDNA present in **96** results in the reduction of FRET emission. The paper-based bioassay **96** was able to detect cancer biomarker protein EpCAM in buffer solution as well as in 10% bovine serum solution. Paper-based bioassay **96** showed a limit of detection 250 pM in the dynamic range 1–100 nM (Fig. 38b, c) for cancer biomarker protein EpCAM [95]. In the same year (2017), Wei and his group utilised the self-assembly of nitrogen-doped carbon dots (CDs) and anchored it on bacterial cellulose (BC) forming **97** (Fig. 38d) and applied it for the detection of Fe^{3+} ions. The nitrogen-doped carbon dots were synthesised utilizing citric acid and ethylenediamine in a facile hydrothermal technique. In the presence of Fe^{3+}, the fluorescence intensity of **97** on excitation at 350 nm is quenched (Fig. 38e). The ($–NH_2$, –COOH, –OH) groups in **97** are capable of selectively chelating Fe^{3+} forming stable Fe^{3+}-**97** complexes. The formation of this complexes leads to the electron transfer from the surface of **97** causing fluorescence quenching phenomenon. The detection limit of cellulose-modified **97** for Fe^{3+} was estimated as 84 nM. The authors predict that material **97** can be used for the detection of Fe^{3+} ions in real-time analysis [96].

In a similar work, Wu and co-workers sourced cellulose from biowaste for the preparation of nitrogen and sulfur co-doped CDs **98** (Fig. 39a). The heteroatom-doped CDs come with a high quantum yield of 13.3%. The nitrogen and sulfur functional groups in **98** were achieved by the burning of urea and sulphuric acid. The cellulose-derived CD **98** were further used for the selective detection of Fe^{3+} ions (Fig. 39b, c) in biological samples. Electron transfer mechanism between the surface of **98** and Fe^{3+} ions is accredited for the fluorescence quenching phenomenon. CD **98** have a diameter of 7.3 nm and demonstrated superior photostability, pH stability and low cytotoxicity. The authors have tested the Fe^{3+} detection efficacy of CD **98** in intracellular samples [97]. Later, Wei and co-workers built a 3D network structure of BC made by layer-by-layer in situ cultivation containing nitrogen-doped graphene oxide quantum dot **99** (Fig. 39d). The QDs were homogeneously distributed in the bacterial cellulose mats via hydrogen bonding to form **99** (Fig. 39e). The bacterial cellulose QDs **99** showed a quenching effect when in contact with Fe^{3+}. The strong coordination between Fe^{3+} ions and ($–NH_2$ and –OH) groups in **99** is held responsible for the selective quenching of fluorescence. The LOD

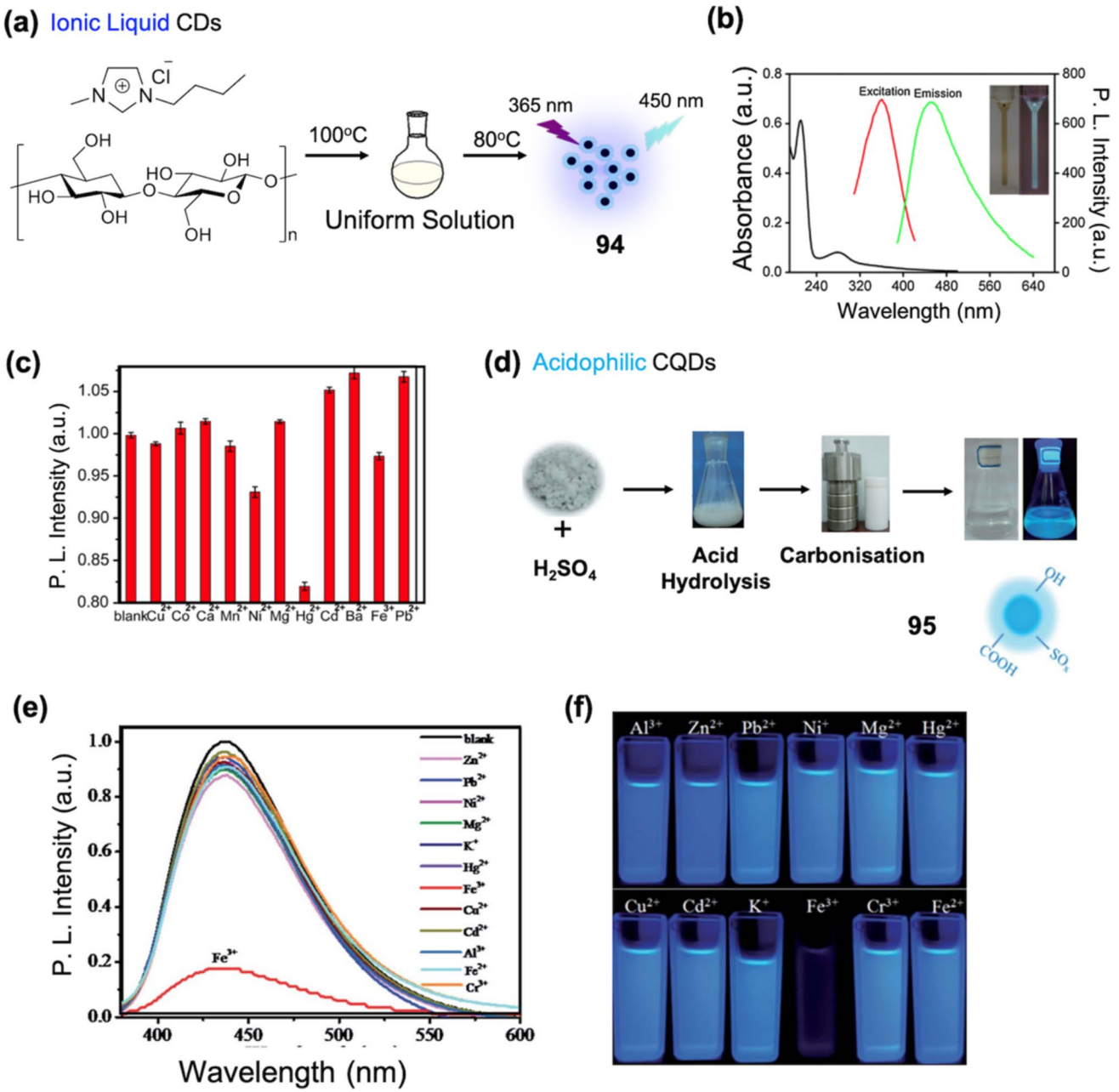

Fig. 37 **a** Synthetic track for the preparation of **94**. **b** Photophysical profile for **94**. **c** Selectivity profile of **94** for Hg^{2+} in the presence of different counter cations. (Refer to the web version of this article for the legend colour). Reproduced from Ref. 93 with permission of Springer. **d** Complete synthesis mechanism for **95**. **e** Selectivity profile of **95** for Fe^{3+} in the presence of various counter cations. **f** Naked eye selectivity images of **95** for Fe^{3+}. (Refer to the web version of this article for the legend colour). Reproduced from Ref. 94 with permission of RSC

of **99** for Fe^{3+} was determined as 69 nM. Probe **99** was utilised for the detection of Fe^{3+} in water samples [98].

In a separate effort, Lin and co-workers developed fluorescent aerogels based on the chemical crosslinking between nanocellulose and carbon dots for advanced optical sensing applications. Nanocellulose-based aerogels mentioned in this work are known for their features like sustainability, lightweight, available surface reactivity, high porosity and specific surface area. The aerogel **100** revealed in the report is attained by the crosslinking of naturally obtained cellulose nanofibre and amine-functionalised CDs (Fig. 40a). Cellulose-aerogel **100** was utilised for the sensitive and selective recognition of NO_x and aldehyde species. The fluorescence selection patterns

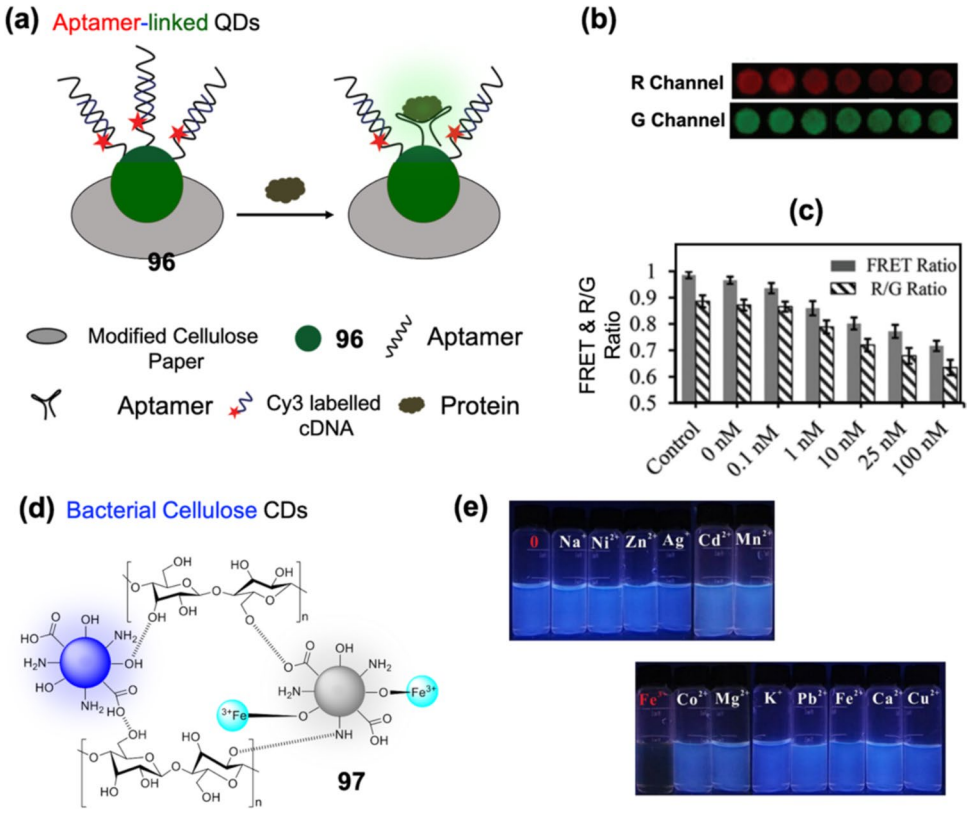

Fig. 38 **a** Procedure for the generation of **96**. **b** Red (R) and green (G) channels of digital fluorescence images and **c** FRET ratio measured from different sources using **96**. (Refer to the web version of this article for the legend colour). Reproduced from Ref. 95 with permission of RSC. **d** Chemical structure of cellulosic material **97**. **e** Naked eye detection images of **97** for Fe^{3+} under UV lamp 365 nm. (Refer to the web version of this article for the legend colour). Reproduced from Ref. 96 with permission of Elsevier

of **100** were quenched in the presence of specific gaseous and liquid molecules. The adsorption and trapping of NO_x inside the porous holes of **100** leads to the prevention of radiative recombination of electrons generated from the interaction between the electron-donating group of **100** and electron withdrawing group of NO_x, resulting in the fluorescence quenching. On the other hand, in the case of aldehyde detection, the covalent interactions between the aldehyde-groups and free amino groups in **100** are held responsible for the fluorescence quenching in aqueous medium. Moreover, for glutaraldehyde (GA) the cellulose-derived aerogel displayed high sensitivity to trap the GA molecules at ppm concentrations [99]. Later, Minami and his team designed and prepared a fluorescent spherical sponge cellulose sensor **101** for the selective and semi-quantitative visual detection of Hg^{2+} and Cu^{2+}. The spherical sponge **101** constituted of cellulose as base material and CDs generated from nitrogen-doping reagent and citric acid as an external carbon source (Fig. 40b). The microwave technique was used for the synthesis of **101**. The porous structure of fluorescent cellulose sponge **101** gave it the capability to adsorb and detect Hg^{2+} and Cu^{2+} ions. Figure 38 c depicts the selectivity mechanism and detection profile of **101** towards Hg^{2+} and Cu^{2+}. The detection limit of probe **101** is estimated as 26 nM and 20 µM respectively. According to the authors, the fluorescent cellulose sponge **101** aided in the protection of probes from environmental interference and comes with a recyclability of 22 cycles when exposed to ethylenediaminetetraacetic acid (EDTA) [100].

In 2020, Ji et al. applied fluorescent cellulose paper–based chemosensor **103** loaded with CDs for the detection of folic acid. The fluorescent paper platform **103** was constructed on a hybrid polydimethylsiloxane (PDMS)/paper platform where cellulose papers fabricated with CDs as luminophores by Schiff base chemistry were laden on the grooves array of designed PDMS plate (Fig. 41a). Under optimal conditions, fluorescent paper platform **103** enabled a rapid fluorescence quenching response towards folic acid through an inner filter effect in a wide range of 1–300 µmol/L^{-1}. The authors expect that **103** will have paramount importance for practical applications in biosensing and clinical diagnostics [101]. In another work, Sun and coworkers designed and developed a strategy for the preparation of nitrogen-doped fluorescent CD **105** by utilising oxidised cellulose by hydrothermal treatment (Fig. 41b). The cellulose-derived CD **105** are monodispersed and spherical with a mean diameter of 1.86 nm. The produced CD **105** demonstrated improved quantum yields of 16.1 and 30.3% with an oxidation treatment. CD **105** showed a selective fluorescence turn-off profile in the presence of Fe^{3+} ions (Fig. 39c). Cellulosic material **105** is rich in amino and hydroxyl groups, which strongly coordinates with Fe^{3+} forming **105**-Fe^{3+} complex, aiding in the electron transfer mechanism, leading to fluorescence

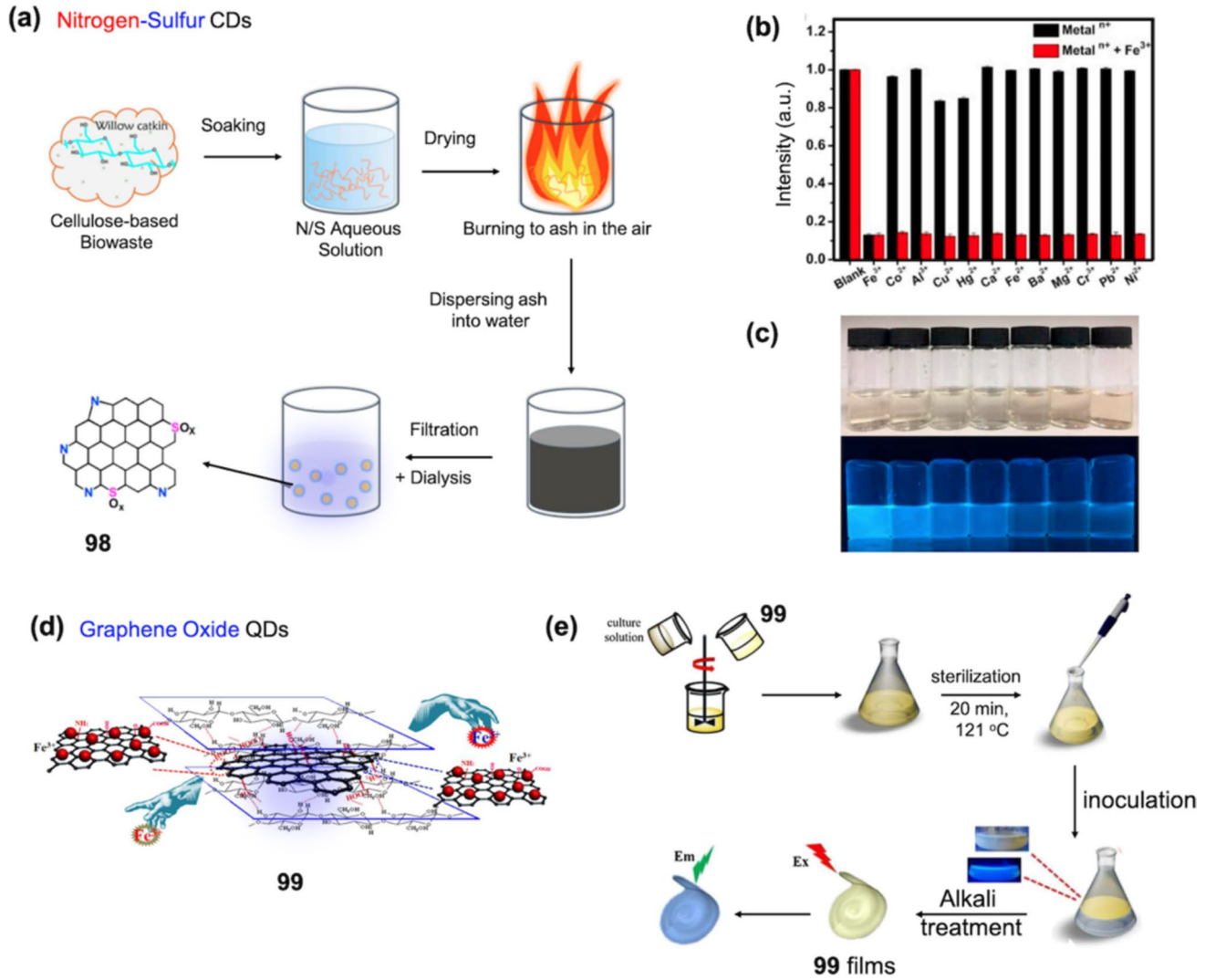

Fig. 39 **a** Procedure for the synthesis of **98**. **b** Interference-based selectivity study of **98** for Fe^{3+}. **c** Visual eye titration profile for **98** with varying Fe^{3+} concentrations. (Refer to the web version of this article for the legend colour). Reproduced from Ref. 97 with permission of Elsevier. **d** Chemical structure and complete detection mechanism of **99** for Fe^{3+}. **e** Chemical synthesis and formation of **99** films. (Refer to the web version of this article for the legend colour). Reproduced from Ref. 98 with permission of Springer

quenching. **105** was capable of detecting Fe^{3+} as low as 1.14 μM. The bioimaging applicability of **105** towards Fe^{3+} detection was tested in Vero cells (Fig. 41d). The authors confirm that **105** can be used for potential applications in sensor, biomedical and bioimaging techniques [102]. In the case of CDs, their aggregation properties limit their wide applications.

To overcome this, Zhang and co-workers synthesised two cellulosic derivatives, **106** and **107**, constituting positive and negative charges. The cellulose derivatives in **106** and **107** act as a protective shell for CDs via electrostatic interactions (Fig. 42a). The embedding of CDs onto the surface of cellulosic matrix (**106** and **107**) prevents the aggregation of CDs, hence improving the retention of its luminescence. Moreover, the use of cellulose in **106** and **107** eases the formation of films (Fig. 42b), inks (Fig. 42c), coatings (Fig. 42d) and many more anti-counterfeiting applicable products. Also, the authors consider **106** and **107** capable of applicability in information encryption [103]. In an approach to reduce waste generation, Sun et al. extracted cellulose diacetate (CDA) from wastes like discarded cigarette filters and used it as a precursor for preparing N-doped carbon dots (N-CDs). The N-CD **108** were prepared by a one-pot hydrothermal carbonization in aqueous solution using a low-cost ammonium hydroxide (passivation agent) (Fig. 42e). The so-developed **108** exhibited an overall quantum yield of 22.4% upon excitation at 320 nm with emission at 415 nm. The authors also found an excellent application for the green material by explicitly using it for the detection of tetracycline. The cellulosic N-CD **108** is capable of detecting tetracycline as

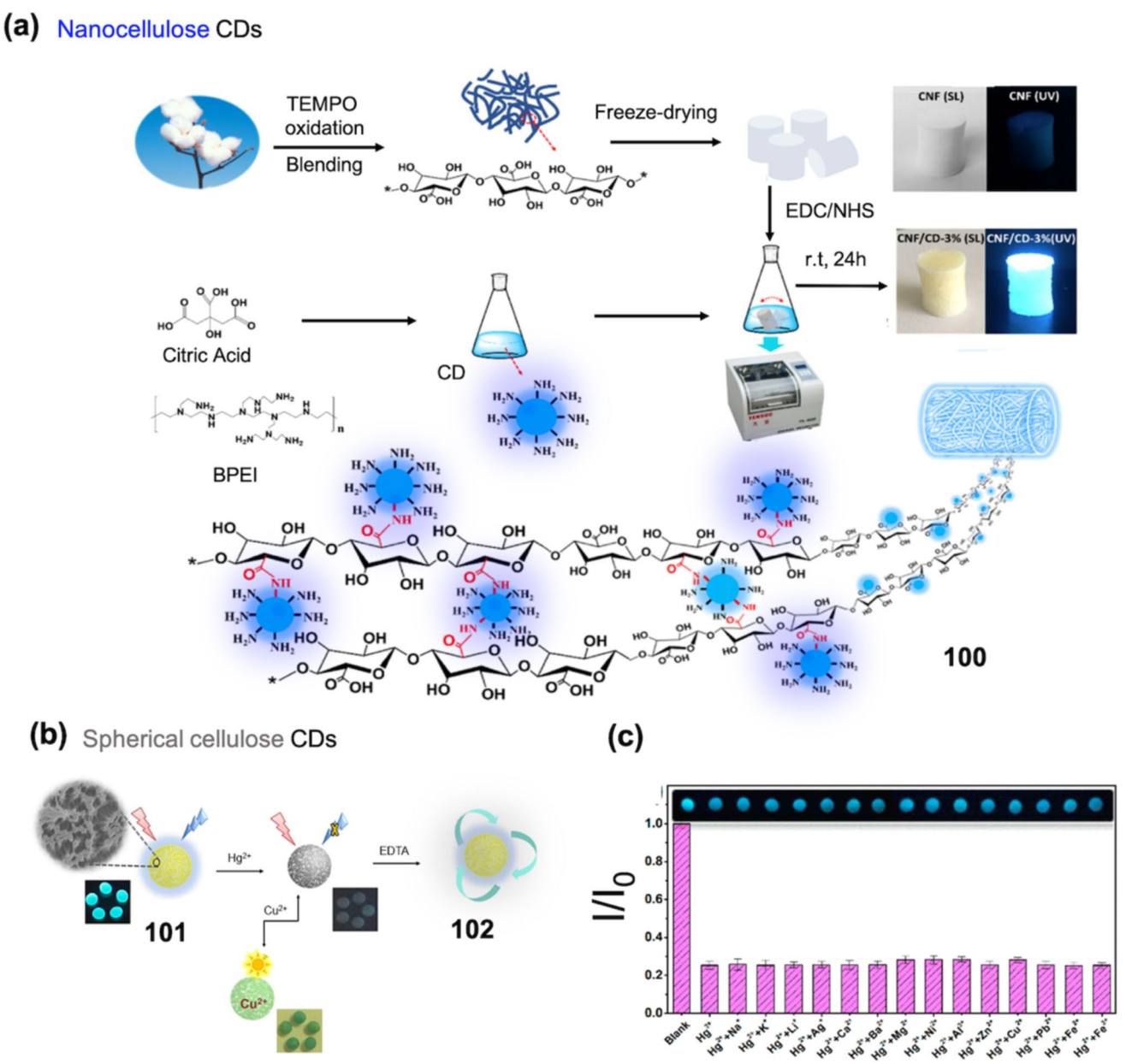

Fig. 40 **a** Complete chemical procedure and mechanism for the construction of nanocellulose QD **100**. (Refer to the web version of this article for the legend colour). Reproduced from Ref. 99 with permission of ACS. **b** Chemical structure and detection mechanism of **101** for Hg^{2+}. **c** Selectivity profile of **101** for Hg^{2+} in the presence of various other counter cations. (Refer to the web version of this article for the legend colour). Reproduced from Ref. 100 with permission of ACS

low as 0.06 µM. The authors also consider the probability of **108** for applicability in fluorescent inks for anti-forgery (Fig. 42f) [104].

Later in the same year (2020), Li and co-workers brought back the combination of quantum dots (QDs) with tunicate cellulose nanofibrils to create a nanohybrid platform **110** for application as 1D ink and 2D film. The synthesis of **110** was achieved by the technique shown in Fig. 43a. The QD factions in **110** are obtained from the CdSe/CdS core/shell, which is further homogenously blended with tunicate cellulose nanofibrils. The so-formed cellulosic nanohybrid **110** exhibits excellent writing fidelity when consumed as a 1D ink. Moreover, **110** displayed properties like good processability during generation, good flexibility and transparency (Fig. 43b). Due to such fantastic qualities of **110**, the authors recommend its utility in anti-counterfeiting technologies [105]. Nanofibrillated cellulose (NFC) is considered to possess excellent anti-counterfeiting properties like renewability, biocompatibility and easy modifiability. In 2020, Chen and their group used Yb and Er-doped CQDs

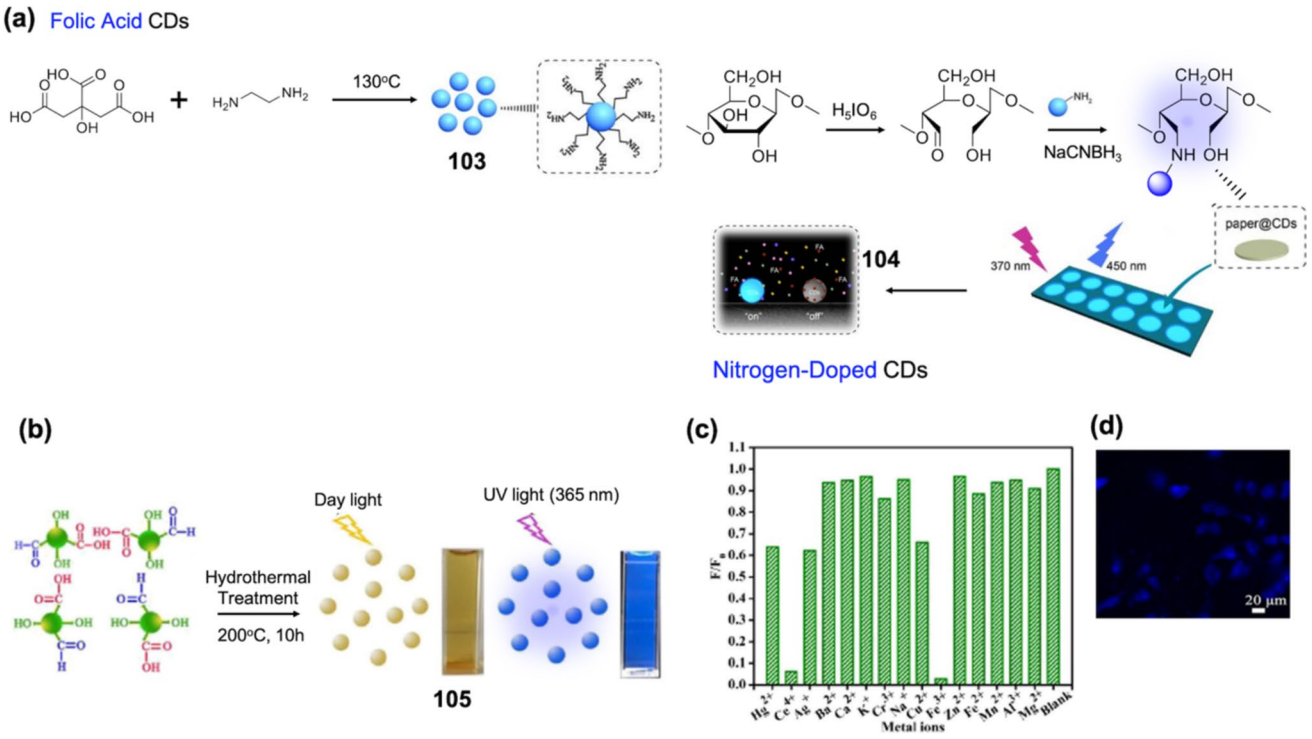

Fig. 41 **a** Complete chemical synthetic route for development of nitrogen doped CD **104**. (Refer to the web version of this article for the legend colour). Reproduced from Ref. 101 with permission of Springer. **b** Synthesis procedure for **105**. **c** Selectivity profile of **105** for Cu^{2+} and Fe^{3+}. (d) Visualisation in HeLa cells. (Refer to the web version of this article for the legend colour). Reproduced from Ref. 102 with permission of Elsevier

for grafting onto dialdehyde NFC forming **111** applicable in anti-counterfeiting technology (Fig. 43c).

The developed material NFC displayed excellent rheological properties and indeed aided in the formation of a waterborne fluorescent dual anti-counterfeiting ink **111**. The presence of Yb and Er doping in CQDs enabled dual photophysical properties of photoluminescence and up-conversion luminescence (Fig. 43d). The authors consider **111** to be productive in the generation of exceptional materials for the printing and packaging industries [106].

In 2021, Ekgasit and co-workers developed a fluorescent nanohybrid **113** constituting of ZnO QDs and cellulose nanocrystals for application as anti-counterfeiting ink. In **113** ZnO QDs, bacterial cellulose nanocrystals were combined by electrostatic self-assembly for improving solvent resistance and message encryption process (Fig. 44a). When investigated on printed areas, **113** can slightly enter into the paper fibres and form a thin layer on the top of paper substrates, conferring a heightened print permanence against wetting conditions while remaining unobservable to the naked eye in under visible light and maintaining luminescent stability. The cellulose based in **113** is water resistant enabling it to develop a higher security level that the print can be submerged in $CuCl_2$ aqueous solution resulting in quenching of luminescence (Fig. 44b). The authors consider that the cellulosic-ink **113** shows potential for use in security devices of anti-counterfeiting [107]. Yang and his group designed and developed a facile strategy for the preparation of carboxymethylcellulose-derived polymer dots (CPDs) **116** and utilised it for the detection of tetracyclines (Fig. 44c). Here, CMC and citric acid are used as precursors for synthesizing **116**. The CPDs **116** have a spherical shape, are water soluble and show blue-green emission. The average diameter of generated CPDs **116** is approximately 11.3 nm. The so-developed CPDs **116** show high selectivity for tetracycline (Fig. 40d). The CPDs **116** were capable of detecting tetracycline using an inner filter effect. The CPDs **116** can detect tetracycline with estimated detection limits of 4.1×10^{-9} M. The authors have utilised the developed CPD **116** for the detection of tetracyclines in real samples, including tap water, milk and river water [108].

In another illustration of multi-modal anti-counterfeiting labels, Li et al. developed **117** prepared by utilising a solvothermal technique for the preparation of $NaGdF_4$:Yb^{3+}, Er^{3+}@CD nanoparticles and dispersed them in hexane solution. The so-dispersed CDs exhibited visible light green emission under NIR light source of 980 nm and light blue–coloured emission while kept under 365-nm UV lamp. Final touches in the formation of **117** were added by painting the dispersed CD on the surface of cholesteric

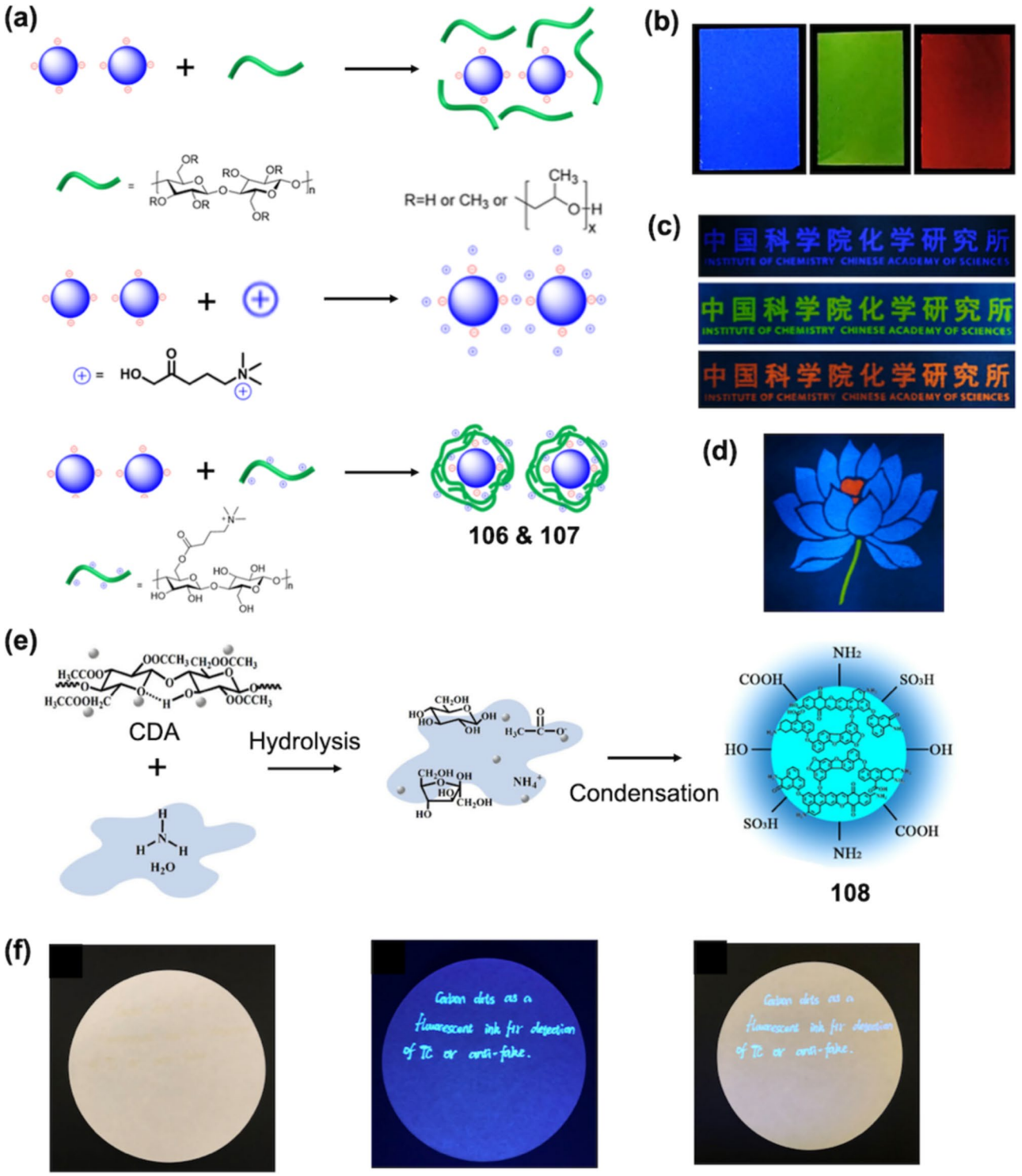

Fig. 42 **a** Complete synthetic procedure for the development of **106** and **107**. **b** Colour changes on **106** and **107** test strips. **c**, **d** Screen printing of **106** and **107** on different patterns like letters and flower. (Refer to the web version of this article for the legend colour). Reproduced from Ref. 103 with permission of ACS. **e** Synthetic route for **108**. **f** Utilisation of **108** ink in encoding and anti-counterfeiting. (Refer to the web version of this article for the legend colour). Reproduced from Ref. 104 with permission of Elsevier

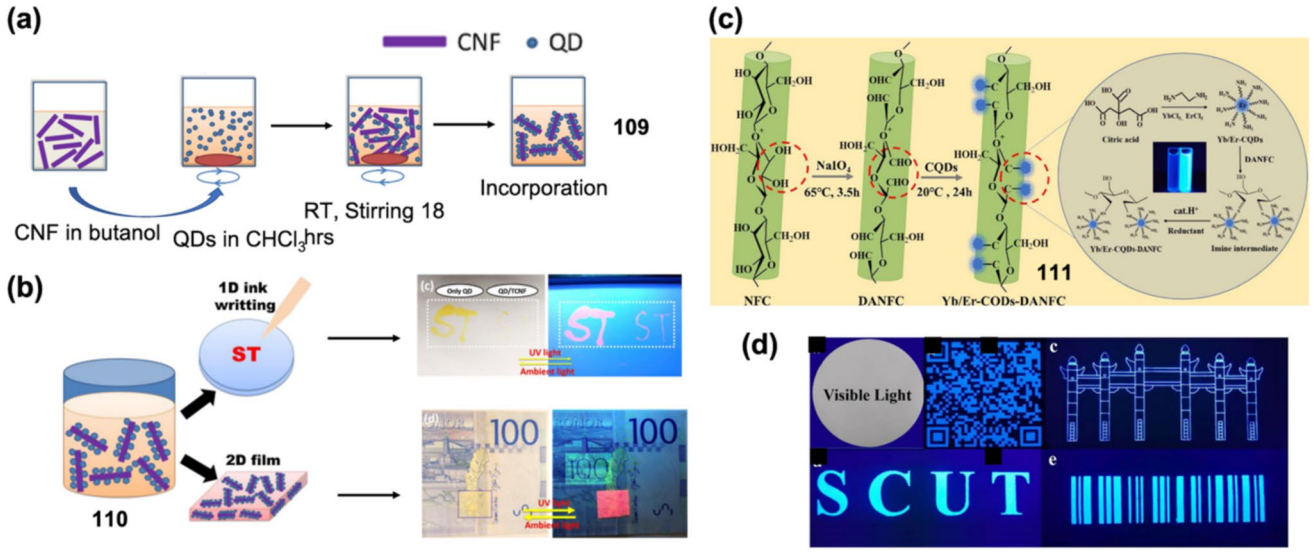

Fig. 43 **a** Chemical structure and synthetic preparation of **110**. **b** Writing on **110** on notes and letters and visibility under UV lamp. (Refer to the web version of this article for the legend colour). Reproduced from Ref. 105 with permission of Elsevier. **c** Schematic illustration of the preparation of **111**. **d** Writing on different papers using **111** ink and visualising under UV lamp. (Refer to the web version of this article for the legend colour). Reproduced from Ref. 106 with permission of Elsevier

nanocellulose film. The cholesteric nanocellulose film in **117** imparted properties which can be applied as a multimodal anti-counterfeiting label (Fig. 45a). The cellulosic label **117** has sharp circular polarisation luminescence properties. Carbon dots (CDs) coating in **117** imparts hydrophobicity to the ink which improves the hydrophobic character resulting in water resistance. The authors used **117** for printing different patterns, QR codes and fonts via manual input, painting and printing (Fig. 45b). Hence, **117** can exhibit three-mode optical properties when observed under natural light, UV light (365 nm) and IR light (980 nm). Additionally, the fluorescent cholesteric nanocellulose film **117** can be adhesively applied to various substrates for anti-counterfeiting applications [109].

In the same year, 2021, Enomae and co-workers utilised a microwave-assisted method for the synthesis of fluorescent CD **118** from precursor nanocellulose for the detection of dual metal ions like Fe^{3+} and Mn^{2+} (Fig. 46a, b). The material **118** constitutes of 2,2,6,6-tetramethylpiperidine-1-oxyl radical-mediated-oxidised cellulose nanofibre (TEMPO-CNF) and 4,7,10-trioxa-1,13-tridecanediamine. The average diameter of the developed CDs **118** was 7.86 nm. The excitation and emission wavelengths of **118** were 390 and 449 nm, respectively. The fluorescence properties of **118** were quenched in the presence of Fe^{3+} and Mn^{2+} within a few seconds and 10 min, respectively (Fig. 46c). The complexation of Fe^{3+} and Mn^{2+} with **118** helps in the electron transfer to the half-filled *3d* orbitals of the respective ions. Hence, this electron transfer mechanism is responsible for the fluorescence quenching of **118** in the presence of Fe^{3+} and Mn^{2+} ions. The authors claim that this work is the first report of CD-related literature used for the quantitative detection of Fe^{3+} and Mn^{2+} [110]. Later, in 2022, Satnami and his group developed alkaline phosphatase immobilised CdTe/ZnS QD **119** for the dual-purpose fluorescent and electrochemical detection of methyl paraoxon (Fig. 46d). The hydrolytic activity of alkaline phosphatase (ALP) with methyl paraoxon generated p-nitrophenol in the presence of QDs **119**. Here, the fluorescence quenching mechanism is attributed to the electron transfer mechanism between **119** and the generated p-nitrophenol moiety. A cellulose paper-based chip sensor was developed by the deposition of CdTe/ZnS material **119** (Fig. 46e). The electrochemical detection of methyl paraoxon by **119** was credited to the linear relationship between oxidation and reduction peak currents against the concentrations of methyl paraoxon. The LOD of **119** for methyl paraoxon was calculated as 0.65 nM and 1.72 nM using fluorescence and paper-based methods and cyclic voltammetry, respectively. The authors believe that probe **119** can present a new insight for the rapid, convenient and trace amount detection of methyl paraoxon [111].

Lin and co-workers reported a solvent-free pyrolysis technique for the preparation of biomass CD **120** and **121** for the selective detection of Fe^{3+} ions. The biomass CDs **120** and **121** were produced from the pyrolysis of two different natural components (cellulose and lignin) (Fig. 47a). Both the cellulose and lignin CDs **120** and **121** were prepared at 300 °C and 350 °C, respectively. CD **120** and **121** exhibited high quantum yields of 11.7% and 23.4%. The so-developed CDs **120** and **121** are sensitive towards Fe^{3+}

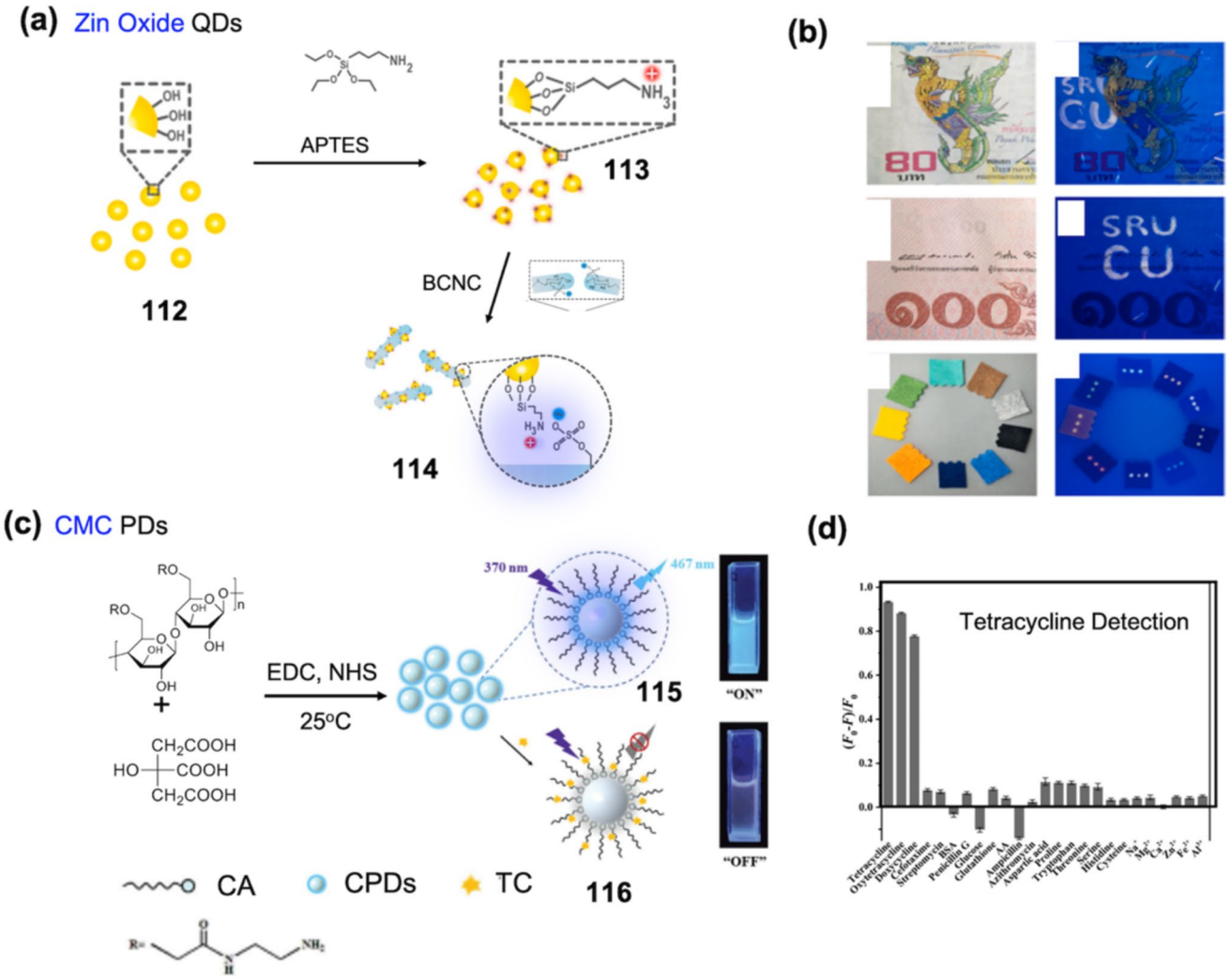

Fig. 44 **a** Chemical mechanism used for the synthesis of **113**. **b** Written patterns **113** for application in anti-counterfeiting notes. (Refer to the web version of this article for the legend colour). Reproduced from Ref. 107 with permission of Elsevier. **c** Chemical method for the synthesis of **116**. **d** Fluorescence selectivity profile of **116** for tetracycline. (Refer to the web version of this article for the legend colour). Reproduced from Ref. 108 with permission of Wiley

ions (Fig. 47b) and show selective quenching. The higher number of hydroxyl group on the surface of **120** and **121** contributes negative charge on the surface, which indeed is crucial for attracting Fe^{3+} ions. The complexation between probes and Fe^{3+} led to the electron transfer phenomenon, resulting in fluorescence quenching of **120** and **121**. The authors consider CDs **120** and **121** as cheap sources for the selective and sensitive detection of Fe^{3+} [112].

In 2022, Wu and their group developed a non-toxic fluorescent molecularly imprinted hydrogel matrix **122** derived from cellulose nanocrystals and CDs for efficient sorption and sensitive detection of tetracycline (Fig. 47c). The specific molecular recognition sites in wood-derived cellulose and CDs of **122** are attributed to the excellent sorption and sensitive detection of tetracycline. The morphology, chemical structure, optical properties and non-cytotoxicity of **122** were investigated. The sorption capacity of **122** was found to be 544.4 mg/g. As depicted in Fig. 47d, cellulosic hydrogel CD **122** show excellent turn-off-based selectivity and sensitivity towards tetracycline. The detection limit of **122** towards tetracycline was determined as 0.11 µg/L. The authors claim that material **122** is very cheap and can be utilised as a green adsorbent for removing antibiotics [113]. Recently, Xiao and co-workers developed fluorescent cellulose nanocrystals with tunable emission wavelengths (Fig. 47e, f). The cellulose nanocrystals (CNCs) were combined with CDs to form tunable emission materials **123**, **124** and **125**. The CDs used in this work were synthesised from citric acid. The nanoscaffolds **123**–**125** reveal quantum yields of > 22%. The nanoprobe **123**–**125** shows high cell

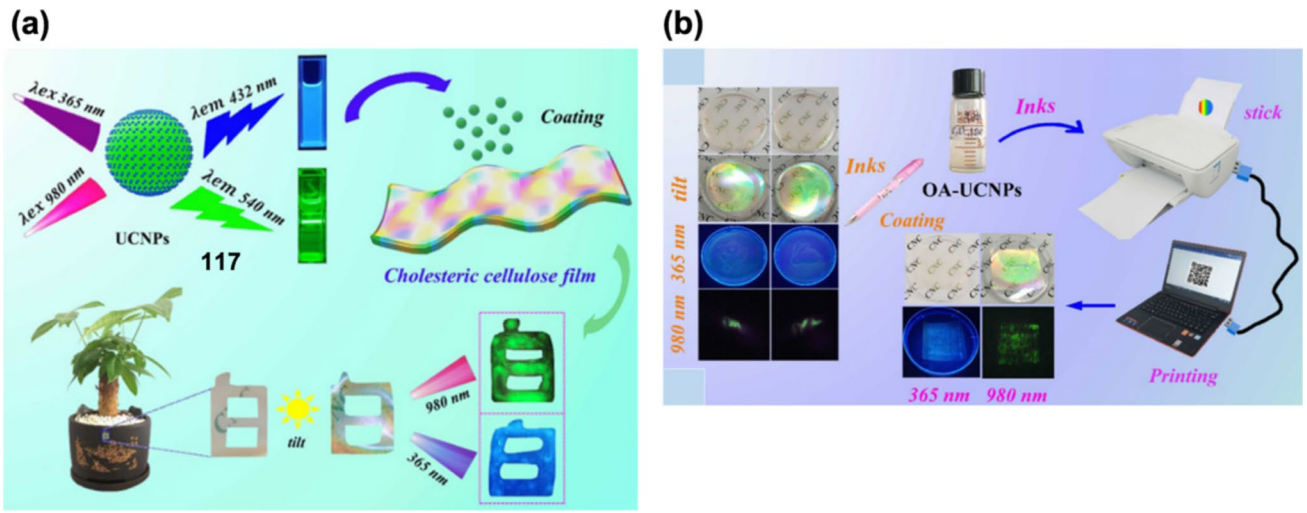

Fig. 45 **a** Schematic example of generation of **117**. **b** Application of **117** in anti-counterfeit printing. (Refer to the web version of this article for the legend colour). Reproduced from Ref. 109 with permission of ACS

membrane penetration and is used for the imaging of multiplexed cytoplasm (Fig. 47 g) [114].

4 Cellulose-derived polymeric materials (Cello-Poly)

Polymers have different physicochemical properties; hence, they are useful in several applications. Polymers may appear in gel, solid, solution, nanoparticle or film form. Appropriate modification of polymeric materials can make them applicable for specific tasks like the development of sensor devices. The polymers applicable in sensor materials or devices include conducting polymers and their composites, molecular imprinted systems (MIPs) and hydrogels. Polymeric materials act as support for functionality immobilisation (e.g. fluorophores, dyes, metal nanoparticles). Moreover, there is a possibility of modifying the chemical tuning properties of polymeric-based sensors [261]. Currently, polymers derived from nature, i.e. natural polymers, are the talk of the town. Natural polymers are large molecules sourced from plants or animals and are employed in every field of biological and environmental importance (ailments, pharmaceutics, sensors, cosmetics and chemistry). As they are available from natural sources, these polymers are economical, modifiable, readily available, tunable, biocompatible and biodegradable. Natural polymers are derived from cellulose, glucomannan, hemicellulose, lignin, agar, starch, pectin, rosin, inulin and acacia gum [262]. Natural polymers constitute different textures depending on the nature of the monomers used. For instance, carboxymethyl cellulose (CMC) is a water-soluble monomer, and owing to its hydrophilicity, CMC forms a hydrogel in solution. This section will discuss natural cellulose–derived polymeric materials and their application in the optical chemosensing field.

4.1 Hydrogels (Cello-HG)

Hydrogels are prepared from cellulose by utilizing chemical crosslinking, physical crosslinking and other polymerization techniques by applying a combinatorial approach [263, 264]. Hydrogels are known for their water insolubility attained due to their crosslinked structure and large molar mass. Hydrogels developed from cellulosic precursors have gained popularity as they can store considerable amounts of moisture inside their structures due to the presence of hydrophilic cavities owing to functionalities like –OH, –COOH, $–NH_2$, $–CONH_2$ and SO_3H. Moreover, high attention is paid to the production of cellulose polymers from biomass as they add biocompatibility and biodegradable properties. The dimensions of cellulosic hydrogels are higher than other types of polymeric gels. They have a diameter in the range of 5–50 nm [197]. Another similar gel category is aerogel, mainly renewable aerogel, also known as cellulose aerogel. Compared to other aerogels, those derived from cellulose are sustainable, inexpensive and eco-friendly. Nanocellulose aerogels are formed by the dispersion of nanocellulose particles in water using mechanical and ultrasonic techniques. Moreover, cellulose aerogels can be easily extracted from water sources and are more stable in water. It can be easily used as supporting materials owing to their high porosity, low density, high strength, low cost, renewability, biocompatibility and large specific surface area [197]. In this section, we will introduce different cellulosic hydrogels and aerogels employed in fluorescence and colourimetric chemosensing.

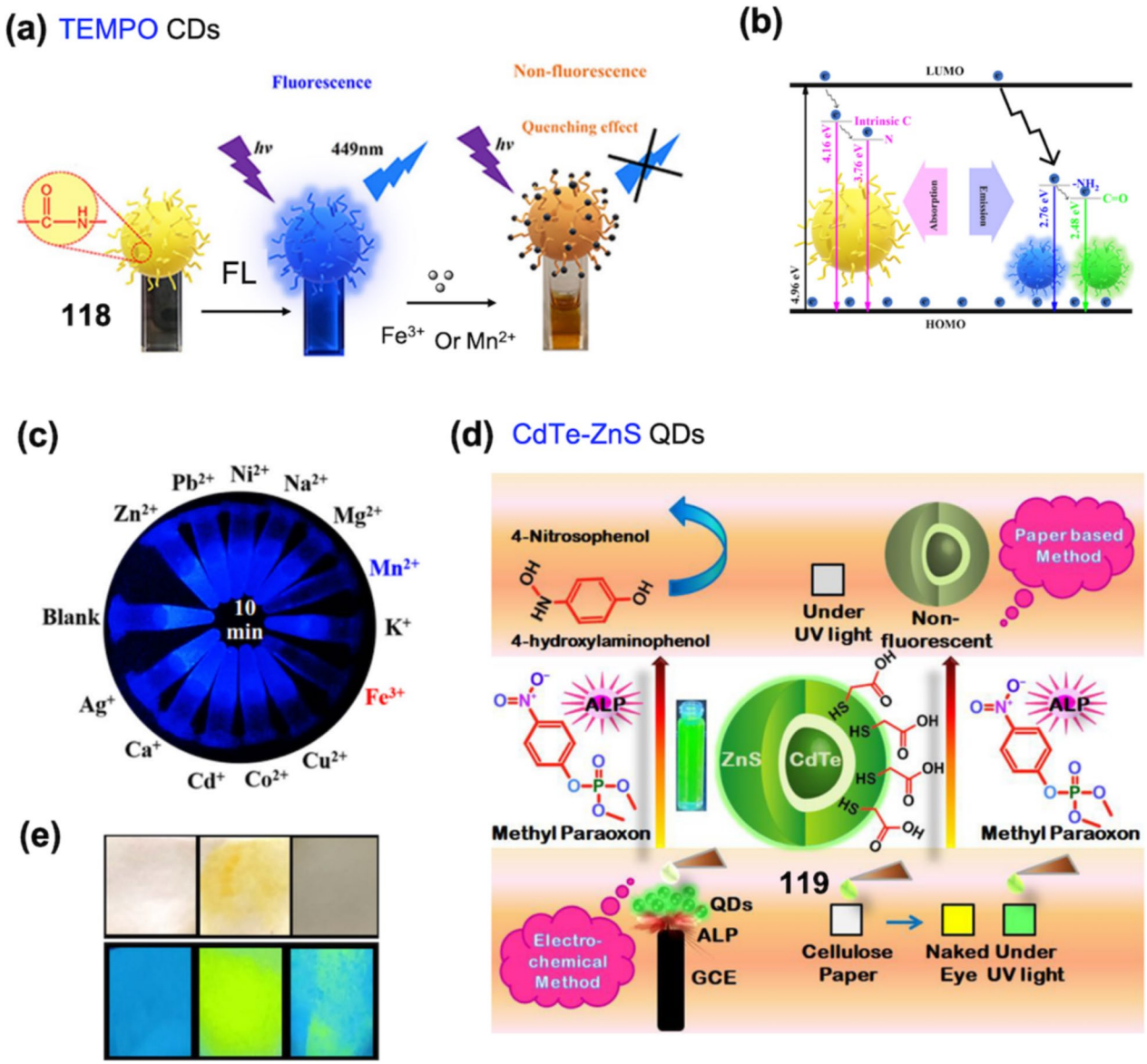

Fig. 46 **a** Schematic diagram depicting the synthesis and detection mechanism of CDs **118** for Fe^{3+} and Mn^{2+}. **b** Schematic of energy band structure and possible luminescence process for TEMPO-CDs **118**. **c** Visualisation of **118** for the selective detection of Fe^{3+} under UV lamp. (Refer to the web version of this article for the legend colour). Reproduced from Ref. 110 with permission of Springer. **d** Schematic representation of detection mechanism of **119** for methyl paraoxon via both fluorescence and electrochemical techniques. **e** Naked eye, (top) and under UV light (bottom) images of **119** doped cellulose paper in the presence of methyl paraoxon. (Refer to the web version of this article for the legend colour). Reproduced from Ref. 111 with permission of ACS

4.1.1 Fluorescence-based hydrogels (Cello-HG)

In 2017, Valcarcel and the group developed nanocellulosic hydrogels based on graphene QD **126** for the efficient detection of laccase. The fluorimetric platform is derived from sulfur and nitrogen-codoped graphene QD **126** dropped into the nanocellulosic hydrogel platform (Fig. 48a). The hydrogel matrix improves the fluorescence signal of **126** and avoids their self-quenching. Moreover, it also stabilises the fluorescence signal and improves the sensitivity of **126** towards laccase. The detection mechanism of **126** is owed to the non-covalent interactions between the sensor and the analyte. The non-covalent interaction between **126** and laccase causes comprehensive quenching without peak shifts of **126** fluorescence using simple energy transfer. The detection limit of cellulosic-hydrogel matrix **126** for laccase is estimated as 0.048 U mL^{-1} with a recovery rate of 86.2 – 94.1%. Using the straightforward strategy, the authors confirm that **126** can stabilise laccase and can be applied for the storage and recycling of enzymes [115]. In another work,

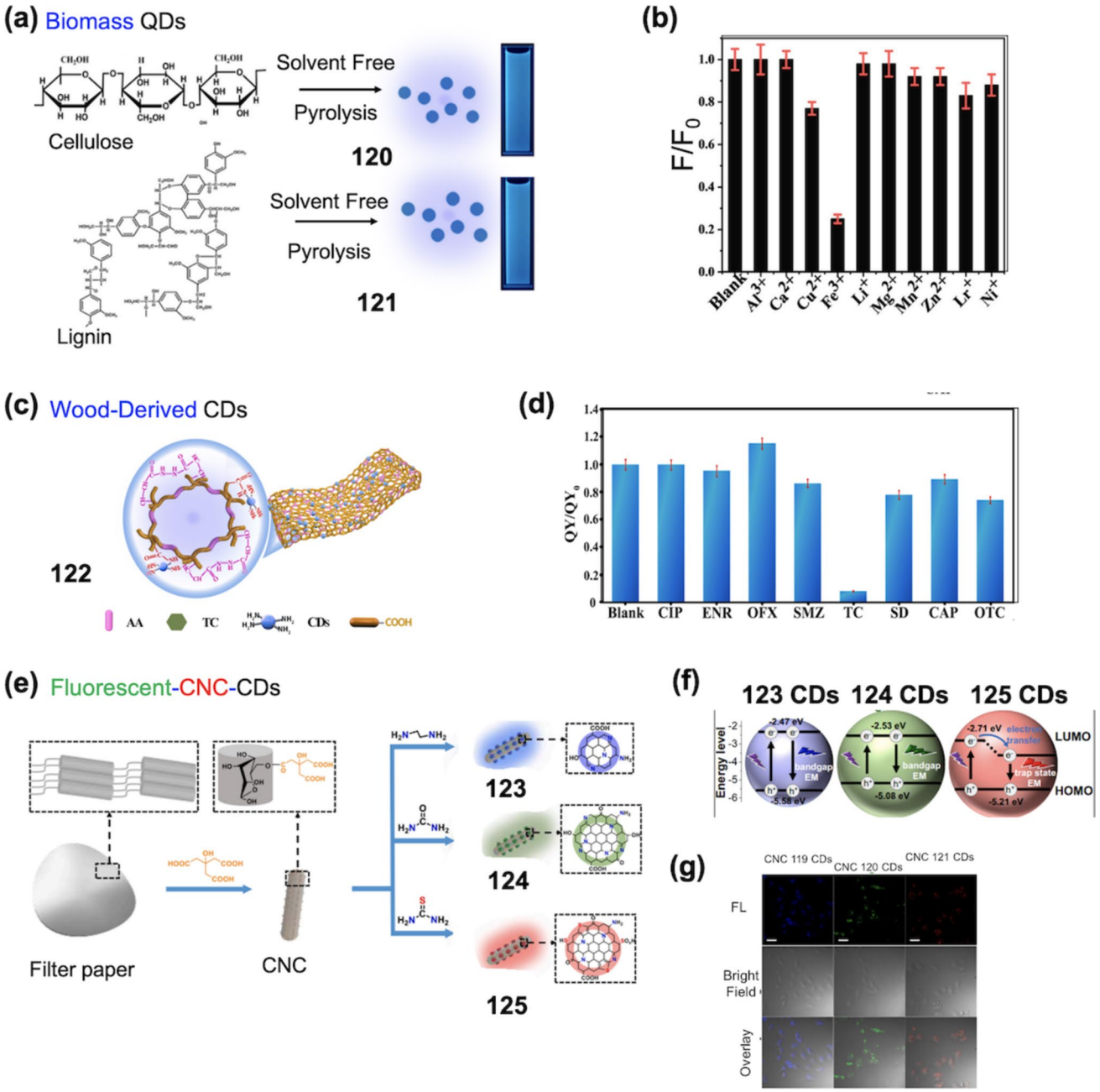

Fig. 47 **a** Synthesis of biomass-based QDs **120** and **121**. **b** Quenching mechanism of **120** and **121** for Fe^{3+} in the presence of different counter cations. (Refer to the web version of this article for the legend colour). Reproduced from Ref. 112 with permission of Frontiers. **c** Chemical structure of wood-derived CD **122**. **d** Selectivity profile of **122** for tetracycline. (Refer to the web version of this article for the legend colour). Reproduced from Ref. 113 with permission of Elsevier. **e** Preparation of materials **123**–**125**. **f** Energy level diagrams for materials **123**–**125**. **g** Imaging profile of **123**–**125** in HeLa cells. (Refer to the web version of this article for the legend colour). Reproduced from Ref. 114 with permission of Elsevier

Wang and co-workers developed an all-biomass fluorescent hydrogel fabricated by the functionalization of alginate (Alg) and cellulose nanofibre (CNF) hydrogels with fluorescent carbon dots (CQDs) generated from xylose, glucose and glucosamine forming probe **127** applicable in biosensing. The CQDs used in probe **127** have dual functions in the composite hydrogels. CQDs endow good fluorescent character and enhance the mechanical properties of the hydrogel **127** (Fig. 48b). The cellulosic hydrogel **127** was used for the detection of Fe^{3+} and gold nanoparticles (AuNPs). In case of Fe^{3+}, the detection is attributed to the PET mechanism in **127**. Moreover, the sensing property of **127** for Fe^{3+} is

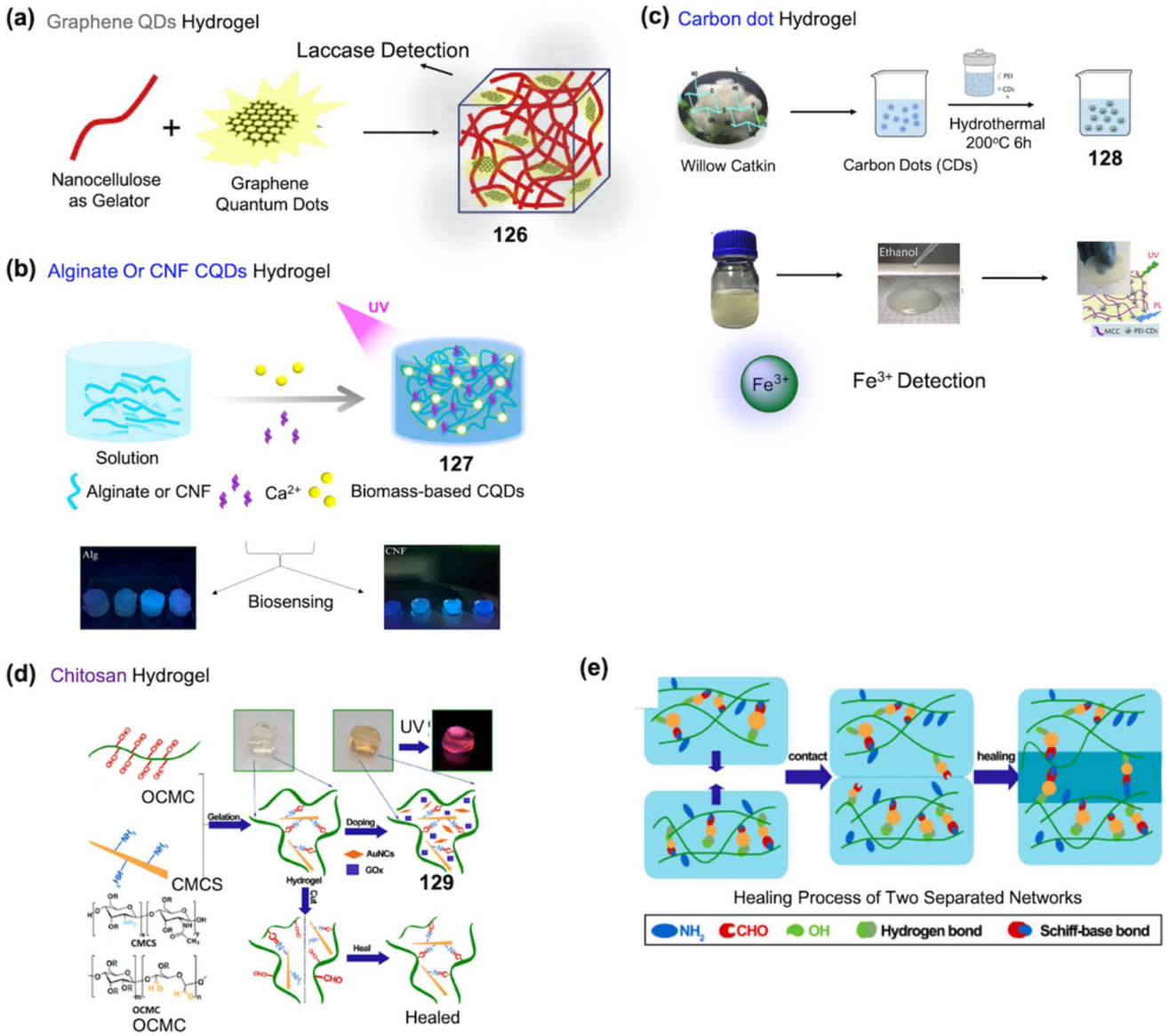

Fig. 48 **a** Chemical synthesis of graphene QDs based hydrogel **126**. (Refer to the web version of this article for the legend colour). Reproduced from Ref. 115 with permission of Elsevier. **b** Synthesis of Alginate hydrogel **127** for biosensing application. (Refer to the web version of this article for the legend colour). Reproduced from Ref. 116 with permission of Elsevier. **c** Synthesis and mechanism of **128** for detection of Fe^{3+}. (Refer to the web version of this article for the legend colour). Reproduced from Ref. 117 with permission of Elsevier. **d** Preparation of chitosan hydrogel **129**. **e** Self-healing mechanism of **129**. (Refer to the web version of this article for the legend colour). Reproduced from Ref. 118 with permission of Elsevier

preserved in the all-biomass hydrogel core of **127**. Further, rapid response fluorescence of **127** for Fe^{3+} is also accredited to the efficient mass transfer enabled by the 3D porous structure of **127**. On the other hand, fluorescence energy transfer mechanism (FRET) is responsible for the detection of AuNPs by **127**. The authors claim that prepared cellulosic hydrogel **127** can be applied in biosensing, biological imaging and biological monitoring fields [116].

Wu and co-workers in 2019 designed and created smart hydrogel based on CDs forming hydrogel nanocomposite **128** for stable detection of Fe^{3+} ions. The cellulosic hydrogel material **128** is formed by the modification of CDs by polyethylenimine (PEI) and then immersing it into microcrystalline cellulose (MCC) hydrogel (Fig. 48c). The hydrogel material **128** was spherical in shape and monodispersed in water with a quantum yield of 28%. Hydrogel **128** has high photostability, which prevents self-quenching of the probe. The authors reveal that fluorescent smart hydrogel **128** is an attractive solution for the detection of stable Fe^{3+} ion-sensing applications. The cellulosic material **128** forms highly

stable complex with Fe^{3+}, when compared with the weaker complexation with other metal ions, leading to the selective detection of Fe^{3+} [117]. In another work, Zhao and the group developed a self-healing hydrogel **129** derived from carboxymethyl chitosan/oxidised carboxymethyl cellulose combined with fluorescent probes (Fig. 48d) and utilised it for the detection of glucose and also wound healing. Here, hydrogel material **129** consists of carboxymethyl chitosan/oxidised carboxymethyl cellulose as the self-healing unit and is doped with gold nanoclusters and glucose oxidase as the sensory unit (Fig. 48e). Cellulosic hydrogel **129** can detect glucose with high sensitivity up to a detection limit of 0.029 mM. Hydrogel **129** exhibited good biocompatibility with applicability in the detection of glucose in vitro and in vivo samples. As per the authors, cellulosic hydrogel material **129** can be used for the clinical detection of glucose and also in wound healing applications [118].

Pu and co-workers developed a cellulose-based hydrogel **130** using carboxymethyl cellulose and CDs for application in information storage and fluorescent anti-counterfeiting. Figure 49 a depicts the synthetic mechanism involved in the generation of cellulosic hydrogel **130**. The cellulosic hydrogel **130** displayed a bright blue emission under UV light, which got quenched in the presence of Fe^{3+} ions (excitation = 340 nm and emission 460 nm (Fig. 49b)), thereby aiding in information storage and anti-counterfeiting. The fluorescence of **130** can be restored by the addition of ascorbic acid, improving the reusability of the material for information storage and anti-counterfeiting. The authors predict a bright prospect for the application of **130** in recyclable information storage and anti-counterfeiting [119].

Later in the same year, Lu and co-workers developed fluorescent hydrogels **131** derived from oxidised carboxymethyl cellulose (Fig. 49c) and utilised it for the adsorption and detection of Ag^+ (Fig. 49d). The $–NH_2$, OH and –COOH groups in **131** form a strong binding with Ag^+ ions via strong chelation. On forming complex with **131**, the silver ions were reduced to metallic silver, which indeed is responsible for the fluorescence quenching. Hydrogel **131** comes with sensing and self-healing properties. Cellulosic hydrogel material **131** can detect Ag^+ as low as 3.798 µM. Moreover, the hydrogel **131** can heal itself without interference from any external stimuli. Also, hydrogel material **131** can be reused seven times without any loss in adsorption performance. The prepared hydrogel matrix **131** holds excellent properties of self-healing, simultaneous adsorption and detection of heavy metal ions, and good mechanical strength, providing its capability for wastewater treatment [120]. In another work, Wu and co-workers utilised a hydrothermal synthetic approach for the synthesis of nanocellulose-based fluorescent hydrogel **132** for the detection of Hg^{2+} ions. The hydrogel material **132** was prepared by a one-pot synthetic strategy from cellulose nanofibres, enabling the in situ formation of CQDs (Fig. 49e). The cellulosic hydrogel **132** had a 3D network structure, and epichlorohydrin depicted positive effects on the mechanical properties of **132**. Cellulosic hydrogel **132** can detect Hg^{2+} in (Fig. 49f, g) in the concentration range of 0–300 mmol/L. The strong complexation of Hg^{2+} ions with **132** initiated the lowering of overall negative charge on the surface of **132**. Moreover, the PET phenomenon in **132** was inhibited by the addition of Hg^{2+} ions, resulting in the electron transfer from **132** to Hg^{2+}. The authors confirm that probe **132** can be used for various ion detection applications [121].

Wu and group developed a non-toxic chitosan-derived hydrogel **133** capable of strong adsorption and sensitive detection of antibiotic tetracycline. The chitosan hydrogel **133** is developed using CNCs and CDs (Fig. 50a). In the presence of tetracycline, the hydrogel **133** exhibits an excellent sorption capacity of 541.3 mg/g and sensitive detection ability in the linear range 1–200 mg/L and a detection limit of 0.12 µg/L (Fig. 50b). The selective quenching profile of **133** for tetracycline is attributed to the decrease in absolute quantum yield of **133** only in the presence of tetracycline. The CNCs in **133** offered a skeleton structure for elevating the adsorption capacity, and the CDs served as remarkable fluorophore moiety for the selective and sensitive detection of tetracycline [122].

In 2023, Liu and co-workers constructed a multifunctional polysaccharide-based aerogel for the efficient fluorescent detection and removal of formaldehyde. The robust aerogel **134** consists of cotton cellulose and chitosan units (Fig. 51a). The aerogel **134** showed 600-fold fluorescence enhancement (F_{540}/F_{450}) under a formaldehyde atmosphere. The titration profile is depicted in Fig. 51b, from which the estimated detection limit of **134** towards formaldehyde is approximately 0.5×10^{-7} M. The cellulosic aerogel **134** could efficiently detect formaldehyde in live zebrafish with notable fluorescence changes [123].

Later in the same year, Yang and team developed stimuli-responsive fluorescent hydrogels **135** derived from natural cellulose for off–on-off detection of Cu^{2+} and GSH. The fluorescent hydrogels **135** consist of cellulose, ionic liquids and lanthanide complexes. The preparation of **135** was achieved by utilizing two steps. In the first step, cellulose was dissolved in 1-allyl-3-methylimidazolium chloride (AmimCl) via a dissolution-regeneration process. In the following step, lanthanide complexes are immersed into the earlier-mentioned aqueous solution. The lanthanide complexes formed in this work utilised Eu^{3+}/Tb^{3+} as the metal bed. In the presence of Cu^{2+}, the fluorescent emission of **135** is quenched, indicating the formation of Cu^{2+} complex. Further, upon the addition of GSH, the fluorescence intensity of **135** is retained (Fig. 51c, d). In the case of Cu^{2+} detection, the coordination reaction between **135** and Cu^{2+} effectively decreases the energy transfer capacity from **135**

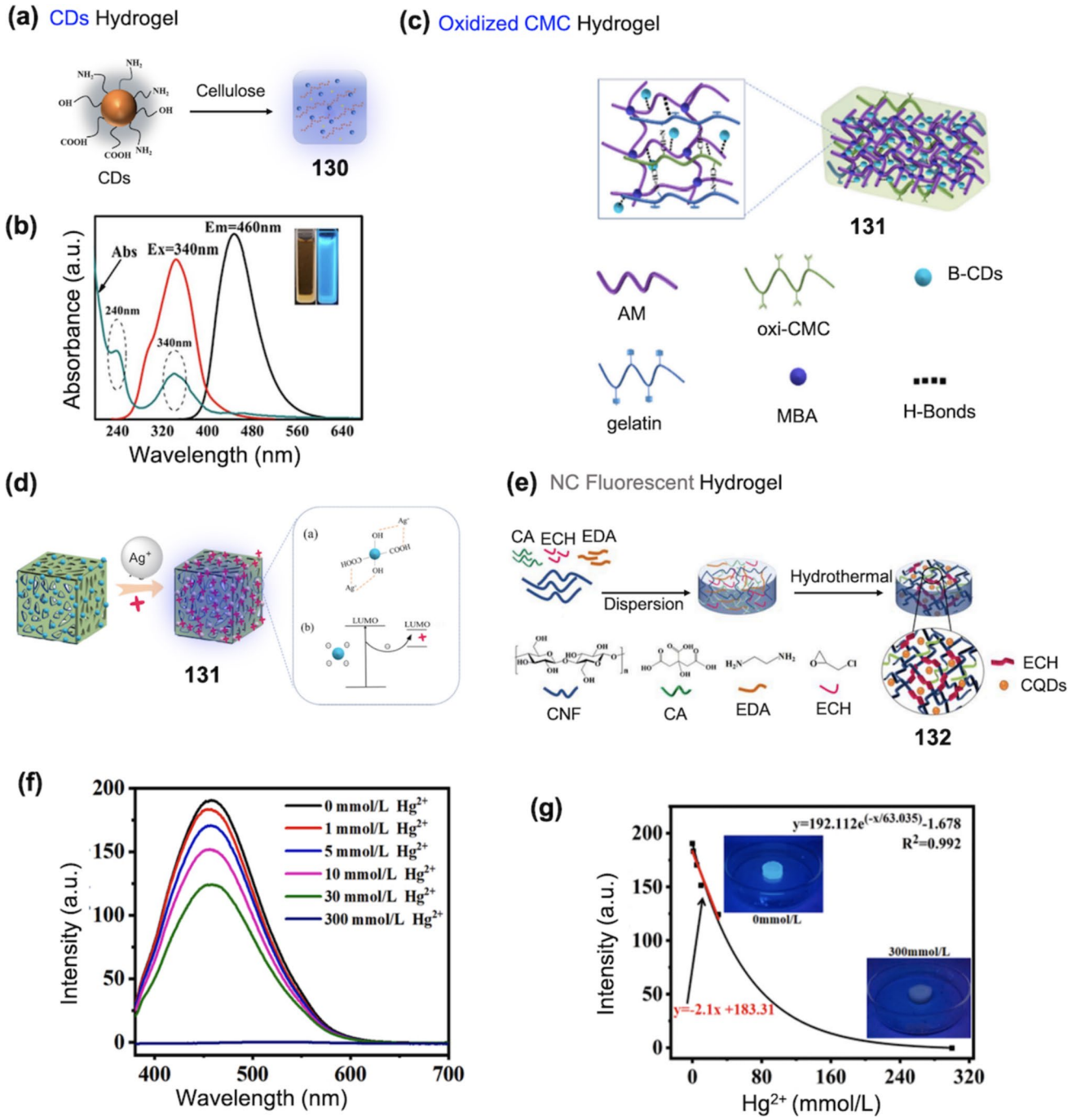

Fig. 49 **a** Chemical synthesis of cellulosic CDs **130**. **b** Emission profile of **130** on excitation at 340 nm. (Refer to the web version of this article for the legend colour). Reproduced from Ref. 119 with permission of Springer. **c** Synthesis of oxidised CMC hydrogel **131**. **d** Structure and detection mechanism of **131** for Ag^{+}. (Refer to the web version of this article for the legend colour). Reproduced from Ref. 120 with permission of Elsevier. **e** Synthetic procedure for development of **132**. **f** Changes in emission profile of **132** on addition of different levels of Hg^{2+}. **g** Titration profile of **132** in the presence of Hg^{2+}. (Refer to the web version of this article for the legend colour). Reproduced from Ref. 121 with permission of Elsevier

to Tb^{3+} ions, resulting in the fluorescence quenching. On the other hand, the chelation of copper by GSH leads to the recovery of fluorescence of probe **135**. The authors consider **135** as capable of usage as biocompatible and biodegradable off–on-off luminescence switches in aqueous medium [124]. Lin and team developed fluorescent starch-based hydrogel **136** encompassed with cellulose nanofibrils and CDs for the simultaneous adsorption and detection of Pb^{2+} (Fig. 51e).

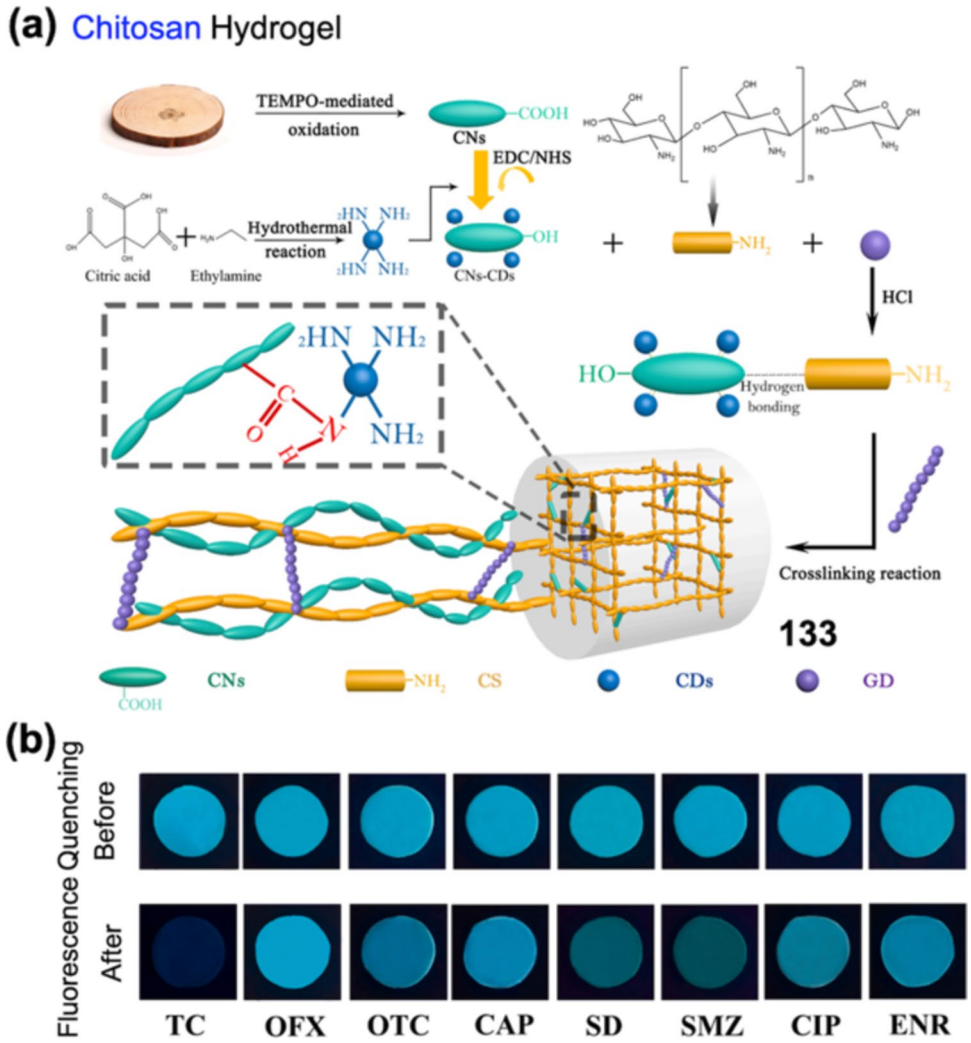

Fig. 50 **a** Chemical synthetic procedure for **133**. **b** Naked eye detection of tetracycline by **133** under UV lamp 365 nm. (Refer to the web version of this article for the legend colour). Reproduced from Ref. 122 with permission of Elsevier

Natural materials like starch and cellulose nanofibrils were loaded with CDs for the fabrication of **136**. In the presence of Pb^{2+}, the emission intensity of **136** was quenched (Fig. 51f). On addition of Pb^{2+} to the probe, it attaches on the surface of 136 via electrostatic interaction and penetrates the 3D pores of **136** using iron transport channels, paving way for the selective quenching profile. The detection limit of **136** for Pb^{2+} was estimated as 0.06 µg/L and an adsorption capacity of 265.9 mg/g. The hydrogel **136** can be used for the real-time detection of Pb^{2+} [125].

4.1.2 Colourimetric-based hydrogels (Cello-HG)

In 2019, Wu and their group developed a colourimetric immune sensor based on Au@g-C3N4-doped sponge-like 3D network cellulose hydrogel **137** for the selective detection of α-fetoprotein. In the mentioned system **137**, AuNPs with a diameter of 18.5 nm were loaded on the g-C_3N_4 nanosheets that were fixed in a 3D porous cellulose hydrogel and used as a binding site for antibody/antigen (Fig. 52a). In the presence of α-Fetoprotein, the AuNPs in **137** are catalysed due to the reduction of 4-nitrophenol to 4-aminophenol (Fig. 52b). In the presence of α-fetoprotein, the colourimetric immunoassay exhibited a linear relationship in the range of 0.1–10000 ng/mL and the detection limit of 0.46 ng/mL. The authors claim that the immune-sensor **137** showed good selectivity, repeatability and stability, which demonstrates applicability for practical diagnostic applications [126].

Cho and co-workers developed nanocellulose-based smart colourimetric hydrogel **138** integrated with anthocyanins for the sensitive detection of ammonia for monitoring pork freshness. Hydrogel **138** was prepared from TEMPO-oxidised cellulose nanofibril (TOCNF)-based hydrogels activated with different crosslinkers and anthocyanins attained from different sources (Fig. 52c). After several evaluations, Al^{3+} was used as the optimum crosslinker for TOCNF-based hydrogel **138**. The cellulosic hydrogel **138** showed a critical colour change in the neutral pH range. The action of **138** on NH_3 was nonlinear, and the naked eye (Fig. 52c) and instrumental colour

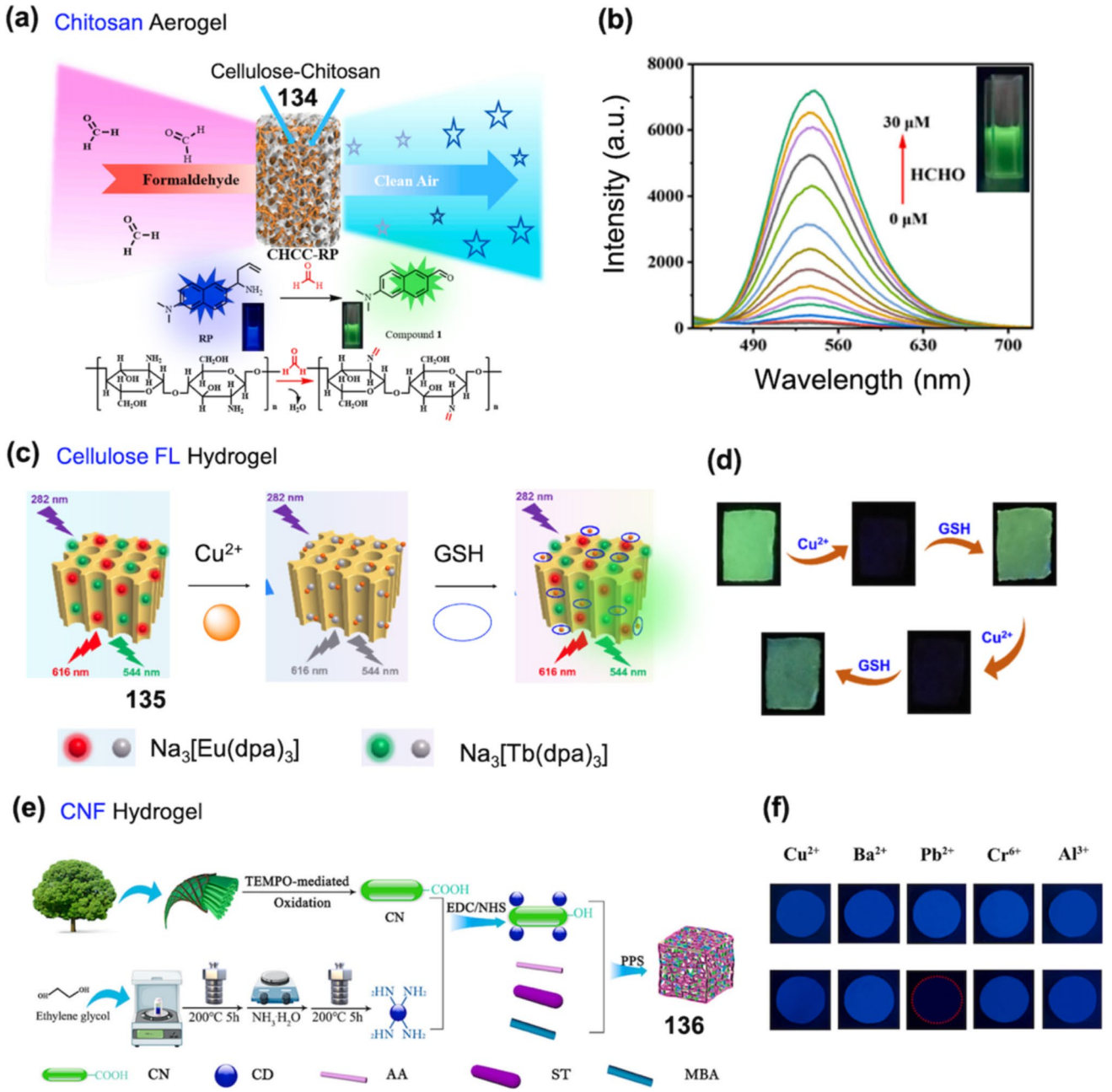

Fig. 51 **a** Procedure for the preparation of **134**. **b** Titration profile of **134** in the presence of varying amounts of HCHO. (Refer to the web version of this article for the legend colour). Reproduced from Ref. 123 with permission of Elsevier. **c** Synthetic procedure and reversible detection mechanism of **135** for Cu^{2+} and GSH. **d** Naked eye visualisation of Cu^{2+} and GSH using **135** doped cellulose test strips. (Refer to the web version of this article for the legend colour). Reproduced from Ref. 124 with permission of ACS. **e** Synthetic procedure for **136**. **f** Visual detection of Pb^{2+} under UV lamp 365 nm by utilising **136**. (Refer to the web version of this article for the legend colour). Reproduced from Ref. 125 with permission of Elsevier

measurement–based limit of detection was estimated to be 150 and 50 ppm, 150 and 50 ppm and 50 and 25 ppm for **138** doped with Aronia, Liriope and red cabbage respectively. The authors applied cellulosic hydrogel **138** for the qualitative and quantitative estimation of pork freshness [127].

4.2 Coordination network polymers (Cello-CNP)

Cellulose comprises functional groups such as hydroxyl and carboxyl species, which enable the interaction with positively charged cations [265]. These interactions pave the way for the synthesis of cellulose-based coordination

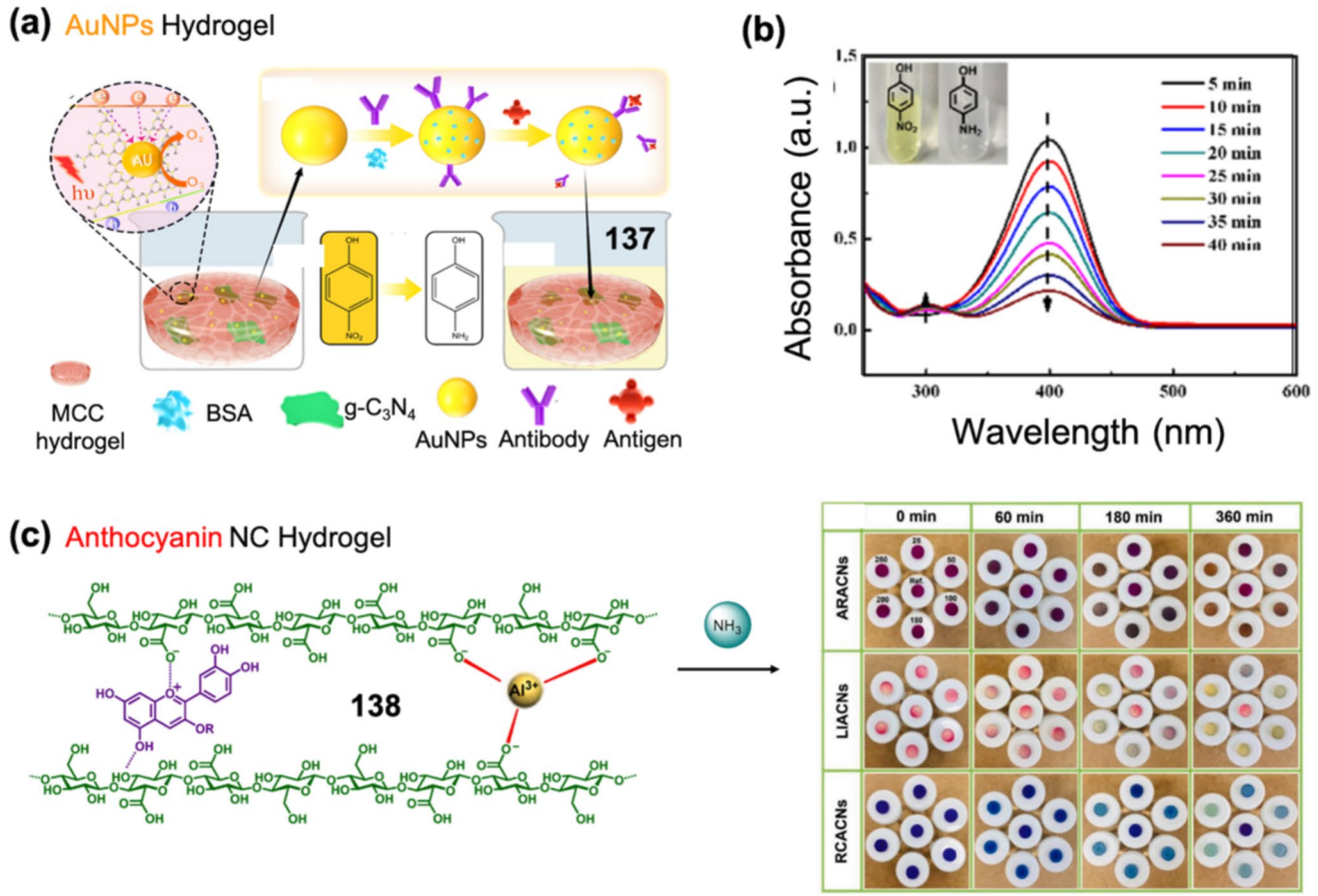

Fig. 52 **a** Procedure for the development of **137**. **b** Time-based titration profile of **137** for explosive detection. (Refer to the web version of this article for the legend colour). Reproduced from Ref. 126 with permission of ACS. **c** Chemical structure of **138** for the detection of ammonia. **d** Visible changes in **138** after treating with NH_3. (Refer to the web version of this article for the legend colour). Reproduced from Ref. 127 with permission of Elsevier

polymers. Reactive molecular dynamics simulations of the interaction of different metals with cellulose depict the formation of different materials. For instance, the interaction between Cu^{2+} and TOCNF revealed that after adsorption onto the nanocellulose surface, Cu^{2+} ions formed nanoclusters and TOCNF-GO biohybrid [265, 266]. The conformational structure of cellulosic chains is modified by the inclusion of multivalent metal ions [267]. Moreover, zinc ions displayed a high propensity to form complexes with the hydroxyl group and hemiacetal oxygen atom unit of cellulose. The synthesis of cellulose MOFs is achieved via the addition of metal salts and organic linkers to the cellulose matrix. Additionally, the involvement of sulphate [268], phosphorylated [269], xanthate [270] and carboxylate [271] increased the adsorption capacity of metals. Cellulose-based coordination network polymers are hybrid materials. Synthesis of cellulose-derived coordination network polymers can be achieved by different techniques including in situ and ex situ methods. The in situ technique includes the addition of MOF precursors, such as metal ions or linkers to the cellulosic-derived materials. The MOF substrates can be added to raw cellulose or cellulose forms like aerogels and foams. Further, conventional techniques such as freeze-drying and casting are used to fabricate foams and aerogels. Another in situ method involves the reaction between MOF precursors and cellulose scaffolds. The ex situ method of synthesis involves the modification of cellulose fibres and cellulose form with the synthesised MOFs. Cellulosic coordination network polymers have appealing features like large specific surface area; enhanced electrochemical, mechanical and antibacterial properties and, most importantly, porous structure. Owing to these excellent features, Cello-CNP has found wide applications in sectors such as water remediation [272], drug release [273], solar power generation [274], electromagnetic interference shielding [275], thermal insulation and fire retardancy [276], information security [277], air purification [278] and chemosensing. In this section, Cello-CNPs with applications in fluorescence and colourimetric optical sensing are discussed.

4.2.1 Fluorescence-based coordination network polymers (Cello-CNP)

Sweat components avail adequate amounts of potential biomarkers that can indicate the health state of a subject. A fluorescent wearable platform for the non-invasive analysis of Cl^- in sweat was developed. Yan et al. prepared a logic smart-device fabrication based on colour-adjustable lanthanide MOFs. The wearable Cl^- monitoring platform **139** was generated using a simple ultrasonic technique for integrating a combination of flexible host material (cotton piece) and two fluorescent materials such as lanthanide MOFs DUT-101 and Ag^+/Eu^{3+}@UiO-67 (Fig. 53a). Compared to large circuit boards, the device **139** is comfortable for human body contact and can be regularly worn. In the cellulose-MOF material **139**, the two lanthanide-based fluorescent moieties afford high colour purity and measurement accuracy. From the two lanthanide moieties, DUT-101 represents the reference fluorescence centre and Ag^+/Eu^{3+}@UiO-67 acts as the working fluorescence centre (Fig. 53b). The cellulosic-MOF material **139** showed excellent selectivity with high sensitivity for quantitative Cl^- measurements. The efficacy and applicability of **139** for Cl– were also tested in real-time, on-body tests with healthy human subjects. Moreover, a codec device was constructed by designing Cl^- and fluorescence signals for the logic circuit, which is considered a mimetic "red-green indicator light" for testing its applicability in healthcare and sports [128]. In this review, we have noticed many cellulosic materials which are capable of detecting Cu^{2+} ions. In another illustration, An and co-workers developed Eu-metal organic frameworks@ TEMPO-oxidised cellulose nanofibril-based fluorescent film **142** for the detection of Cu^{2+} ions (Fig. 53c). The fabrication of **142** was achieved by the in situ synthesis in the hydroalcoholic medium. The cellulosic material **142** was characterised by using X-ray diffraction, scanning electron microscopy, Fourier transform infrared spectroscopy and fluorescence spectrometer, along a few more techniques. The authors claim that film **142** performed a high quenching–based selectivity (Exi = 254 nm, Emi = 614 nm) towards Cu^{2+} ions in the presence of other interfering metal ions. However, from Fig. 53 d and e, it is noticed that there is clear interference from Zn^{2+}, Na^+, Ni^{2+}, Mg^{2+} and Ca^{2+} ions. The reason behind the interference is **142** has high negative charge and so can attract different cations. Elevated quenching of **142** was noticed with the addition of increasing levels of Cu^{2+} ions. Moreover, cellulosic material **142** developed a good linear relationship with Cu^{2+}, which made its utility promising for detection in

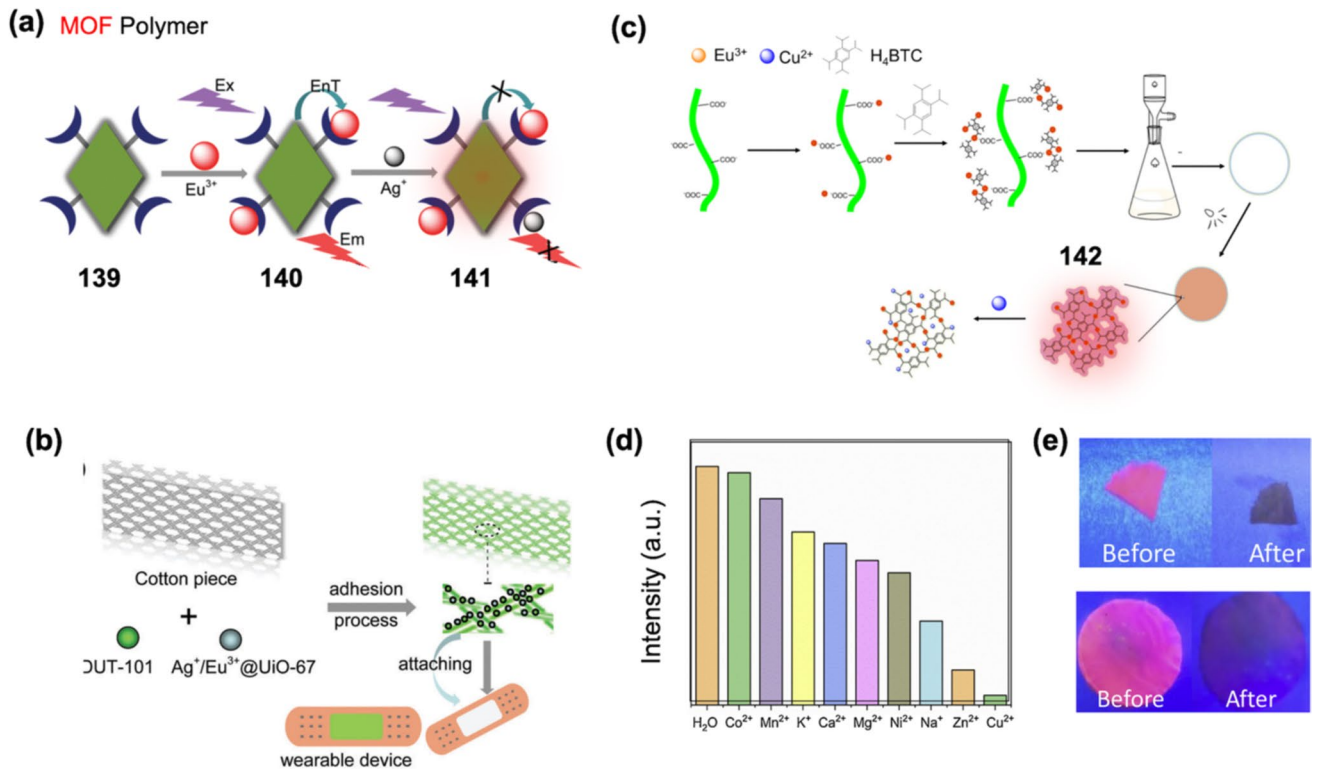

Fig. 53 **a** Reversible detection mechanism of Eu^{3+} and Ag^+ by **139**. **b** Preparation of wearable device using **139**. (Refer to the web version of this article for the legend colour). Reproduced from Ref. 128 with permission of RSC. **c** Synthetic procedure for **142**. **d** Quenching profile of **142** for Cu^{2+} in presence of other counter cations. **e** Visual detection of Cu^{2+} using **142** doped cellulose paper. (Refer to the web version of this article for the legend colour). Reproduced from Ref. 128 with permission of Elsevier

water bodies. However, as mentioned earlier, the report lacks selectivity and proof of concept in its claims [129].

In 2022, Neogi and his team introduced in situ fabricated MOF-cellulose composite **143** (Fig. 54a) as a ROS deactivator-convertor, fluoro switchable bi-phasic tweezers for free chlorine detoxification and size-exclusive catalytic insertion of aqueous H_2O_2. The chemo-robust and hydrogen-bonded framework **143** which encompassed free $–NH_2$ moiety affixed pores that act as an ultra-fast and highly regenerable luminophore for the selective detection of hazardous ROS producers such as ClO^- and H_2O_2 with a nanomolar level sensitivity. In the cello-MOF **143**, bio-relevant antioxidant L-ascorbic acid delivers notable quenching of 3.5-fold to the probe along with bi-phasic colourimetric variation in the presence of ClO^- (Fig. 54b). The on–off-on detection mechanism of **143** for ROS analytes was proved by density functional theory (DFT) calculations. The authors consider that cellulosic material **143** can perform as a smart composite material for bimodal deactivation and conversion of ROS species. Moreover, the multi-cyclic alkene epoxidation by **143** proves its effectiveness for application in futuristic continuous flow reactors. MOF materials have been excessively utilised as fluorescent probes for the detection of Cr(VI) [130]. Yilamz and group utilised a cellulose-based material for fabricating MOF probes **144** and **145** for the detection of Cr(VI) ions and investigation of their antimicrobial properties. Cellulosic materials **144** and **145** constitute two different MOF units, UiO-66 and ZIF-8, linked with 1,8-naphthalimide, respectively (Fig. 54c). The 1,8-naphthalimide unit in **144** and **145** displays a significant selective quenching for Cr(VI) (Fig. 54d, e). Moreover, cellulosic materials **144** and **145** also contain Ag^+, which gives the probe an effective hand for determining the antimicrobial properties. Probes **144** and **145** can detect Cr(VI) as low as 1.07 µM. Moreover, the Ag^+ capped **144** and **145** showed a significant antibacterial effect against *E. coli* at a MIC value of 0.0024 mg/mL [131]. Consumption of antibiotics is on a constant rise. Therefore, monitoring and detection of antibiotics such as ciprofloxacin is of great necessity.

Earlier in 2022, An et al. developed a Tb-coordination polymer-anchored nanocellulose composite film **146** for the selective and sensitive detection of antibiotic ciprofloxacin. The nanocellulose composite film **146** was prepared by the combination of terbium coordination polymer (Tb-AMP) and TEMPO-oxidised cellulose nanofibres, in aqueous media via the in situ synthetic route (Fig. 55a). In the presence of ciprofloxacin energy is supplied for terbium ion in **146** through antenna effect to attain green fluorescence under a 365-nm UV lamp (Fig. 55b). Probe **146** shows high selectivity and sensitivity for detection of ciprofloxacin (Fig. 55c). Nanocellulosic material **146** can detect ciprofloxacin in a good linear range of 1–8 µM with a LOD determined at 0.0392 µM. The authors consider **146** capable of the future quantitative colourimetric analysis of antibiotic pollutants [132]. In another illustration of Cr(VI) detection, Wu and the team utilised a bacterial cellulose-fabricated Zr-MOF probe **147** (Fig. 55d). The Zr-MOF material showed strong aggregation-induced emission (AIE) when grown with bacterial cellulose. Cellulosic material **147** was formed by uniformly wrapping bacterial cellulose-abundant hydroxyl groups in the interior of the MOF layer. Cellulosic material **147** exhibited selective quenching–based detection

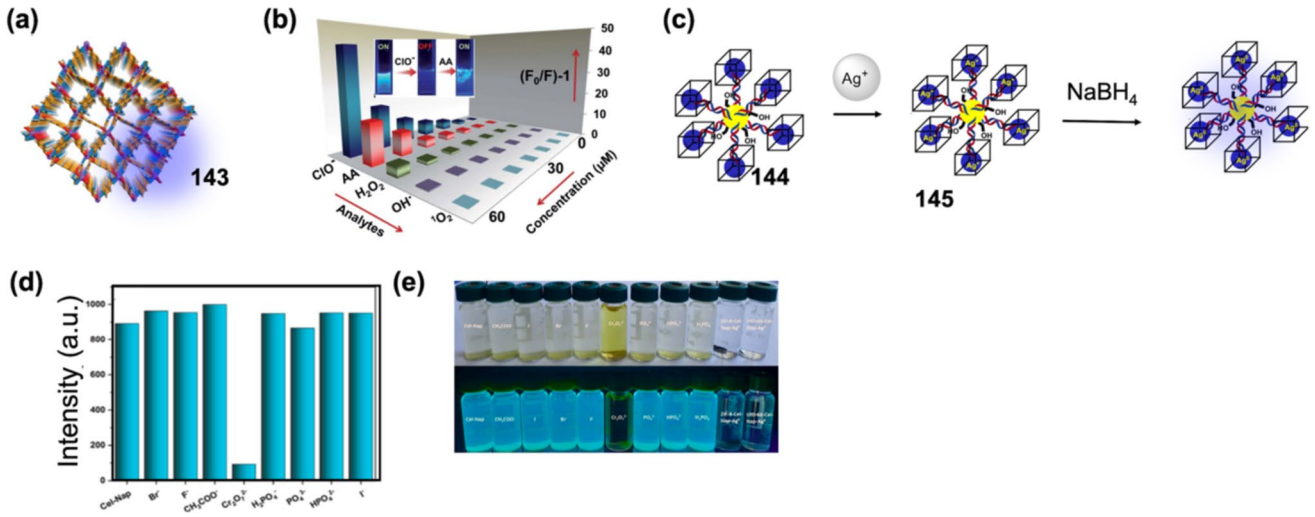

Fig. 54 **a** Structure of MOF **143**. **b** Selectivity plot of **143** towards anions. (Refer to the web version of this article for the legend colour). Reproduced from Ref. 130 with permission of RSC. **c** Construction of MOF material **144** used for the reversible detection of Ag^+ and chromate. **d** Selectivity plot of **144** for anions. **e** Naked eye detection of anions under visible and UV light. (Refer to the web version of this article for the legend colour). Reproduced from Ref. 131 with permission of Elsevier

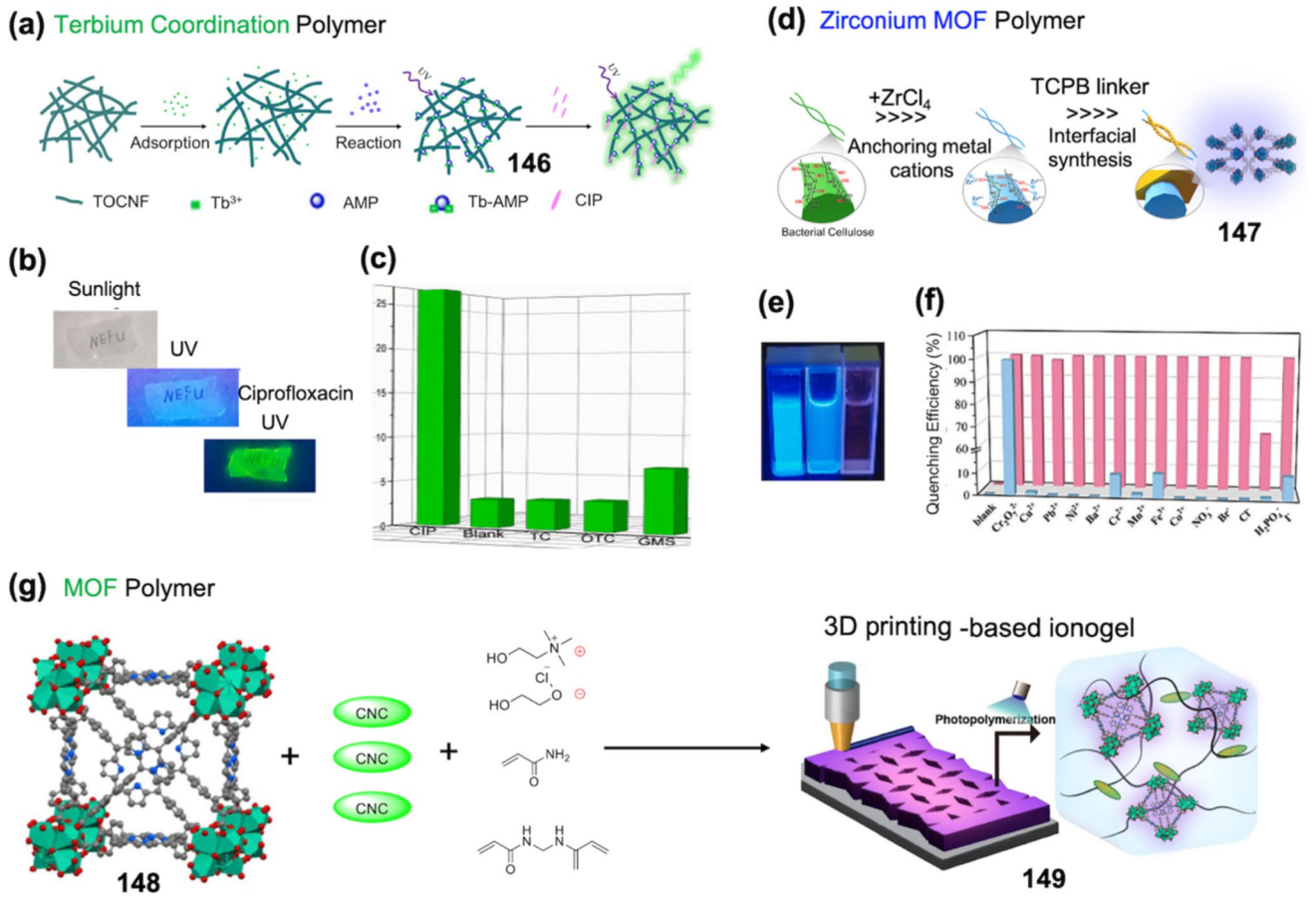

Fig. 55 **a** Synthetic procedure for **146**. **b** Visual detection of ciprofloxacin by **146** under UV lamp 365 nm. **c** Selectivity profile of **146** for ciprofloxacin. (Refer to the web version of this article for the legend colour). Reproduced from Ref. 132 with permission of Elsevier. **d** Synthetic track for zirconium-based MOF **147**. **e** Naked eye detection profile of **147** for chromate. **f** Quenching efficiency of **147** for chromate in the presence of various anions. (Refer to the web version of this article for the legend colour). Reproduced from Ref. 133 with permission of Elsevier. **g** Synthetic procedure for preparing **148** and 3d printing mechanism forming **149**. (Refer to the web version of this article for the legend colour). Reproduced from Ref. 134 with permission of ACS

and enrichment of Cr(VI) with a high adsorption capacity of 90 mg/g (Fig. 55e, f). The abundant hydroxyl groups in **147** allow the binding of Cr(VI), resulting in the fluorescence quenching effect. Probe **147** can detect Cr(VI) with an estimated LOD of 41.8 nM. Cellulosic material **147** can be utilised for the detection and adsorption of Cr(VI) in real time [133].

4.2.2 Colourimetric-based coordination network polymers (Cello-CNP)

In 2022, Yu and co-workers demonstrated the 3D printing of MOFs-based ionogel (MIG) **149** for applicability as wearable sensors with colourimetric and mechanical responses (Fig. 55g). For this purpose, the 3D printing ink was prepared from a combination of deep eutectic solvents (DESs), cellulose nanocrystals (CNCs), MOF crystals and acrylamide. After printing, a second covalently crosslinked poly(acrylamide) network and solidification of MIG were achieved by a photopolymerization technique. Moreover, a porphyrinic Zr-based MOF, MOF-525, was utilised as a functional filler providing sharper colour changes when exposed to acidic compounds. The so-developed MOF material **149** was used as an auxetic sensor for the detection of human body movements [134]. Phenol is a chemical agent excessively utilised in different industries. As per the European community, the permissible limits for concentrations of phenol in water should be below 1 mg/L. Wang et al. involved a MOF-based bimetallic oxide composite nanozyme fibre membrane for the colourimetric detection of phenol. For this purpose, the authors have used variable-valence metal Co/Mn bimetallic MOF-74 as a precursor to generating a bimetallic oxide composite nanozyme with peroxidase-like activity.

Further, the developed nanozyme is combined with cellulose via suction filtration to form nanozyme fibre

membrane (NFM) **150** (Fig. 56a). As depicted in Fig. 56 b and c, the MOF-derived cellulosic membrane **150** was used for the selective absorbance and colourimetric detection of hazardous phenol. The developed membrane-based test strips **150** can detect phenol in a wide linear range from 0.5 to 500 µM with an LOD of 0.2 µM. The membrane-based test strips **150** displayed excellent properties like porous nanostructures, efficient catalytic activity and surface physicochemical properties. Hence, the authors consider that the development of **150** will pave a new path for future high-performance in situ detection of phenol platforms [135].

4.3 Other polymers (Cello-other-poly)

Until now in this section on cellulose-based polymers (Cello-Poly), discussion related to reports on cellulose-hydrogel (Cello-HG) and cellulose-coordination network polymers (Cello-CNP) and their application in optical chemosensing is pursued. However, there are many other cellulose-polymer interactions such as micelle, nanofibre films, zwitterionic units, chiral molecules, proteins and organic molecules which are also utilised in optical chemosensing applications [279]. In this segment of the review, the mentioned cellulose-polymer interactions and their optical chemosensing application are examined.

4.3.1 Fluorescence-based polymers (Cello-other-poly)

In another work, Kanoh et al. reported an illustration of chiral fluorescent molecule-modified cellulose materials **152** for the detection of aromatic nitro-compounds exhibiting central, axial and planar chirality. The cellulose-modified chiral probe **152** constitutes microcrystalline cellulose as the precursor, benzo[1,2-b:4,5-b′]dithiophene-based π-conjugated group as a fluorescent signalling unit adapted via a two-step polymer reaction, which includes cross-coupling and carbamoylation reactions (Fig. 57a). In the presence of aromatic nitro compounds, the fluorescence of cellulose-modified chiral probe **152** is quenched. Probe **152** utilises an enantioselective fluorescence response path for the selective detection of nitro aromatics. The detection of aromatic nitro compounds using **152** can also be visualised with the naked eye (Fig. 57b). This report was an excellent example of the applicability of cellulosic polymer material for the detection of aromatic nitrochiral compounds [136]. The substitution of protein on the nanocellulose paper surface was illustrated for the first time by Faccio et al. The authors utilised cyanobacterial C-phycocyanin as a protein unit and integrated it into the nanocellulose matrix forming **154** for further application in the detection of Cu^{2+} ions at the nano to micromolar level (Fig. 57c). Covalent coupling accompanied by physisorption between Cu^{2+} ions and **154** is responsible for the detection. Moreover, **154** was doped with red fluorescent copper

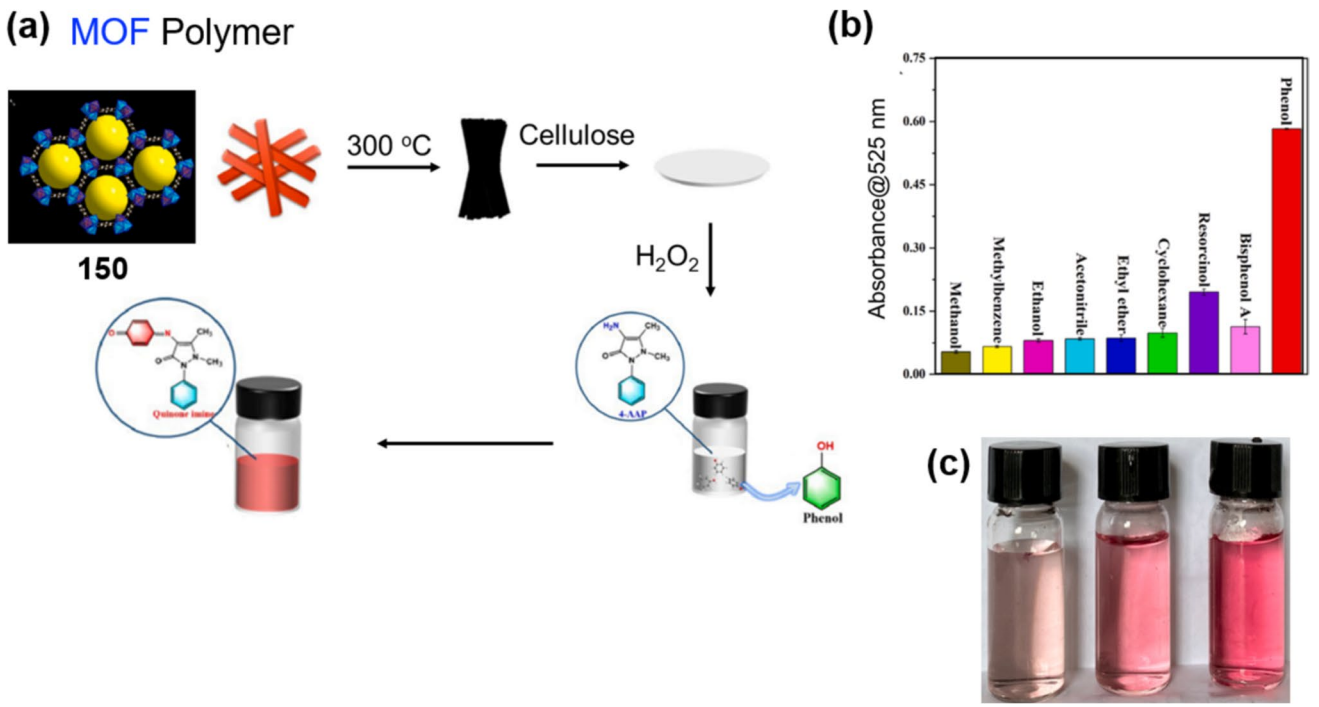

Fig. 56 **a** Synthetic and detection mechanism of **150** for phenol. **b** Selectivity profile of **150** for phenol in the presence of different counter analytes. **c** Naked eye profile of **150** after addition of phenol. (Refer to the web version of this article for the legend colour). Reproduced from Ref. 135 with permission of Elsevier

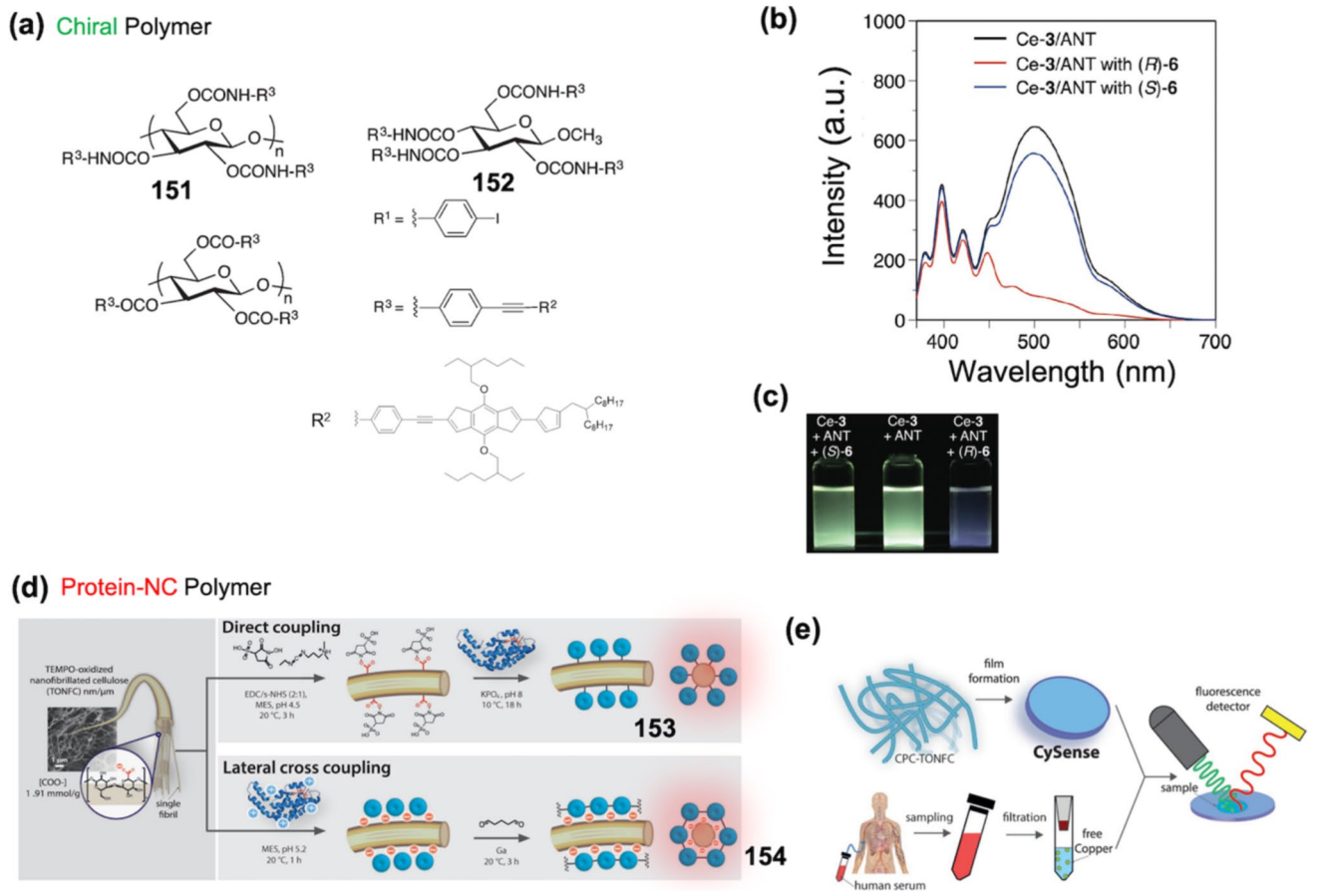

Fig. 57 **a** Chemical structure of **151** and **152**. **b**, **c** Photophysical properties of **151** and **152**. (Refer to the web version of this article for the legend colour). Reproduced from Ref. 136 with permission of RSC. **d** Procedure for preparing **153** and **154**. **e** Testing of **153** and **154** in human serum samples. (Refer to the web version of this article for the legend colour). Reproduced from Ref. 137 with permission of Wiley

sensitive hybrid film. The nanocellulosic hybrid film **154** can detect Cu^{2+} with an estimated LOD of 200×10^{-9} M (Fig. 57d). The hybrid film **154** can be used for measuring Cu^{2+} levels in a fluorimeter or a microarray laser scanner (Fig. 57e) [137].

In 2017, Chen et al. developed a cellulose-based material **155** by using facile citric acid/cysteine (CCF) treatment. The advantage of using this method was that the alteration of cellulose-based materials **155** could be accomplished without cellulose dissolution (Fig. 58a). Moreover, the mentioned route also enables preserving the original morphology of **155**. Additionally, CCF-modified cellulose material **155** displays selective quenching and excellent UV absorption capacity. Hence, the authors consider cellulosic material **155** can be employed in anti-counterfeiting, chemical shielding and UV shielding applications (Fig. 58b, c) [138].

Nishio and co-workers developed napthalimide-based fluorescent cellulose derivatives **156–161** for sensing of nitroaromatic compounds. For achieving materials **156–161**, first, allyl cellulose was synthesised from cellulose in an aqueous solution consisting of NaOH/urea, with the simultaneous addition of amino ethanethiol (AET). Finally, napthalimide-derived fluorescent units were integrated by the reaction of AET-modified AC with 4-dimethylamine-1,8-naphthalic anhydride (DMANA) (Fig. 59a). The structures of cellulosic materials **156–161**were well characterised and further used for fluorescence quenching-based detection of 2,4,6-trinitrophenol (TNP) and 2,4-dinitrophenylhydrazine (DNH) (Fig. 59b, c). The authors predict that either the quenching occurs as a result of electron transfer from probe to nitroaromatics or due to resonance energy transfer (RET) mechanism. The estimated LODs of **156–161** for TNP and DNH were 2.5×10^{-8} and 3.2×10^{-8} mol/L, respectively. The authors claim that probes **156–161**can be used for the detection of specific nitroaromatic entities in aqueous and nonaqueous media [139].

Organic polymers have found high weightage in the field of optical chemosensing. In 2018, Fragouli and their team developed photochromic paper indicators for the determination of acidic food spoilage. Cellulosic paper **162** was

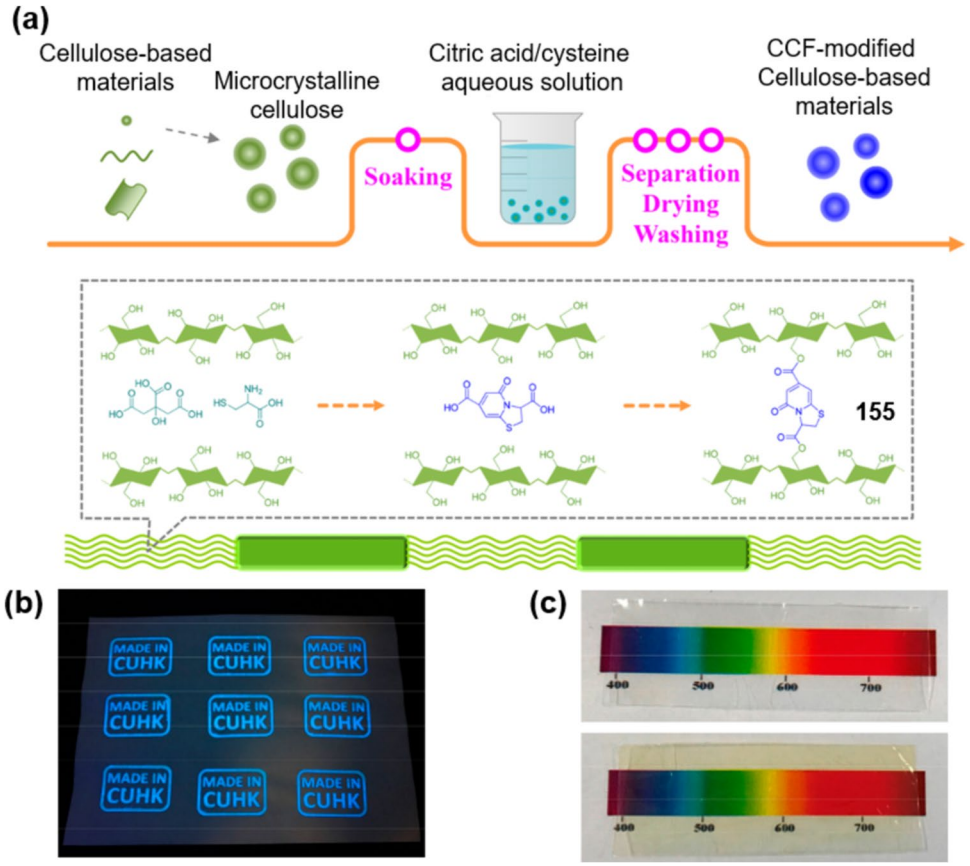

Fig. 58 **a** Complete preparation of cellulosic material **155**. **b** Screen printing and writing of molecular using **155**. **c** Colour ruler prepared using **155**. (Refer to the web version of this article for the legend colour). Reproduced from Ref. 138 with permission of ACS

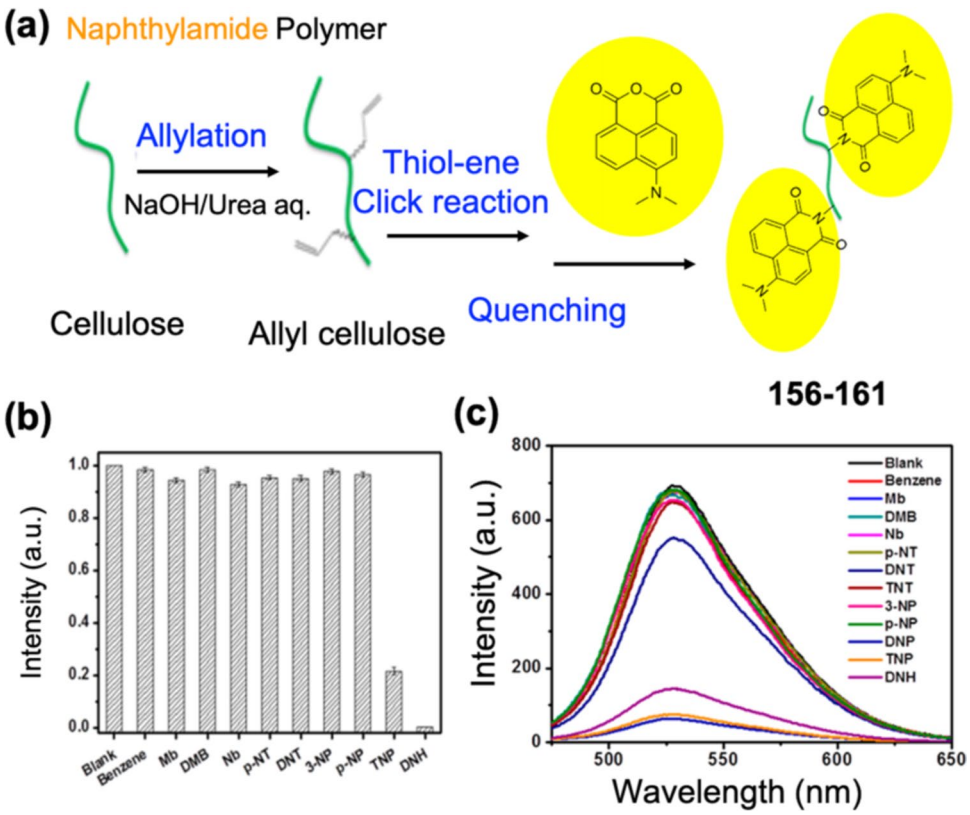

Fig. 59 **a** Synthetic route for preparation of cellulosic materials **156**–**161**. **b** Selectivity profile of **156** for nitroaromatic compounds. **c** Quenching profile for different nitroaromatics by **156**. (Refer to the web version of this article for the legend colour). Reproduced from Ref. 139 with permission of ACS

prepared by the incorporation of spiropyran-modified poly(2-hydroxyethyl methacrylate) via a noncovalent functionalization onto the paper strip surface (Fig. 60a). In the presence of acidic vapours, i.e. spoiled food samples, the fluorescence of **162** is changed from pink to colourless (Fig. 60b, c). The naked-eye visualization of food spoilage is achieved using cellulosic papers **162**. The authors have used the potential of cellulosic material **162** in food packaging and food spoilage sensors [140]. In the current review, we have come across many sensing materials for the detection of Fe^{3+} ions. A reduced form of Fe^{3+}, i.e. is Fe^{2+}, also plays a crucial role in many biological processes, and determining their concentrations in the human body is vital for human health. In 2018, Zhang et al. developed a cellulose-derived sensor encompassing phenanthroline for the highly selective and rapid naked-eye and fluorescent detection of Fe^{2+} ions. Cellulosic probe **164** constitutes of 1,10-phenanthroline-5-amine (Phen) as fluorophore unit, cellulose acetate-based matrix and 4,4′-methylene diphenyl diisocyanate (MDI) as crosslinker (Fig. 60d). Cellulosic polymer **164** was capable of detecting Fe^{2+} via a chemical bonding strategy. High and rapid fluorescence quenching of **164** was achieved with the addition of Fe^{2+} (Fig. 60e). The limit of detection of cellulosic material **164** for Fe^{2+} was estimated as 2.6 ppb. The visualization of Fe^{2+} using **177** was tested via printing, films and coating on glass (Fig. 60f).

The authors consider that the Fe^{2+} responsive material **164** has huge potential in the detection and extraction of Fe^{2+} ions [141]. Later, in 2019, Kamel and co-workers introduced fluorescein-based chitosan nanoparticles and imprinted them

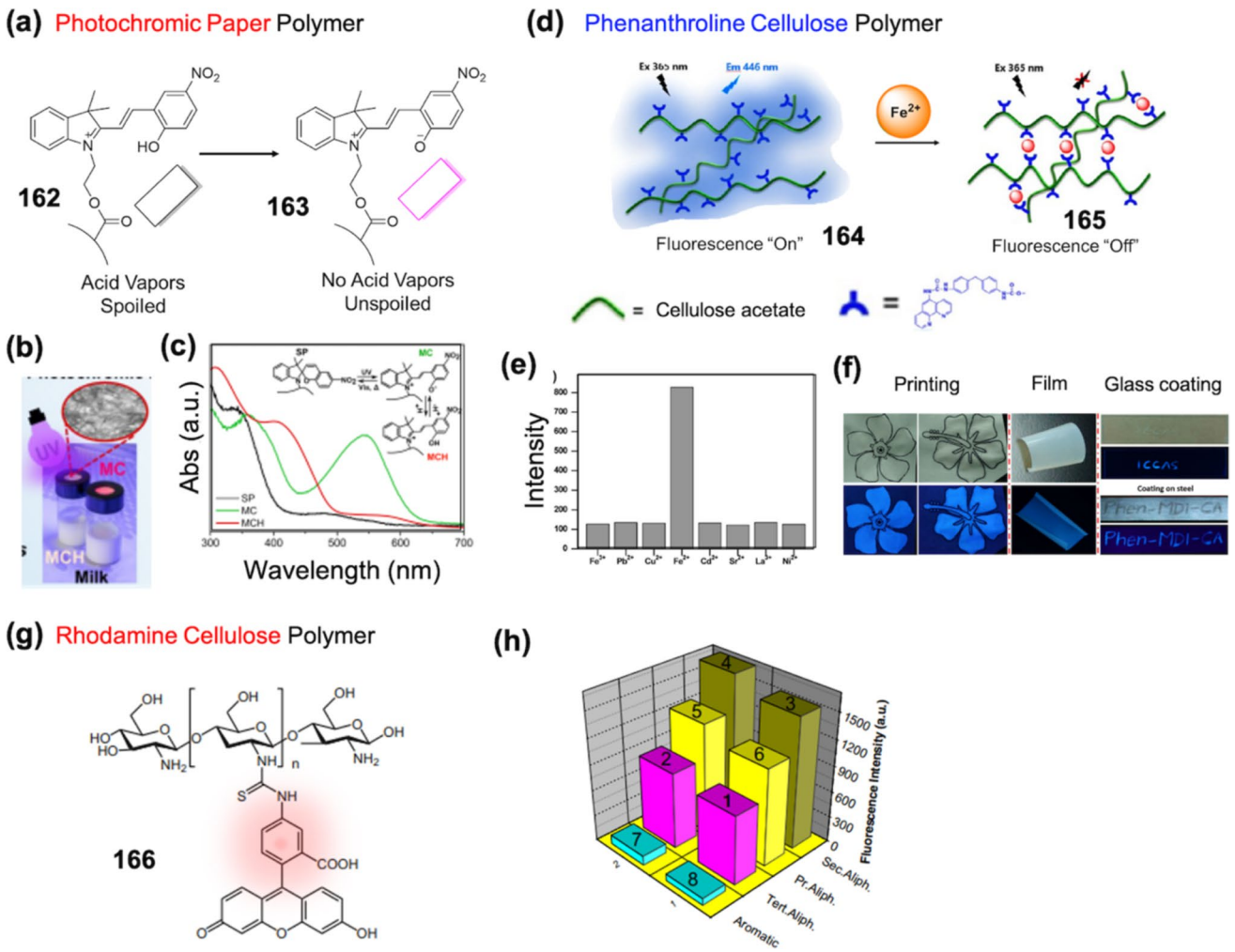

Fig. 60 **a** Structure and synthetic procedure for preparing **162**. **b**, **c** Colourimetric detection of acid vapours. (Refer to the web version of this article for the legend colour). Reproduced from Ref. 140 with permission of ACS. **d** Synthesis and fluorimetric detection mechanism for **164**. **e** Selectivity profile of **164** for Fe^{2+} in the presence of various cations. **f** Glass printing of **164** and applied in detection of Fe^{2+}. (Refer to the web version of this article for the legend colour). Reproduced from Ref. 141 with permission of ACS. **g** Chemical structure of **166**. **h** Fluorescence selectivity of **166** for aromatic molecules. (Refer to the web version of this article for the legend colour). Reproduced from Ref. 142 with permission of Springer

on cellulose strips for the naked eye and fluorescence-based detection of ammonia and amine vapours. Cellulose material **166** was synthesised by appending fluorescein-modified chitosan nanoparticles onto cellulose matrix (Fig. 60g). In the presence of alkaline species, the protonated portions of fluoresceins are deprotonated resulting in the turn-on emission (Fig. 60h). The readout limit of **166** for ammonia and amine vapours is determined as 280 ppm in a linear concentration range of 0.13–280 ppm. The cellulosic material **166** can be applied for the detection of ammonia and amine vapours in real samples [142].

A similar sensing application was pursued by Zhang et al. (2019), wherein they developed an amine-responsive cellulose-based ratiometric fluorescent material **167** for the real-time and visual determination of shrimp and crab freshness. Probe **167** constituted of an immobilisation of fluorescein isothiocyanate-based fluorophore indicator and protoporphyrin IX as internal reference onto cellulose acetate, respectively [143]. The blending of green-emitting cellulose fluorescein isothiocyanate and red-emitting protoporphyrin IX cellulose generated a series of dual-emissive fluorescent material **167** with varying ratios (Fig. 61a). In a sample when fluorescein isothiocyanate cellulose and protoporphyrin IX cellulose were blended in a 5:1 ratio, they emitted red fluorescence. However, when exposed to ammonia fluorescein, isothiocyanate was deprived with a proton, a result of which the molecular structure of **167** changed causing green emission. Cellulosic material **167** displays a sensitive, colour responsive, linear and rapid response to ammonia within a range of 5.0 ppm to 2.5×10^4 ppm. The authors have successfully employed **167** for high contrasting, low cost and rapid responsive detection of shrimp and crab spoilage (Fig. 61b). Later in 2021, Cheng and team utilised naphthalimide-based fluorescent molecules for modifying cellulose surface and applied in the detection of 2,4,6-trinitrophenol (TNP). In the process, etherification of cellulose led to the formation of $BrCH_2CH_2NH_2$, $–NH_2$ group bearing cellulose. Further, the formed $–NH_2$ groups were reacted with bromo-1,8-naphthalic anhydride forming a naphthalimide cellulose derivative. Moreover, three different recognition units were introduced by replacing the Br atoms forming cellulosic probes **168**–**170** (Fig. 61c). Cellulosic fluorophore **168**–**170** showed selective fluorescence quenching when in contact with TNP (Fig. 61d). The LODs for **168**–**170** to TNP were

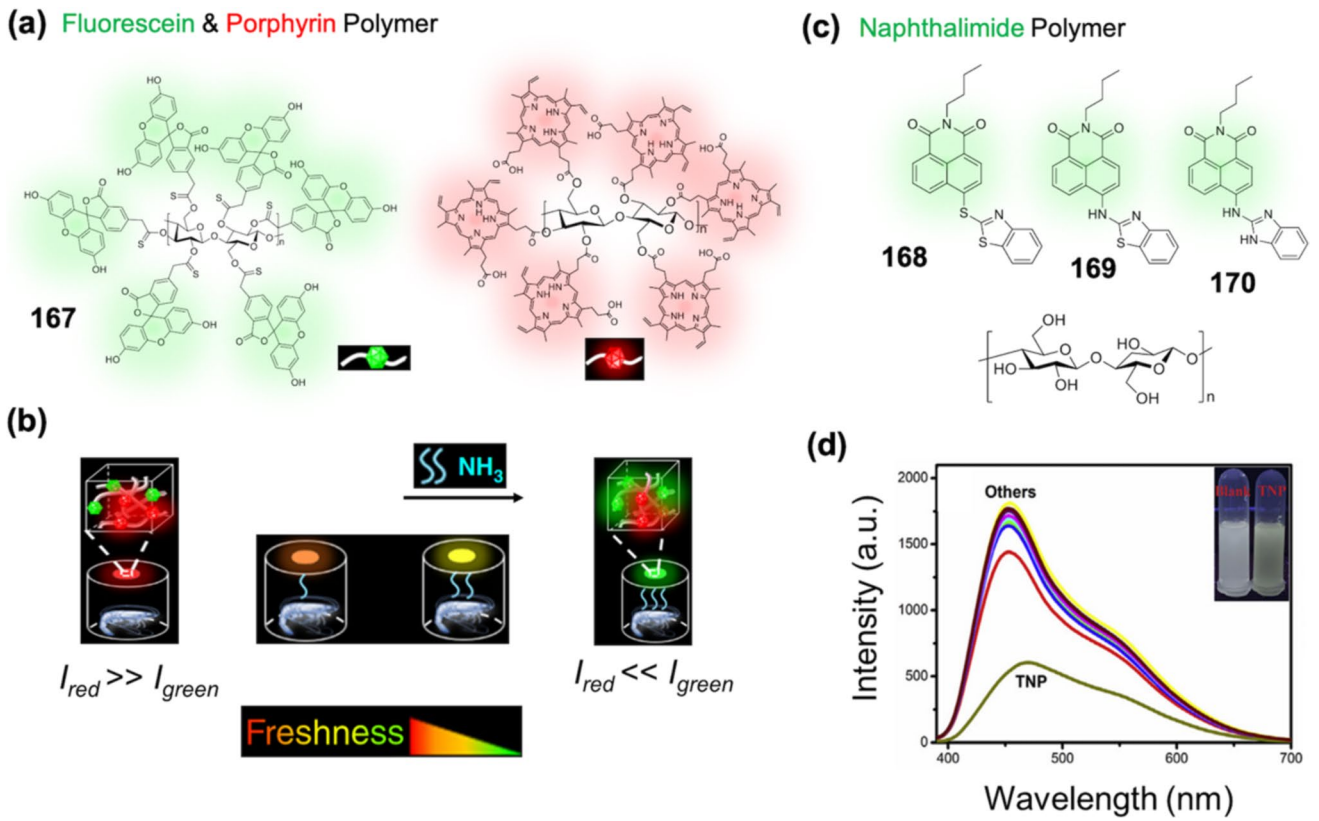

Fig. 61 **a** Chemical structure of **167** and derivative. **b** Estimation of fish freshness using a combination of **167** and derivative. (Refer to the web version of this article for the legend colour). Reproduced from Ref. 143 with permission of Nature. **c** Chemical structure of **168**, **169** and **170**. **d** Quenching-based selectivity profile of **168** for trinitrophenol. (Refer to the web version of this article for the legend colour). Reproduced from Ref. 144 with permission of Elsevier

estimated as 0.52, 0.76 and 0.81 µM, respectively. The aim of the work was to develop a selective sensor for explosive TNP in real-time situations [144].

Liu et al. utilised an oxidation process and two consecutive Schiff bases strategies for modifying the cellulose surface with polyethylenimine (PEI) and salicylaldehyde forming **174** (Fig. 62a). Microcrystalline cellulose was used as the cellulose unit in **174**. Cellulose material **174** exhibited selective fluorescence quenching with Fe^{3+} even in the presence of different counter analytes. Moreover, a colourimetric change was also observed in the profile of **174** with Fe^{3+}. The addition of Fe^{3+} to Salen molecule **174** aids in the formation of a strong complex bond. Moreover, Fe^{3+} induces PET mechanism resulting in the fluorescence quenching of **174**. The fluorescence emission from green to quenched for **174** to Fe^{3+} is also noticeable to the naked eye under the UV lamp (Fig. 62b, c). The detection limit of **174** to Fe^{3+} is determined as 0.01 ppm. The authors consider the potential of **174** to be used in the practical application of on-site Fe^{3+} detection [145]. Yang and co-workers developed a pyrimidine-2-amine derivative-grafted cellulose ratiometric probe **177** for determining pH in extremely acidic media. As depicted in Fig. 62d, probe **177** was synthesised by grafting camphor-derived pyrimidine-2-amine onto dialdehyde cellulose. Cellulosic material **177** can monitor extremely acidic conditions with a p*Ka* of 1.57. On varying the pH of **177** solutions from 6.86 to 1.04, a distinct red shift in fluorescence emission is noticed from 416 to 486 nm (Fig. 62e). Moreover, no interference was observed when treated with metal ions. The cellulosic probe **177** showed prominent stability, high selectivity, good repeatability and rapid response towards H^+. The authors have tested the efficacy of cellulosic material **177** in highly acidic conditions like real vinegar samples [146].

In 2022, Yang et al. developed a cellulose-based fluorescent probe **180** with carboxymethyl cellulose as the skeleton and 8-aminoquinoline as the fluorophore unit for selective, specific and sensitive detection of Cu^{2+}

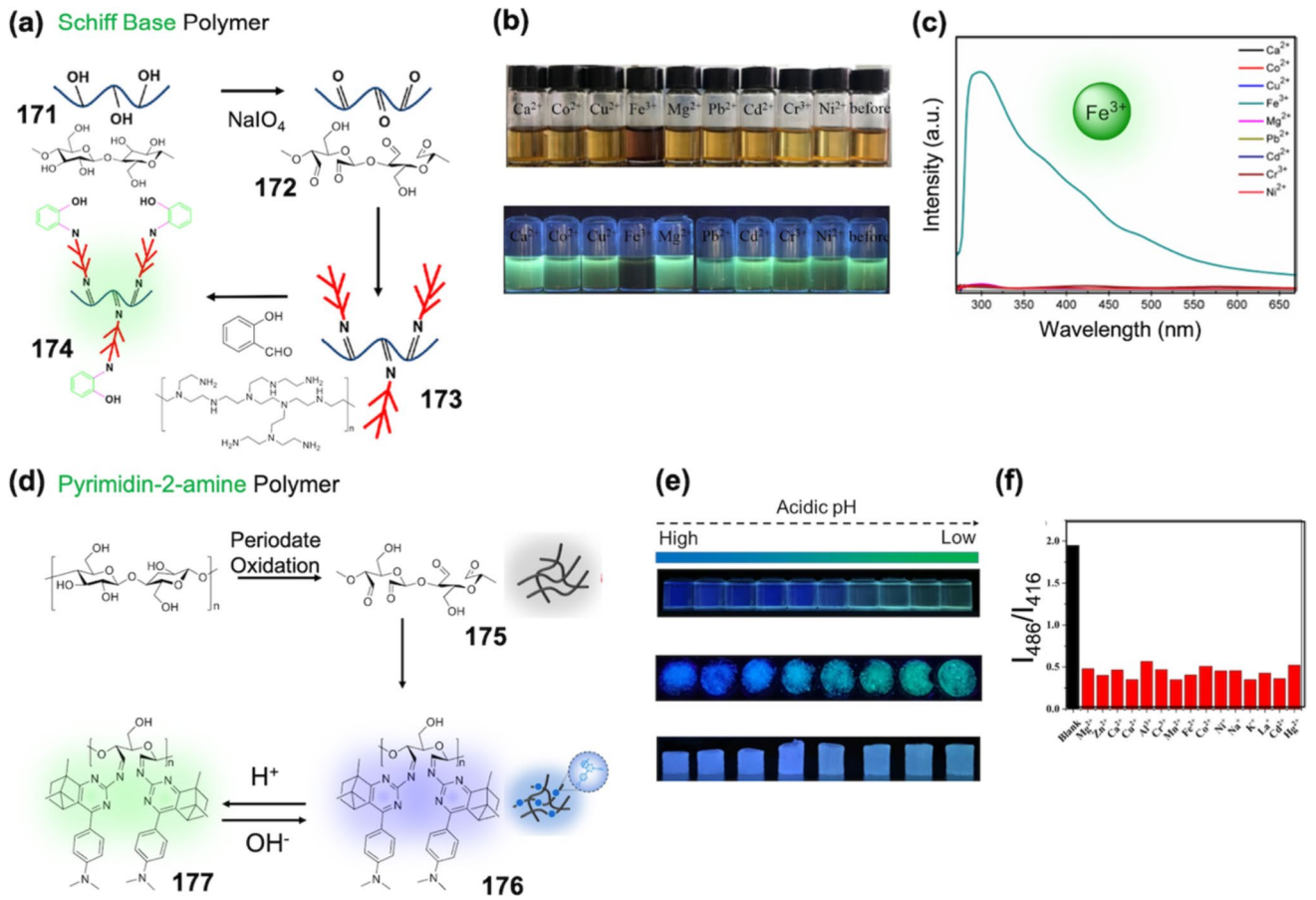

Fig. 62 **a** Chemical structure and synthesis of **174**. **b** Visual detection of Fe^{3+} using **174** both colourimetrically and under UV light. **c** Fluorescence selectivity profile of **174** for Fe^{3+}. (Refer to the web version of this article for the legend colour). Reproduced from Ref. 145 with permission of Elsevier. **d** Chemical techniques and mechanism for the preparation of **177**. **e** Changes in pH visualised on cellulose material. **f** Selectivity profile of **177** in presence of cations. (Refer to the web version of this article for the legend colour). Reproduced from Ref. 146 with permission of Springer

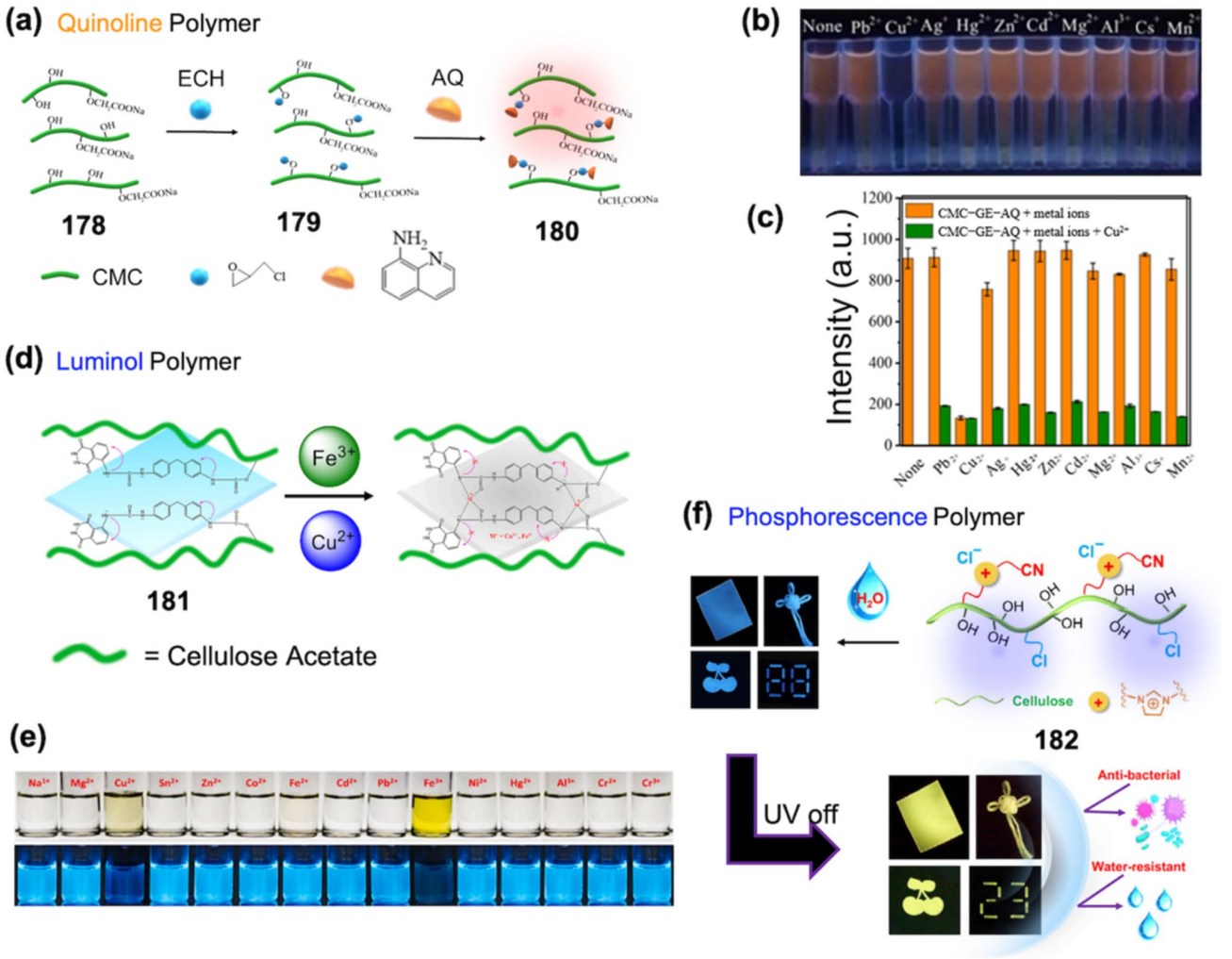

Fig. 63 **a** Preparation method for **180**. **b** Naked eye detection of Cu^{2+} by **180** under UV lamp 365 nm. **c** Interference-based selectivity profile of **180** for Cu^{2+}. (Refer to the web version of this article for the legend colour). Reproduced from Ref. 147 with permission of MDPI. **d** Detection mechanism of **181** for cations. **e** Visual selectivity profile of **181** towards Cu^{2+} and Fe^{3+}. (Refer to the web version of this article for the legend colour). Reproduced from Ref. 148 with permission of Elsevier. **f** Complete study of phosphorescence by **182**. (Refer to the web version of this article for the legend colour). Reproduced from Ref. 149 with permission of Nature

(Fig. 63a). Cellulosic material **180** displayed highly specific turn-off fluorescence response towards Cu^{2+} (Fig. 63b, c). Probe **180** has large oxygen functionality, which assists in the complexation with Cu^{2+} ions. Further, complexation with Cu^{2+} ions induce PET phenomenon in **180**. Moreover, coordination with copper generates a planar structured **180**. All these reasons are attributed for the selective fluorescence quenching of Cu^{2+} by **180**. The LOD of **180** to Cu^{2+} was calculated to be 6.4×10^{-8} mol/L^{-1}. The authors used X-ray photoelectron spectroscopy (XPS) and density functional theory (DFT) techniques to determine the sensing detection mechanism. The authors have tested the efficacy of cellulosic material **180** for the detection of Cu^{2+} ions in real water samples [147].

In another work, Xu and co-workers developed cellulose-based smart materials **181** for colourimetric and fluorescent detection of Cu^{2+} and Fe^{3+} ions and evaluated their application in anti-counterfeiting applications. Cellulosic material **181** was achieved by combining luminol (fluorophore unit) with 4,4′-methylene diphenyl diisocyanate (MDI) as the crosslinker (Fig. 63d). Addition of Cu^{2+} and Fe^{3+} to **181** induced fluorescence quenching (Fig. 63e). Cellulosic material **181** can detect Cu^{2+} and Fe^{3+} as low as 56 ppb and 37 ppb in fluorescence mode. Probe **181** was modified into polymeric films for applicability in anti-counterfeiting experiments. The authors confirm that cellulosic material **181** has outstanding biodegradability and renewability and is cost-effective and non-toxic [148]. Zhang et al. developed a

cellulose-based phosphorescent material **182** with excellent anti-bacterial, water-resistance and easy processability. The phosphorescent cationised cellulose derivative **182** was prepared by introducing ionic structures, which include cyanomethyl imidazolium cations and chloride anions, into the cellulose matrix. The phosphorescence of cellulosic material **182** was achieved by intersystem crossing enabled by the cyano group and nitrogen element in imidazolium cations. The cations (chloride anions) in the cyano group undergo multiple hydrogen bonding and electrostatic attraction interactions with the hydroxyl group in cellulose, forming **182** and resulting in the effective inhibition of non-radiative transitions. The cellulose-based phosphorescent material can be easily modified into films, fibres, patterns and coatings by utilizing eco-friendly aqueous solution processing strategies. The authors have tested the worth of cellulosic material **182** for antibacterial properties and water resistance (Fig. 63f) [149].

Formaldehyde (HCHO) is a simple reactive carbonyl compound that plays a crucial role in pathological processes as a biomarker. In living organisms, HCHO is exclusively linked to the synthesis of neurotransmitters and amino acids. Hence, it is important to monitor the levels of HCHO. Kong and co-workers introduced a cellulose-based fluorescent probe **183** for the quantitative detection of HCHO, aiding in the determination of spoilage of real food samples and bioimaging in living cells. In probe **183**, cellulose is functionalised with hydrazine naphthalimide (fluorophore unit) (Fig. 64a). In the presence of HCHO, cellulosic material **183** exhibits a strong fluorescence turn-on response (Fig. 64b). Cellulosic material **183** can rapidly detect HCHO with 12.3-fold increase in the emission intensity. The limit of detection (Fig. 64c) of **183** towards HCHO is calculated as 0.09 ppm. Probe **183** was used to estimate levels of HCHO in HepG2 cells. Moreover, the efficacy of **183** test papers for HCHO was also tested in food and water samples (Fig. 64d) [150]. In another work, Yang and group introduced a coumarin-grafted dialdehyde cellulose-based fluorescent material **184** for the sensitive and selective detection of Fe^{3+} ions (Fig. 64e). Cellulosic material **184** was prepared by condensation reaction between dialdehyde cellulose and coumarin derivative. In the presence of Fe^{3+} ions, the fluorescence

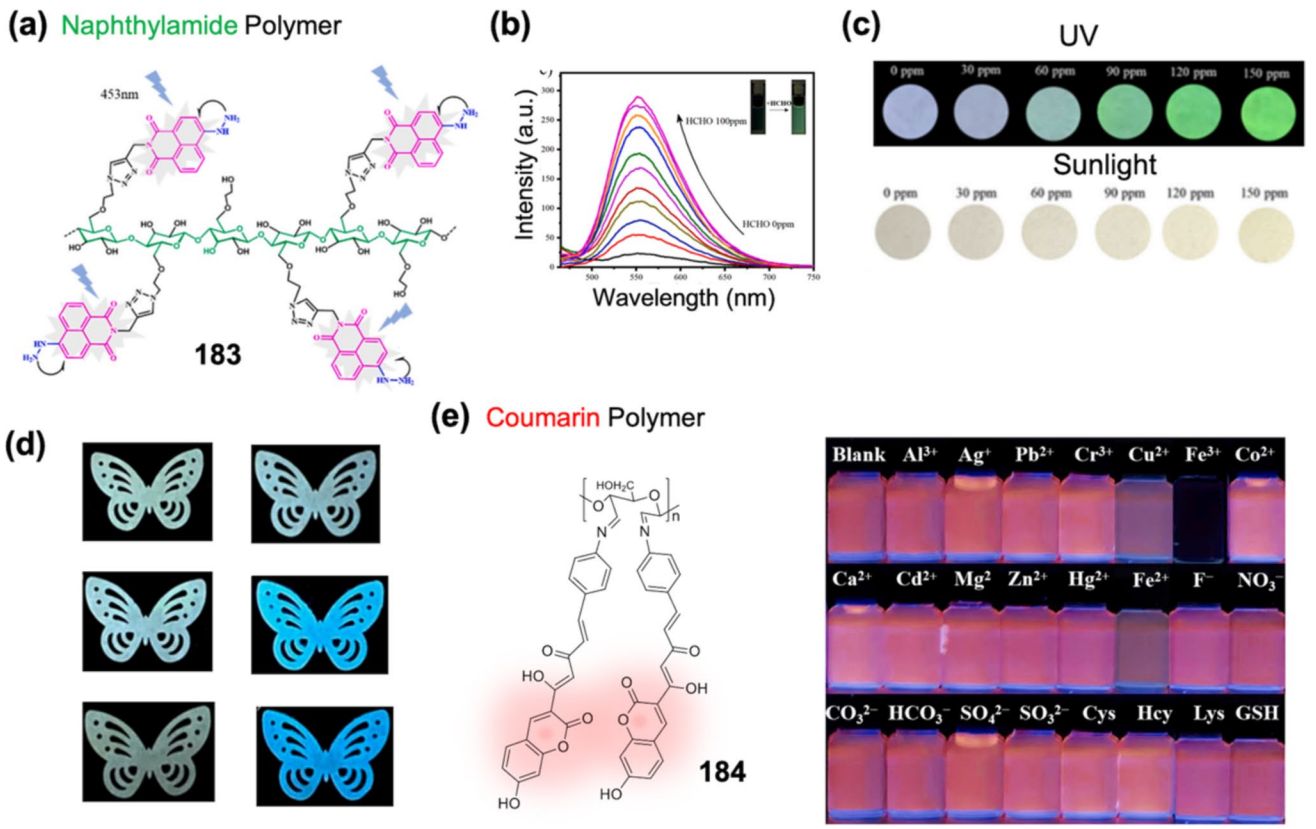

Fig. 64 **a** Chemical structure of **183**. **b** The changes of fluorescence spectra of probe **183** at different HCHO concentrations. **c** Colour change of the strips doped with **183** on treatment with different concentration gradients of HCHO. **d** Images for test paper application of **183** to HCHO. (Refer to the web version of this article for the legend colour). Reproduced from Ref. 150 with permission of Elsevier. **e** Chemical structure of **184** and fluorescence selective images of **184** towards Fe^{3+}. (Refer to the web version of this article for the legend colour). Reproduced from Ref. 151 with permission of Elsevier

emission of **184** is quenched, with a naked eye colour change from pink to colourless under a UV lamp (Fig. 64e (right)). The quenching profile resulted from the complexation between 184 and Fe^{3+} inducing PET mechanism. The LOD of **184** to Fe^{3+} was estimated as 91.7 nM. The authors consider coumarin-embedded cellulosic material **184** as capable of monitoring levels of Fe^{3+} in water samples [151].

In another illustration of coumarin cellulose interaction, Yang et al. synthesised a coumarin-modified fluorescent cellulose probe for sensitive and selective detection of CN^- in food samples. Cellulosic material **185** (Fig. 65a) was synthesised by utilizing cellulose acetate as the skeleton matrix and the coumarin derivative as the fluorophore unit. The presence of CN^- produced a fluorescence quenching effect on **185** (Fig. 65b). The interaction between **185** and CN^- generates a new species, i.e. **185**-CN^-, which is non-fluorescent. Cellulosic material **185** can detect CN– as low as 5.8×10^{-7} M, which is lower than the recommended limit of CN^- by WHO in drinking water. The fluorescent cellulosic film **185** was capable of detecting CN^- in food samples like bitter almonds and germinated potatoes (Fig. 65c) [152]. In a crucial report, Zhu and co-workers developed a dual-responsive cellulose-based fluorescent material fabricated **186** in a CO_2 switchable solvent for multifunctional applications (Fig. 65d). Cellulosic material **186** was successfully grafted by using 7-hydroxy-4-trifluoromethyl coumarin (HFC) and poly (lactic acid) onto the cellulose backbone. Cellulose probe **186** showed effective quenching of fluorescence towards Fe^{3+} (Fig. 65e, f). As reported earlier here, also the binding of Fe^{3+} with **186** induces the PET mechanism, leading to fluorescence quenching. The authors consider cellulosic material **186** capable of real-time, accurate and visual monitoring levels of Fe^{3+} in aquatic products [153].

In the same year, Yang and the group utilised an efficient ethyl cellulose fluorescent probe **187** for quick detection of Fe^{3+} and its multifaceted applications. The authors grafted flavanol on an ethyl cellulose bed to form **187** and applied it for the detection of Fe^{3+} ions (Fig. 66a). The addition of Fe^{3+} to cellulosic material **187** resulted in fluorescence quenching. Here also on complexation with Fe^{3+}, PET phenomenon is activated resulting in the fluorescence quenching. The detection of Fe^{3+} by **187** can be visualised under a UV lamp (Fig. 66b). The detection limit of Fe^{3+} by **187**. The LOD is determined as 2.65×10^{-7} mol/L. The **187**-loaded filter paper can be used for the estimation of Fe^{3+} in real water samples (Fig. 66b) [154].

In another illustration of cellulosic probes for the detection of Fe^{3+}, Cheng and co-workers developed highly soluble cellulose-derived fluorescent probes **188**–**190** for the simultaneous detection and removal of Fe^{3+}. Cellulosic probes **188**–**190** were produced in different steps. In the first step, the hydroxyl group in glucose units was reacted with thionyl chloride to generate chloro-cellulose (Cell-Cl). In the second step, Cell-Cl was reacted with 2-mercaptobenzothiazole, and CS_2 paved the way for the creation of a cellulose-based macromolecular RAFT reagent (Cell-CTA). Finally, naphthalimide units, fluorescent monomers bearing

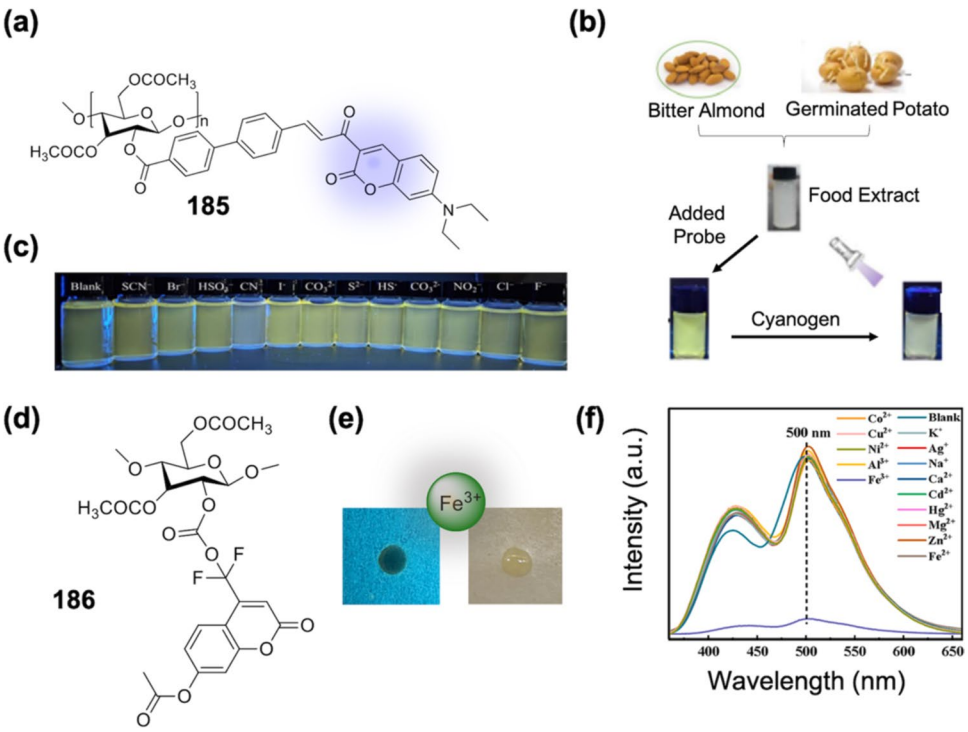

Fig. 65 **a** Chemical structure of **185**. **b** Detection strategy used by **185** for estimating CN^- in food samples. **c** Naked eye change in fluorescence of **185** in presence of CN^-. (Refer to the web version of this article for the legend colour). Reproduced from Ref. 152 with permission of RSC. **d** Chemical structure of **186**. **e** Naked eye change in the profile of **186** coated cellulose paper in presence of Fe^{3+}. **f** Quenching profile of **186** in the presence of Fe^{3+}. (Refer to the web version of this article for the legend colour). Reproduced from Ref. 153 with permission of Elsevier

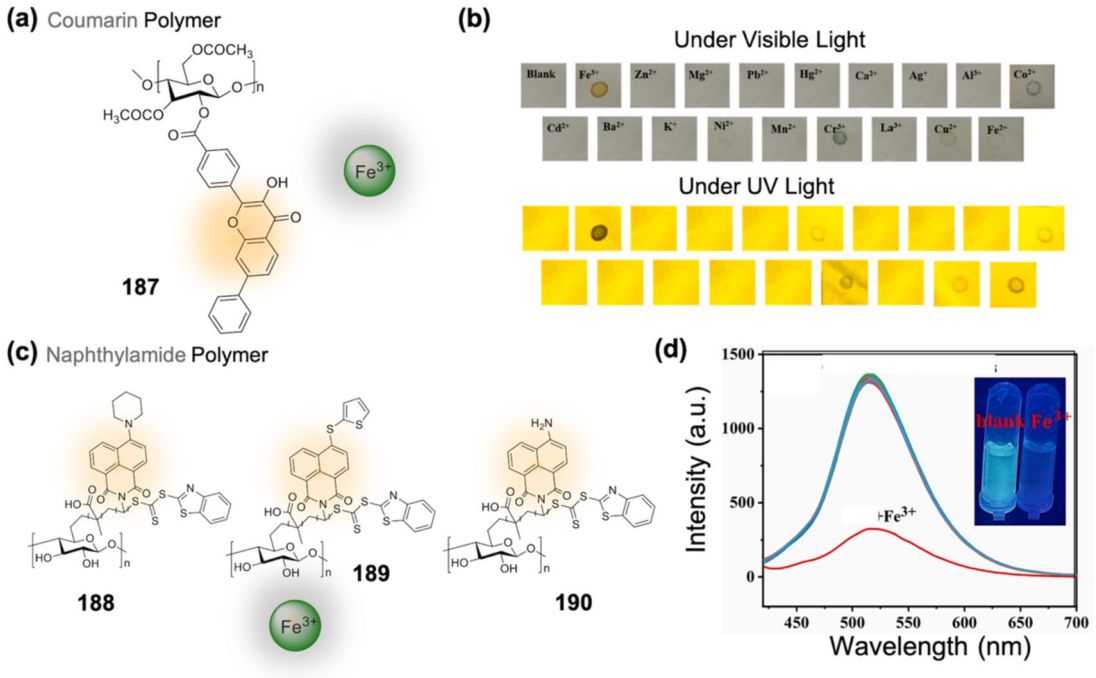

Fig. 66 **a** Chemical structure of **187**. **b** Naked eye selectivity of **187** doped cellulose paper for Fe^{3+}. (Refer to the web version of this article for the legend colour). Reproduced from Ref. 154 with permission of Elsevier. **c** Chemical structure of napthalimide-cellulose molecules **188–190**. **d** Quenching profile of **190** for Fe^{3+} in the presence of various counter analytes. (Refer to the web version of this article for the legend colour). Reproduced from Ref. 155 with permission of Elsevier

–C = C– and methacrylic acid were grafted on the cellulose chain via the RAFT polymerization technique forming **188–190** (Fig. 66c). The soluble cellulose macromolecular materials **188–190** are capable of selectively recognizing Fe^{3+} (fluorescence quenching) in pure water with excellent recyclability and regeneration (Fig. 66d). The modification of cellulose improves the hydrophilicity and introduces fluorophore unit while decreasing the crystallinity enabling solubility of **188–190** both in water and organic solvents. As per the authors, the cellulosic probe **188–190** can be utilised for the simultaneous detection and adsorption of Fe^{3+} ions in water [155].

Later in the same year, Cheng et al. doped cellulose surface with fluorescent naphthalimide forming polymeric fluorescent probes **191**, **192** and **193**. Figure 67 a depicts the solid emission images of probes **191–193** under a UV lamp. To attain products **191–193**, at first esterification reaction between the –OH group of cellulose and acryloyl chloride was pursued. Further, using the thiol-ene click reaction, –C = C on cellulose, –SH on cysteamine and $–NH_2$ groups at the chain ends were conferred on cellulose. This pre-treated cellulose was reacted with 4-bromo-1,8-naphthalene anhydride derivatives forming **191–193**. Cellulosic materials **191–193** exhibit selective quenching in the presence of Fe^{2+} (Fig. 67b, c). Under basic conditions, the electron-donating nature of N atom of **191–193** is impaired by the –OH group, leading to the intramolecular charge transfer (ICT) phenomenon. However, on addition of Fe^{2+}, the PET mechanism is induced in **191–193**, causing fluorescence quenching. As the prepared probes **191–193** are fabricated into cellulose membrane, their utility as a portable device is conceivable [156]. Mercurous ions (Hg^+) are inorganic elements or simply inorganic mercury that possess high-end neuro and nephrotoxicity. Recently, in 2024, Cheng and co-workers introduced an organic-solvent-soluble cellulose doped with fluorescent polyurethanes and utilised it for the simultaneous detection and removal of Hg^+ ions. In this study, the authors have integrated fluorophore naphthalimide into cellulose-based polyurethane films to generate **195** (Fig. 67d). Upon contact with mercurous ions (Hg^+), the fluorescence profile of **195** is quenched (Fig. 67e). Hg^+ is considered to have strong electrophilicity as it is a Lewis acid. The lone pairs of N and O atoms in **195** interact with Hg^+ forming strong binding. These result in the fluorescence quenching of **195** as Hg^+ is a strong quencher. Moreover, **195** displays an adsorption capacity of 8.4 mg cm^{-2} for Hg^+. The cellulosic film **195** can be applied for monitoring and reducing the mercurous-related environmental pollution [157].

In 2023, Shi and their team developed cellulose-based fluorescent films **196** and **197** with enamine bonds for applicability in anti-counterfeiting and UV shielding. The preparation of **196** and **197** was made possible in two steps

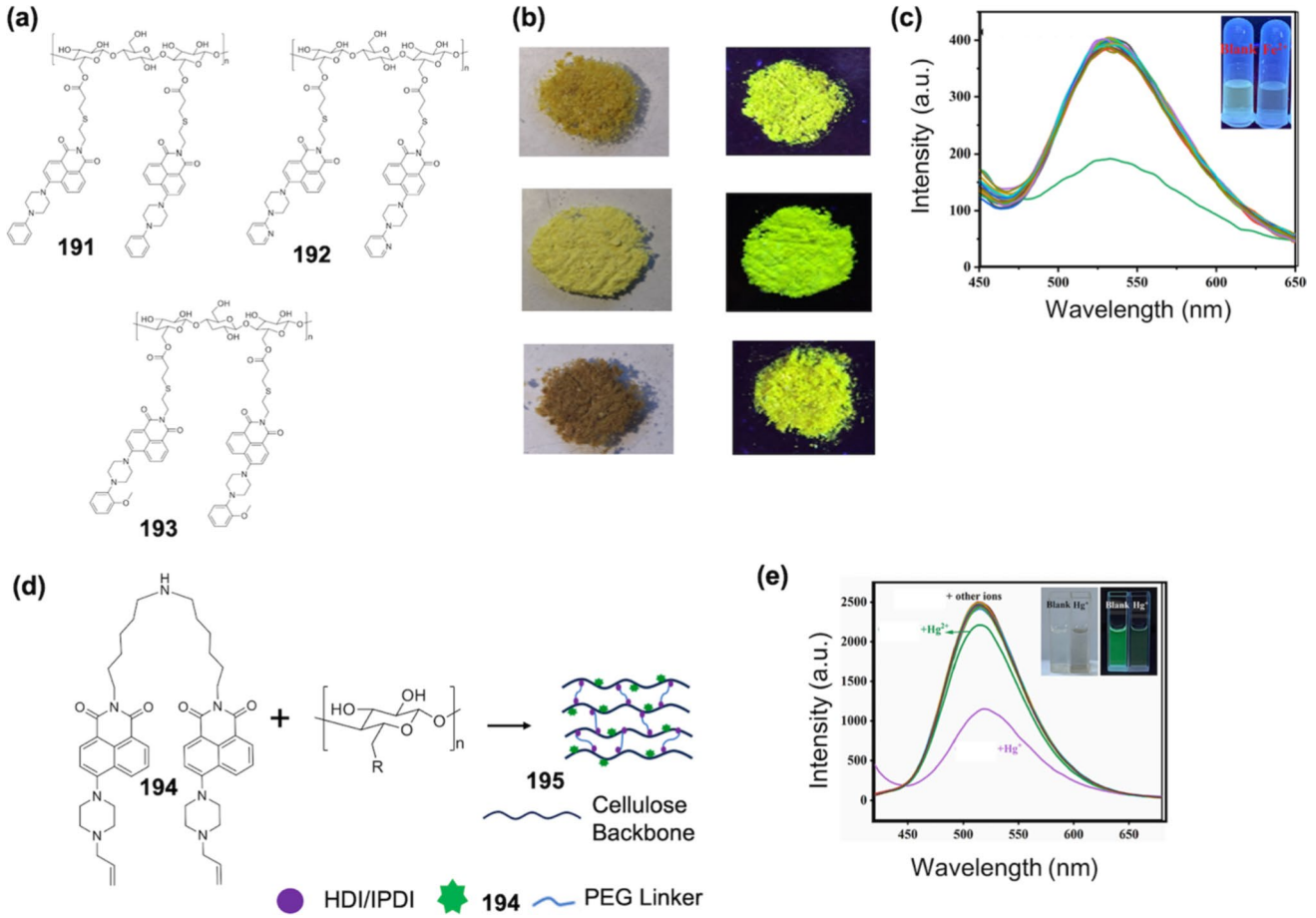

Fig. 67 **a** Chemical structure of cellulosic material **191**–**193**. **b** Solid state emission profile of **191**–**193**. **c** Quenching profile of **193** for Fe^{3+} in presence of different counter cations. (Refer to the web version of this article for the legend colour). Reproduced from Ref. 156 with permission of Springer. **d** Chemical synthesis of cellulosic material **195**. **e** Quenching profile of **195** for Hg^{+} in the presence of other counter cations. (Refer to the web version of this article for the legend colour). Reproduced from Ref. 157 with permission of Elsevier

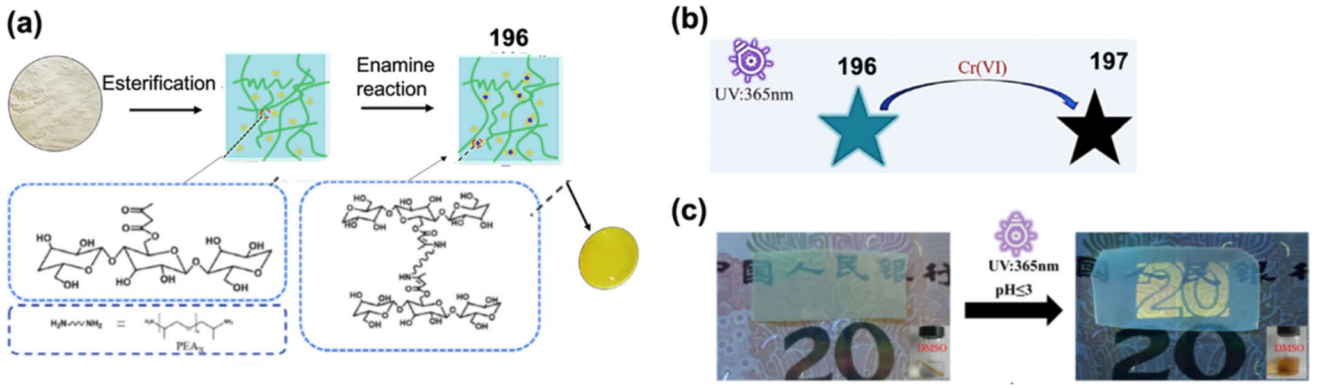

Fig. 68 **a** Chemical method for the synthesis of **196**. **b** Mechanism for the detection of Cr(VI) by **196**. **c** Cellulose film coated with **196** used in anti-counterfeiting application. (Refer to the web version of this article for the legend colour). Reproduced from Ref. 158 with permission of RSC

by grafting microcrystalline celluloses with acetoacetyl groups, followed by crosslinking with polyetherimide (Fig. 68a). The mechanical properties of **196** and **197** polymeric films are drastically improved by the crosslinking procedure. Moreover, the enamine bonds in **196** and **197** help in inducing recyclability to the polymer films. The fluorescence of **196** and **197** got quenched in the presence of Cr(VI) solution (Fig. 68b). Further, the polymeric films **196** and **197** can be utilised for anti-counterfeiting and UV shielding applications (Fig. 68c) [158].

In the same year (2023), Qin et al. developed dual-emitting cellulose nanocrystal hybrid material **198**. Product **198** comes with circularly polarised luminescence and can be easily applied in anti-counterfeiting labels. Material **198** constitutes lanthanide complexes as luminescent units and CNCs as chiral nematic moieties (Fig. 69a, b). The so-obtained **198** films show excellent broadband reflection across the visible spectrum. The so-mentioned feature is attributed to the chiral nematic domains from CNCs. The broad reflection band of **198** covers both green and red fluorescent emission centres and also generates circularly polarised luminescence emission (Fig. 69c). The CNC-based material **198** with tailored shapes is further employed as anti-counterfeit tags and decorative applications [159].

4.3.2 Colourimetric-based polymers (Cello-Other-Poly)

There are very few illustrations of Cello-Other-Poly as colourimetric chemosensors. Pangon and co-workers developed colourimetric probe **199** based on urethane-linked imidazole-cellulose microcrystals for the detection of different important metal ions. The surface modification of cellulose microcrystals (CMCs) was performed by using 1,1-carbonyldiimidazole and 1-(3-aminopropyl)imidazole, respectively, producing **199** (Fig. 70a, b). The colourimetric changes in the profile of **199** with different metal ions like Fe^{2+}, Fe^{3+}, Co^{2+}, Ni^{2+}, Cu^{2+}, Zn^{2+}, Ag^{+} and Cd^{2+} are depicted in Fig. 70c. The presence of urethane linked- imidazole on cellulose is credited for the increased adsorption capacity of **199** towards Zn^{2+} (3 times) and Ni^{2+} (23 times). The authors consider **199** to be capable of being utilised as sustainable bioadsorbents and sensing materials for metal separation and water purification [160]. Later in 2019, Liu and co-workers developed high-purity cellulose membrane **200** based on a sensitive enzyme colourimetric assay for the determination

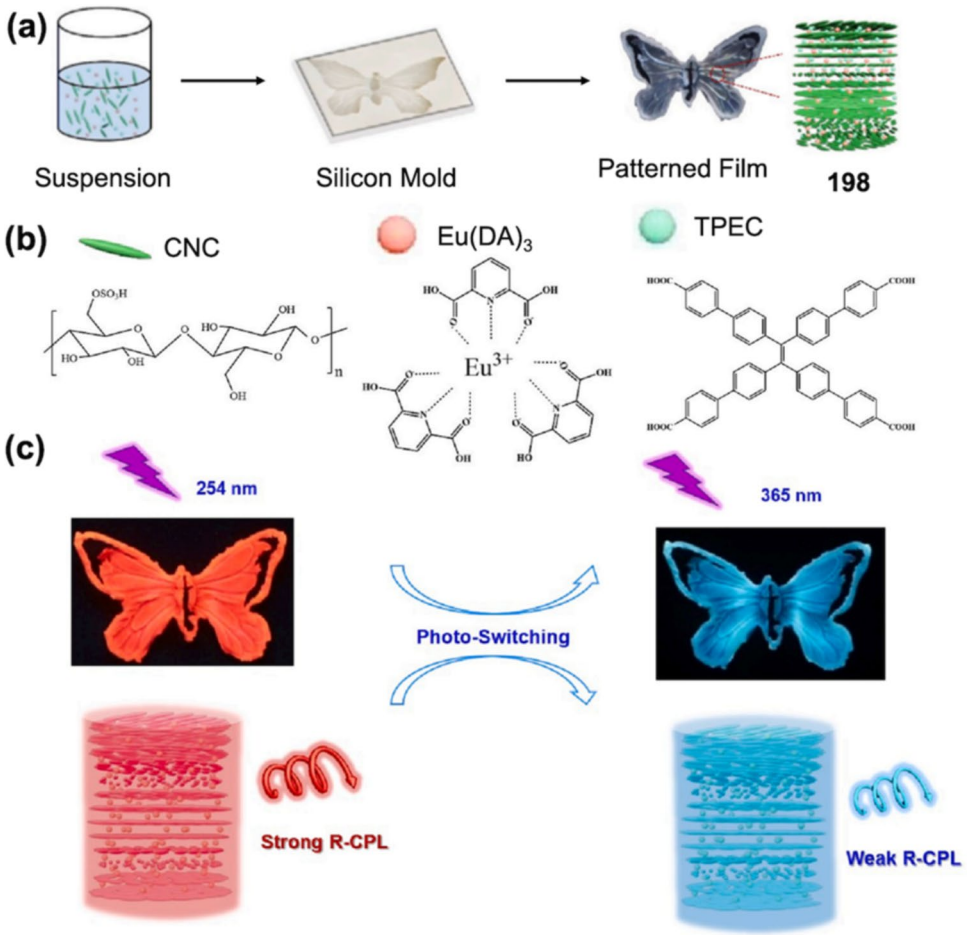

Fig. 69 **a** Chemical method to synthesise cellulose film **198**. **b** Different moieties involved in the preparation of **198**. **c** Photo switching ability of **198** in butterfly patterns. (Refer to the web version of this article for the legend colour). Reproduced from Ref. 159 with permission of Elsevier

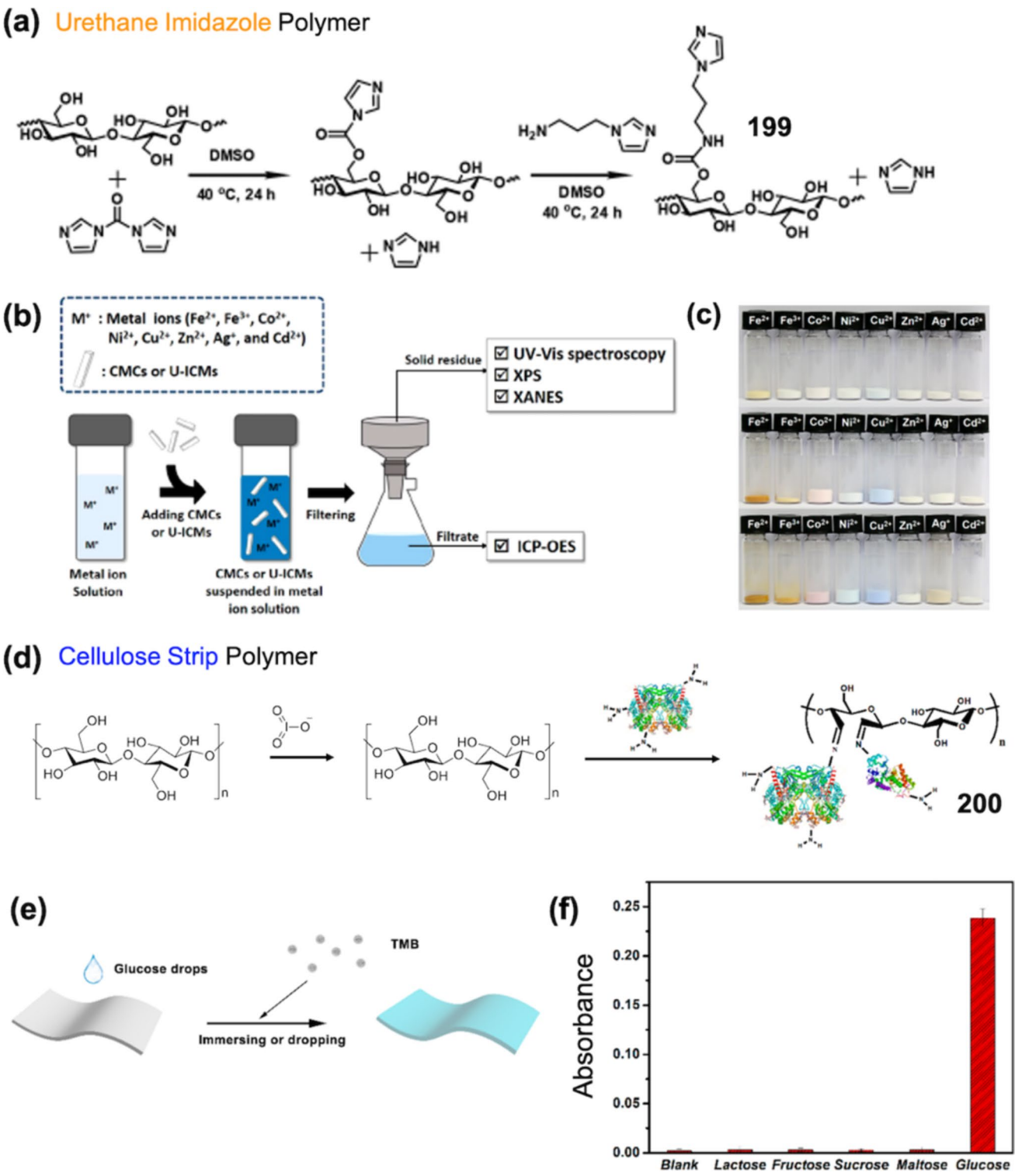

Fig. 70 **a** Synthesis route for preparation of **199**. **b** Experimental setup for studying metal adsorption and sensing. **c** Images of **199** after exposure to various metal ion solutions. (Refer to the web version of this article for the legend colour). Reproduced from Ref. 160 with permission of ACS. **d** Synthesis methodology for **200**. **e** Detection mechanism of **200** towards glucose. **f** Selectivity profile of **200** towards glucose in the presence of different counter analytes. (Refer to the web version of this article for the legend colour). Reproduced from Ref. 161 with permission of ACS

of low concentrations of glucose (Fig. 70d). At first, cellulose was dissolved in NaOH/urea solution and then modified with sodium periodate oxidation technique resulting in the immobilization of glucose oxidase (GOx) and horseradish peroxidase (HRP) with Schiff-base (Fig. 70e). The enzymatic cellulosic probe **200** can selectively detect low concentrations of glucose (Fig. 70f). The sensing mechanism is as follows: in probe **200**, the GOx unit can catalyse the oxidation of glucose forming H_2O_2. Further, the reaction of H_2O_2 with 3,3',5,5'-tetramethylbenzidine (TMB) under the oxidation of horseradish peroxidase yields a blue colour, indicating the presence of glucose. The LOD of **200** to glucose was estimated as 0.45 nM in the linear range of 1 to 11 nM. The authors consider that this work will provide a new strategy for the development of cellulose-based functional materials applicable in biosensors, drug carriers and biomedicine [161].

In another work (2019), Wang and co-workers developed a biomass cellulose–derived simple colourimetric probe for in situ visual recognition of Cu^{2+} (Fig. 71a). Cellulosic material **201** was synthesised by a Schiff base reaction between the aldehyde moieties in dialdehyde cellulose and the amino functionality of 2,6-pyridine dihydrazide. The as-prepared sensor **201** displayed a selective visual and colourimetric detection towards Cu^{2+}. The visual detection limit of **201** towards Cu^{2+} was estimated as 10^{-7} mol/L (Fig. 71b). The detection of Cu^{2+} was attributed to the different functionalities like –C = O, –NH and $–NH_2$ in **201**, also possessing a large external surface area, short transit distance and flexibility. The cellulose grafted material **201** can be used for the in situ detection of Cu^{2+} ions [162]. In 2023, Zhang and co-workers introduced a cellulose membrane–based nanozyme immobilization platform **202** for the colourimetric detection of hydrogen peroxide (H_2O_2) and uric acid (UA) (Fig. 71c). The cellulose membrane platform is immobilised with gold nanoclusters, which can mimic peroxidase and also catalyse the oxidation of 3,3′,5,5′-tetramethylbenzidine (TMB) by H_2O_2.Cellulosic material **202** can detect H_2O_2 with a visual detection limit of 7 µM and uric acid in a concentration range of 50–500 µM. The development of cellulosic material **202** provides new insights into the effective immobilization of enzymes on cellulose surfaces [163].

In 2021, Sarute et al. utilised cellulose developed from recycled office waste and formed a colourimetric composite platform **203** for the colourimetric detection of food spoilage (Fig. 72a). The cellulose composite **203**

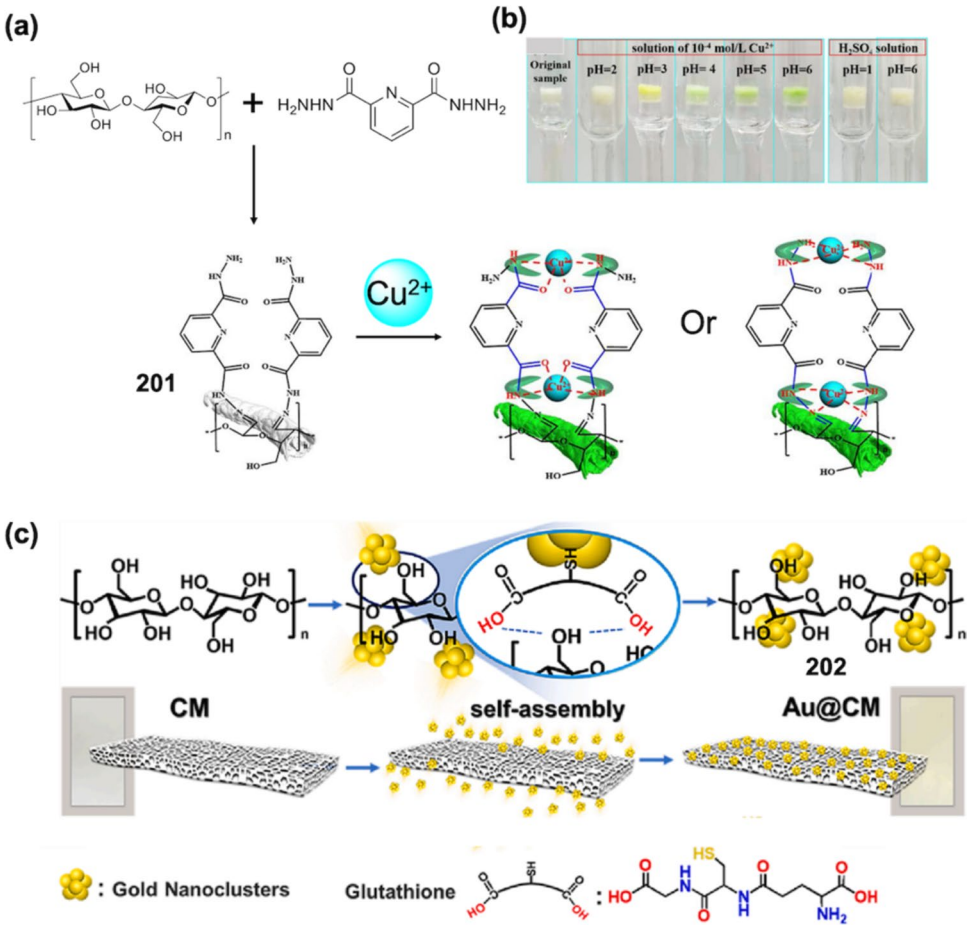

Fig. 71 **a** Synthetic profile of **201** and detection mechanism of Cu^{2+}. **b** Colourimetric change in **201** doped cellulose by changing pH. (Refer to the web version of this article for the legend colour). Reproduced from Ref. 162 with permission of Elsevier. **c** Complete procedure for the formation of **202**. (Refer to the web version of this article for the legend colour). Reproduced from Ref. 163 with permission of Elsevier

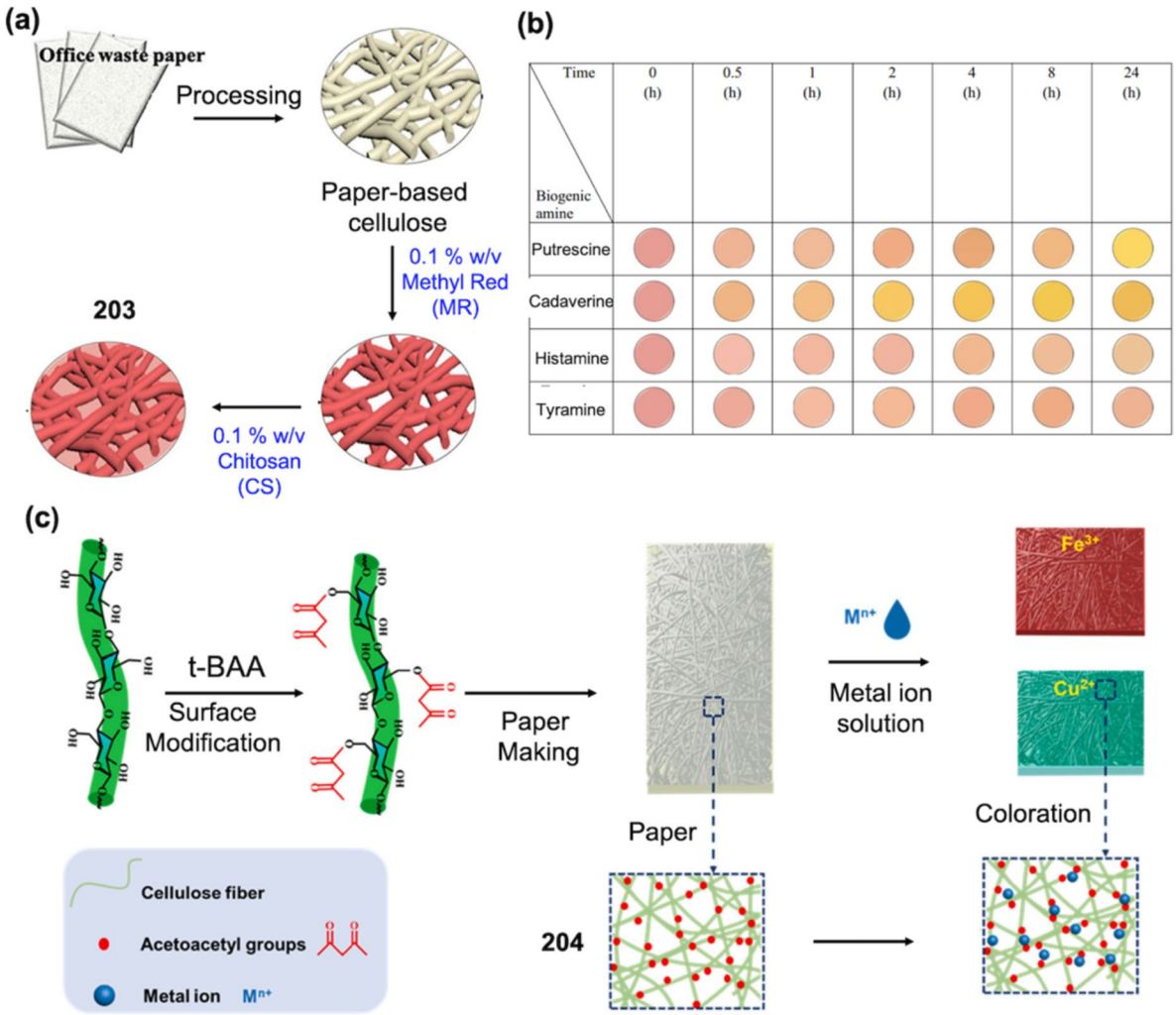

Fig. 72 **a** Chemical proportions in the formation of **203**. **b** Visible changes in the colour patterns of **203** doped cellulose in the presence of different biogenic amines. (Refer to the web version of this article for the legend colour). Reproduced from Ref. 164 with permission of Springer. **c** Preparation of **204** and its use in colourimetric detection of Fe^{3+} and Cu^{2+}. (Refer to the web version of this article for the legend colour). Reproduced from Ref. 165 with permission of Elsevier

constituted of a dye methyl red and chitosan. The so-developed cellulose composite was capable of colourimetrically visualizing biogenic amines such as putrescine, cadaverine, histamine and tyramine. Probe **203** can discriminate different biogenic amine vapours based on different detection times (Fig. 72b). In the presence of biogenic amine vapours, the colourimetric change in **203** was retained for 8 h. The authors consider cellulosic composite **203** capable of determining food spoilage [164]. Qi and co-workers introduced an efficient and portable cellulose-based colourimetric test paper for metal ion detection. The authors have used a surface esterification approach for impending acetyl groups on the surface of cellulose fibres (Fig. 72c). Further, utilizing a paper-making process, the developed cellulose acetoacetate fibres were transformed into cellulose acetoacetate paper **204**. The cellulosic paper **204** is known to have robust mechanical properties, good thermal stability and rapid selectivity to Fe^{3+} and Cu^{2+}. The acetoacetyl groups in **204** are coordinatively chelated with metal ions to form a six-membered ring aiding in the visual recognition of metal ions. The mechanism utilised in this work is promising for future applications. However, the selectivity profile is doubtful [165].

5 Future and challenges

In this section, we will review the future prospects and challenges in cellulosic materials as optical chemosensors.

5.1 Future and challenges in cellulose-derived organic materials (Cello-Org)

Cellulose is a renewable, highly efficient, eco-friendly and low-cost material with remarkable adsorption efficiency. Cellulose consists of several –OH functional groups that can be easily modified using different organic molecules [187]. Organic molecule–based optical sensors can be either adsorbed on the surface of cellulose matrix like paper or can undergo reaction and form new colourimetric and fluorimetric templates. The so-mentioned features enable cellulosic material to act as template for holding organic dyes and fluorophores capable of usage as optical chemosensors. Adsorption of fluorophore and dyes on the surface of cellulose is related with different characteristics like the initial concentration of fluorophore, the dose of adsorbent, pH of the solution and temperature. However, to pursue proper integration of organic molecules on cellulose matrix, it is important to modify the cellulose surface with different functional groups.

1. Modifications of the cellulose matrix can help in the enhancement of adsorption capacity and reactive sites on the cellulose surface. For the real-time monitoring of different toxic, hazardous environmental and biological materials, the organic fluorophore and colourimetric dye embedded in the cellulose matrix is highly useful.
2. Cellulose-based organic materials can generate low-cost, high-end and portable devices for the monitoring of different analytes. Generally, researchers employ cellulose papers for adsorbing fluorescent and colourimetric organic chemosensors and use it as dip-in device for real-time detection of analytes. However, in the absence of proper adsorption, some of the organic dyes are released into the water during real-time examinations. Moreover, this leakage also reduces the efficacy of the developed sensor system. Hence, the actual reported LODs for probes cannot be achieved during real-time examination.
3. It is very important to fabricate organic dyes with cellulose matrix by synthetic approach. Moreover, optimization of cellulose PAD matrix, repetitive deposition of sample onto cellulose substrate and preconcentration by solid-phase extraction can be used for the development of optical chemosensors.
4. New innovative techniques for modification of cellulose surface and sequential integration of organic chromo and fluorophores should be ensured for enhancing the real-time applicability of optical chemosensors.

5.2 Future and challenges in cellulose-derived nanomaterials (Cello-Nano)

As discussed in the review, cellulose matrix displays high bio and haemocompatibility and good biodegradability. Moreover, cellulose materials show slow degradation both in vivo and in vitro. The mentioned property of cellulose makes it an excellent candidate for application in different scaffolds. Different chemical oxidation strategies on bacterial cellulose surfaces, such as TEMPO-mediated oxidation [280], exposure to γ-radiation [281], periodate [280] or incorporation of an enzyme, can improve the degradability of cellulose [282]. Utilizing cellulose nanomaterials aids in the improvement of the mechanical strength of nanomaterials. The hydroxyl functional groups in cellulose induce high functionality, which is crucial for interfacial interactions during a composite formation. As discussed in this review, nanocellulose such as cellulose nanocrystals (CNCs) and cellulose nanofibres (CNFs) have been excessively employed for modifying organic dyes and different nanoparticles forming cellulosic hybrids. CNCs and CNFs have abundant hydroxyl groups, which aid in surface functionalization for applicability in optical chemosensing.

1. CNCs attain properties like high strength, high degree of crystallinity, high degree of hydrophilicity, hydrophobicity and self-affinity that are comparable to pure cellulose. Nevertheless, CNC inclusion and dispersion into polymeric systems are both vital and difficult.
2. It will be of great interest to study the hierarchical CNC structures for photonic applications. Aligned CNCs with the capability of detecting biomolecules and essential biomarkers should be explored. Moreover, the alignment of CNCs can be achieved by utilizing minimum resources.
3. Raw cellulose is extensively used for the preparation of carbon and quantum dots. However, the CDs and QDs developed from cellulose face the challenge of low luminescent intensity and quantum yield. This drawback of cellulose-generated CDs and QDs can be corrected by combining them with metallic and non-metallic heteroatoms.
4. Another drawback of CDs as fluorophores is their colour availability. Most of the developed CDs show blue and green emission; other less energy colours like orange and red are rarely produced. The focus should be on the development of cellulose-derived CDs, which can emit low energy emission frequencies of orange, pink and red for their applications in bioimaging.
5. There is room for the generation of high-performance cellulose-based fluorescence composites by the innovation of high-quality CDs, with properties like high fluorescence at solid states, thermal activation resultant

delayed fluorescence and room temperature phosphorescence.
6. Different dimensional cellulose-derived CDs should be prepared for improving energy consumption, decreased hydrophobicity and poor stability caution. CDs are easily detachable from the cellulose architecture. Hence, special attention should be paid to improving the attachability of CDs to the cellulose surfaces.
7. Quantitative and strong binding between CDs and cellulose should be promoted to maintain fluorescence stability even under the influence of diverse external environments.
8. It is very important to understand the underlying significance of cellulose-based nanomaterials and accordingly modify them with different organic, inorganic and nano moieties for application in optical chemosensing.

5.3 Future and challenges in cellulose-derived polymeric materials (Cello-Poly)

In this review, we have noticed several polymer-cellulose (hydrogel, coordination networks, micelle and organic) interactions and their applications in optical chemosensing. In the case of cellulose hydrogels, it is easy to incorporate biological elements and analytes into its core. Hence, the usage of cellulose hydrogels in optical chemosensing has a very bright future. The hydrophilic hydroxyl groups in cellulose allow it to bind easily with different hydrogels and can increase the stability of synthesised hydrogels. Hydrogels synthesised from cellulose are promising soft matters that can accommodate many important species as a result enhancing their properties. Cellulose hydrogels can be used in the development of luminescent materials for packaging and anti-counterfeiting applications. Moreover, extensive application of cellulose hydrogels can be pursued for the design and development of 3D-printed optical chemosensors. Cellulose hydrogels can also undergo trial for application for real-time monitoring of relevant biological analytes. Cellulose hydrogels can also be fabricated into biodegradable films for real-time sensing applications.

Cellulose is capable of usage as a binder, modulator and support for different polymeric materials. For instance, the TEMPO-cellulose nanofibrils changed the formation of nucleation and growth for MOF crystals [283]. Cellulose helps to improve the mechanical properties of coordination polymers like MOFs. It is very important to focus on synthetic factors like synthesis, drying and others for improving the quality of generated cellulose MOFs. Loading coordination polymers into cellulose can add properties such as crystallinity, surface accessibility and high specific area to the composites. However, the hydrophilic nature of cellulose increases the levels of moisture in the coordination polymer cellulose composite causing unstable mechanical and electrochemical properties. Templating issues related to MOF cellulose composites should be solved. However, coordination polymer cellulose composites are least used in optical chemosensing due to their quenching-based detection profiles.

1. Polymers can be incorporated into cellulose only if the moisture resistance profile of cellulose is improved. For this purpose, cellulosic materials can be modified by grafting long-chain aliphatic compounds to the surface.
2. Another approach is to use a chemical crosslinker resin capable of inducing hydrophobicity. Hydrophobic nano coating and hydrophobic plastic lamination can aid in elevating the hydrophobicity.
3. Improving the quality of cellulose-derived polymers will enhance their capability as optical chemosensors.
4. In the current review, we have noticed that most of the cellulose-derived or linked polymers have found application in the optical sensing of metals, anions and a few other analytes. However, biologically important analytes like neurotransmitters, ROS and RSS species are ignored.
5. Cellulose-hydrogel hybrids have good bio-applicability and, hence, should be applied for the detection of biologically relevant species. Further, explorations should be made to improve the strength, stability and applicability of different cellulose polymer materials for utility in optical chemosensing.

6 Conclusion

In this review, we have summarised the research based on the synthesis of different cellulose-based materials and their applications in optical chemosensing. We expect that this review will be used as a concrete base for the future development of cellulosic optical chemosensors. Most probably, cellulose-based optical probes will gain very high significance in the fields of analyte detection, security printing and biological applications. However, a few points are to be considered for the future development of cellulosic materials. More use of natural cellulose should be made in the synthesis of cellulose-based chromo and fluorophores. Proper care must be taken to improve the quantum yield of fluorophores after combining with cellulose derivatives. The safety and lifetime of the cellulosic materials should be accurately investigated. The toxicity of such hybrid materials should be monitored. Besides the chemosensing of metallic and anionic analytes, researchers should pay additional focus to employ cellulosic materials for detection of pesticides and other biologically essential and important analytes. Although many cellulosic material entries for optical chemosensing are presented, more work is required to develop such optical chemosensors

to enhance efficiency, portability, reduced cost and response time of cellulosic optical chemosensors. Finally, the current review will hold high importance for the readers, the broader scientific community and investigators working in the development of optical chemosensors for large-scale applicability and real-time monitoring utilities. This review will yield at least a few novel cellulosic materials with excellent properties and applicability that will be prepared in the near future.

Abbreviations AIE: Aggregation-induced emission; μ(PAD): Polystyrene-coated cellulose paper; CNF: Cellulose nanofibre; DCP: Diethyl chlorophosphite; LOD: Limit of detection; MCC: Microcrystalline cellulose; MFC: Microfibrillated cellulose; CNC: Cellulose nanocrystals; CNPs: Carbon nanoparticles; DPA: Dipicolinic acid; UCPs: Upconverting phosphors; LRET: Luminescence resonance energy transfer; BPM: Base pair mismatched; CF: Charge transfer; TCNQ: 7, 7, 8, 8-Tetracyanoquino-dimethane; TCNB: 1,2,4,5-Tetracyano-benzene; TCNE: Tetracyano-ethylene; APTES: 3-Aminopropyl triethoxysilane; CMC: Carboxymethyl cellulose; UCNPs: Up-converting nanoparticles; QC: Quaternised cellulose; SPOTPE: 1,1,2-Triphenyl-2-[4-(3-sulfonatopropoxyl)-phenyl]-ethene sodium salt; TEM: Transmission electron microscopy; ROS: Reactive oxygen species; LD: Levodopa; DA: Dopamine; NAD: Nicotinamide adenine dinucleotide; NADH: Dihydronicotinamide adenine dinucleotide; CTAB: Cetyltrimethylammonium bromide; OP: Organophosphorous; TCh: Thiocholine; TEMPO: 2,2,6,6-Tetramethylpiperidin-1-piperidinyloxy; EDTAD: Ethylenediaminetetraacetic dianhydride; AMC: 7-Amino-4-methylcoumarin; TLm: 6-Thienyllumazine; ESPT: Excited-state proton transfer; BC: Bacterial cellulose; CDs: Carbon dots; QDs: Quantum dots; PDMS: Hybrid polydimethylsiloxane; CPDs: Carboxymethylcellulose-derived polymer dots; HG: Hydrogels; Alg: Alginate; TOCNF: TEMPO-oxidised cellulose nanofibril; MOF: Metal organic frameworks; MIG: MOF-based ionogels; TNT: Trinitrotoluene; DNT: Dinitrotoluene; MDI: 4,4′-Methylene diphenyl diisocyanate; XPS: X-ray photoelectron spectroscopy; DFT: Density functional theory; WHO: World Health Organisation; TMB: 3,3′,5,5′-Tetramethylbenzidine; GOx: Glucose oxidase; 7-AC: &-Acryloxycoumarin; COF: Coordination organic frameworks

Author contribution Ratish R. Nair prepared the concept, complete draft, figure preparation and overview & editing. Joo Hee Hyun helped in figure preparation of cellulose-based nanoparticle, Jahyun Kim helped in figure preparation of cellulose-based polymers, Kyung Oh Jung performed useful discussions and gave views in conclusion. Dokyoung Kim concept preparation, funding acquisition, supervision, visualization, writing – review & editing. All authors reviewed the manuscript.

Funding This work was supported by grants from the National Research Foundation (NRF) of Korea (2022-R1F1A1069954) and the Bio & Medical Technology Development Program of the NRF of Korea (2021-M3A9I5030523). This research was also supported by the Core Research Institute (CRI) Program, the Basic Science Research Program through the NRF of Korea, Ministry of Education (2018-R1A6A1A03025124).

Data availability No datasets were generated or analysed during the current study.

Declarations

Ethical approval Not applicable.

Competing interests The authors declare no competing interests.

References

1. Klemm D, Heublein B, Fink H-P, Bohn A (2005) Cellulose: fascinating biopolymer and sustainable raw material. Angew Chem Int Ed 44(22):3358–3393. https://doi.org/10.1002/anie.200460587
2. Moon RJ, Martini A, Nairn J, Simonsen J, Youngblood J (2011) Cellulose nanomaterials review: structure, properties and nanocomposites. Chem Society Rev 40(7):3941–3994. https://doi.org/10.1039/C0CS00108B
3. Georgouvelas D, Jalvo B, Valencia L, Papawassiliou W, Pell AJ, Edlund U et al (2020) Residual lignin and zwitterionic polymer grafts on cellulose nanocrystals for antifouling and antibacterial applications. ACS Appl Polym Mater 2(8):3060–3071. https://doi.org/10.1021/acsapm.0c00212
4. Nasrollahzadeh M, Sajjadi M, Iravani S, Varma RS (2021) Starch, cellulose, pectin, gum, alginate, chitin and chitosan derived (nano)materials for sustainable water treatment: a review. Carbohyd Polym 251:116986. https://doi.org/10.1016/j.carbpol.2020.116986
5. Abdelhamid HN (2021) 8 - Self-decontaminating antimicrobial textiles. In: Mondal MIH (ed) Antimicrobial Textiles from Natural Resources. Woodhead Publishing, pp 259–294
6. Li X, Zhang X, Wang N, Chang H, Wang Y, Zhang Z (2019) Range-broadening ultraviolet-blocking regulation of cellulose nanopaper via surface self-absorption with poly(methyl methacrylate)/avobenzone. ACS Appl Polym Mater 1(11):2981–2989. https://doi.org/10.1021/acsapm.9b00686
7. Li H, He Y, Yang J, Wang X, Lan T, Peng L (2019) Fabrication of food-safe superhydrophobic cellulose paper with improved moisture and air barrier properties. Carbohyd Polym 211:22–30. https://doi.org/10.1016/j.carbpol.2019.01.107
8. Aguilar-Sanchez A, Jalvo B, Mautner A, Rissanen V, Kontturi KS, Abdelhamid HN et al (2021) Charged ultrafiltration membranes based on TEMPO-oxidized cellulose nanofibrils/poly(vinyl alcohol) antifouling coating. RSC Advances 11(12):6859–6868. https://doi.org/10.1039/D0RA10220B
9. Grishkewich N, Mohammed N, Tang J, Tam KC (2017) Recent advances in the application of cellulose nanocrystals. Curr Opin Colloid Interface Sci 29:32–45. https://doi.org/10.1016/j.cocis.2017.01.005
10. Chen W, Yu H, Lee S-Y, Wei T, Li J, Fan Z (2018) Nanocellulose: a promising nanomaterial for advanced electrochemical energy storage. Chem Society Rev 47(8):2837–2872. https://doi.org/10.1039/C7CS00790F

11. Chibac-Scutaru AL, Coseri S (2023) Advances in the use of cellulose-based proton exchange membranes in fuel cell technology: a review. Int J Biol Macromol 247:125810. https://doi.org/10.1016/j.ijbiomac.2023.125810
12. Dias OAT, Konar S, Leão AL, Yang W, Tjong J, Sain M (2020) Current state of applications of nanocellulose in flexible energy and electronic devices. Front Chem 8:420
13. Chen S, Jiang J, Xu F, Gong S (2019) Crepe cellulose paper and nitrocellulose membrane-based triboelectric nanogenerators for energy harvesting and self-powered human-machine interaction. Nano Energy 61:69–77. https://doi.org/10.1016/j.nanoen.2019.04.043
14. Pal RK, Goyal P, Sehgal S (2021) Effect of cellulose fibre based insulation on thermal performance of buildings. Mater Today: Proceedings 45:5778–5781. https://doi.org/10.1016/j.matpr.2021.02.749
15. Valencia L, Kumar S, Jalvo B, Mautner A, Salazar-Alvarez G, Mathew AP (2018) Fully bio-based zwitterionic membranes with superior antifouling and antibacterial properties prepared via surface-initiated free-radical polymerization of poly(cysteine methacrylate). J Mater Chem A 6(34):16361–16370. https://doi.org/10.1039/C8TA06095A
16. Khine YY, Stenzel MH (2020) Surface modified cellulose nanomaterials: a source of non-spherical nanoparticles for drug delivery. Materials Horizons 7(7):1727–1758. https://doi.org/10.1039/C9MH01727E
17. Georgouvelas D, Abdelhamid HN, Li J, Edlund U, Mathew AP (2021) All-cellulose functional membranes for water treatment: adsorption of metal ions and catalytic decolorization of dyes. Carbohyd Polym 264:118044. https://doi.org/10.1016/j.carbpol.2021.118044
18. Bacakova L, Pajorova J, Bacakova M, Skogberg A, Kallio P, Kolarova K et al (2019) Versatile application of nanocellulose: from industry to skin tissue engineering and wound healing. Nanomaterials (Basel) 9(2):164. https://doi.org/10.3390/nano9020164
19. Gorgieva S (2020) Bacterial cellulose as a versatile platform for research and development of biomedical materials. Processes 8(5):624. https://doi.org/10.3390/pr8050624
20. Pang M, Huang Y, Meng F, Zhuang Y, Liu H, Du M et al (2020) Application of bacterial cellulose in skin and bone tissue engineering. Eur Polymer J 122:109365. https://doi.org/10.1016/j.eurpolymj.2019.109365
21. van Zyl EM, Coburn JM (2019) Hierarchical structure of bacterial-derived cellulose and its impact on biomedical applications. Curr Opin Chem Eng 24:122–130. https://doi.org/10.1016/j.coche.2019.04.005
22. Zhang Z, Liu G, Li X, Zhang S, Lü X, Wang Y (2020) Design and synthesis of fluorescent nanocelluloses for sensing and bioimaging applications. ChemPlusChem 85(3):487–502. https://doi.org/10.1002/cplu.201900746
23. Abdelhamid HN, Mathew AP (2022) Cellulose-based nanomaterials advance biomedicine: a review. Int J Mol Sci 23(10):5405. https://doi.org/10.3390/ijms23105405
24. Yang J, Li J (2018) Self-assembled cellulose materials for biomedicine: a review. Carbohyd Polym 181:264–274. https://doi.org/10.1016/j.carbpol.2017.10.067
25. Nehra P, Chauhan RP (2021) Eco-friendly nanocellulose and its biomedical applications: current status and future prospect. J Biomater Sci Polym Ed 32(1):112–149. https://doi.org/10.1080/09205063.2020.1817706
26. Ullah S, Chen X (2020) Fabrication, applications and challenges of natural biomaterials in tissue engineering. Appl Mater Today 20:100656. https://doi.org/10.1016/j.apmt.2020.100656
27. Jorfi M, Foster EJ (2015) Recent advances in nanocellulose for biomedical applications. J Appl Polym Sci 132(14), https://doi.org/10.1002/app.41719.
28. Long W, Ouyang H, Hu X, Liu M, Zhang X, Feng Y et al (2021) State-of-art review on preparation, surface functionalization and biomedical applications of cellulose nanocrystals-based materials. Int J Biol Macromol 186:591–615. https://doi.org/10.1016/j.ijbiomac.2021.07.066
29. Sunasee R, Hemraz UD, Ckless K (2016) Cellulose nanocrystals: a versatile nanoplatform for emerging biomedical applications. Expert Opin Drug Deliv 13(9):1243–1256. https://doi.org/10.1080/17425247.2016.1182491
30. Derikvand F, Yin DT, Barrett R, Brumer H (2016) Cellulose-based biosensors for esterase detection. Anal Chem 88(6):2989–2993. https://doi.org/10.1021/acs.analchem.5b04661
31. Milindanuth P, Pisitsak P (2018) A novel colorimetric sensor based on rhodamine-B derivative and bacterial cellulose for the detection of Cu(II) ions in water. Mater Chem Phys 216:325–331. https://doi.org/10.1016/j.matchemphys.2018.06.003
32. Samanta S, Halder S, Dey P, Manna U, Ramesh A, Das G (2018) A ratiometric fluorogenic probe for the real-time detection of SO32− in aqueous medium: application in a cellulose paper based device and potential to sense SO32− in mitochondria. Analyst 143(1):250–257. https://doi.org/10.1039/C7AN01368J
33. Chen L, Hu B, Zhang J, Zhang J, Huang S, Ren P et al (2019) A facile synthesis of 1,3,6,8-pyrenesulfonic acid tetrasodium salt as a hydrosoluble fluorescent ink for anti-counterfeiting applications. RSC Advances 9(1):476–481. https://doi.org/10.1039/C8RA09106D
34. Taweetanavanich T, Wanno B, Tuntulani T, Pulpoka B, Kaewtong C (2019) A pH optical and fluorescent sensor based on rhodamine modified on activated cellulose paper. J Chin Chem Soc 66(5):493–499. https://doi.org/10.1002/jccs.201800327
35. Saravana Kumar S, Selva Kumar R, Ashok Kumar SK (2020) An "Off-On-Off" type fluorescent chemosensor for the relay detection of Zn2+ and H2PO4− in aqueous environment. Inorg Chim Acta 502:119348. https://doi.org/10.1016/j.ica.2019.119348
36. Nawaz H, Zhang J, Tian W, Jin K, Jia R, Yang T et al (2020) Cellulose-based fluorescent sensor for visual and versatile detection of amines and anions. J Hazard Mater 387:121719. https://doi.org/10.1016/j.jhazmat.2019.121719
37. Oguz M, Kursunlu AN, Yilmaz M (2020) Low-cost and environmentally sensitive fluorescent cellulose paper for naked-eye detection of Fe(III) in aqueous media. Dyes Pigm 173:107974. https://doi.org/10.1016/j.dyepig.2019.107974
38. Zhang Y, Cui X, Wang X, Feng X, Cheng W, Xiong R et al (2023) Biomass-based indole derived fluorescence sensor composited with cellulose paper: detection of picric acid in food and environment samples. Int J Biol Macromol 253:126963. https://doi.org/10.1016/j.ijbiomac.2023.126963
39. Abdollahi A, Hanaei N, Rahmanidoust M, Dashti A (2023) Photoluminescent Janus oxazolidine nanoparticles for development of organic light-emitting diodes, anticounterfeiting, information encryption, and optical detection of scratch. J Colloid Interface Sci 630:242–256. https://doi.org/10.1016/j.jcis.2022.10.013
40. Rull-Barrull J, d'Halluin M, Le Grognec E, Felpin F-X (2016) Chemically-modified cellulose paper as smart sensor device for colorimetric and optical detection of hydrogen sulfate in water. Chem Commun 52(12):2525–2528. https://doi.org/10.1039/C5CC09889K
41. Abou-Yousef H, Khattab TA, Youssef YA, Al-Balakocy N, Kamel S (2017) Novel cellulose-based halochromic test strips for naked-eye detection of alkaline vapors and analytes. Talanta 170:137–145. https://doi.org/10.1016/j.talanta.2017.04.002

42. Patil P, Sehlangia S, Patil A, Pradeep C, Sahoo SK, Patil U (2019) A new phthalimide based chemosensor for selective spectrophotometric detection of Cu(II) from aqueous medium. Spectrochim Acta Part A Mol Biomol Spectrosc 220:117129. https://doi.org/10.1016/j.saa.2019.05.034
43. Fettouche S, Boukhriss A, Tahiri M, Cherkaoui O, Bazi F, Gmouh S (2019) Naked eye and selective detection of copper(II) in mixed aqueous media using a cellulose-based support. Chem Res Chin Univ 35(4):598–603. https://doi.org/10.1007/s40242-019-8313-4
44. Jeong E, Kim J-K, Jin J, Lee H-I (2022) Transparent nanocellulose paper-based biodegradable colorimetric nerve agent detectors. Carbohyd Polym 295:119845. https://doi.org/10.1016/j.carbpol.2022.119845
45. Zhang H, Xu Y, Xu Y, Lu J, Song X, Luo X (2023) An ingenious cellulose membrane sensor design strategy for colorimetric detection of Ag+/Hg2+ based on redox reaction. Talanta 255:124209. https://doi.org/10.1016/j.talanta.2022.124209
46. Nagai A, Miller JB, Du J, Kos P, Stefan MC, Siegwart DJ (2015) Correction: Biocompatible organic charge transfer complex nanoparticles based on a semi-crystalline cellulose template. Chem Commun 51(96):17178–17178. https://doi.org/10.1039/C5CC90504D
47. Wang F, Li W, Wang J, Ren J, Qu X (2015) Detection of telomerase on upconversion nanoparticle modified cellulose paper. Chem Commun 51(58):11630–11633. https://doi.org/10.1039/C5CC03902A
48. Xiong F, Han Y, Li G, Qin T, Wang S, Chu F (2016) Synthesis and characterization of renewable woody nanoparticles fluorescently labeled by pyrene. Ind Crops Prod 83:663–669. https://doi.org/10.1016/j.indcrop.2015.12.055
49. Bothra S, Upadhyay Y, Kumar R, Ashok Kumar SK, Sahoo SK (2017) Chemically modified cellulose strips with pyridoxal conjugated red fluorescent gold nanoclusters for nanomolar detection of mercuric ions. Biosens Bioelectron 90:329–335. https://doi.org/10.1016/j.bios.2016.11.066
50. Li G, Sun Y, Liu H (2018) Gold-carboxymethyl cellulose nanocomposites greenly synthesized for fluorescent sensitive detection of Hg(II). J Cluster Sci 29(1):177–184. https://doi.org/10.1007/s10876-017-1317-7
51. Ye J, Zhang M, Xiong J (2018) Fluorescence probe based carboxymethyl cellulose/Tb(III) nanocomposites for detection of Mn2+ with simpleness, rapidness and high sensitivity. Carbohyd Polym 190:156–161. https://doi.org/10.1016/j.carbpol.2018.02.042
52. Fu AC, Hu Y, Zhao Z-H, Su R, Song Y, Zhu D (2018) Functionalized paper microzone plate for colorimetry and up-conversion fluorescence dual-mode detection of telomerase based on elongation and capturing amplification. Sens Actuators, B Chem 259:642–649. https://doi.org/10.1016/j.snb.2017.12.124
53. Patel R, Bothra S, Kumar R, Crisponi G, Sahoo SK (2018) Pyridoxamine driven selective turn-off detection of picric acid using glutathione stabilized fluorescent copper nanoclusters and its applications with chemically modified cellulose strips. Biosens Bioelectron 102:196–203. https://doi.org/10.1016/j.bios.2017.11.031
54. Mu L, Shi L, Wang Y, Zhou Q, Ye J, Feng X (2018) Transparent luminescent nanopaper based on g-C3N4 nanosheet grafted oxidized cellulose nanofibrils with excellent thermal and mechanical properties. J Mater Chem C 6(46):12660–12667. https://doi.org/10.1039/C8TC03812K
55. Wang H, Ye X, Zhou J (2019) Self-assembly fluorescent cationic cellulose nanocomplex via electrostatic interaction for the detection of Fe(3+) ions. Nanomaterials (Basel) 9(2):279. https://doi.org/10.3390/nano9020279
56. Fu J, Zhu J, Tian Y, He K, Yu H, Chen L et al (2020) Green and transparent cellulose nanofiber substrate-supported luminescent gold nanoparticles: a stable and sensitive solid-state sensing membrane for Hg(II) detection. Sens Actuators, B Chem 319:128295. https://doi.org/10.1016/j.snb.2020.128295
57. Delavari S, Ziadzade S, Keyvan Rad J, Hamrang V, Mahdavian AR (2020) Anticounterfeiting and photoluminescent cellulosic papers based on fluorescent acrylic copolymer nanoparticles containing coumarin. Carbohyd Polym 247:116756. https://doi.org/10.1016/j.carbpol.2020.116756
58. Bhamore JR, Gul AR, Chae W-S, Kim K-W, Lee JS, Park H et al (2020) One-pot fabrication of amino acid and peptide stabilized gold nanoclusters for the measurement of the lead in plasma samples using chemically modified cellulose paper. Sens Actuators, B Chem 322:128603. https://doi.org/10.1016/j.snb.2020.128603
59. Quan Z, Xue F, Li H, Chen Z, Wang L, Zhu H et al (2022) A bioinspired ratiometric fluorescence probe based on cellulose nanocrystal-stabilized gold nanoclusters for live-cell and zebrafish imaging of highly reactive oxygen species. Chem Eng J 431:133954. https://doi.org/10.1016/j.cej.2021.133954
60. Mahdavi M, Emadi H, Nabavi SR (2023) A bacterial cellulose-based LiSrVO4:Eu3+ nanosensor platform for smartphone sensing of levodopa and dopamine: point-of-care diagnosis of Parkinson's disease. Nanoscale Adv 5(18):4782–4797. https://doi.org/10.1039/D3NA00297G
61. You J, Hu H, Zhou J, Zhang L, Zhang Y, Kondo T (2013) Novel cellulose polyampholyte–gold nanoparticle-based colorimetric competition assay for the detection of cysteine and mercury(II). Langmuir 29(16):5085–5092. https://doi.org/10.1021/la3050913
62. Liang P, Yu H, Guntupalli B, Xiao Y (2015) Paper-based device for rapid visualization of NADH based on dissolution of gold nanoparticles. ACS Appl Mater Interfaces 7(27):15023–15030. https://doi.org/10.1021/acsami.5b04104
63. Wu S, Li D, Gao Z, Wang J (2017) Controlled etching of gold nanorods by the Au(III)-CTAB complex, and its application to semi-quantitative visual determination of organophosphorus pesticides. Microchim Acta 184(11):4383–4391. https://doi.org/10.1007/s00604-017-2468-9
64. Li J-J, Hou C-J, Huo D-Q, Shen C-H, Luo X-G, Fa H-B et al (2017) Detection of trace nickel ions with a colorimetric sensor based on indicator displacement mechanism. Sens Actuators, B Chem 241:1294–1302. https://doi.org/10.1016/j.snb.2016.09.191
65. Zor E (2018) Silver nanoparticles-embedded nanopaper as a colorimetric chiral sensing platform. Talanta 184:149–155. https://doi.org/10.1016/j.talanta.2018.02.096
66. Bagheri N, Saraji M (2019) Combining gold nanoparticle-based headspace single-drop microextraction and a paper-based colorimetric assay for selenium determination. Anal Bioanal Chem 411(28):7441–7449. https://doi.org/10.1007/s00216-019-02106-4
67. Teodoro KBR, Migliorini FL, Christinelli WA, Correa DS (2019) Detection of hydrogen peroxide (H2O2) using a colorimetric sensor based on cellulose nanowhiskers and silver nanoparticles. Carbohyd Polym 212:235–241. https://doi.org/10.1016/j.carbpol.2019.02.053
68. Ali M, Khalid MAU, Shah I, Kim SW, Kim YS, Lim JH et al (2019) Paper-based selective and quantitative detection of uric acid using citrate-capped Pt nanoparticles (PtNPs) as a colorimetric sensing probe through a simple and remote-based device. New J Chem 43(20):7636–7645. https://doi.org/10.1039/C9NJ01257E
69. Ganguly K, Patel DK, Dutta SD, Lim K-T (2021) TEMPO-cellulose nanocrystal-capped gold nanoparticles for colorimetric detection of pathogenic DNA. ACS Omega 6(19):12424–12431. https://doi.org/10.1021/acsomega.1c00359

70. Sanjabi S, Keyvan Rad J, Salehi-Mobarakeh H, Mahdavian AR (2024) Dual-chromic cellulose paper modified with nanocapsules containing leuco dye and spiropyran derivatives: a colorimetric portable chemosensor for detection of some heavy metal cations. J Environ Chem Eng 12(1):111724. https://doi.org/10.1016/j.jece.2023.111724
71. Grate JW, Mo K-F, Shin Y, Vasdekis A, Warner MG, Kelly RT et al (2015) Alexa Fluor-labeled fluorescent cellulose nanocrystals for bioimaging solid cellulose in spatially structured microenvironments. Bioconjug Chem 26(3):593–601. https://doi.org/10.1021/acs.bioconjchem.5b00048
72. Tang L, Li T, Zhuang S, Lu Q, Li P, Huang B (2016) Synthesis of pH-sensitive fluorescein grafted cellulose nanocrystals with an amino acid spacer. ACS Sustain Chem Eng 4(9):4842–4849. https://doi.org/10.1021/acssuschemeng.6b01124
73. Gu Y, Wang M, Li G (2017) CNT-anchored cellulose fluorescent nanofiber membranes as a fluorescence sensor for Cu2+ and Cr3+. Analytical Methods 9(42):6044–6048. https://doi.org/10.1039/C7AY01994G
74. Chen J, Zhou Z, Chen Z, Yuan W, Li M (2017) A fluorescent nanoprobe based on cellulose nanocrystals with porphyrin pendants for selective quantitative trace detection of Hg2+. New J Chem 41(18):10272–10280. https://doi.org/10.1039/C7NJ01263B
75. Zhang Y-J, Ma X-Z, Gan L, Xia T, Shen J, Huang J (2018) Fabrication of fluorescent cellulose nanocrystal via controllable chemical modification towards selective and quantitative detection of Cu(II) ion. Cellulose 25(10):5831–5842. https://doi.org/10.1007/s10570-018-1995-9
76. Chen H, Huang J, Hao B, Yang B, Chen S, Yang G et al (2019) Citrate-based fluorophore-modified cellulose nanocrystals as a biocompatible fluorescent probe for detecting ferric ions and intracellular imaging. Carbohyd Polym 224:115198. https://doi.org/10.1016/j.carbpol.2019.115198
77. Al-Shamsi N, Laptenok SP, Bufaroosha MS, Greish YE, Saleh NI (2019) Time-resolved photoluminescence of 6-thienyllumazine fluorophores in cellulose acetate nanofibers for detection of mercury ions. Spectrochim Acta Part A Mol Biomol Spectrosc 222:117189. https://doi.org/10.1016/j.saa.2019.117189
78. Hou A, Chen H, Zheng C, Xie K, Gao A (2020) Assembly of a fluorescent chiral photonic crystal membrane and its sensitive responses to multiple signals induced by small molecules. ACS Nano 14(6):7380–7388. https://doi.org/10.1021/acsnano.0c02883
79. Ye X, Kang Y, Zhou J (2020) Rhodamine labeled cellulose nanocrystals as selective "naked-eye" colorimetric and fluorescence sensor for Hg2+ in aqueous solutions. Cellulose 27(9):5197–5210. https://doi.org/10.1007/s10570-020-03126-5
80. Patel I, Woodcock J, Beams R, Stranick SJ, Nieuwendaal R, Gilman JW et al (2021) Fluorescently labeled cellulose nanofibers for environmental health and safety studies. Nanomaterials 11(4):1015. https://doi.org/10.3390/nano11041015
81. Ye X, Zhang D, Wang S, Zhou P, Zhu P (2022) Fluorescent cellulose nanocrystals based on AIE luminogen for rapid detection of Fe3+ in aqueous solutions. RSC Adv 12(38):24633–24639. https://doi.org/10.1039/D2RA04272J
82. Tewatia P, Kumar V, Samota S, Singhal S, Kaushik A (2022) Sensing and annihilation of ultra-trace level arsenic (III) using fluoranthene decorated fluorescent nanofibrous cellulose probe. J Hazard Mater 424:127722. https://doi.org/10.1016/j.jhazmat.2021.127722
83. Cai C, Wei Z, Huang Y, Wang P, Song J, Deng L et al (2021) "Rigid-stretchable" unity of shape memory composites with fluorescence via crystallinity tailoring for anti-counterfeiting application. Compos Sci Technol 201:108524. https://doi.org/10.1016/j.compscitech.2020.108524
84. Zhang F, Li Q, Wang C, Wang D, Song M, Li Z et al (2022) Multimodal, convertible, and chiral optical films for anti-counterfeiting labels. Adv Func Mater 32(33):2204487. https://doi.org/10.1002/adfm.202204487
85. Jiang Y, Su W, Li G, Fu Y, Li Z, Qin M et al (2022) Highly strong luminescent chiral nematic cellulose nanocrystal/PEI composites for anticounterfeiting. Chem Eng J 430:132780. https://doi.org/10.1016/j.cej.2021.132780
86. Raj S, Shankaran DR (2016) Curcumin based biocompatible nanofibers for lead ion detection. Sens Actuators, B Chem 226:318–325. https://doi.org/10.1016/j.snb.2015.12.006
87. Song W, Lee J-K, Gong MS, Heo K, Chung W-J, Lee BY (2018) Cellulose nanocrystal-based colored thin films for colorimetric detection of aldehyde gases. ACS Appl Mater Interfaces 10(12):10353–10361. https://doi.org/10.1021/acsami.7b19738
88. Ram B, Chauhan GS, Mehta A, Gupta R, Chauhan K (2018) Spherical nanocellulose-based highly efficient and rapid multifunctional naked-eye Cr(VI) ion chemosensor and adsorbent with mild antimicrobial properties. Chem Eng J 349:146–155. https://doi.org/10.1016/j.cej.2018.05.085
89. Faham S, Golmohammadi H, Ghavami R, Khayatian G (2019) A nanocellulose-based colorimetric assay kit for smartphone sensing of iron and iron-chelating deferoxamine drug in biofluids. Anal Chim Acta 1087:104–112. https://doi.org/10.1016/j.aca.2019.08.056
90. Naghdi T, Golmohammadi H, Vosough M, Atashi M, Saeedi I, Maghsoudi MT (2019) Lab-on-nanopaper: an optical sensing bioplatform based on curcumin embedded in bacterial nanocellulose as an albumin assay kit. Anal Chim Acta 1070:104–111. https://doi.org/10.1016/j.aca.2019.04.037
91. Wang C, Xu Z, Cheng H, Lin H, Humphrey MG, Zhang C (2015) A hydrothermal route to water-stable luminescent carbon dots as nanosensors for pH and temperature. Carbon 82:87–95. https://doi.org/10.1016/j.carbon.2014.10.035
92. Ge Y, Chen S, Yang J, Wang B, Wang H (2015) Color-tunable luminescent CdTe quantum dot membranes based on bacterial cellulose (BC) and application in ion detection. RSC Adv 5(69):55756–55761. https://doi.org/10.1039/C5RA08361C
93. Wang C, Wang C, Xu P, Li A, Chen Y, Zhuo K (2016) Synthesis of cellulose-derived carbon dots using acidic ionic liquid as a catalyst and its application for detection of Hg2+. J Mater Sci 51(2):861–867. https://doi.org/10.1007/s10853-015-9410-5
94. Yang G, Wan X, Su Y, Zeng X, Tang J (2016) Acidophilic S-doped carbon quantum dots derived from cellulose fibers and their fluorescence sensing performance for metal ions in an extremely strong acid environment. J Mater Chem A 4(33):12841–12849. https://doi.org/10.1039/C6TA05943K
95. Das P, Krull UJ (2017) Detection of a cancer biomarker protein on modified cellulose paper by fluorescence using aptamer-linked quantum dots. Analyst 142(17):3132–3135. https://doi.org/10.1039/C7AN00624A
96. Lv P, Yao Y, Li D, Zhou H, Naeem MA, Feng Q et al (2017) Self-assembly of nitrogen-doped carbon dots anchored on bacterial cellulose and their application in iron ion detection. Carbohyd Polym 172:93–101. https://doi.org/10.1016/j.carbpol.2017.04.086
97. Cheng C, Xing M, Wu Q (2019) A universal facile synthesis of nitrogen and sulfur co-doped carbon dots from cellulose-based biowaste for fluorescent detection of Fe3+ ions and intracellular bioimaging. Mater Sci Eng, C 99:611–619. https://doi.org/10.1016/j.msec.2019.02.003
98. Lv P, Zhou H, Mensah A, Feng Q, Lu K, Huang J et al (2019) In situ 3D bacterial cellulose/nitrogen-doped graphene oxide quantum dot-based membrane fluorescent probes

for aggregation-induced detection of iron ions. Cellulose 26(10):6073–6086. https://doi.org/10.1007/s10570-019-02476-z
99. Wu B, Zhu G, Dufresne A, Lin N (2019) Fluorescent aerogels based on chemical crosslinking between nanocellulose and carbon dots for optical sensor. ACS Appl Mater Interfaces 11(17):16048–16058. https://doi.org/10.1021/acsami.9b02754
100. Yu S, Li W, Fujii Y, Omura T, Minami H (2019) Fluorescent spherical sponge cellulose sensors for highly selective and semi-quantitative visual analysis: detection of Hg2+ and Cu2+ ions. ACS Sustain Chem Eng 7(23):19157–19166. https://doi.org/10.1021/acssuschemeng.9b05142
101. Li W, Zhang X, Miao C, Li R, Ji Y (2020) Fluorescent paper–based sensor based on carbon dots for detection of folic acid. Anal Bioanal Chem 412(12):2805–2813. https://doi.org/10.1007/s00216-020-02507-w
102. Liu Z, Chen M, Guo Y, Zhou J, Shi Q, Sun R (2020) Oxidized nanocellulose facilitates preparing photoluminescent nitrogen-doped fluorescent carbon dots for Fe3+ ions detection and bio-imaging. Chem Eng J 384:123260. https://doi.org/10.1016/j.cej.2019.123260
103. Jin K, Zhang J, Tian W, Ji X, Yu J, Zhang J (2020) Facile access to solid-state carbon dots with high luminescence efficiency and excellent formability via cellulose derivative coatings. ACS Sustain Chem Eng 8(15):5937–5945. https://doi.org/10.1021/acssuschemeng.0c00237
104. Zhao Y, Li J (2020) Unique and outstanding quantum dots (QD)/tunicate cellulose nanofibrils (TCNF) nanohybrid platform material for use as 1D ink and 2D film. Carbohyd Polym 242:116396. https://doi.org/10.1016/j.carbpol.2020.116396
105. Zhao Z, Guo Y, Zhang T, Ma J, Li H, Zhou J et al (2020) Preparation of carbon dots from waste cellulose diacetate as a sensor for tetracycline detection and fluorescence ink. Int J Biol Macromol 164:4289–4298. https://doi.org/10.1016/j.ijbiomac.2020.08.243
106. Li P, Zeng J, Wang B, Cheng Z, Xu J, Gao W et al (2020) Water-borne fluorescent dual anti-counterfeiting ink based on Yb/Er-carbon quantum dots grafted with dialdehyde nano-fibrillated cellulose. Carbohyd Polym 247:116721. https://doi.org/10.1016/j.carbpol.2020.116721
107. Ngoensawat U, Parnsubsakul A, Kaitphaiboonwet S, Wutikhun T, Sapcharoenkun C, Pienpinijtham P et al (2021) Luminescent nanohybrid of ZnO quantum dot and cellulose nanocrystal as anti-counterfeiting ink. Carbohyd Polym 262:117864. https://doi.org/10.1016/j.carbpol.2021.117864
108. Zhang S, Wang Y, Yang G (2021) A facile strategy for the preparation of carboxymethylcellulose-derived polymer dots and their application to detect tetracyclines. Macromol Chem Phys 222(22):2100267. https://doi.org/10.1002/macp.202100267
109. Dong Y, Zhao H, Wang S, Cheng Q, Liu S, Li Y (2022) Multimode anticounterfeiting labels based on a flexible and water-resistant NaGdF4Yb3+, Er3+@carbon dots chiral fluorescent cellulose film. ACS Appl Mater Interfaces 14(35):40313–40321. https://doi.org/10.1021/acsami.2c09971
110. Hu D, Lin K-H, Xu Y, Kajiyama M, Neves MA, Ogawa K et al (2021) Microwave-assisted synthesis of fluorescent carbon dots from nanocellulose for dual-metal ion-sensor probe: Fe (III) and Mn (II). Cellulose 28(15):9705–9724. https://doi.org/10.1007/s10570-021-04126-9
111. Dewangan L, Korram J, Karbhal I, Nagwanshi R, Ghosh KK, Pervez S et al (2022) Alkaline phosphatase immobilized CdTe/ZnS quantum dots for dual-purpose fluorescent and electrochemical detection of methyl paraoxon. Ind Eng Chem Res 61(10):3636–3646. https://doi.org/10.1021/acs.iecr.1c05065
112. Chen M, Zhai J, An Y, Li Y, Zheng Y, Tian H et al (2022) Solvent-free pyrolysis strategy for the preparation of biomass carbon dots for the selective detection of Fe3+ ions. Front Chem 10:940398
113. Luo Q, He S, Huang Y, Lei Z, Qiao J, Li Q et al (2022) Non-toxic fluorescent molecularly imprinted hydrogel based on wood-derived cellulose nanocrystals and carbon dots for efficient sorption and sensitive detection of tetracycline. Ind Crops Prod 177:114528. https://doi.org/10.1016/j.indcrop.2022.114528
114. Liang F, Liu Y, Sun J, Liu C, Deng C, Seidi F et al (2024) Facile preparation, optical mechanism elaboration, and bio-imaging application of fluorescent cellulose nanocrystals with tunable emission wavelength. Int J Biol Macromol 257:128648. https://doi.org/10.1016/j.ijbiomac.2023.128648
115. Ruiz-Palomero C, Benítez-Martínez S, Soriano ML, Valcárcel M (2017) Fluorescent nanocellulosic hydrogels based on graphene quantum dots for sensing laccase. Anal Chim Acta 974:93–99. https://doi.org/10.1016/j.aca.2017.04.018
116. Wang Y, Liang Z, Su Z, Zhang K, Ren J, Sun R et al (2018) All-biomass fluorescent hydrogels based on biomass carbon dots and alginate/nanocellulose for biosensing. ACS Appl Bio Mater 1(5):1398–1407. https://doi.org/10.1021/acsabm.8b00348
117. Cheng C, Xing M, Wu Q (2019) Green synthesis of fluorescent carbon dots/hydrogel nanocomposite with stable Fe3+ sensing capability. J Alloy Compd 790:221–227. https://doi.org/10.1016/j.jallcom.2019.03.053
118. Shen Y, Wang Z, Wang Y, Meng Z, Zhao Z (2021) A self-healing carboxymethyl chitosan/oxidized carboxymethyl cellulose hydrogel with fluorescent bioprobes for glucose detection. Carbohyd Polym 274:118642. https://doi.org/10.1016/j.carbpol.2021.118642
119. Lv H, Wang S, Wang Z, Meng W, Han X, Pu J (2022) Fluorescent cellulose-based hydrogel with carboxymethyl cellulose and carbon quantum dots for information storage and fluorescent anti-counterfeiting. Cellulose 29(11):6193–6204. https://doi.org/10.1007/s10570-022-04643-1
120. He X, Jia H, Sun N, Hou M, Tan Z, Lu X (2022) Fluorescent hydrogels based on oxidized carboxymethyl cellulose with excellent adsorption and sensing abilities for Ag+. Int J Biol Macromol 213:955–966. https://doi.org/10.1016/j.ijbiomac.2022.06.029
121. Cheng F, Zhang S, Zhang L, Sun J, Wu Y (2022) Hydrothermal synthesis of nanocellulose-based fluorescent hydrogel for mercury ion detection. Colloids Surf, A 636:128149. https://doi.org/10.1016/j.colsurfa.2021.128149
122. Luo Q, Ren T, Lei Z, Huang Y, Huang Y, Xu D et al (2022) Non-toxic chitosan-based hydrogel with strong adsorption and sensitive detection abilities for tetracycline. Chem Eng J 427:131738. https://doi.org/10.1016/j.cej.2021.131738
123. Zong P, Qin W, Luo J, Wang X, Bi J, Kong F et al (2023) Construction of a multifunctional polysaccharide-based aerogel for highly efficient fluorescence detection and removal of formaldehyde. Sens Actuators, B Chem 380:133391. https://doi.org/10.1016/j.snb.2023.133391
124. Zhao W, Li H, Chen Y, Yang D (2023) Cu2+-induced "off–on–off" switching luminescence of cellulose-based luminescent hydrogels. ACS Sustainable Chem Eng 11(11):4509–4516. https://doi.org/10.1021/acssuschemeng.3c00107
125. Zhang Z, Huang Z, Qin D, Liu D, Guo X, Lin H (2024) Fluorescent starch-based hydrogel with cellulose nanofibrils and carbon dots for simultaneous adsorption and detection of Pb(II). Carbohyd Polym 323:121427. https://doi.org/10.1016/j.carbpol.2023.121427
126. Ma F, Yuan C-W, Liu J-N, Cao J-H, Wu D-Y (2019) Colorimetric immunosensor based on Au@g-C3N4-doped spongelike 3D network cellulose hydrogels for detecting α- fetoprotein. ACS Appl Mater Interfaces 11(22):19902–19912. https://doi.org/10.1021/acsami.9b06769
127. Pirayesh H, Park B-D, Khanjanzadeh H, Park H-J, Cho Y-J (2023) Nanocellulose-based ammonia sensitive smart

colorimetric hydrogels integrated with anthocyanins to monitor pork freshness. Food Control 147:109595. https://doi.org/10.1016/j.foodcont.2022.109595
128. Xu X-Y, Yan B (2018) A fluorescent wearable platform for sweat Cl− analysis and logic smart-device fabrication based on color adjustable lanthanide MOFs. J Mater Chem C 6(7):1863–1869. https://doi.org/10.1039/C7TC05204A
129. Wang H, Pei Y, Qian X, An X (2020) Eu-metal organic framework@TEMPO-oxidized cellulose nanofibrils photoluminescence film for detecting copper ions. Carbohyd Polym 236:116030. https://doi.org/10.1016/j.carbpol.2020.116030
130. Goswami R, Bankar BD, Rajput S, Seal N, Pillai RS, Biradar AV et al (2022) In situ fabricated MOF–cellulose composite as an advanced ROS deactivator-convertor: fluoroswitchable bi-phasic tweezers for free chlorine detoxification and size-exclusive catalytic insertion of aqueous H2O2. J Mater Chem A 10(8):4316–4332. https://doi.org/10.1039/D1TA10504C
131. Kayhan EY, Yildirim A, Kocer MB, Uysal A, Yilmaz M (2023) A cellulose-based material as a fluorescent sensor for Cr(VI) detection and investigation of antimicrobial properties of its encapsulated form in two different MOFs. Int J Biol Macromol 240:124426. https://doi.org/10.1016/j.ijbiomac.2023.124426
132. Wang H, Qian X, An X (2022) Tb-coordination polymer-anchored nanocellulose composite film for selective and sensitive detection of ciprofloxacin. Carbohyd Polym 287:119337. https://doi.org/10.1016/j.carbpol.2022.119337
133. Jiang S, Yan Z, Deng Y, Deng W, Xiao H, Wu W (2024) Fluorescent bacterial cellulose@Zr-MOF via in-situ synthesis for efficient enrichment and sensitive detection of Cr(VI). Int J Biol Macromol 262:129854. https://doi.org/10.1016/j.ijbiomac.2024.129854
134. Pal S, Su Y-Z, Chen Y-W, Yu C-H, Kung C-W, Yu S-S (2022) 3D printing of metal–organic framework-based ionogels: wearable sensors with colorimetric and mechanical responses. ACS Appl Mater Interfaces 14(24):28247–28257. https://doi.org/10.1021/acsami.2c02690
135. Zhang K, Lu L, Liu Z, Cao X, Lv L, Xia J et al (2022) Metal-organic frameworks-derived bimetallic oxide composite nanozyme fiber membrane and the application to colorimetric detection of phenol. Colloids Surf, A 650:129662. https://doi.org/10.1016/j.colsurfa.2022.129662
136. Ikai T, Suzuki D, Shinohara K-I, Maeda K, Kanoh S (2017) A cellulose-based chiral fluorescent sensor for aromatic nitro compounds with central, axial and planar chirality. Polym Chem 8(14):2257–2265. https://doi.org/10.1039/C7PY00285H
137. Weishaupt R, Siqueira G, Schubert M, Kämpf MM, Zimmermann T, Maniura-Weber K et al (2017) A protein-nanocellulose paper for sensing copper ions at the nano- to micromolar level. Adv Func Mater 27(4):1604291. https://doi.org/10.1002/adfm.201604291
138. Chen H, Yan X, Feng Q, Zhao P, Xu X, Ng DHL et al (2017) Citric acid/cysteine-modified cellulose-based materials: green preparation and their applications in anticounterfeiting, chemical sensing, and UV shielding. ACS Sustain Chem Eng 5(12):11387–11394. https://doi.org/10.1021/acssuschemeng.7b02473
139. Hu H, Wang F, Yu L, Sugimura K, Zhou J, Nishio Y (2018) Synthesis of novel fluorescent cellulose derivatives and their applications in detection of nitroaromatic compounds. ACS Sustain Chem Eng 6(1):1436–1445. https://doi.org/10.1021/acssuschemeng.7b03855
140. Genovese ME, Abraham S, Caputo G, Nanni G, Kumaran SK, Montemagno CD et al (2018) Photochromic paper indicators for acidic food spoilage detection. ACS Omega 3(10):13484–13493. https://doi.org/10.1021/acsomega.8b02570
141. Nawaz H, Tian W, Zhang J, Jia R, Chen Z, Zhang J (2018) Cellulose-based sensor containing phenanthroline for the highly selective and rapid detectioN of Fe2+ ions with naked eye and fluorescent dual modes. ACS Appl Mater Interfaces 10(2):2114–2121. https://doi.org/10.1021/acsami.7b17342
142. Khattab TA, Kassem NF, Adel AM, Kamel S (2019) Optical recognition of ammonia and amine vapor using "turn-on" fluorescent chitosan nanoparticles imprinted on cellulose strips. J Fluoresc 29(3):693–702. https://doi.org/10.1007/s10895-019-02381-5
143. Jia R, Tian W, Bai H, Zhang J, Wang S, Zhang J (2019) Amine-responsive cellulose-based ratiometric fluorescent materials for real-time and visual detection of shrimp and crab freshness. Nat Commun 10(1):795. https://doi.org/10.1038/s41467-019-08675-3
144. Jiao X, Li H, Cheng X (2021) Cellulose-based fluorescent macromolecular sensors and their ability in 2, 4, 6-trinitrophenol detection. Materials Today Chem 22:100615. https://doi.org/10.1016/j.mtchem.2021.100615
145. Fan J, Zhang S, Xu Y, Wei N, Wan B, Qian L et al (2020) A polyethylenimine/salicylaldehyde modified cellulose Schiff base for selective and sensitive Fe3+ detection. Carbohyd Polym 228:115379. https://doi.org/10.1016/j.carbpol.2019.115379
146. Yin J, Zhang Y, Meng Z-Y, Li M-X, Zhao F, Wang S-F et al (2021) Pyrimidin-2-amine derivative-grafted cellulose ratiometric fluorescent probe for pH detection in extremely acidic media. Cellulose 28(16):10441–10455. https://doi.org/10.1007/s10570-021-04194-x
147. Zhao F, Meng Z, Wang Z, Yang Y (2022) A new cellulose-based fluorescent probe for specific and sensitive detection of Cu(2+) and its applications in the analysis of environmental water. Polymers (Basel) 14(11):2164. https://doi.org/10.3390/polym14112146
148. Nawaz H, Chen S, Li X, Zhang X, Zhang X, Wang J-Q et al (2022) Cellulose-based environment-friendly smart materials for colorimetric and fluorescent detection of Cu2+/Fe3+ ions and their anti-counterfeiting applications. Chem Eng J 438:135595. https://doi.org/10.1016/j.cej.2022.135595
149. Zhang X, Cheng Y, You J, Zhang J, Yin C, Zhang J (2022) Ultralong phosphorescence cellulose with excellent anti-bacterial, water-resistant and ease-to-process performance. Nat Commun 13(1):1117. https://doi.org/10.1038/s41467-022-28759-x
150. Xu Q, Sun H, Ren M, Kong F (2023) A novel cellulose-based fluorescent probe for the quantitative detection of HCHO in real food samples and living cells. Ind Crops Prod 204:117406. https://doi.org/10.1016/j.indcrop.2023.117406
151. Wang X, Meng Z, Tian X, Kou J, Xu K, Wang Z et al (2023) A novel coumarin derivative-grafted dialdehyde cellulose-based fluorescent sensor for selective and sensitive detection of Fe3+. Spectrochim Acta Part A Mol Biomol Spectrosc 292:122378. https://doi.org/10.1016/j.saa.2023.122378
152. Kou J, Meng Z, Wang X, Wang Z, Yang Y (2023) A novel coumarin derivative-modified cellulose fluorescent probe for selective and sensitive detection of CN− in food samples. Anal Methods 15(13):1639–1648. https://doi.org/10.1039/D2AY01886A
153. Xu Y, Yu X, Chen M, Sun Y, Zhang W, Fang Y et al (2023) Dual responsive cellulose-based fluorescent material fabricated in a CO2 switchable solvent for multifunctional applications. Chem Eng J 477:147272. https://doi.org/10.1016/j.cej.2023.147272
154. Wu Y, Meng Z, Zhao F, Wang S, Wang Z, Yang Y (2023) An efficient ethylcellulose fluorescent probe for rapid detection of Fe3+ and its multi-functional applications. Spectrochim Acta Part A Mol Biomol Spectrosc 284:121767. https://doi.org/10.1016/j.saa.2022.121767
155. Ma Y, Cheng X (2023) Readily soluble cellulose-based fluorescent probes for the detection and removal of Fe3+ ion. Int J Biol

Macromol 253:127393. https://doi.org/10.1016/j.ijbiomac.2023.127393
156. Yun L, Cheng X (2023) Synthesis of fluorescent probes based on cellulose for Fe2+ recognition. Cellulose 30(2):933–951. https://doi.org/10.1007/s10570-022-04930-x
157. Yun L, He J, Cheng X (2024) Synthesis of organic-solvent-soluble cellulose and preparation of fluorescent polyurethanes for the detection and removal of Hg+ ions. Int J Biol Macromol 254:127727. https://doi.org/10.1016/j.ijbiomac.2023.127727
158. Qiao Y, Ma Y, Chen X, Guo W, Min Y, Fan J et al (2023) Cellulose-based fluorescent films with anti-counterfeiting and UV shielding capabilities enabled by enamine bonds. Mater Adv 4(14):2940–2949. https://doi.org/10.1039/D3MA00132F
159. Xing L, Li G, Sun Y, Wang X, Yuan Z, Fu Y et al (2023) Dual-emitting cellulose nanocrystal hybrid materials with circularly polarized luminescence for anti-counterfeiting labels. Carbohyd Polym 313:120856. https://doi.org/10.1016/j.carbpol.2023.120856
160. Pramual K, Intasanta V, Chirachanchai S, Chanlek N, Kidkhunthod P, Pangon A (2018) Urethane-linked imidazole-cellulose microcrystals: synthesis and their dual functions in adsorption and naked eye sensing with colorimetric enhancement of metal ions. ACS Sustain Chem Eng 6(3):3686–3695. https://doi.org/10.1021/acssuschemeng.7b04028
161. Luo X, Xia J, Jiang X, Yang M, Liu S (2019) Cellulose-based strips designed based on a sensitive enzyme colorimetric assay for the low concentration of glucose detection. Anal Chem 91(24):15461–15468. https://doi.org/10.1021/acs.analchem.9b03180
162. Zhou S, He H, Guo W, Zhu H, Xue F, Cheng M et al (2019) Structural design of a high sensitivity biomass cellulose-based colorimetric sensor and its in situ visual recognition mechanism for Cu2+. Carbohyd Polym 219:95–104. https://doi.org/10.1016/j.carbpol.2019.04.094
163. Wei Y, Lu J, Xu Y, Song X, Yu Y, Zhang H et al (2023) Nanozyme-immobilized cellulose membranes designed by a simple hydrogen bond-dominated for colorimetric detection of hydrogen peroxide and uric acid. Microchem J 193:109113. https://doi.org/10.1016/j.microc.2023.109113
164. Phookum T, Siripongpreda T, Rodthongkum N, Ummartyotin S (2021) Development of cellulose from recycled office waste paper-based composite as a platform for the colorimetric sensor in food spoilage indicator. J Polym Res 28(11):416. https://doi.org/10.1007/s10965-021-02785-7
165. Guo L, Liu H, Peng F, Qi H (2021) Efficient and portable cellulose-based colorimetric test paper for metal ion detection. Carbohyd Polym 274:118635. https://doi.org/10.1016/j.carbpol.2021.118635
166. Zhang Y, He P, Luo M, Xu X, Dai G, Yang J (2020) Highly stretchable polymer/silver nanowires composite sensor for human health monitoring. Nano Res 13(4):919–926. https://doi.org/10.1007/s12274-020-2730-z
167. Zhao G, Zhang X, Cui X, Wang S, Liu Z, Deng L et al (2018) Piezoelectric polyacrylonitrile nanofiber film-based dual-function self-powered flexible sensor. ACS Appl Mater Interfaces 10(18):15855–15863. https://doi.org/10.1021/acsami.8b02564
168. Kano S, Kim K, Fujii M (2017) Fast-response and flexible nanocrystal-based humidity sensor for monitoring human respiration and water evaporation on skin. ACS Sensors 2(6):828–833. https://doi.org/10.1021/acssensors.7b00199
169. Li N, Jiang Y, Zhou C, Xiao Y, Meng B, Wang Z et al (2019) High-performance humidity sensor based on urchin-like composite of Ti3C2 MXene-derived TiO2 nanowires. ACS Appl Mater Interfaces 11(41):38116–38125. https://doi.org/10.1021/acsami.9b12168
170. Ma H, Liu Z, Lou J, Ding Q, Jiang Y, Li X et al (2023) Bacterial cellulose/MWCNT coatings for highly sensitive and flexible paper-based humidity sensors. Cellulose 30(2):1193–1204. https://doi.org/10.1007/s10570-022-04960-5
171. Lan L, Le X, Dong H, Xie J, Ying Y, Ping J (2020) One-step and large-scale fabrication of flexible and wearable humidity sensor based on laser-induced graphene for real-time tracking of plant transpiration at bio-interface. Biosens Bioelectron 165:112360. https://doi.org/10.1016/j.bios.2020.112360
172. Chaudhary P, Maurya DK, Pandey A, Verma A, Tripathi RK, Kumar S et al (2022) Design and development of flexible humidity sensor for baby diaper alarm: experimental and theoretical study. Sens Actuators, B Chem 350:130818. https://doi.org/10.1016/j.snb.2021.130818
173. Wang Y, Hou S, Li T, Jin S, Shao Y, Yang H et al (2020) Flexible capacitive humidity sensors based on ionic conductive wood-derived cellulose nanopapers. ACS Appl Mater Interfaces 12(37):41896–41904. https://doi.org/10.1021/acsami.0c12868
174. Gabrielli V, Frasconi M (2022) Cellulose-based functional materials for sensing. Chemosensors 10(9):352. https://doi.org/10.3390/chemosensors10090352
175. Franco P, Senso A, Oliveros L, Minguillón C (2001) Covalently bonded polysaccharide derivatives as chiral stationary phases in high-performance liquid chromatography. J Chromatogr A 906(1):155–170. https://doi.org/10.1016/S0021-9673(00)00531-8
176. Sternberg R, Bindra DS, Wilson GS, Thevenot DR (1988) Covalent enzyme coupling on cellulose acetate membranes for glucose sensor development. Anal Chem 60(24):2781–2786. https://doi.org/10.1021/ac00175a028
177. Edwards JV, Prevost N, Sethumadhavan K, Ullah A, Condon B (2013) Peptide conjugated cellulose nanocrystals with sensitive human neutrophil elastase sensor activity. Cellulose 20(3):1223–1235. https://doi.org/10.1007/s10570-013-9901-y
178. Orelma H, Teerinen T, Johansson L-S, Holappa S, Laine J (2012) CMC-modified cellulose biointerface for antibody conjugation. Biomacromol 13(4):1051–1058. https://doi.org/10.1021/bm201771m
179. Berlin P, Klemm D, Tiller J, Rieseler R (2000) A novel soluble aminocellulose derivative type: its transparent film-forming properties and its efficient coupling with enzyme proteins for biosensors. Macromol Chem Phys 201(15):2070–2082. https://doi.org/10.1002/1521-3935(20001001)201:15%3c2070::AID-MACP2070%3e3.0.CO;2-E
180. Lee K-Y, Tammelin T, Schulfter K, Kiiskinen H, Samela J, Bismarck A (2012) High performance cellulose nanocomposites: comparing the reinforcing ability of bacterial cellulose and nanofibrillated cellulose. ACS Appl Mater Interfaces 4(8):4078–4086. https://doi.org/10.1021/am300852a
181. Siqueira G, Bras J, Dufresne A (2010) Cellulosic bionanocomposites: a review of preparation, properties and applications. Polymers 2(4):728–765. https://doi.org/10.3390/polym2040728
182. Golmohammadi H, Morales-Narváez E, Naghdi T, Merkoçi A (2017) Nanocellulose in sensing and biosensing. Chem Mater 29(13):5426–5446. https://doi.org/10.1021/acs.chemmater.7b01170
183. Wang D, Yu H, Fan X, Gu J, Ye S, Yao J et al (2018) High aspect ratio carboxylated cellulose nanofibers cross-linked to robust aerogels for superabsorption–flocculants: paving way from nanoscale to macroscale. ACS Appl Mater Interfaces 10(24):20755–20766. https://doi.org/10.1021/acsami.8b04211
184. Kontturi E, Laaksonen P, Linder MB, Nonappa Gröschel AH, Rojas OJ et al (2018) Advanced materials through assembly of

nanocelluloses. Adv Mater 30(24):1703779. https://doi.org/10.1002/adma.201703779
185. Fei G, Wang Y, Wang H, Ma Y, Guo Q, Huang W et al (2019) Fabrication of bacterial cellulose/polyaniline nanocomposite paper with excellent conductivity, strength, and flexibility. ACS Sustain Chem Eng 7(9):8215–8225. https://doi.org/10.1021/acssuschemeng.8b06306
186. Dai L, Wang Y, Zou X, Chen Z, Liu H, Ni Y (2020) Ultrasensitive physical, bio, and chemical sensors derived from 1-, 2-, and 3-D nanocellulosic materials. Small 16(13):1906567. https://doi.org/10.1002/smll.201906567
187. Ng H-M, Sin LT, Tee T-T, Bee S-T, Hui D, Low C-Y et al (2015) Extraction of cellulose nanocrystals from plant sources for application as reinforcing agent in polymers. Compos B Eng 75:176–200. https://doi.org/10.1016/j.compositesb.2015.01.008
188. Avcioglu NH (2022) Bacterial cellulose: recent progress in production and industrial applications. World J Microbiol Biotechnol 38(5):86. https://doi.org/10.1007/s11274-022-03271-y
189. Dandegaonkar G, Ahmed A, Sun L, Adak B, Mukhopadhyay S (2022) Cellulose based flexible and wearable sensors for health monitoring. Mater Adv 3(9):3766–3783. https://doi.org/10.1039/D1MA01210J
190. Fan J, Zhang S, Li F, Shi J (2020) Cellulose-based sensors for metal ions detection. Cellulose 27(10):5477–5507. https://doi.org/10.1007/s10570-020-03158-x
191. Abdelhamid HN, Mathew AP (2022) Cellulose–metal organic frameworks (CelloMOFs) hybrid materials and their multifaceted applications: a review. Coord Chem Rev 451:214263. https://doi.org/10.1016/j.ccr.2021.214263
192. Pena-Pereira F, Lavilla I, de la Calle I, Romero V, Bendicho C (2023) Detection of gases and organic vapors by cellulose-based sensors. Anal Bioanal Chem 415(18):4039–4060. https://doi.org/10.1007/s00216-023-04649-z
193. Prathapan R, Tabor RF, Garnier G, Hu J (2020) Recent progress in cellulose nanocrystal alignment and its applications. ACS Appl Bio Mater 3(4):1828–1844. https://doi.org/10.1021/acsabm.0c00104
194. Lu Y, Liu C, Mei C, Sun J, Lee J, Wu Q et al (2022) Recent advances in metal organic framework and cellulose nanomaterial composites. Coord Chem Rev 461:214496. https://doi.org/10.1016/j.ccr.2022.214496
195. Huang L, Hu Q, Gao S, Liu W, Wei X (2023) Recent progress and applications of cellulose and its derivatives-based humidity sensors: a review. Carbohyd Polym 318:121139. https://doi.org/10.1016/j.carbpol.2023.121139
196. Nawaz H, Zhang X, Chen S, You T, Xu F (2021) Recent studies on cellulose-based fluorescent smart materials and their applications: a comprehensive review. Carbohyd Polym 267:118135. https://doi.org/10.1016/j.carbpol.2021.118135
197. Carolin CF, Kamalesh T, Kumar PS, Hemavathy RV, Rangasamy G (2023) A critical review on sustainable cellulose materials and its multifaceted applications. Industrial Crops Products 203:117221. https://doi.org/10.1016/j.indcrop.2023.117221
198. Chang S, Weng Z, Zhang C, Jiang S, Duan G (2023) Cellulose-based intelligent responsive materials: a review. Polymers 15(19). https://doi.org/10.3390/polym15193905
199. Wang D-C, Lei S-N, Zhong S, Xiao X, Guo Q-H (2023) Cellulose-based conductive materials for energy and sensing applications. Polymers 15(20):4159. https://doi.org/10.3390/polym15204159
200. Ma H, Cheng Z, Li X, Li B, Fu Y, Jiang J (2023) Advances and challenges of cellulose functional materials in sensors. J Bioresources Bioproducts 8(1):15–32. https://doi.org/10.1016/j.jobab.2022.11.001
201. Singh S, Bhardwaj S, Tiwari P, Dev K, Ghosh K, Maji PK (2024) Recent advances in cellulose nanocrystals-based sensors: a review. Materials Advances 5(7):2622–2654. https://doi.org/10.1039/D3MA00601H
202. Al-Saidi HM, Khan S (n.d.) A review on organic fluorimetric and colorimetric chemosensors for the detection of Ag(I) ions. Critical Rev Anal Chem 1–27, https://doi.org/10.1080/10408347.2022.2133561.
203. Abu-Rayyan A, Ahmad I, Bahtiti NH, Muhmood T, Bondock S, Abohashrh M et al (2023) Recent progress in the development of organic chemosensors for formaldehyde detection. ACS Omega 8(17):14859–14872. https://doi.org/10.1021/acsomega.2c07724
204. El-Sewify IM, Radwan A, Elghazawy NH, Fritzsche W, Azzazy HME (2022) Optical chemosensors for environmental monitoring of toxic metals related to Alzheimer's disease. RSC Adv 12(50):32744–32755. https://doi.org/10.1039/D2RA05384E
205. Wu D, Sedgwick AC, Gunnlaugsson T, Akkaya EU, Yoon J, James TD (2017) Fluorescent chemosensors: the past, present and future. Chem Soc Rev 46(23):7105–7123. https://doi.org/10.1039/C7CS00240H
206. Alyami AY (2023) Recent progress in organic fluorescence and colorimetric chemosensors for Cu2+ detection: a comprehensive review (2018–2023). Dyes Pigm 220:111740. https://doi.org/10.1016/j.dyepig.2023.111740
207. Nair RR, Debnath S, Das S, Wakchaure P, Ganguly B, Chatterjee PB (2019) A highly selective turn-on biosensor for measuring spermine/spermidine in human urine and blood. ACS Appl Bio Mater 2(6):2374–2387. https://doi.org/10.1021/acsabm.9b00084
208. Nair RR, Raju M, Patel NP, Raval IH, Suresh E, Haldar S et al (2015) Naked eye instant reversible sensing of Cu2+ and its in situ imaging in live brine shrimp Artemia. Analyst 140(16):5464–5468. https://doi.org/10.1039/C5AN00957J
209. Raju M, Nair RR, Raval IH, Haldar S, Chatterjee PB (2018) A water soluble Cu2+-specific colorimetric probe can also detect Zn2+ in live shrimp and aqueous environmental samples by fluorescence channel. Sens Actuators, B Chem 260:364–370. https://doi.org/10.1016/j.snb.2018.01.010
210. Raju M, Nair RR, Raval IH, Haldar S, Chatterjee PB (2015) Reporting a new siderophore based Ca2+ selective chemosensor that works as a staining agent in the live organism Artemia. Analyst 140(22):7799–7809. https://doi.org/10.1039/C5AN01733E
211. Debnath S, Ghosh R, Nair RR, Pradhan D, Chatterjee PB (2022) Advances in the development of water-soluble fluorogenic probes for bioimaging of hypochlorite/hypochlorous acid in cells and organisms. ACS Omega 7(43):38122–38149. https://doi.org/10.1021/acsomega.2c04840
212. Nair RR, Raju M, Bhai S, Raval IH, Haldar S, Ganguly B et al (2019) Estimation of bisulfate in edible plant foods, dog urine, and drugs: picomolar level detection and bio-imaging in living organisms. Analyst 144(19):5724–5737. https://doi.org/10.1039/C9AN01078E
213. Mudhulkar R, Nair RR, Raval IH, Haldar S, Chatterjee PB (2017) Visualizing Zn2+ in living whole organism artemia by a natural fluorimetric intermediate siderophore. ChemistrySelect 2(22):6407–6412. https://doi.org/10.1002/slct.201701071
214. Nair RR, Raju M, Jana K, Mondal D, Suresh E, Ganguly B et al (2018) Instant detection of hydrogen cyanide gas and cyanide salts in solid matrices and water by using CuII and NiII complexes of intramolecularly hydrogen bonded zwitterions. Chem - A Eur J 24(42):10721–10731. https://doi.org/10.1002/chem.201800894
215. Nair RR, An JM, Kim J, Kim D (2023) Review: recent progress in fluorescent molecular systems for the detection of disease-related biomarkers in biofluids. Coord Chem Rev 494:215336. https://doi.org/10.1016/j.ccr.2023.215336

216. Nair RR, Raju M, Debnath S, Ghosh R, Chatterjee PB (2020) Concurrent detection and treatment of cyanide-contaminated water using mechanosynthesized receptors. Analyst 145(16):5647–5656. https://doi.org/10.1039/D0AN00449A
217. Raju M, Patel TJ, Nair RR, Chatterjee PB (2016) Xanthurenic acid: a natural ionophore with high selectivity and sensitivity for potassium ions in an aqueous solution. New J Chem 40(3):1930–1934. https://doi.org/10.1039/C5NJ02540K
218. Debnath S, Chatterjee PB (2022) Enantiopure chiroptical probes for circular dichroism and absorbance based detection of nerve gas simulants. Chem Commun 58(64):9006–9009. https://doi.org/10.1039/D2CC03392E
219. Debnath S, Nair RR, Bhattacharya A, Ghosh R, Chatterjee PB (2021) Smartphone assisted chromogenic sensing of halogenated solvents and monoaromatic hydrocarbons. Dyes Pigm 196:109821. https://doi.org/10.1016/j.dyepig.2021.109821
220. Nair RR, Seo EW, Hong S, Jung KO, Kim D (2023) Pentafluorobenzene: promising applications in diagnostics and therapeutics. ACS Appl Bio Mater 6(10):4081–4099. https://doi.org/10.1021/acsabm.3c00676
221. Nair RR, Debnath S, Ghosh R, Bhattacharya A, Raju M, Chatterjee PB (2024) Label-free detection of unbound bilirubin and nitrophenol explosives in water by a mechanosynthesized dual functional zinc complex: recognition of picric acid in various common organic media. Chem - A Eur J 30(9):e202303068. https://doi.org/10.1002/chem.202303068
222. Ghosh R, Nair RR, Ghosh S, Debnath S, Chatterjee PB (2024) A water-soluble wavy coordination polymer of Cu(II) as a turn-on luminescent probe for histidine and histidine-rich proteins/peptides. Inorg Chem 63(18):8320–8328. https://doi.org/10.1021/acs.inorgchem.4c00665
223. Debnath S, Nair RR, Ghosh R, Kiranmai G, Radhakishan N, Nagesh N et al (2022) A unique water soluble probe for measuring the cardiac marker homocysteine and its clinical validation. Chem Commun 58(66):9210–9213. https://doi.org/10.1039/D2CC01515C
224. Nair RR, Jin JH, An JM, Kang J, Kim J, Jeong H et al (2024) Single-benzene-based fluorescent probe for the detection of inhale-toxic triphosgene and its practical applications. Dyes Pigm 228:112237. https://doi.org/10.1016/j.dyepig.2024.112237
225. Das P, Ghosh A, Bhatt H, Das A (2012) A highly selective and dual responsive test paper sensor of Hg2+/Cr3+ for naked eye detection in neutral water. RSC Adv 2(9):3714–3721. https://doi.org/10.1039/C2RA00788F
226. Xu LQ, Neoh K-G, Kang E-T, Fu GD (2013) Rhodamine derivative-modified filter papers for colorimetric and fluorescent detection of Hg2+ in aqueous media. J Mater Chem A 1(7):2526–2532. https://doi.org/10.1039/C2TA01072K
227. Ashokkumar P, Weißhoff H, Kraus W, Rurack K (2014) Test-strip-based fluorometric detection of fluoride in aqueous media with a BODIPY-linked hydrogen-bonding receptor. Angew Chem Int Ed 53(8):2225–2229. https://doi.org/10.1002/anie.201307848
228. Ruan Z, Li C, Li J-R, Qin J, Li Z (2015) A relay strategy for the mercury (II) chemodosimeter with ultra-sensitivity as test strips. Sci Rep 5(1):15987. https://doi.org/10.1038/srep15987
229. Wang D-H, Zhang Y, Sun R, Zhao D-Z (2016) Dimethyl yellow-based colorimetric chemosensors for "naked eye" detection of Cr3+ in aqueous media via test papers. RSC Adv 6(6):4640–4646. https://doi.org/10.1039/C5RA22127G
230. Nair RR, Paul A, Raju M, Suresh E, Srivastava DN, Chatterjee PB (2017) Can mechanochemical synthesis be utilized in the progress of chemosensing technology? A case study with a series of Cu2+ selective receptors. Sens Actuators, B Chem 253:213–223. https://doi.org/10.1016/j.snb.2017.06.097
231. Jarangdet T, Pratumyot K, Srikittiwanna K, Dungchai W, Mingvanish W, Techakriengkrai I et al (2018) A fluorometric paper-based sensor array for the discrimination of volatile organic compounds (VOCs) with novel salicylidene derivatives. Dyes Pigm 159:378–383. https://doi.org/10.1016/j.dyepig.2018.06.044
232. Sutariya PG, Soni H, Gandhi SA, Pandya A (2019) Luminescent behavior of pyrene-allied calix[4]arene for the highly pH-selective recognition and determination of Zn2+, Hg2+ and I−via the CHEF-PET mechanism: computational experiment and paper-based device. New J Chem 43(25):9855–9864. https://doi.org/10.1039/C9NJ01388A
233. Ramesh S, Kumaresan S (2021) A highly selective coumarin-based chemosensor for naked-eye detection of cyanide anions via nucleophilic addition in pure aqueous environment. Microchem J 169:106584. https://doi.org/10.1016/j.microc.2021.106584
234. Kim NH, Kang RH, Kim D (2022) Pentafluoro-benzene functionalized AIEgen: a highly sensitive and fast responsive fluorescent nanoprobe for the detection of gold ions. Dyes Pigm 198:110007. https://doi.org/10.1016/j.dyepig.2021.110007
235. Kang J, An JM, Seo EW, Lee J, Huh Y, Park C et al (2023) Single-benzene-based ratiometric fluorescent probe for hydrazine visualization. Dyes Pigm 218:111487. https://doi.org/10.1016/j.dyepig.2023.111487
236. Chen X, Pradhan T, Wang F, Kim JS, Yoon J (2012) Fluorescent chemosensors based on spiroring-opening of xanthenes and related derivatives. Chem Rev 112(3):1910–1956. https://doi.org/10.1021/cr200201z
237. Zhu D, Liu B, Wei G (2021) Two-dimensional material-based colorimetric biosensors: a review. Biosensors 11(8):259. https://doi.org/10.3390/bios11080259
238. Xiao W, Luo Y, Zhang X, Huang J (2013) Highly sensitive colourimetric anion chemosensors fabricated by functional surface modification of natural cellulose substance. RSC Adv 3(16):5318–5323. https://doi.org/10.1039/C3RA00074E
239. Swingler S, Gupta A, Gibson H, Kowalczuk M, Heaselgrave W, Radecka I (2021) Recent advances and applications of bacterial cellulose in biomedicine. Polymers (Basel) 13(3):412. https://doi.org/10.3390/polym13030412
240. Martinez AW, Phillips ST, Butte MJ, Whitesides GM (2007) Patterned paper as a platform for inexpensive, low-volume, portable bioassays. Angew Chem Int Ed 46(8):1318–1320. https://doi.org/10.1002/anie.200603817
241. Koppaka V, Thompson DC, Chen Y, Ellermann M, Nicolaou KC, Juvonen RO et al (2012) Aldehyde dehydrogenase inhibitors: a comprehensive review of the pharmacology, mechanism of action, substrate specificity, and clinical application. Pharmacol Rev 64(3):520–539. https://doi.org/10.1124/pr.111.005538
242. Kabir MM, Wang H, Lau KT, Cardona F (2012) Chemical treatments on plant-based natural fibre reinforced polymer composites: an overview. Compos B Eng 43(7):2883–2892. https://doi.org/10.1016/j.compositesb.2012.04.053
243. de Mesquita JP, Donnici CL, Pereira FV (2010) Biobased nanocomposites from layer-by-layer assembly of cellulose nanowhiskers with chitosan. Biomacromol 11(2):473–480. https://doi.org/10.1021/bm9011985

244. Xue B, Yang Y, Sun Y, Fan J, Li X, Zhang Z (2019) Photoluminescent lignin hybridized carbon quantum dots composites for bioimaging applications. Int J Biol Macromol 122:954–961. https://doi.org/10.1016/j.ijbiomac.2018.11.018
245. Joshi PN, Mathias A, Mishra A (2018) Synthesis of ecofriendly fluorescent carbon dots and their biomedical and environmental applications. Mater Technol 33(10):672–680. https://doi.org/10.1080/10667857.2018.1492683
246. Qin K, Zhang D, Ding Y, Zheng X, Xiang Y, Hua J et al (2020) Applications of hydrothermal synthesis of Escherichia coli derived carbon dots in in vitro and in vivo imaging and p-nitrophenol detection. Analyst 145(1):177–183. https://doi.org/10.1039/C9AN01753D
247. Zhang M, Su R, Zhong J, Fei L, Cai W, Guan Q et al (2019) Red/orange dual-emissive carbon dots for pH sensing and cell imaging. Nano Res 12(4):815–821. https://doi.org/10.1007/s12274-019-2293-z
248. Yang T, Huang J-L, Wang Y-T, Zheng A-Q, Shu Y, Wang J-H (2019) β-cyclodextrin-decorated carbon dots serve as nanocarriers for targeted drug delivery and controlled release. ChemNanoMat 5(4):479–487. https://doi.org/10.1002/cnma.201800528
249. Han M, Zhu S, Lu S, Song Y, Feng T, Tao S et al (2018) Recent progress on the photocatalysis of carbon dots: classification, mechanism and applications. Nano Today 19:201–218. https://doi.org/10.1016/j.nantod.2018.02.008
250. Jana J, Lee HJ, Chung JS, Kim MH, Hur SH (2019) Blue emitting nitrogen-doped carbon dots as a fluorescent probe for nitrite ion sensing and cell-imaging. Anal Chim Acta 1079:212–219. https://doi.org/10.1016/j.aca.2019.06.064
251. Yuan F, Yuan T, Sui L, Wang Z, Xi Z, Li Y et al (2018) Engineering triangular carbon quantum dots with unprecedented narrow bandwidth emission for multicolored LEDs. Nat Commun 9(1):2249. https://doi.org/10.1038/s41467-018-04635-5
252. Hu C, Li M, Qiu J, Sun Y-P (2019) Design and fabrication of carbon dots for energy conversion and storage. Chem Society Rev 48(8):2315–2337. https://doi.org/10.1039/C8CS00750K
253. Joseph J, Anappara AA (2017) White-light-emitting carbon dots prepared by the electrochemical exfoliation of graphite. ChemPhysChem 18(3):292–298. https://doi.org/10.1002/cphc.201601020
254. Dey S, Govindaraj A, Biswas K, Rao CNR (2014) Luminescence properties of boron and nitrogen doped graphene quantum dots prepared from arc-discharge-generated doped graphene samples. Chem Phys Lett 595–596:203–208. https://doi.org/10.1016/j.cplett.2014.02.012
255. Nguyen V, Zhao N, Yan L, Zhong P, Nguyen VC, Le PH (2020) Double-pulse femtosecond laser ablation for synthesis of ultrasmall carbon nanodots. Mater Res Express 7(1):015606. https://doi.org/10.1088/2053-1591/ab6124
256. Hu Y, Wang Y, Wang C, Ye Y, Zhao H, Li J et al (2019) One-pot pyrolysis preparation of carbon dots as eco-friendly nanoadditives of water-based lubricants. Carbon 152:511–520. https://doi.org/10.1016/j.carbon.2019.06.047
257. Tabaraki R, Abdi O (2019) Microwave assisted synthesis of N-doped carbon dots: an easy, fast and cheap sensor for determination of aspartic acid in sport supplements. J Fluoresc 29(3):751–756. https://doi.org/10.1007/s10895-019-02387-z
258. Huang H, Cui Y, Liu M, Chen J, Wan Q, Wen Y et al (2018) A one-step ultrasonic irradiation assisted strategy for the preparation of polymer-functionalized carbon quantum dots and their biological imaging. J Colloid Interface Sci 532:767–773. https://doi.org/10.1016/j.jcis.2018.07.099
259. Lu Z, Su T, Feng Y, Jiang S, Zhou C, Hong P et al (2019) Potential application of nitrogen-doped carbon quantum dots synthesized by a solvothermal method for detecting silver ions in food packaging. Int J Environ Res Public Health 16(14):2518. https://doi.org/10.3390/ijerph16142518
260. Yarur F, Macairan J-R, Naccache R (2019) Ratiometric detection of heavy metal ions using fluorescent carbon dots. Environ Sci: Nano 6(4):1121–1130. https://doi.org/10.1039/C8EN01418C
261. Cichosz S, Masek A, Zaborski M (2018) Polymer-based sensors: a review. Polym Testing 67:342–348. https://doi.org/10.1016/j.polymertesting.2018.03.024
262. Alberti G, Zanoni C, Losi V, Magnaghi LR, Biesuz R (2021) Current trends in polymer based sensors. Chemosensors 9(5):108. https://doi.org/10.3390/chemosensors9050108
263. Zainal SH, Mohd NH, Suhaili N, Anuar FH, Lazim AM, Othaman R (2021) Preparation of cellulose-based hydrogel: a review. J Market Res 10:935–952. https://doi.org/10.1016/j.jmrt.2020.12.012
264. Thivya P, Akalya S, Sinija VR (2022) A comprehensive review on cellulose-based hydrogel and its potential application in the food industry. Appl Food Res 2(2):100161. https://doi.org/10.1016/j.afres.2022.100161
265. Zhu C, Monti S, Mathew AP (2020) Evaluation of nanocellulose interaction with water pollutants using nanocellulose colloidal probes and molecular dynamic simulations. Carbohyd Polym 229:115510. https://doi.org/10.1016/j.carbpol.2019.115510
266. Zhu C, Monti S, Mathew AP (2018) Cellulose nanofiber–graphene oxide biohybrids: disclosing the self-assembly and copper-ion adsorption using advanced microscopy and ReaxFF simulations. ACS Nano 12(7):7028–7038. https://doi.org/10.1021/acsnano.8b02734
267. Valencia L, Nomena EM, Monti S, Rosas-Arbelaez W, Mathew AP, Kumar S et al (2020) Multivalent ion-induced re-entrant transition of carboxylated cellulose nanofibrils and its influence on nanomaterials' properties. Nanoscale 12(29):15652–15662. https://doi.org/10.1039/D0NR02888F
268. Liu P, Sehaqui H, Tingaut P, Wichser A, Oksman K, Mathew AP (2014) Cellulose and chitin nanomaterials for capturing silver ions (Ag+) from water via surface adsorption. Cellulose 21(1):449–461. https://doi.org/10.1007/s10570-013-0139-5
269. Liu P, Borrell PF, Božič M, Kokol V, Oksman K, Mathew AP (2015) Nanocelluloses and their phosphorylated derivatives for selective adsorption of Ag+, Cu2+ and Fe3+ from industrial effluents. J Hazard Mater 294:177–185. https://doi.org/10.1016/j.jhazmat.2015.04.001
270. Pillai SS, Deepa B, Abraham E, Girija N, Geetha P, Jacob L et al (2013) Biosorption of Cd(II) from aqueous solution using xanthated nano banana cellulose: equilibrium and kinetic studies. Ecotoxicol Environ Saf 98:352–360. https://doi.org/10.1016/j.ecoenv.2013.09.003
271. Yu X, Tong S, Ge M, Wu L, Zuo J, Cao C et al (2013) Adsorption of heavy metal ions from aqueous solution by carboxylated cellulose nanocrystals. J Environ Sci 25(5):933–943. https://doi.org/10.1016/S1001-0742(12)60145-4
272. Li D, Tian X, Wang Z, Guan Z, Li X, Qiao H et al (2020) Multifunctional adsorbent based on metal-organic framework modified bacterial cellulose/chitosan composite aerogel for high efficient removal of heavy metal ion and organic pollutant. Chem Eng J 383:123127. https://doi.org/10.1016/j.cej.2019.123127

273. Liu Y, Huo Y, Fan Q, Li M, Liu H, Li B et al (2021) Cellulose nanofibrils composite hydrogel with polydopamine@zeolitic imidazolate framework-8 encapsulated in used as efficient vehicles for controlled drug release. J Ind Eng Chem 102:343–350. https://doi.org/10.1016/j.jiec.2021.07.023
274. Zhou S, Qiu Z, Strømme M, Xu C (2021) Solar-driven ionic power generation via a film of nanocellulose @ conductive metal–organic framework. Energy Environ Sci 14(2):900–905. https://doi.org/10.1039/D0EE02730H
275. Fei Y, Liang M, Zhou T, Chen Y, Zou H (2020) Unique carbon nanofiber@ Co/C aerogel derived bacterial cellulose embedded zeolitic imidazolate frameworks for high-performance electromagnetic interference shielding. Carbon 167:575–584. https://doi.org/10.1016/j.carbon.2020.06.013
276. Zhou S, Apostolopoulou-Kalkavoura V, Tavares da Costa MV, Bergström L, Strømme M, Xu C (2019) Elastic aerogels of cellulose nanofibers@metal–organic frameworks for thermal insulation and fire retardancy. Nano-Micro Letters 12(1):9. https://doi.org/10.1007/s40820-019-0343-4
277. Zheng S, Liu S, Xiao B, Liu L, Wan X, Gong Y et al (2021) Integrate nanoscale assembly and plasmonic resonance to enhance photoluminescence of cellulose nanocrystals for optical information hiding and reading. Carbohyd Polym 253:117260. https://doi.org/10.1016/j.carbpol.2020.117260
278. Ma S, Zhang M, Nie J, Tan J, Yang B, Song S (2019) Design of double-component metal–organic framework air filters with PM2.5 capture, gas adsorption and antibacterial capacities. Carbohyd Polym 203:415–422. https://doi.org/10.1016/j.carbpol.2018.09.039
279. Paria S, Maity P, Siddiqui R, Patra R, Maity SB, Jana A (2022) Nanostructured luminescent micelles: efficient "functional materials" for sensing nitroaromatic and nitramine explosives. Photochem 2(1):32–57. https://doi.org/10.3390/photochem2010004
280. Li J, Wan Y, Li L, Liang H, Wang J (2009) Preparation and characterization of 2,3-dialdehyde bacterial cellulose for potential biodegradable tissue engineering scaffolds. Mater Sci Eng, C 29(5):1635–1642. https://doi.org/10.1016/j.msec.2009.01.006
281. Czaja W, Kyryliouk D, DePaula CA, Buechter DD (2014) Oxidation of γ-irradiated microbial cellulose results in bioresorbable, highly conformable biomaterial. J Appl Polym Sci 131(6). https://doi.org/10.1002/app.39995.
282. Hu Y, Catchmark JM (2011) In vitro biodegradability and mechanical properties of bioabsorbable bacterial cellulose incorporating cellulases. Acta Biomater 7(7):2835–2845. https://doi.org/10.1016/j.actbio.2011.03.028
283. Zhu L, Zong L, Wu X, Li M, Wang H, You J et al (2018) Shapeable fibrous aerogels of metal–organic-frameworks templated with nanocellulose for rapid and large-capacity adsorption. ACS Nano 12(5):4462–4468. https://doi.org/10.1021/acsnano.8b00566